



Development of a Novel Bioconjugation Platform for the Generation of Homogenous Antibody-Drug Conjugates

Friederike M. Dannheim

Clare Hall

University of Cambridge

August 2021

Supervised by Professor David R. Spring

This dissertation is submitted for the degree of **Doctor of Philosophy**

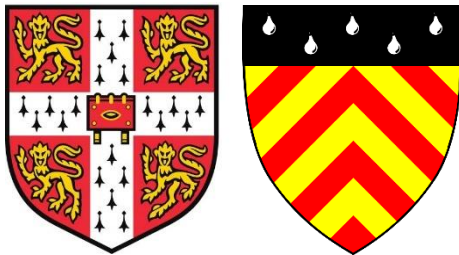
Declaration

This dissertation is submitted in fulfilment of the requirements for the degree of Doctor of Philosophy. This dissertation describes my own work and is not the product of collaboration, unless otherwise stated. The work presented has not been submitted for any other degree. It does not exceed the prescribed word count for the Physics and Chemistry Degree Committee.

Friederike M. Dannheim

August 2021

Clare Hall, University of Cambridge



Abstract

Antibody-drug conjugates (ADCs) are therapeutic entities which leverage the specificity of antibodies to selectively deliver potent cytotoxins to specific cell types, such as cancer cells. The pharmacology of an ADC is critically dependent on its stability, homogeneity, and drug-to-antibody ratio (DAR) – all of which are controlled by the chemistry used to attach the drug to the antibody. Thus, to optimise these ADC characteristics, significant effort has been invested in the development of bioconjugation methods which yield homogenous ADCs with stable linkages and well-defined modification sites. However, despite many recent advances in the field, significant limitations remain. For instance, many methods necessitate the use of antibody engineering which typically requires laborious case-by-case optimisation. Additionally, efficient modulation of DAR in integer increments while maintaining homogeneity and stability remains exceptionally challenging.

The primary aim of this work was the establishment of a linker technology that yields homogenous, stable, and functional ADCs from native antibodies. The secondary aim of this work was the derivatisation of these linkers to allow for the facile modulation of DAR in integer increments. Both of these goals could be achieved by the development of a novel class of disulfide rebridging linkers, based on the previously reported divinylpyrimidine (DVP) motif.

This report details the development of a novel set of disulfide rebridging linkers, which contain four DVP motifs (termed ‘TetraDVPs’). The TetraDVP motif can conjugate to eight distinct cysteine residues, allowing simultaneous rebridging of all four interchain disulfides in an IgG1 antibody with a single linker molecule, a strategy which generates antibody conjugates with excellent homogeneity. Derivatisation of the initial TetraDVP linker with varying numbers of payload attachment handles enabled facile modulation of drug loading. Thus, antibody conjugates were functionalised with varying numbers of biologically relevant moieties (e.g. fluorophores, cytotoxins) through bioorthogonal chemistry. Assessment of the biological activity of the resultant conjugates demonstrated exceptional stability in human plasma along with potent and selective cytotoxicity in a series of cell-based assays.

Acknowledgements

First and foremost, I would like to thank Prof David Spring for welcoming me into his research group and introducing me to the field of antibody-drug conjugates, and for his guidance and encouragement throughout the years. I would also like to thank Prof Jason Carroll for allowing me to work in his lab at CRUK and dive into the wonderful world of cancer research. It has been an honour and a pleasure to work with you, and I am very grateful for the opportunities I was given. Thank you also to Dr Jeremy Parker for helpful discussions and advice over the last few years. I would like to acknowledge AstraZeneca and the BBSRC for funding this research.

A massive thanks to my mentor Dr Stephen Walsh, who has spent countless hours teaching me about protein chemistry and cell biology and supported my professional development all throughout my PhD. Thank you for believing in me, and for helping me move forward, even when the going gets tough.

Thanks to the whole Spring group – past and present – for being such a social, lovable bunch. I will sorely miss our tea breaks, Friday pub trips, Christmas dinners, barbeques, badminton/bouldering sessions and, yes, even our mid-pandemic ‘Trivia Murder Party’ games. A special shout-out goes to my fellow 2017 starters, Sam and Abi. Thank you for your friendship and camaraderie. I still remember our early days in lab 122 with fondness!

Thanks also to the Carroll lab for being such a welcoming and wonderful group, and for everything they’ve taught me about cells and biology in general. Special thanks to Danya for always going out of her way to help me learn new techniques, and for many entertaining coffee mornings.

I would also like to thank my parents whose unwavering support and numerous care packages of German chocolates have kept me going throughout my degree. Your support throughout all my endeavours, great and small, means the world to me.

Finally, I would like to thank Steve, Andrew, Nicola, Tom and Anders for proofreading this thesis.

Abbreviations

°C	degrees centigrade
aaRS	amino acyl-tRNA synthetase
ADC	antibody-drug conjugate
ADCC	antibody-dependent cell-mediated cytotoxicity
ADPN	arylene dipropionitrile
AFC	antibody-fluorophore conjugate
ALC	antibody-linker conjugate
ALL	acute lymphoblastic leukaemia
AML	acute myeloid leukaemia
APN	arylpropionitrile
aq.	aqueous
Boc	<i>tert</i> -butoxycarbonyl
Boc-ON	2-(<i>tert</i> -butoxycarbonyloxyimino)-2-phenylacetonitrile
BTFFH	fluoro-dipyrrolidinocarbenium hexafluorophosphate
Bu	butyl
CAR-T	chimeric antigen receptor T cells
CDC	complement dependent cytotoxicity
CRISPR	clustered regularly interspaced short palindromic repeats
CuAAC	copper-catalysed azide-alkyne cycloaddition
CV	column volume
DAR	drug-to-antibody ratio
DIC	<i>N,N'</i> -diisopropylcarbodiimide
DIPEA	<i>N,N</i> -diisopropylethylamine
DLBCL	diffuse large B-cell lymphoma
DMAP	4-dimethylaminopyridine
DMF	<i>N,N</i> -dimethylformamide
DMSO	dimethylsulfoxide
DNA	deoxyribonucleic acid
DoE	design of experiments
dppf	1,1'-bis(diphenylphosphino)ferrocene
DSC	differential scanning calorimetry
DTT	dithiothreitol

DVP	divinylpyrimidine
DVT	divinyltriazine
EDC	1-Ethyl-3-(3-dimethylaminopropyl) carbodiimide
EDTA	ethylenediaminetetraacetic acid
ELISA	enzyme-linked immunosorbent assay
ER	oestrogen receptor
ESI	electrospray ionisation
Et	ethyl
Fab	fragment, antigen-binding
FACS	fluorescence-activated cell sorting
FAR	fluorophore-to-antibody ratio
Fc	fragment, crystallisable
FDA	Food and Drug Administration
FGE	formylglycine-generating enzyme
g	gram(s)
GSH	glutathione
h	hour(s)
HBTU	hexafluorophosphate benzotriazole tetramethyl uronium
HDX-MS	hydrogen-deuterium exchange mass spectrometry
HER2	human epidermal growth factor receptor type 2
HIC	hydrophobic interaction chromatography
HIPS	hydrazine- <i>iso</i> -Pictet–Spengler
HMWS	high molecular weight species
HOBt	hydroxybenzotriazole
HPLC	high performance liquid chromatography
HMBC	heteronuclear multiple bond correlation
HRMS	high resolution mass spectrometry
HSA	human serum albumin
HSQC	heteronuclear single quantum correlation
IgG	immunoglobulin G
IPA	isopropyl alcohol
IR	infrared (spectroscopy)
L	litre
LC-MS	liquid chromatography mass spectrometry
LLS	longest linear sequence

M	molar
mAb	monoclonal antibody
mc	maleimidocaproyl
MCC	4-(maleimidomethyl)cyclohexane-1-carboxylate
MEC	minimum effective concentration
Me	methyl
min	minute(s)
miRNA	microRNA
MMAE	monomethyl auristatin E
MMAF	monomethyl auristatin F
MoA	mechanism of action
mol	mole(s)
m.p.	melting point
MTD	maximum tolerated dose
MTGase	microbial transglutaminase
MTI	microtubule inhibitor
MWCO	molecular weight cut off
NGM	next-generation maleimide
NHS	<i>N</i> -hydroxysuccinimide
NMR	nuclear magnetic resonance (spectroscopy)
<i>p</i> -	para
PABC	<i>para</i> -aminobenzoyloxycarbonyl
PBD	pyrrolobenzodiazepine
PBS	Phosphate-buffered saline
PD	pyridazinedione
PDC	peptide-drug conjugate
PE	petroleum ether
PEG	polyethylene glycol
ppm	parts per million
R _f	retention factor
RNA	ribonucleic acid
rt	room temperature
sat.	saturated
SDS-PAGE	sodium dodecyl sulfate polyacrylamide gel electrophoresis
SEC	size-exclusion chromatography

SERD	selective oestrogen receptor degrader
SERM	selective oestrogen receptor modulator
siRNA	small interfering RNA
SMCC	succinimidyl-4-(<i>N</i> -maleimidomethyl)cyclohexane-1-carboxylate
S _N Ar	nucleophilic aromatic substitution
SPAAC	strain-promoted azide-alkyne cycloaddition
<i>t</i>	tertiary
TCEP	tris(2-carboxyethyl)phosphine hydrochloride
TBS	Tris-buffered saline
TFA	trifluoroacetic acid
THF	tetrahydrofuran
THPTA	tris(benzyltriazolymethyl)amine
TLC	thin-layer chromatography
TMS	trimethylsilyl
UAA	unnatural amino acid
v/v	volume concentration

Standard one and three letter codes are used for amino acids.

Table of Contents

DECLARATION	III
ABSTRACT	V
ACKNOWLEDGEMENTS	VII
ABBREVIATIONS	IX
TABLE OF CONTENTS	XIII
CHAPTER 1 - INTRODUCTION	1
1.1 Cancer therapy	1
1.2 Antibody-drug conjugates (ADCs)	4
1.3 The Antibody	8
1.4 The Payload	10
1.5 The Linker	12
1.5.1 Release mechanisms	13
1.5.1.1 Cleavable linkers	13
1.5.1.2 Non-cleavable linkers	15
1.5.2 Antibody modification	16
1.5.2.1 Stochastic conjugation methods	17
1.5.2.2 Site-selective conjugation methods	21
CHAPTER 2 – PROJECT OVERVIEW AND AIMS	29
CHAPTER 3 – BISDVP DISULFIDE REBRIDGING LINKERS	31
3.1 Introduction	31
3.2 Divinylpyrimidine (DVP) Linker Synthesis	32
3.3 BisDVP Linker Synthesis	37
3.3 Trastuzumab Bioconjugation	40
3.4 Functionalisation with AlexaFluor™ 488	42
3.5 Conclusions	45
CHAPTER 4 – TETRADVP DISULFIDE REBRIDGING LINKERS	46
4.1 Introduction	46
4.2 TetraDVP Linker Synthesis	47

4.2.1 Synthesis of TetraDVPs with one or two alkyne groups	47
4.2.2 Synthesis of a TetraDVP with three alkyne groups	50
4.2.3 Synthesis of TetraDVPs with one or two alkyne groups (revisited)	54
4.2.4 Synthesis of TetraDVPs with four alkyne groups	56
4.3 Trastuzumab Bioconjugation	59
4.4 Functionalisation with AlexaFluor™ 488	64
4.5 Biological Evaluation	68
4.5.1 Stability	68
4.5.2 Aggregation	71
4.5.3 Binding affinity	72
4.5.4 Cellular selectivity	72
4.6 Functionalisation with cytotoxic payloads	74
4.6.1 Post-conjugation functionalisation with MMAE	74
4.6.1.1 N ₃ -PEG ₄ -Val-Cit-PABC-MMAE	74
4.6.1.2 N ₃ -PEG ₂₄ -Val-Cit-PABC-MMAE	79
4.6.1.3 N ₃ -PEG ₄ -Glu ₂ -PEG ₂ -Val-Cit-PABC-MMAE	81
4.6.1.4 N ₃ -PEG ₄ -MMAE	83
4.6.2 Post-conjugation functionalisation with SN-38	85
4.6.3 Pre-conjugation functionalisation with MMAE	91
4.7 Cytotoxicity	94
4.7.1 Cleavable MMAE ADCs	94
4.7.2 Non-cleavable MMAE ADCs	95
4.8 PEGylated TetraDVP Linker	97
4.9 Conclusions	101
CHAPTER 5 – CONCLUSIONS AND FUTURE WORK	102
5.1 Conclusions	102
5.2 Future work	104
5.2.1 Improving post-conjugation payload attachment	104
5.2.2 <i>In vivo</i> evaluation of ADCs	105
5.2.3 Structural investigations	106
5.2.4 Fc fusion compounds	106
CHAPTER 6 - EXPERIMENTAL	108
6.1 General Experimental	108
6.2 Synthetic procedures	110
6.3 Protein Chemistry	135
6.4 Biological Evaluation	148
REFERENCES	151

APPENDIX A – NMR SPECTRA	163
APPENDIX B – HPLC TRACES	199
APPENDIX C – PROTEIN LC-MS	202
APPENDIX D – HIC TRACES	210
APPENDIX E – PUBLICATIONS	227

Chapter 1 - Introduction

1.1 Cancer therapy

According to recent reports by Cancer Research UK, over 360,000 people in the UK are diagnosed with cancer every year.¹ In fact, it is estimated that 1 in 2 people in the UK born after 1960 will be diagnosed with some form of cancer during their lifetime. While survival rates have increased significantly in recent years, only 54% of patients survive for more than 5 years after their initial diagnosis.²

Chemotherapy has been utilised as a means of treating cancer since the 1940s.^{3,4} At present, nearly a third of cancer patients in the UK receive chemotherapy as part of their treatment.⁵ Chemotherapy entails the administration of cytotoxic small molecules which accumulate within tumour cells and cause cell death *via* a variety of mechanisms.⁶ For example, DNA cross-linking agents such as cisplatin, carboplatin and oxaliplatin react with nuclear DNA by forming covalent linkages between adenine and guanine bases (Figure 1). These cross-links result in a distortion of the DNA structure, which inhibits transcription and ultimately leads to cell cycle arrest and apoptosis.^{7,8} Another common class of chemotherapy agents – microtubule inhibitors (MTI) – induce apoptosis by stabilising or destabilising microtubules, thereby interfering with mitotic function and cell cycle progression.^{9,10} Taxanes (e.g. paclitaxel) and vinca alkaloids (e.g. vinblastine) are both types of MTIs which function *via* microtubule stabilisation and depolymerisation respectively.^{11,12}

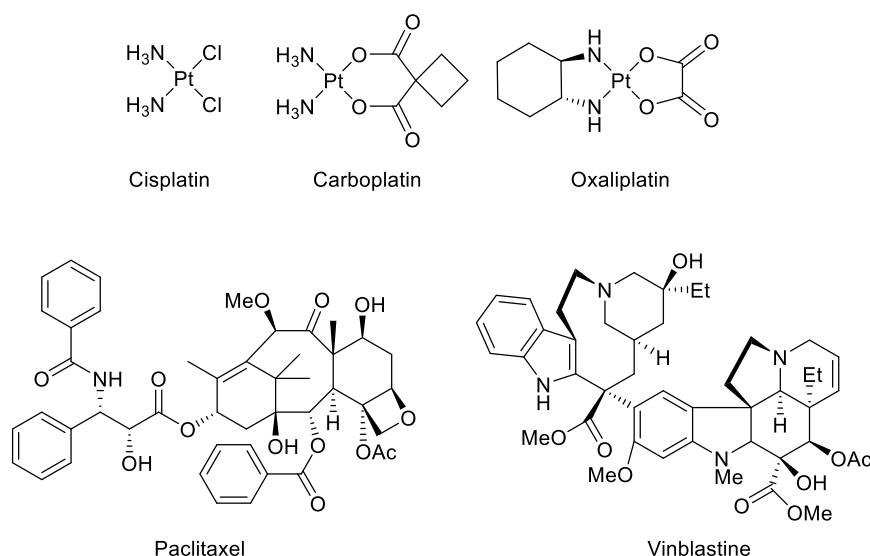


Figure 1: DNA-crosslinking agents (top) and microtubule inhibitors (bottom) are commonly used small molecule chemotherapeutics.

While these traditional chemotherapy agents kill tumour cells with admirable efficiency, they lack the ability to adequately differentiate between diseased and healthy cells. This lack of selectivity can lead to patients experiencing severe adverse effects in response to therapy and force premature termination of treatment.^{6,13,14} Thus, a plethora of research has been dedicated to the design of targeted therapeutics which specifically target cancer cells while sparing normal cells.¹⁵

Many cancerous cells are distinguishable from healthy cells through the overexpression or mutation of certain proteins, which may be inhibited using targeted small molecule therapeutics. For example, most cases of chronic myeloid leukaemia are characterised by a genetic mutation which causes the expression of BCR-ALB, a unique tyrosine kinase fusion protein which is permanently active and accelerates cell proliferation.¹⁶ A targeted approach to the treatment of such cases is the administration of imatinib, a small molecule inhibitor of BCR-ALB (Figure 2).¹⁷ Oestrogen receptor (ER) positive breast cancer is another type of cancer that may be modulated with small molecule inhibitors. The ER transcription factor is a driving force in approximately 75% of breast cancers and can be regulated using selective ER modulators (SERMs) such as tamoxifen or selective ER degraders (SERDs) such as fulvestrant.^{18–20} However, while these small molecule drugs have undoubtedly had a positive effect on cancer survival rates, they still frequently result in the death of healthy cells and harmful side effects. This is partly due to the fact that small molecule inhibitors – particularly

tyrosine kinase inhibitors – are not entirely selective and usually have a broad spectrum of proteins with which they interfere.^{16,21,22}

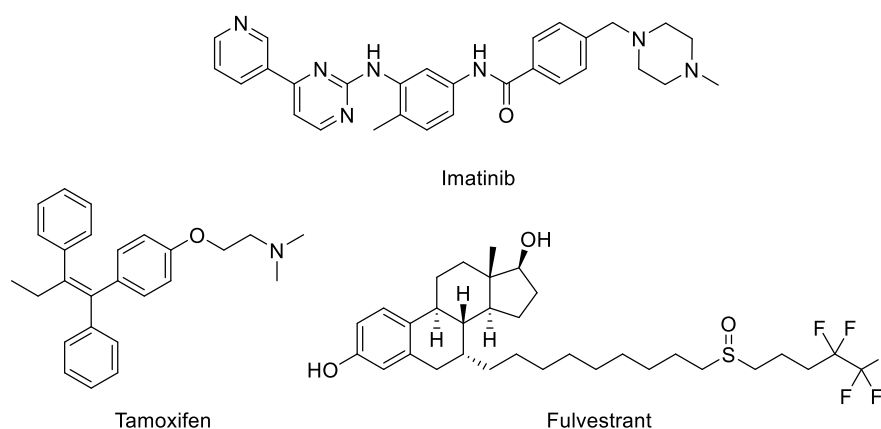


Figure 2: Small molecule inhibitors such as imatinib, tamoxifen or fulvestrant target cancer cells by inhibiting proteins which are unique to or overexpressed by the cancer.

In recent years, the search for more selective cancer therapies has resulted in a growing interest in biotherapeutics. The field of biotherapeutics (also referred to as ‘biologics’) encompasses all therapeutics that are based on protein, peptide or oligonucleotide structures. The most prominent class of biotherapeutics are monoclonal antibodies (mAb) which accounted for five of the top ten best-selling drugs in 2019.²³

Antibodies are proteins with the ability to bind to antigens (typically cell surface receptors) with high affinity and selectivity. Many cancers are characterised through the overexpression of certain receptors and can thus be selectively targeted using mAbs. Once an antibody has bound its target antigen it may then inhibit cell proliferation by blocking the receptor signalling pathway, or kill the malignant cell by mobilising the immune system *via* complement dependent cytotoxicity (CDC) or antibody-dependent cell-mediated cytotoxicity (ADCC).^{24,25} For example, the first mAb to be approved for cancer therapy, rituximab, targets CD20, an antigen expressed by non-Hodgkin lymphoma cells, and subsequently induces cell death *via* a combination of CDC, ADCC and direct blockage of cell signalling pathways.^{26,27} Since the approval of rituximab by the US Food and Drug Administration (FDA) in 1997, over 80 therapeutic mAbs have reached the market and many more are under evaluation in clinical trials.^{28,29} However, despite their widespread success, antibody therapeutics are not without their faults. For instance, many antibodies are not sufficiently potent as a monotherapy to eradicate the cancer and must be administered in combination with traditional chemotherapy

drugs.³⁰ Furthermore, cancers frequently develop resistance to antibodies, rendering the therapy ineffective after only a few cycles of treatment.³¹ Thus, new antibody modalities with enhanced potency such as antibody-drug conjugates (ADCs) are attracting increased attention.

Apart from antibodies, the field of biotherapeutics includes small biologics such as microRNAs (miRNA), small interfering RNAs (siRNA), antisense oligonucleotides and peptide-drug conjugates (PDCs),^{32–35} as well as complex immunotherapies such as chimeric antigen receptor T cells (CAR-T) or clustered regularly interspaced short palindromic repeats (CRISPR)/Cas therapy.^{36–38} While all of these modalities represent highly promising concepts, most are still in early stage development and issues with cost, safety and delivery remain to be overcome before they can be considered feasible for widespread use. Therefore, antibodies are predicted to remain a key driver of the biopharmaceutical market for the foreseeable future.^{29,39}

1.2 Antibody-drug conjugates (ADCs)

The concept of antibody-drug conjugates (ADCs) is derived from the idea of combining the powerful cell-killing ability of cytotoxic small molecules with the target specificity of antibodies. An ADC is a complex macromolecule consisting of three components: a monoclonal antibody (mAb), a cytotoxic drug (also often referred to as a ‘payload’ or ‘warhead’), and a linker to connect the two and modulate various properties of the therapeutics, such as solubility and drug loading (Figure 3).

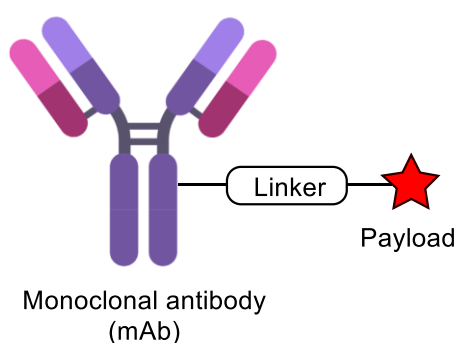


Figure 3: General structure of an antibody-drug conjugate (ADC).

Much like the mechanism of action (MoA) of an unmodified antibody, the typical MoA of an ADC involves binding of the mAb to an antigen on the surface of a target cell (Figure 4). The ADC is subsequently internalised, typically *via* receptor-mediated endocytosis. Once inside

the cell, the ADC is trafficked through several cellular compartments including the lysosome, where the antibody is degraded. Degradation of the antibody causes release of the payload which then initiates apoptosis of the target cell through various mechanisms, such as the inhibition of DNA replication or microtubule formation.⁴⁰ Some ADCs contain additional release mechanisms in the form of cleavable linkers, which allow for payload release independent of antibody degradation in response to intracellular stimuli such as low pH or protease enzymes.⁴¹ This aspect is described in more detail in Chapter 1.5.1.1. Depending on the nature of payload release, it may also be possible for the free payload to diffuse into other nearby cells; This is called the ‘bystander effect’ and can be useful in the treatment of cancers with heterogeneous antigen expression or solid tumours which may otherwise be difficult to penetrate.⁴²

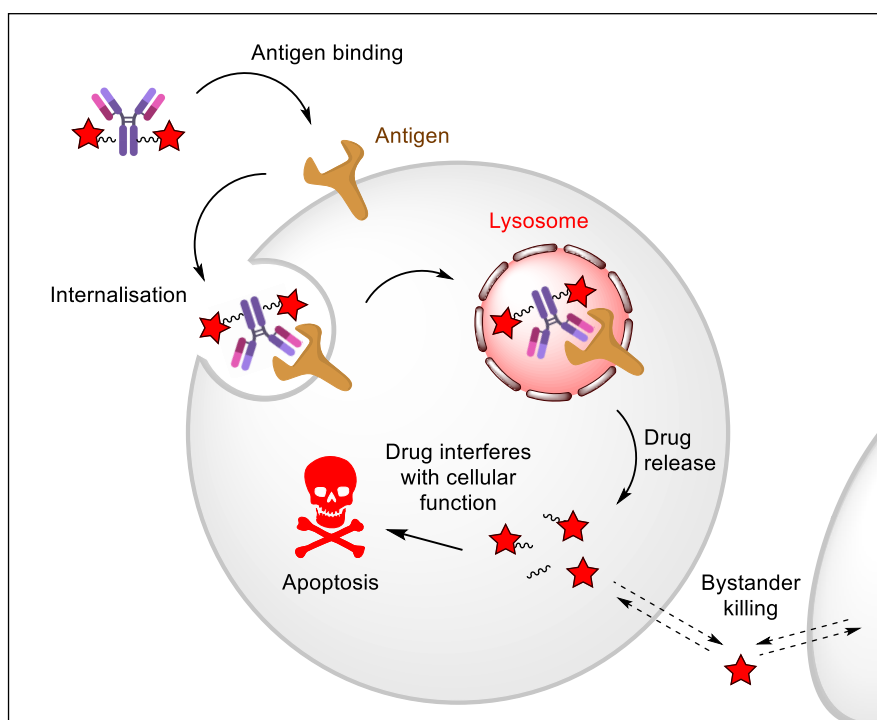


Figure 4: Typical mechanism of ADC internalisation and drug release.

In order to create a successful ADC, all three components – antibody, linker and warhead – need to be carefully chosen and optimised. Thus, despite the first ADC being reported as early as 1958,⁴³ ADCs did not reach the market until 2000 when gemtuzumab ozogamicin (Mylotarg®) gained FDA approval for the treatment of acute myeloid leukaemia (AML).^{44,45} Yet even then ADCs struggled to gain a foothold in the clinic, and Mylotarg® was voluntarily removed from the market in 2010 due to post-approval studies showing that the drug

provided no clinical benefit over standard chemotherapy and in some cases led to acute adverse effects. Mylotarg® was eventually reintroduced to the market in 2017 with lower dosing strategies, aimed at a more specific patient population.⁴⁶

While Mylotarg®'s initial removal from the market was a disappointment, it also provided valuable lessons to the community which in turn sped up the pace of ADC development. Thus, in 2011 brentuximab vedotin (Adcetris®) was approved for the treatment of relapsed or refractory Hodgkin's lymphoma and anaplastic large cell lymphoma.^{47,48} In 2013, trastuzumab emtansine (T-DM1, Kadcyla®) was approved for the treatment of HER2-positive metastatic breast cancer.^{49–51} Apart from the re-introduction of Mylotarg®, 2017 also saw the approval of inotuzumab ozogamicin (Besponsa®) to treat acute lymphoblastic leukaemia (ALL).^{52–54} In 2019, ADCs truly found their stride as three new constructs were approved within a single year: polatuzumab vedotin (Polivy®) for the treatment of relapsed or refractory diffuse large B-cell lymphoma (DLBCL), enfortumab vedotin (Padcev®) for the treatment of metastatic or locally advanced urothelial cancer, and trastuzumab deruxtecan (Enhertu®) for the treatment of HER2-positive metastatic breast cancer.^{55–58} Following on from there, 2020 witnessed the approval of sacituzumab govitecan (Trodelvy®) for the treatment of triple-negative breast cancer and belantamab mafodotin (Blenrep®) for the treatment of multiple myeloma.^{59–62} The most recent ADC to receive FDA approval was loncastuximab tesirine (Zynlonta®), which was approved for the treatment of relapsed or refractory DLBCL in 2021.⁶³ Overall, there are currently ten ADCs on the market and over 80 others in clinical/preclinical trials (Figure 5).²⁹

Despite the apparent popularity of ADCs in recent years, there remains room for improvement. For example, all clinically approved ADCs (with the exception of Enhertu® and Trodelvy®) are heterogeneous in terms of the number of payload molecules attached to each antibody and the attachment location on the antibody and thus consist of different ADC populations with differing pharmacokinetic profiles (*vide infra*).⁴⁰ Furthermore, many ADCs suffer from premature payload release due to the use of semi-stable linkers.⁶⁴ These factors complicate pharmacokinetic assessment and increase the risk of adverse effects in response to treatment. Thus, there remains an unmet need for optimisation of the three ADC components – antibodies, linkers, and payloads – and the synthetic methods used to combine them.

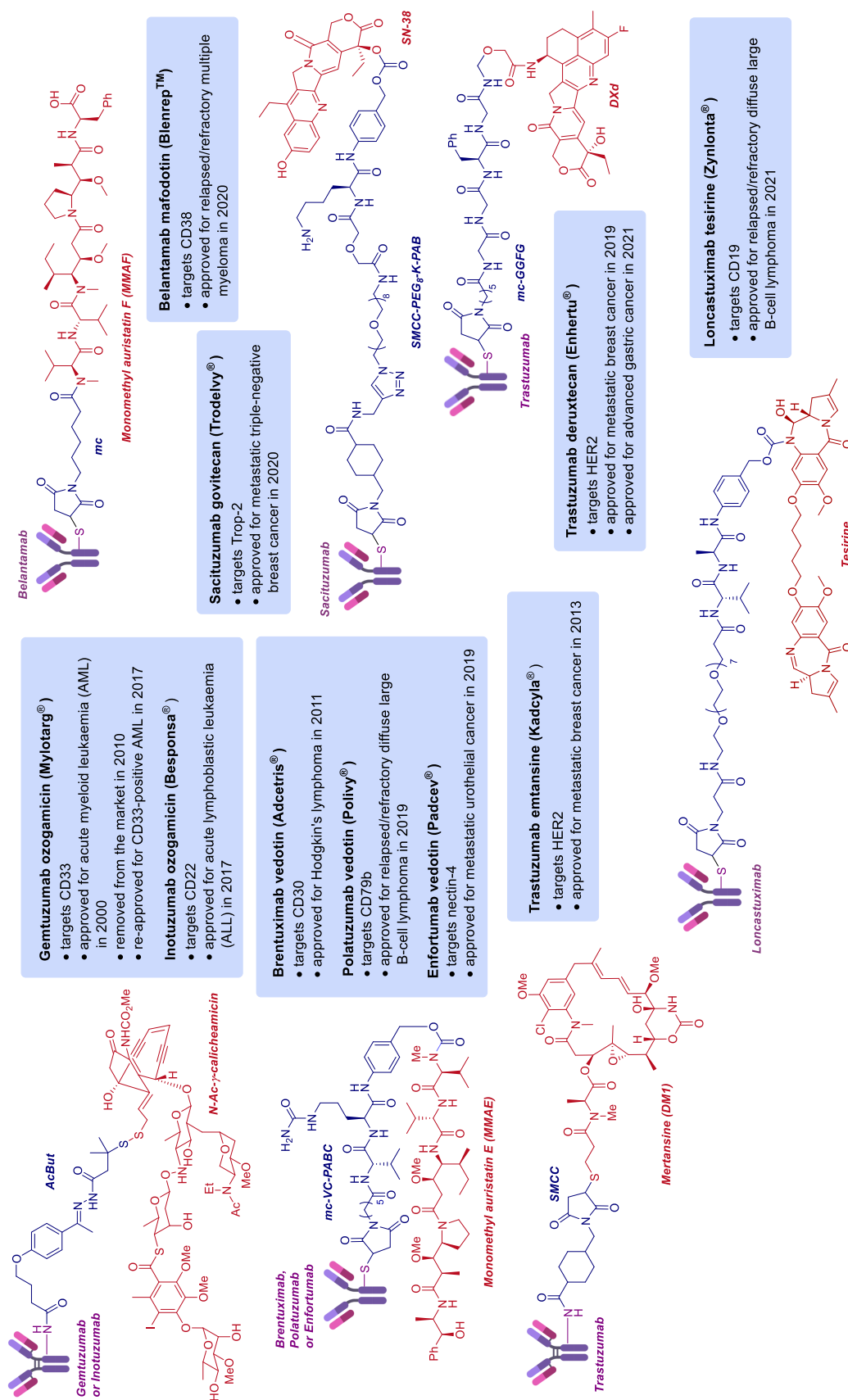


Figure 5: Structures of FDA approved ADCs, with linkers shown in blue and payloads shown in red.

1.3 The Antibody

All ADCs in ongoing clinical and preclinical development are based on antibodies of the immunoglobulin G (IgG) isotype, which is the most abundant type of antibody in the human body.⁶⁵ All IgG antibodies are composed of two heavy chains (~50 kDa) and two light chains (~25 kDa). Each light chain is subdivided into a variable domain (V_L) and a constant domain (C_L). Similarly, each heavy chain is subdivided into a variable domain (V_H) and three constant domains (C_{H1} , C_{H2} and C_{H3}). The light chains and the V_H and C_{H1} domains of the heavy chains form the fragment antigen-binding (Fab) regions, which contain the antigen binding sites.⁶⁶ The C_{H2} and C_{H3} domains of the heavy chains form the fragment crystallisable (Fc) region which ensures recognition of the antibody by the immune system (Figure).^{65,67} The C_{H2} domains are glycosylated at N297. This glycosylation pattern is heterogeneous across different IgGs, and some antibodies can exist as a mixture of glycoforms.⁶⁸ The antibody's structure is maintained by a combination of non-covalent interactions and disulfide bonds (intrachain and interchain).

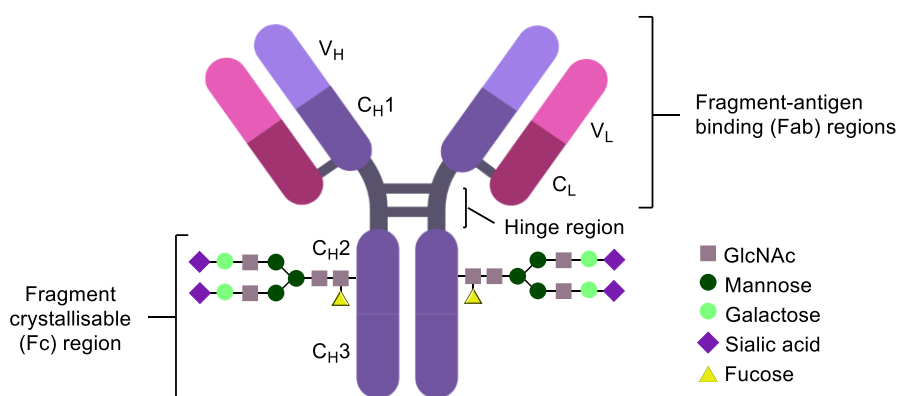
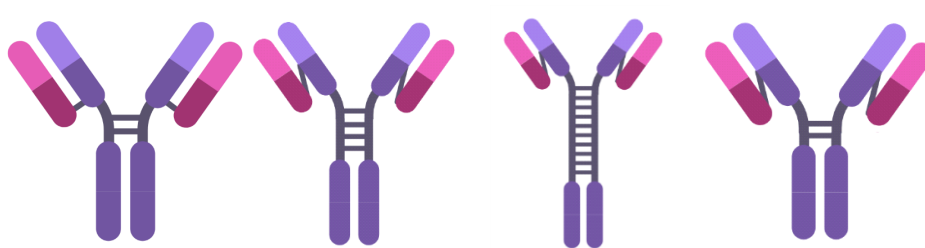


Figure 6: General structure of an IgG1 antibody with four interchain disulfide bonds.

IgGs can be divided into four subclasses: IgG1, IgG2, IgG3 and IgG4. The four subclasses have approximately 90% sequence homology, but vary in terms of serum stability, number of interchain disulfide bonds, and their ability to activate the immune system *via* ADCC or the complement pathway (Figure 7).⁶⁷ Traditionally, IgG1 has been utilised the most in ADC development, due to its favourable balance of long serum half-life and moderate to strong immune activation; however, IgG4 has also been utilised in cases where less immune activation is desirable.⁶⁹ Both IgG1 and IgG4 contain a total of 16 disulfide bonds per antibody. Of these 12 are intrachain bonds and 4 are interchain bonds. While interchain bonds are

highly solvent exposed and may easily be reduced and/or modified by chemical methods, the intrachain bonds are buried within the globular fold of the protein and therefore unreactive to chemical modification unless harsh denaturing conditions are applied.⁷⁰ From a structural perspective, the main difference between IgG1 and IgG4 is that native IgG4 molecules possess the ability to undergo dynamic Fab arm exchange which may result in the formation of hybrid antibodies *in vivo* and lead to undesired off-target effects. However, this can be prevented through a S228P mutation in the hinge region of the heavy chain.^{71,72} All clinically approved ADCs are based on IgG1 antibodies, except Mylotarg[®] and Besponsa[®] which are based on IgG4 antibodies with S228P mutations.



	IgG1	IgG2	IgG3	IgG4
Relative natural abundance	60%	32%	4%	4%
# of interchain disulfide bonds	4	6	13	4 ^a
Serum half-life	~21 days	~21 days	~7 days	~21 days
Immune activation				
via C1q binding	++	+	+++	-
via FcγR binding	+++	+	++++	++
Use in clinically-approved ADCs	Kadcyla [®] , Enhertu [®] , Trodelvy [®] , Blenrep [™] , Adcetris [®] , Polivy [®] , Padcev [®] , Zynlonta [®]		-	Mylotarg [®] ^b , Besponsa [®] ^b

Figure 7: Overview of IgG subclasses for potential use in ADCs; ^aHinge region disulfides are labile, enabling spontaneous Fab arm exchange with other IgG4 antibodies *in vivo*; ^bFab arm exchange is prevented through S228P mutation in the hinge region.

An antibody suitable for ADC development should target an antigen which is either exclusively expressed by cancer cells or expressed at much higher levels relative to those of non-cancerous cells, thus minimising cross-reactivity with healthy tissues.⁷³ Additionally, the mAb should be human-derived or humanised, as such antibodies carry a lower immunogenicity risk than animal-derived antibodies.⁷⁴ Furthermore, the target antigen should be expressed in

large numbers (at least 10,000 – 1,000,000 antigens per cell, depending on cancer type) and internalise efficiently upon antibody binding.^{73,75} The potency of an ADC is closely related to the expression level, internalisation rate, and cellular trafficking pathway of its target antigen, thus these factors should be considered carefully in the design process.^{76,77}

1.4 The Payload

The payload is responsible for killing the target cells. Early ADC research utilised existing chemotherapy agents such as methotrexate or doxorubicin as payloads;⁷⁸ however, these cytotoxins were found to have insufficient potency when used as part of an ADC.⁷⁹ This is predominantly because the number of ADC molecules that can enter each target cell is limited by the density of target antigens on the cell surface and thus the rate of internalisation of the antibody-antigen complex is much lower than the rate of internalisation of simple small molecule chemotherapy drugs.⁶⁴ Therefore, research is now focusing on the use of more potent payloads, many of which were specifically designed for use in ADCs (Figure 8).

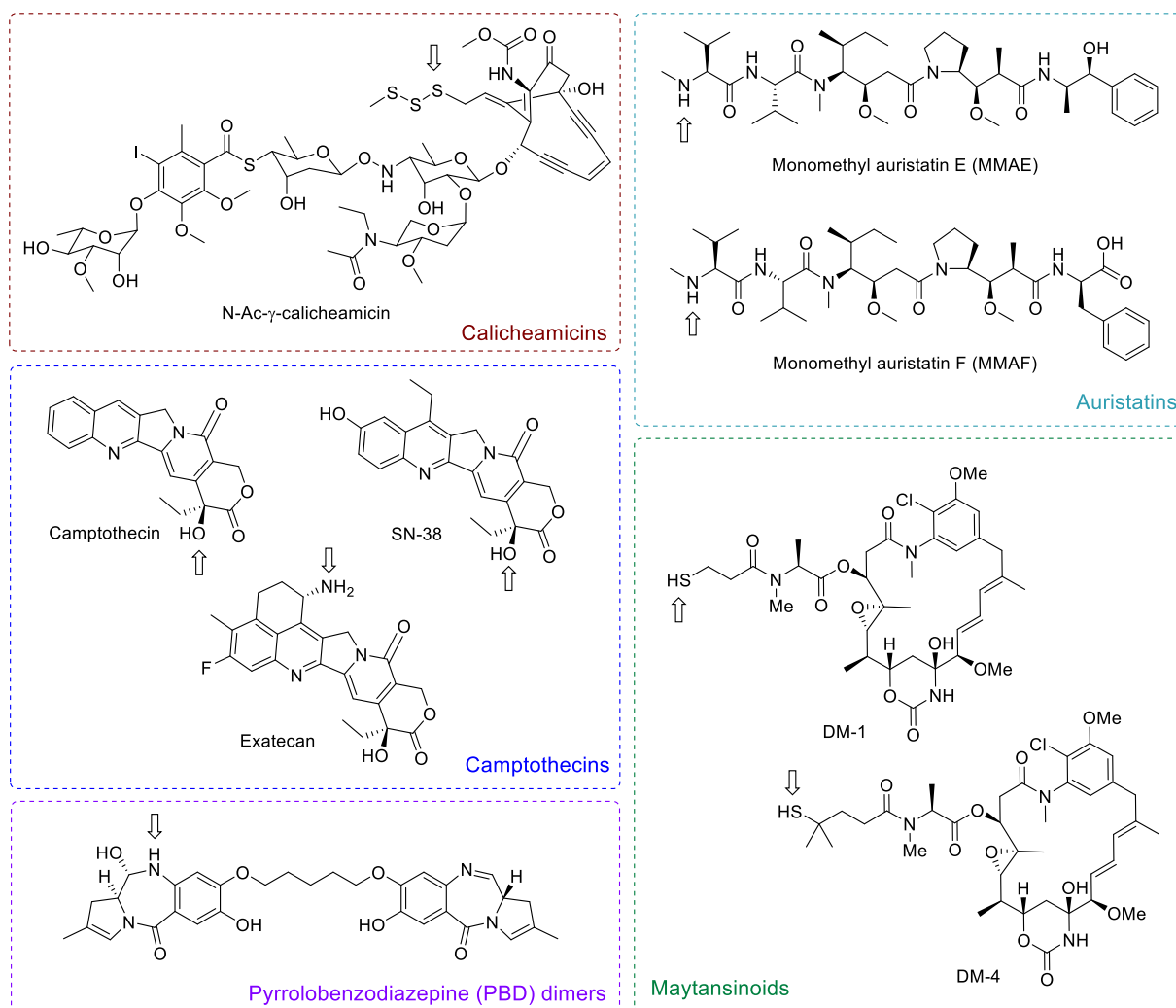


Figure 8: Examples of widely used ADC payloads include DNA targeting agents such as calicheamicins and PBD dimers, tubulin inhibitors such as auristatins and maytansinoids, and topoisomerase inhibitors such as camptothecins. Arrows indicate the typical site of linker attachment.

Most ADC payloads are analogues of natural products. For example, *N*-Ac- γ -calicheamicin – the active payload of Mylotarg® and Besponsa® – is a derivative of the natural product calicheamicin γ first isolated from the bacterial species *Micromonospora echinospora*.⁸⁰ *N*-Ac- γ -calicheamicin is a powerful cytotoxin which induces DNA double-strand breaks by binding to the DNA minor groove and undergoing a Bergman cyclisation which generates a highly reactive diradical species that splits the DNA.^{80,81}

Other commonly employed payload classes are the auristatins and the maytansinoids which induce cell death *via* tubulin inhibition. Five of the ten approved ADCs employ one of these two payload classes (Adcetris®, Kadcyla®, Polivy®, Padcev®, Blenrep®).

Among the more recently introduced payloads are the topoisomerase I inhibitor camptothecin and its synthetic analogues SN-38, exatecan and DXd.⁸¹ In living cells, topoisomerase I relaxes and untangles the DNA in preparation for DNA replication. Inhibition of this enzyme by camptothecins causes arrest of the replication fork and apoptosis.^{82,83} SN-38 and DXd form part of the approved ADCs Trodelvy® and Enhertu®.

The most recently introduced payload class are the pyrrolobenzodiazepine (PBD) dimers. PBD dimers are highly potent DNA damaging agents with the ability to form both intra- and interchain cross-links in the minor groove of the DNA.^{84,85} The PBD dimer tesirine is the payload component of Zynlonta®.

A number of other ADC warheads are currently being evaluated in clinical trials. Among them are DNA alkylating agents such as duocarmycins, antimitotic drugs such as tubulysins, and RNA polymerase inhibitors such as α -amanitin.^{39,86–88}

Most warheads are relatively hydrophobic in nature. This means that the number of payloads attached to each antibody needs to be chosen carefully. While ADCs with a high drug-to-antibody ratio (DAR) can be expected to be more potent than those with fewer payloads attached, the increase in hydrophobicity makes them more prone to aggregation and rapid clearance.⁸⁹ The optimal DAR depends on the types of linker and warhead used. For example, for maytansinoids and auristatins the ideal DAR is considered to be in the range of 3-4, whereas PBD dimers perform optimally at a DAR of 1-2.^{90,91}

1.5 The Linker

The ADC linker is responsible for connecting the cytotoxic warhead to the mAb. To achieve this, the linker reagent must be a bifunctional molecule with orthogonal functional groups to allow chemoselective attachment to the antibody and the payload. The chemical transformations used for this purpose should be highly efficient and reproducible, to allow large scale production with minimal batch-to-batch variability.⁹² Furthermore, it is crucial that the linkages resulting from these reactions are stable in circulation for several days as decomposition of the conjugate could cause premature payload release and systemic toxicity. At the same time, a linker should incorporate an efficient mechanism for releasing the payload upon internalisation of the ADC into the target cell. It is crucial that the linker enables traceless release of an unmodified warhead or that the chosen payload is not inhibited by the

attached linker. Aside from these absolute requirements, the linker can also be used to modulate the physical properties of the ADC. For example, many linkers include polyethylene glycol (PEG) spacers as a means of enhancing solubility.

1.5.1 Release mechanisms

ADC linkers can be categorised in a number of different ways. One such way is the classification of linkers as 'cleavable' or 'non-cleavable' according to their mechanism of payload release.

1.5.1.1 Cleavable linkers

Cleavable linkers contain inbuilt release mechanisms which effect controlled payload release at the site of the target cell in response to specific intracellular stimuli. Depending on the nature of these stimuli, cleavable linkers can be further subcategorised as 'chemically cleavable' or 'enzyme-cleavable'.

Chemically cleavable linkers were the first type of cleavable linker to be employed in the clinic. Among these are acid-labile linkers such as hydrazones and carbonates which exploit the acidic environment of the lysosome (pH 4.5-5.0) to release the free payload *via* hydrolysis during cellular trafficking. The linkers of Mylotarg®, Besponsa® and Trodelvy® contain such acid-cleavable motifs (Figure 9).^{41,93}

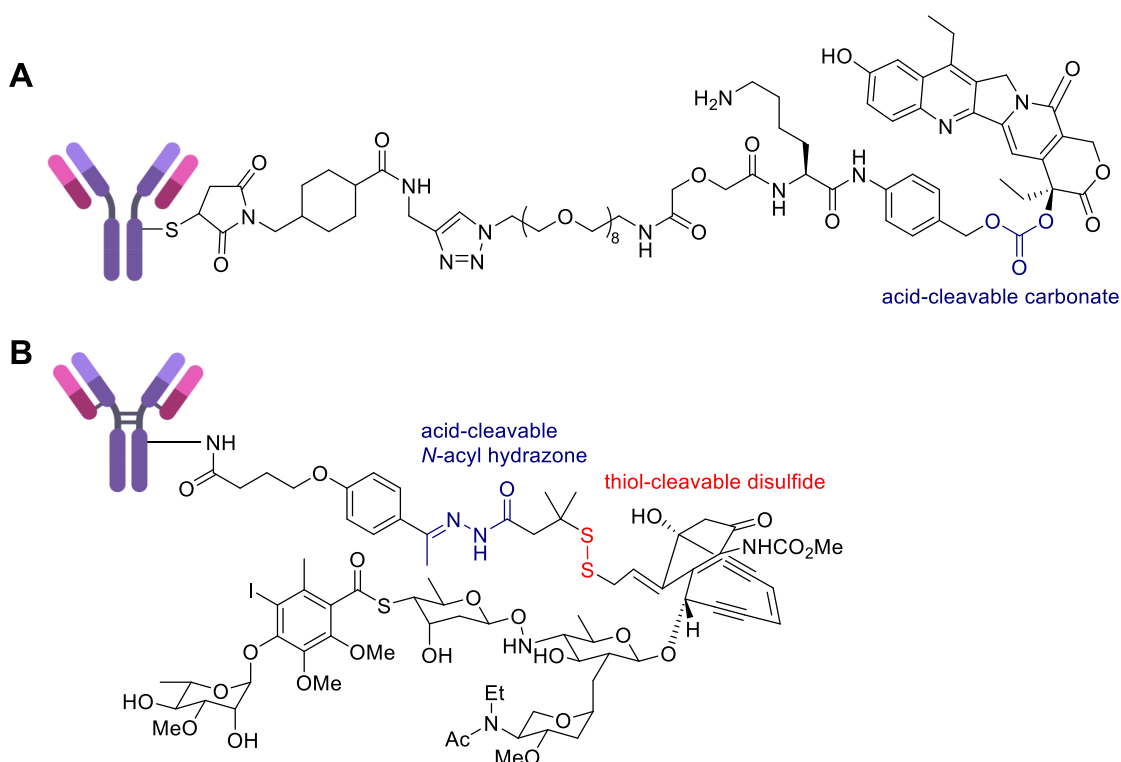


Figure 9: Examples of ADCs containing chemically cleavable linkers. (A) Structure of Trodelvy® with acid-cleavable carbonate shown in blue. (B) Structure of Mylotarg®/Besponsa® with acid-cleavable hydrazone shown in blue and thiol-cleavable disulfide shown in red.

Reducible disulfides are another type of chemically cleavable linkage. The cytoplasm contains high concentrations (1-10 mM) of free thiols such as glutathione (GSH), a small cysteine-containing tripeptide capable of disulfide reduction. In contrast, blood plasma contains thiols in much lower concentrations, and its dominant thiol-containing molecule – human serum albumin (HSA) – is fairly unreactive due to the buried position of its cysteine residue.⁹⁴ This difference allows for the controlled thiol-mediated cleavage of disulfide-containing linkers in the intracellular compartment. While calicheamicin-based ADCs Mylotarg® and Besponsa® both contain reducible disulfides, this type of cleavable group has primarily been employed in combination with maytansinoid payloads. Several studies have been dedicated to the optimisation of steric protection around the disulfide to further increase selectivity for intracellular cleavage.^{75,95,96} In spite of these efforts, most chemically cleavable linkers tend to suffer from poor *in vivo* stability. Thus, most ADCs in clinical trials today rely on enzyme-cleavable linkers.

The most frequently used enzyme-cleavable linkers are those containing valine-citrulline (Val-Cit) or valine-alanine (Val-Ala) dipeptide motifs which are cleaved by the protease cathepsin B

in the lysosome. These are often employed in combination with the self-immolative *p*-aminobenzyloxycarbonyl (PABC) group. PABC undergoes spontaneous 1,6-elimination upon enzymatic cleavage, releasing the free drug along with CO₂ and quinone methide (Figure 10).^{97,98} Adcetris®, Polivy®, Padcev® and Zynlonta® all contain Val-Ala/Cit-PABC motifs.

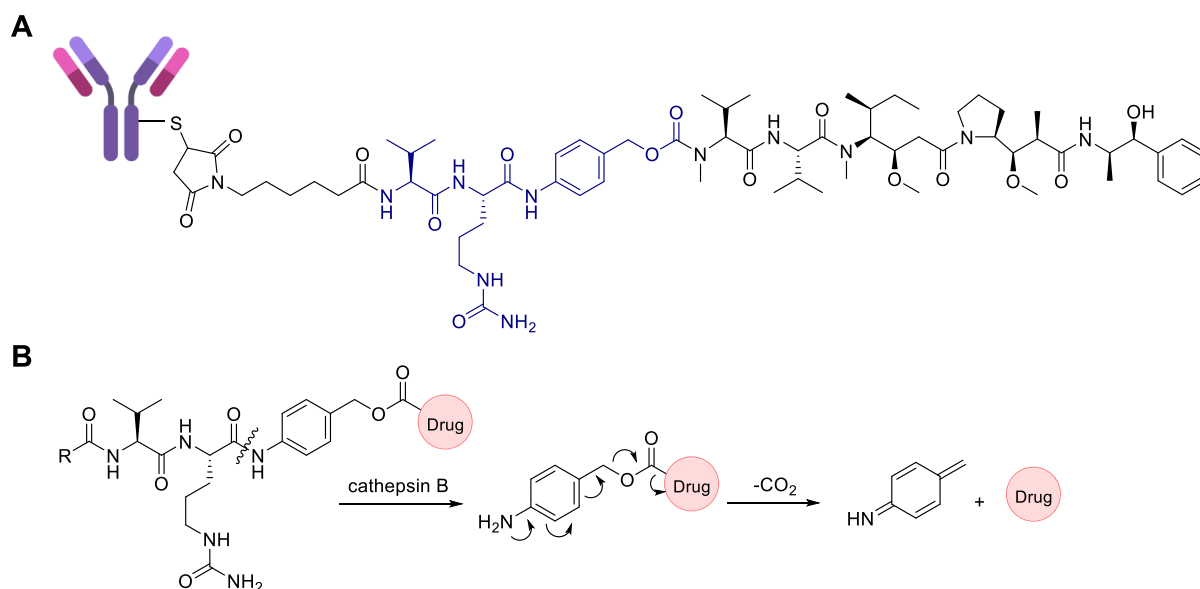


Figure 10: (A) Structure of Adcetris®/Padcev®/Polivy® with enzyme-cleavable Val-Cit-PABC motif shown in blue. (B) Cleavage mechanism of Val-Cit-PABC in response to cathepsin enzymes.

Alternative methods of enzymatic release may utilise β -galactoside motifs which are cleaved by β -galactosidase enzymes, or pyrophosphate diesters which are sequentially cleaved by pyrophosphatases and acid phosphatases.^{99,100} Additionally, Bargh *et al.* of the Spring group have recently developed arylsulfate-containing ADC linkers which have been shown to cleave efficiently in the presence of lysosomal arylsulfatases to facilitate payload release.¹⁰¹ It is also possible to combine multiple enzyme-cleavable motifs in a single linker as has been exemplified by the Spring group and others.^{102,103}

1.5.1.2 Non-cleavable linkers

Non-cleavable linkers lack specific release mechanisms. Instead, the drug is released upon lysosomal degradation of the mAb into its constituent amino acids. This mechanism releases the payload with the linker and point-of-attachment amino acid appendage still attached (Figure 11). Whether these appendages influence the payload's cell-killing ability depends on the size and structure of the linker as well as the nature of the warhead. Studies have shown that it is possible to pair certain payloads – such as auristatins and PBD dimers – with non-

cleavable linkers without diminishing their cytotoxicity.^{104–106} However, in many other cases non-cleavable ADCs have been shown to exert reduced potency compared to their cleavable counterparts. In addition to this, non-cleavable ADCs may be more prone to resistance mechanisms compared to cleavable ADCs. This is because their cytotoxicity is critically dependent on antibody degradation which in turn is dependent on efficient lysosomal trafficking; therefore, genetic mutations resulting in altered expression of lysosomal transporters constitute a major mechanism of acquired resistance to non-cleavable ADCs.⁷⁷ Cleavable ADCs are less dependent on lysosomal trafficking and thus less affected by such mutations.

There are two well-established non-cleavable linkers: succinimidyl-4-(*N*-maleimidomethyl)cyclohexane-1-carboxylate (SMCC), which utilises antibody lysine residues for attachment, and maleimidocaproyl (mc), which enables attachment of the payload to cysteine residues. The approved ADCs Kadcyla® and Blenrep® make use of these linkers.

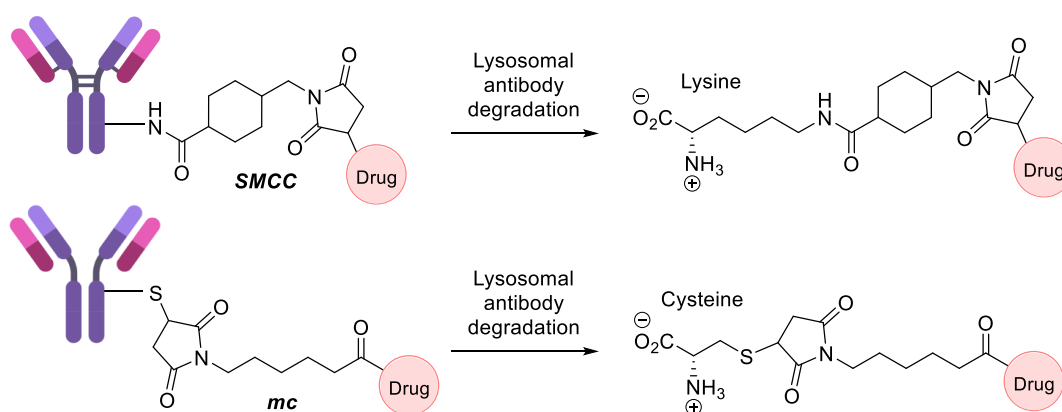


Figure 11: Non-cleavable linkers which lack a specific payload release mechanism result in a maintained attachment of the payload to the linker and the conjugating amino acid appendage after lysosomal degradation of the antibody.

1.5.2 Antibody modification

The main purpose of ADC linkers is to conjugate the payload to the antibody. The type of chemistry used for this purpose can greatly affect the performance of the ADC, as it determines the conjugation site and DAR, and impacts the overall stability of the construct. While attachment of the payload to the linker is usually a straightforward procedure, attachment of the linker and/or linker-payload to the antibody can pose a formidable challenge. Reactions used for protein modification must meet a strict set of requirements to ensure efficient and robust conjugation. As such, the reaction must work under aqueous

conditions, as high concentrations of organic co-solvents (>15%) lead to denaturation of proteins. For similar reasons, the reaction must occur at near physiological pH and temperatures (*ca.* pH 5-9, 37 °C). Furthermore, due to the low reaction concentrations employed in protein chemistry (low micromolar), the conjugation reagent must be highly reactive. At the same time, the reagent must be exceptionally chemoselective, due to the vast number of amino acid residues exposed on the antibody's surface.^{107,108} Adhering to this set of rules, a large toolbox of protein modification reactions have been developed to modify IgG antibodies *via* conjugation to natural amino acids, genetically incorporated unnatural amino acids (UAA) or antibody glycans.^{108,109} The following sections will provide an overview of these methods.

1.5.2.1 Stochastic conjugation methods

The side chains of natural amino acids contain a plethora of functional groups which may be targeted for bioconjugation. In this context, nucleophilic side chains such as the amino group of lysine and the thiol group of cysteine represent the most attractive targets, as they can be easily functionalised *via* reaction with complementary electrophilic groups on the linker. Indeed, all ten of the currently FDA-approved ADCs are generated *via* modification of lysine or cysteine residues on the surface of the antibody.

1.5.2.1.1 Lysine

Lysine residues can be easily functionalised using electrophilic *N*-hydroxysuccinimide (NHS) esters. As such, Mylotarg®, Besponsa® and Kadcyca® are all synthesised *via* reaction of surface-exposed lysines with NHS ester derivatives of their respective payloads.^{45,50,110} However, standard IgG antibodies contain approximately 80 lysine residues, more than half of which are accessible for chemical modification.¹¹¹ Due to this high abundance, synthesising an ADC with a precise DAR and control of the conjugation site *via* lysine modification is virtually impossible. This is best exemplified by the procedure used for the synthesis of Mylotarg® which generates a heterogeneous mixture of ADCs with >40 different conjugation sites and drug loadings ranging from 0 to 8, with almost 50% of antibodies not having any calicheamicin payload attached.¹¹² As already discussed in Chapter 1.4, the DAR affects the pharmacokinetic profile of an ADC in multiple ways. Similarly, the site of conjugation is critical to the pharmacology of an ADC for a variety of reasons. For instance, attachment of the

payload near the antigen binding region of the antibody may impede antigen recognition, with the potential to lower the targeting capability and thus the efficacy of the ADC. Furthermore, several studies have shown that the conjugation site can affect the aggregation potential of the ADC as well as the stability of the linkage between the linker and the antibody.^{113–116} Thus, stochastic conjugation methods such as lysine conjugation may yield a mixture of different ADC products with different pharmacological properties.

In addition to NHS esters, a number of other lysine-selective reagents have been developed (Figure 12).¹¹⁷ These include phenylisothiocyanates and β -lactams, which introduce the payload in a single step,^{118–120} as well as acid fluorides and sulfonyl acrylates, which initially introduce a payload attachment handle (such as an azide) that subsequently facilitates drug attachment in a second step.^{121,122} For example, acid fluorides have been used to introduce azides which can be further functionalised using strain-promoted azide-alkyne cycloaddition (SPAAC), and sulfonyl acrylates to install acrylate electrophiles which allow for further modification *via* aza-Michael addition.

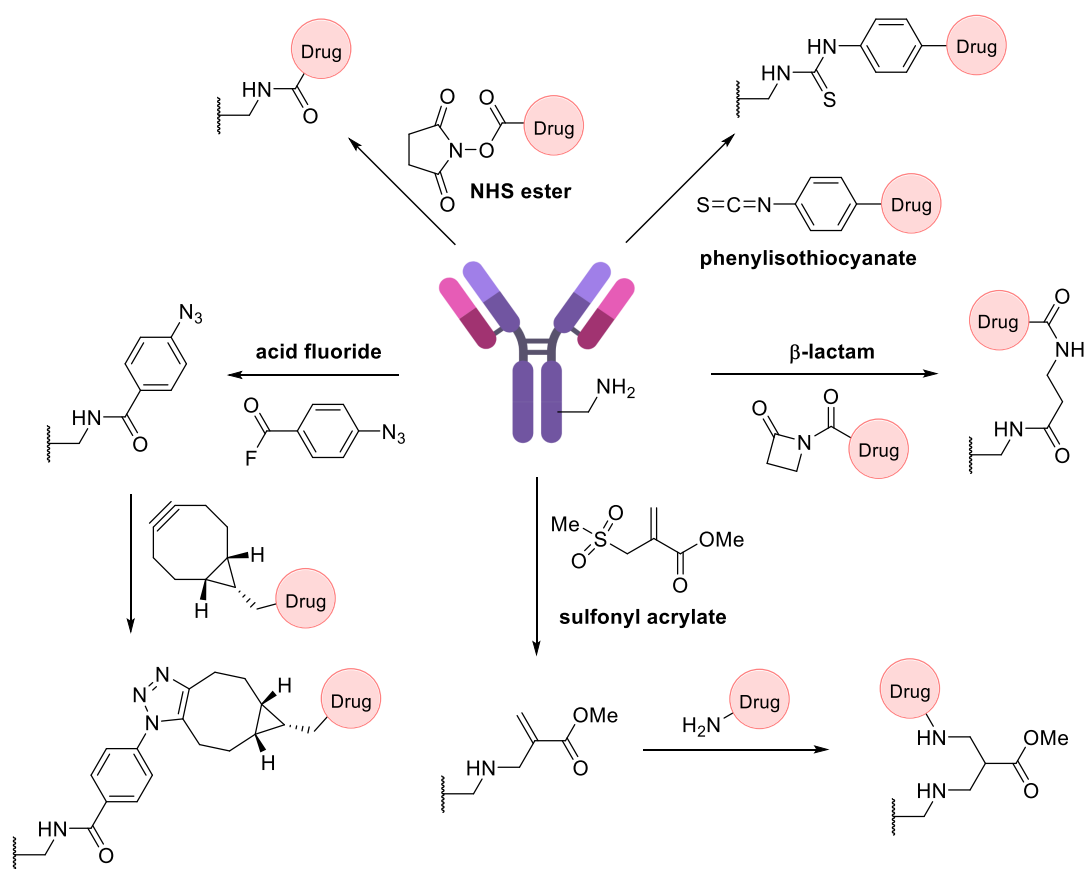


Figure 12: Methods for the modification of antibody lysine residues.

1.5.2.1.2 Cysteine

Cysteine residues are a particularly attractive target for protein bioconjugation due to their low natural abundance and the exceptionally high nucleophilicity of the thiolate side chain. All IgG1 cysteine residues are present in the form of disulfide bonds, of which four are interchain bonds and the rest are intrachain bonds.⁷⁰ The interchain disulfides can be reduced selectively, revealing up to eight reactive thiol groups. Subsequent reaction with soft electrophiles affords selective bioconjugation at the eight different sites. In some cases, including the approved ADCs Enhertu® and Trodelvy®, a resulting DAR 8 conjugate has been achieved with high homogeneity, efficacy, and safety.^{59,123} However, due to differences in toxicity and hydrophobicity, a DAR of 8 is not suitable for many linker-payloads. The generation of ADCs with average DARs of 2–4 can be achieved by a combination of partial disulfide reduction/reoxidation and controlled linker-payload stoichiometry.¹²⁴ However, this process is difficult to control, and the resulting ADCs are inescapably heterogeneous – although with less variability than that seen with stochastic lysine conjugation.^{125,126} Moreover, a recent study has shown that the loss of the interchain disulfides – the only covalent bonds connecting the four antibody chains – may be associated with reduced stability and biological activity of the antibody.¹²⁷

Cysteine conjugation is most commonly achieved *via* 1,4-conjugate addition to *N*-substituted maleimides. Indeed, all of the seven FDA-approved ADCs which are linked through cysteine residues are synthesised using maleimide conjugation. Maleimides are popular reagents due to their synthetic accessibility and fast reaction kinetics. However, the generated thiosuccinimide linkage is inherently unstable, and can undergo retro-Michael addition to release the deconjugated linker-payload (Figure 13).^{128,129} In circulation, the released linker-payload may subsequently react with thiol-containing biomolecules such as HSA or diffuse into nearby cells, thus causing untargeted systemic toxicity. The stability of maleimide bioconjugates can be greatly improved by post-conjugation hydrolysis of the succinimide ring to the maleamic acid. For regular *N*-alkyl maleimides, this process takes several days; however, the rate of hydrolysis can be increased significantly through alteration of the *N*-substituent. As such, a number of “self-hydrolysing” maleimides containing PEG or aryl substituents have been developed.^{130,131}

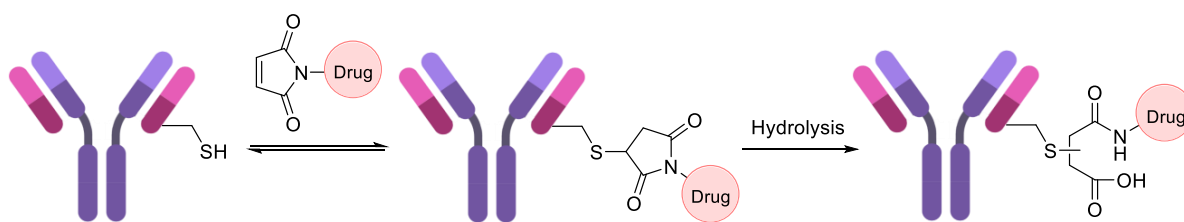


Figure 13: Cysteine conjugation using maleimides yields thiosuccinimide conjugates which may undergo retro-Michael addition to reform the original conjugation reagent or hydrolyse to form stable maleamic acid conjugates.

To forgo the need for post-conjugation hydrolysis, a number of alternative cysteine conjugation reagents, which result in the formation of inherently stable linkages, have been developed. These include vinylpyrimidines,¹³² ethynylphosphonamides,¹³³ 3-arylpropionitrile (APN),¹³⁴ palladium oxidative-addition complexes,¹³⁵ *N*-methylpyridinium salts,¹³⁶ α -halocarbonyls,¹²⁸ and others (Figure 14).

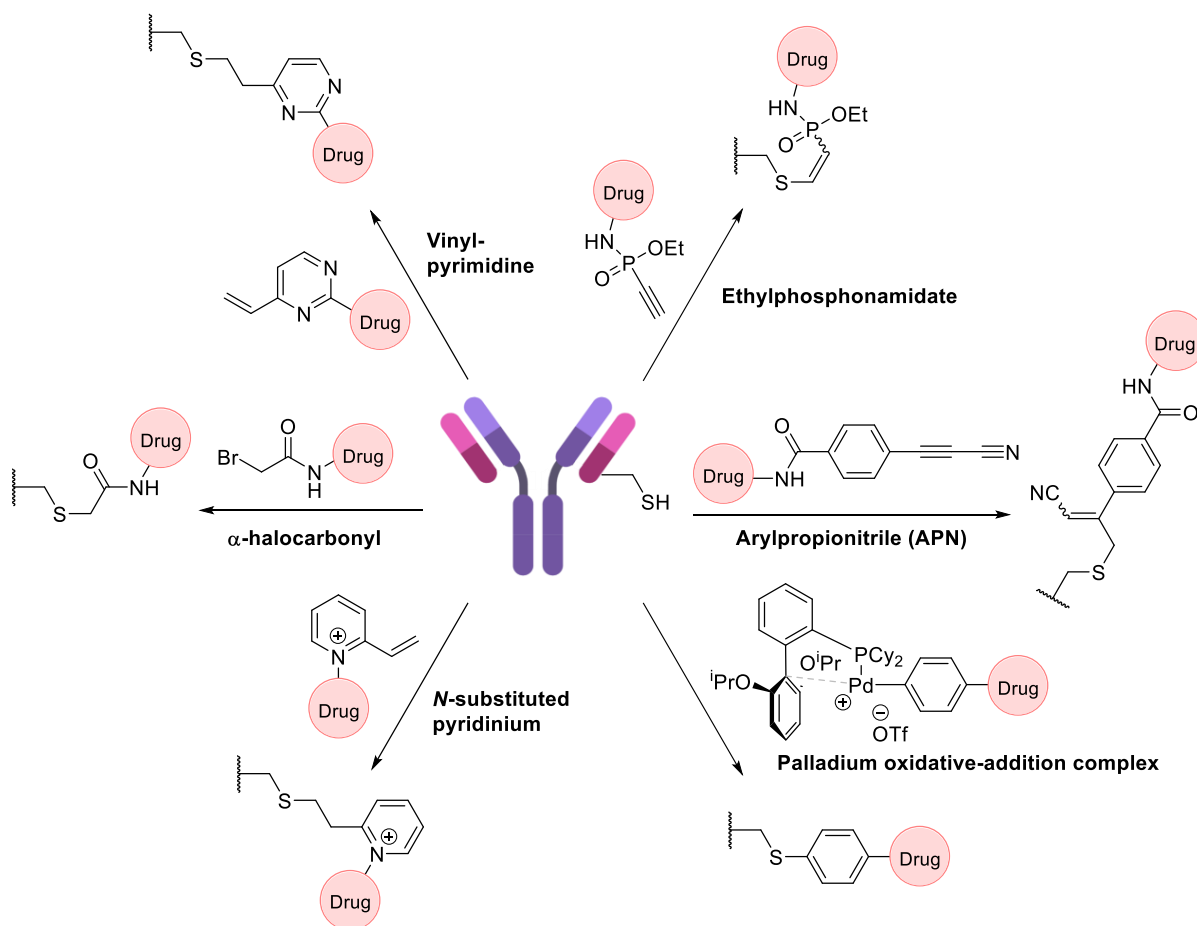


Figure 14: Alternative methods for the modification of antibody cysteine residues.

1.5.2.2 Site-selective conjugation methods

While all the FDA-approved ADCs and a large proportion of ADCs in clinical trials rely on stochastic cysteine/lysine conjugation – which yield heterogeneous conjugates with respect to DAR and conjugation site – advances in site-selective protein modification have enabled the development of a new generation of ADCs with improved homogeneity and increasingly predictable pharmacology. Methods employed for this purpose include the genetic incorporation of additional natural or unnatural amino acids, enzymatic modifications of amino acid sidechains and antibody glycans, and disulfide rebridging. The following sections will provide a brief overview of these methods.

1.5.2.2.1 Antibody engineering

The most widely employed method of achieving site-selective modification of antibodies is the alteration of the antibody primary sequence through genetic engineering to incorporate additional reactive amino acids. As such, genetic modification of the number of accessible cysteine residues has become a popular method to achieve site-selective conjugation. Junutula *et al.* pioneered the field by developing THIOMABs – a class of antibody in which selected serine, valine or alanine residues are mutated to cysteine *via* site-directed mutagenesis.^{113,137} ADCs generated *via* modification of these engineered cysteine residues have been shown to be more homogenous and display improved efficacy and toxicity profiles compared to heterogeneous ADCs made *via* modification of interchain disulfides.¹³⁷ However, the site of cysteine insertion is crucial in this context, as sub-optimal positioning may have detrimental effects on the biophysical properties of the ADC.^{113,114,138,139} Thus, careful optimisation of the insertion site is required for each ADC candidate.

THIOMABs have been used for the generation of ADCs with DARs of 2, 4, 6 or 10, including dual-functional ADCs containing both MMAE and PBD dimer payloads.^{140–142} THIOMAB ADCs with different DARs can be accessed in a number of ways. For example, a DAR 6 ADC was generated through the incorporation of six additional cysteine residues, each of which was reacted with a maleimide linker containing a single payload. In another example, a DAR 4 ADC was generated through incorporation of two cysteine residues, which were each reacted with a maleimide linker linked to two payload molecules.

Conceptually, THIOMABs should allow for the use of cysteine conjugation for payload attachment without any disturbance to the interchain disulfides. However, in practice, most THIOMABs are generated with the engineered cysteine residues capped as disulfides with cysteine or glutathione, and therefore a procedure for partial reduction using tris(2carboxyethyl)phosphine (TCEP) or dithiothreitol (DTT), purification, and selective re-oxidation of the interchain disulfide bonds is typically required to reveal the engineered thiols in their free form prior to bioconjugation (Figure 15).¹⁴³

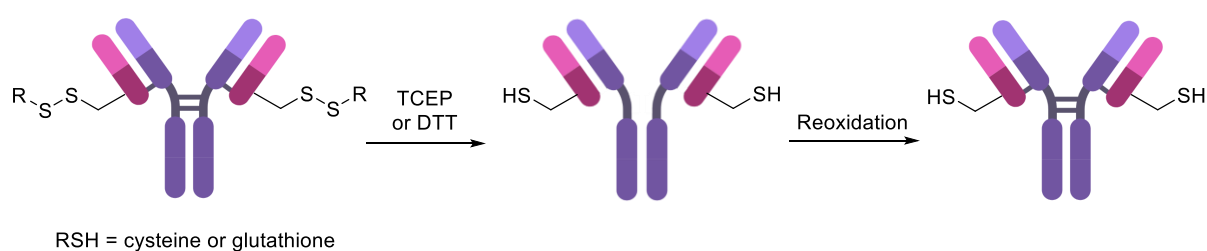


Figure 15: Uncapping of THIOMAB antibodies *via* non-selective disulfide reduction followed by reoxidation of interchain disulfide bonds.

An alternative to the installation of additional cysteine residues is the incorporation of UAAs with bioorthogonal reactivity. The process of introducing UAAs into proteins was pioneered by Noren *et al.* and involves the incorporation of a degenerate stop codon (TAG) representing the desired UAA into the gene encoding the protein of interest. An orthogonal amino acyl-tRNA synthetase (aaRS)-tRNA pair that recognises this codon is then used to install the UAA into the protein sequence during translation.^{144,145} Using this process, a variety of different UAAs have been incorporated into antibodies (Figure 16).¹⁴⁶ These include *p*-acetylphenylalanine, which can undergo oxime ligation with alkoxy-amine-containing payloads (Figure 16A), and cyclopentadiene-lysine, which reacts irreversibly with maleimide-functionalised payloads *via* Diels-Alder cycloaddition (Figure 16B).^{147–150} Furthermore, a variety of azide-containing UAAs have been used to enable payload attachment *via* copper-catalysed azide-alkyne cycloaddition (CuAAC) or SPAAC (Figure 16C).^{151,152} The resulting ADCs have been shown to display improved homogeneity and pharmacology compared to heterogeneous ADCs. However, as with THIOMABs, the position of the inserted amino acids needs to be carefully optimised on a case-by-case basis as inadequate placement may lead to protein aggregation and reduced activity.^{153,154}

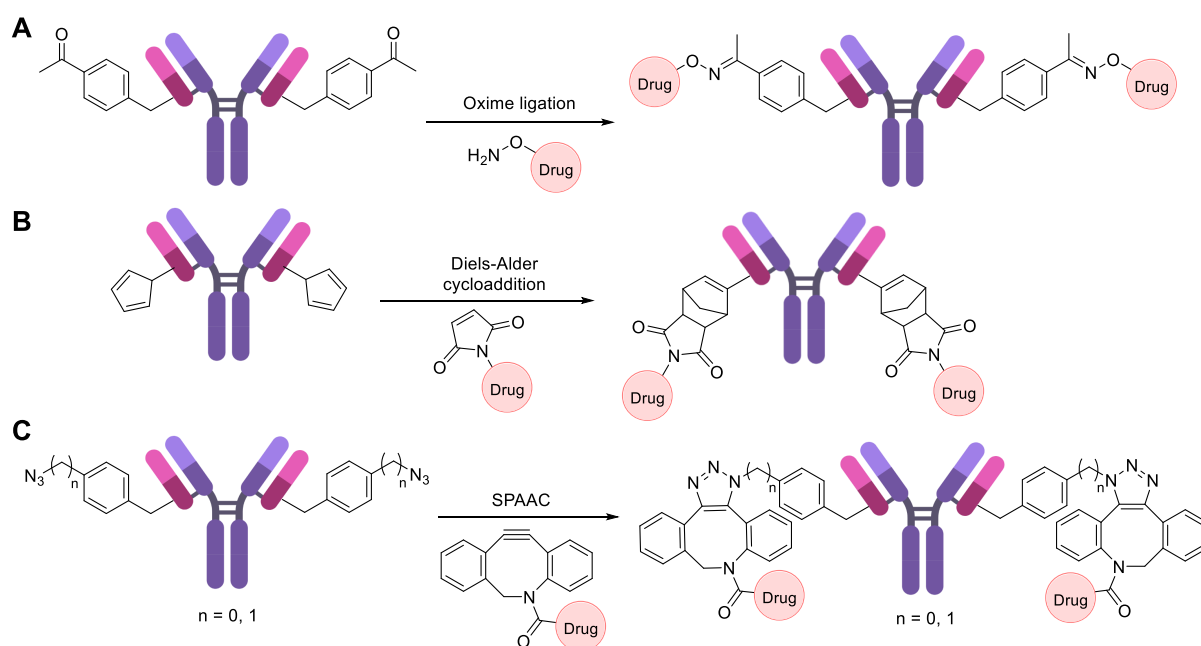


Figure 16: Selected methods for the generation of ADCs using UAAs *via* (A) oxime ligation, (B) Diels-Alder cycloaddition or (C) azide-alkyne cycloaddition.

1.5.2.2.2 Enzymatic methods

Enzymes have been frequently used to achieve site-selective antibody modification due to their high levels of substrate and reaction specificity. As such, enzymatic reactions can directly attach a payload to a specific amino acid sequence or introduce a reactive functionality on the antibody that can be further functionalised with the desired payload.

The most commonly used enzyme for this purpose is microbial transglutaminase (MTGase). MTGase is capable of catalysing the formation of an amide bond between a glutamine side chain and a broad variety of alkylamine substrates.¹⁵⁵ The conserved Q295 residue in the C_H2 domain of IgG1 has been found to be an excellent substrate for this reaction. However, in native IgG1 access to this site is blocked by the adjacent glycosylation at N297. Therefore, to enable modification of Q295, the glycan must first be removed. This can be done by treatment with the deglycosylation enzyme PNGase F, or *via* genetic engineering of a N297A mutation, which prevents biosynthetic antibody glycosylation. Aglycosylated antibodies produced in this way have been modified *via* MTGase-mediated reaction with alkylamine substrates containing one or two azide groups, thus enabling attachment of one or multiple payloads *via* SPAAC to yield ADCs with DARs of 2 or 4 (Figure 17).^{156,157} While the ADCs displayed high homogeneity and favourable efficacy compared to heterogeneous ADCs, it is yet unclear if the necessary deglycosylation has a significant impact on antibody pharmacokinetics. Studies

have shown that aglycosylated antibodies may be more prone to denaturation, aggregation and proteolytic degradation than their glycosylated counterparts.^{158,159} However, whether this variance in biophysical stability translates to a real difference in pharmacokinetic profiles in humans remains to be determined.¹⁶⁰

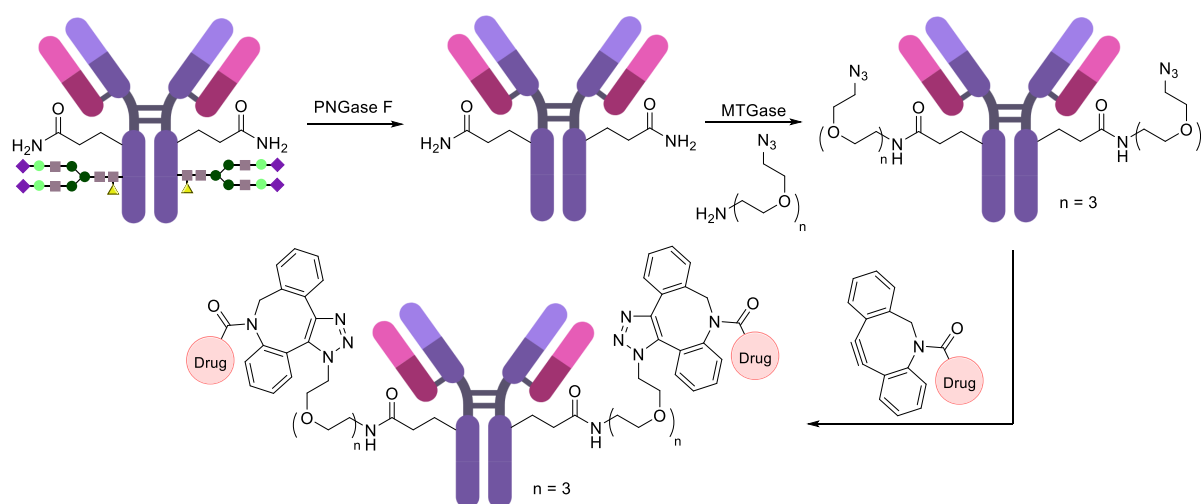


Figure 17: Synthesis of homogenous ADCs *via* MTGase-mediated transglutamination at Q295.

An alternative strategy to the modification of Q295 is to direct the site of MTG-mediated transglutamination *via* the insertion of a glutamine-containing recognition sequence ('Q-tag'). The first such sequences – the LLQG motif – was designed by Strop *et al.* and could be inserted at a range of different positions in the antibody structure to yield ADCs with DARs of 2, 4, 6 or 8 (Figure 18A).^{115,161,162} Similar to the other genetic engineering approaches discussed in Chapter 1.5.2.2.1, the site of insertion was shown to have a significant effect on conjugation efficiency and pharmacokinetics and thus required careful optimisation for each individual ADC candidate.^{115,163}

Recognition tags have been developed for a variety of different enzymes. For example, the CXPXR consensus sequence (X = any amino acid except proline) – also known as SMARTag® – can be genetically incorporated at the C-termini of an antibody to enable formylglycine-generating enzyme (FGE)-mediated oxidation of the inserted cysteine residues to formylglycine. Aldehyde modified antibodies generated in this way have been conjugated with hydrazine-functionalised payloads *via* hydrazine-*iso*-Pictet–Spengler (HIPS) ligation to yield homogenous DAR 2 ADCs (Figure 18B).^{164,165} Other enzymes for which recognition tags have been developed include prenyltransferase,¹⁶⁶ bacterial sortase,¹⁶⁷ and SpyLigase.¹⁶⁸

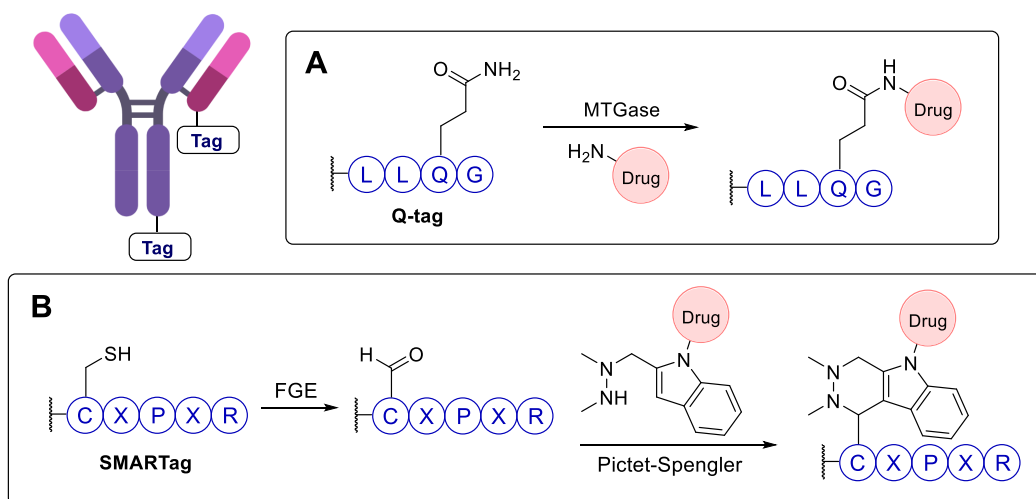


Figure 18: Examples of enzymatic bioconjugation methods using recognition tags. (A) MTGase-mediated modification of Q-tag recognition sequence; (B) FGE-mediated modification of SMARTag recognition sequence.

1.5.2.2.3 Disulfide rebridging

Disulfide rebridging involves the reduction of the four interchain disulfide bonds of an IgG1 followed by reaction with a cysteine-selective cross-linking reagent. This process enables the reconnection of the polypeptide chains while simultaneously installing drug molecules or bioorthogonal functionalities amenable to further modification. By covalently reconnecting the cysteine residues, a stabilising effect akin to that of the precursor disulfide bonds is maintained and a controlled loading of one linker molecule per disulfide can be achieved. Depending on the number of drug molecules attached to each linker, a DAR of 4, 8 or 16 can be attained in this way.¹⁶⁹ Since the conjugation utilises native cysteine residues in the antibody hinge region, no alteration of the genetic code or the glycosylation pattern is required. Furthermore, there is usually little need for case-by-case optimisation since the interchain disulfide bonds are highly conserved across all antibodies of the same isotype.⁶⁷

A variety of different disulfide rebridging groups have been developed (Figure 19).¹⁰⁸ Among the most commonly used are bissulfones,^{170–172} next-generation maleimides (NGMs),^{173–176} and pyridazinediones (PDs);^{177–181} however, in recent years numerous other reagents have emerged, including arylene dipropiolonitrile (ADPN),¹⁸² divinylheteroarenes (such as divinylpyrimidine [DVP] and divinyltriazine [DVT]),^{183–185} dibromomethyl heterocycles (C-Lock™),¹⁰⁶ diethynyl phosphinates,¹⁸⁶ and dichloroacetone.¹⁸⁷

Classical disulfide rebridging reagents react with two cysteine residues per linker molecule. As reduction of the interchain disulfides of a human IgG1 antibody yields eight reactive

cysteine residues, most standard reagents therefore have a scope of DAR values which is limited to multiples of four. However, such DAR values are not suitable for all payloads. Therefore, Lee *et al.* recently developed a bis-dibromopyridazinedione (bis-diBrPD) linker capable of reacting with four cysteine residues. The linker comprised a single alkyne, and thus enabled the synthesis of a DAR 2 ADC *via* post-conjugation CuAAC with azide-functionalised doxorubicin.¹⁸⁸ In a similar bid, Novartis utilised a 1,3-dichloroacetone linker to rebridge disulfides in an IgG1, and subsequently performed oxime ligation with a linker-payload containing two hydroxylamine groups to generate a DAR 2 ADC.¹⁸⁹ Finally, MedImmune/Spirogen have succeeded in generating a homogenous DAR 1 ADC *via* rebridging of an engineered Flexmab antibody – which contains only a single reducible disulfide – with a PBD dimer functionalised with two maleimide groups.¹⁹⁰

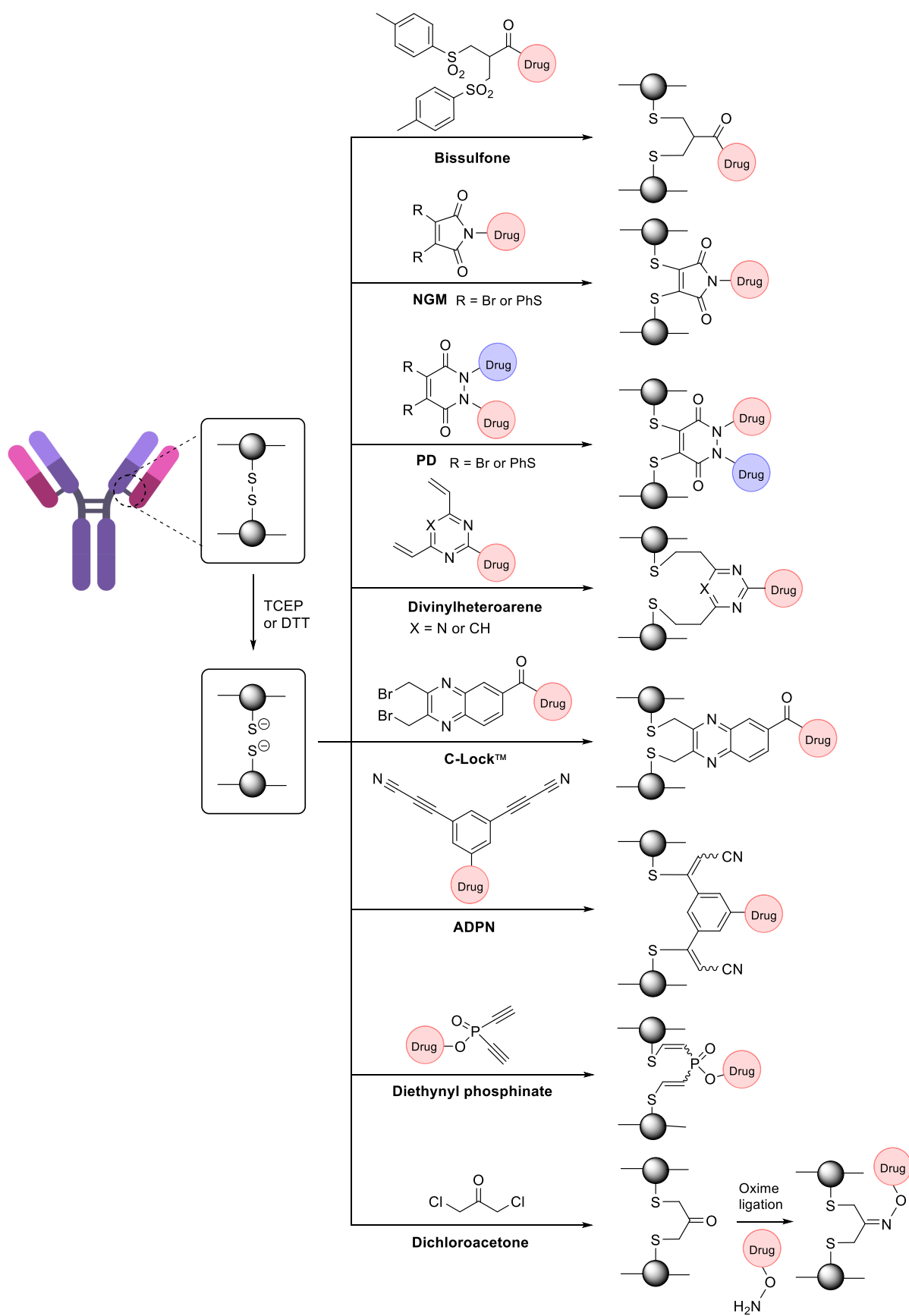


Figure 19: Disulfide rebridging linkers used for the synthesis of homogenous ADCs.

The main drawback of disulfide rebridging is the formation of half antibody species which originate from non-native intrachain rebridging of the hinge region disulfides (Figure 20). These half antibody species lack the native covalent link between the two heavy chains but remain held together by strong non-covalent interactions. Depending on reagent and reaction conditions, the half antibody content of rebridged ADCs can range from 5-95%.¹⁰⁸ A recent study suggests that half antibodies may suffer from reduced thermal stability and receptor binding affinities compared to unmodified or natively rebridged antibodies;¹²⁷ therefore, the development of methods to reduce half antibody formation is highly desirable. One such method was developed by Lee *et al.* who designed a dithioaryl(TCEP)pyridazinedione reagent, which could effectuate both disulfide reduction and rebridging, thus reducing the residence time of the reduced cysteine residues and their potential for scrambling.¹⁹¹ This “2-in-1” reagent led to reduced half-antibody formation in comparison to a two-step reduction-rebridging protocol. However, it was noted that the reagent suffered from low synthetic tractability and poor oxidative stability, hampering its wide-spread application.¹⁹² Therefore, the development of additional methods to reduce half antibody formation is warranted.

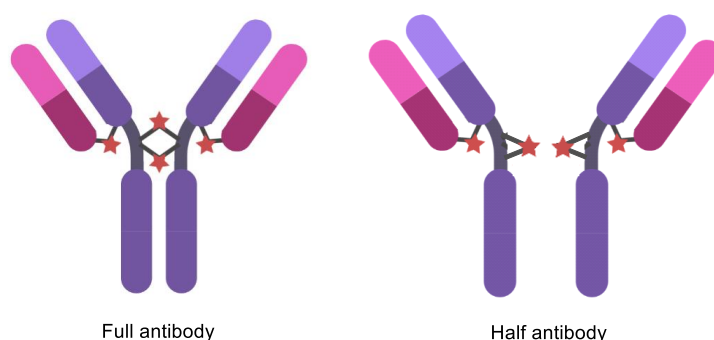


Figure 20: Classical disulfide rebridging results in a mixture of natively rebridged full antibody and non-natively rebridged half antibody species.

Chapter 2 – Project Overview and Aims

The primary aim of this project is the development of a novel method for the site-selective generation of homogenous ADCs. Ideally, this method should be applicable to any IgG1 without the need for genetic engineering or extensive case-by-case optimisation. Disulfide rebridging has emerged as an attractive conjugation method for the synthesis of ADCs which fulfils these criteria. However, this approach remains limited by its propensity to form fragmented antibody species ('half antibodies') during rebridging. Therefore, the development of a new method of rebridging which alleviates the problem of half antibody formation is desirable.

In addition to the issue of half antibody formation, disulfide rebridging – along with all current antibody modification methods – is limited in its ability to modulate the DAR while maintaining homogeneity. Even slight differences in DAR can have a profound effect on ADC pharmacology.^{90,170} Therefore, the investigation of ADCs with different DARs during the preclinical stages of the drug development process could expedite clinical efforts and reduce attrition. While many bioconjugation methods allow alteration of the number of drugs attached to each antibody, most of these methods generate a mixture of species with an *average* DAR, rather than a single ADC species with a *precise* DAR. DAR heterogeneity has been linked to reduced therapeutic performance, making the development of methods which yield ADCs with precise DARs highly desirable.^{137,156,175} Additionally, many contemporary antibody modification methods require alterations in the primary structure of the antibody to facilitate the generation of ADCs with different DARs – a process which usually requires extensive case-by-case optimisation, thus decelerating the drug development process. Lastly, all current methods – even those that succeed at generating a precise DAR without the need for genetic engineering – are limited to producing ADCs with even DAR values (2, 4, 6, etc.) as any modification made on one of the heavy/light chains is always mirrored on the other heavy/light chain. The development of methods that enable access to the full scope of integer DAR values ≥ 1 would be advantageous to allow for more thorough investigation into the effect of DAR on therapeutic performance. For these reasons, the primary objective of this project is the development of a new class of disulfide rebridging linkers which not only overcome the problem of half antibody formation, but enable the generation of ADCs with

precise DAR *via* a modular strategy to access conjugates with DARs from across a wider range of integer values than those that are currently attainable.

As outlined in Chapter 1.5.2, suitable linkers should be stable, reasonably soluble in aqueous media, and generate a linkage which is stable in human plasma for several days. Furthermore, the bioconjugation reaction should be fast, efficient, and proceed with high conversion without negatively affecting the structure or biological activity of the antibody. Lastly, functionalisation of the linker with a variety of payloads should be synthetically tractable and not significantly affect the activity of the attached payload.

The work described in this thesis can be divided into two distinct sections.

Chapter 3 describes investigations into the use of bis-divinylpyrimidine (BisDVP) linkers as a novel method for functional disulfide rebridging. Following a convergent synthetic strategy, a BisDVP linker was synthesised, and then reacted with a model antibody to evaluate its rebridging ability. Compared to a MonoDVP linker, the BisDVP was found to reduce half antibody formation, but not prevent it altogether.

In Chapter 4, the concept of combining multiple DVP motifs in a single linker molecule was further investigated by the design and synthesis of a series of TetraDVP linkers. Antibody bioconjugation studies showed the TetraDVP scaffold to be capable of rebridging all four interchain disulfides of an IgG1 and thus prevent half antibody formation completely. Furthermore, the synthesis of a set of TetraDVP linkers containing different numbers of alkyne functionalities enabled the generation of antibody conjugates with modular cargo loading *via* post-conjugation CuAAC with azide-functionalised fluorophores and cytotoxins. Finally, biological evaluation of the modified antibodies demonstrated their exquisite stability, binding affinity, and cell-selective cytotoxicity.

Chapter 3 – BisDVP Disulfide Rebridging Linkers

3.1 Introduction

Classical disulfide rebridging reagents typically react with two cysteine residues. As reduction of the interchain disulfides of a human IgG1 antibody yields eight reactive cysteine residues, most standard reagents modify antibodies in a 4:1 ratio, and therefore have a scope of DAR values which is limited to multiples of four. It was hypothesised that increasing the number of cysteine reactive groups on each linker would decrease the linker-to-antibody ratio and thus expand the scope of DAR values attainable. Furthermore, it was anticipated that this approach could reduce the risk of losing the covalent link between the two antibody heavy chains that is often observed with standard disulfide rebridging reagents.

Disulfide rebridging linkers which bridge multiple disulfide bonds have previously been explored by Lee *et al.* who designed a series of bis-dibromopyridazinedione (bis-diBrPD) linkers capable of connecting four cysteine residues within an IgG1 antibody.¹⁸⁸ These bis-diBrPD linkers enabled the generation of ADCs and antibody-fluorophore conjugates (AFCs) with encouragingly low levels of half antibody formation and drug loadings of two or four through the incorporation of either one or two alkyne handles per linker molecule (Figure 21A).

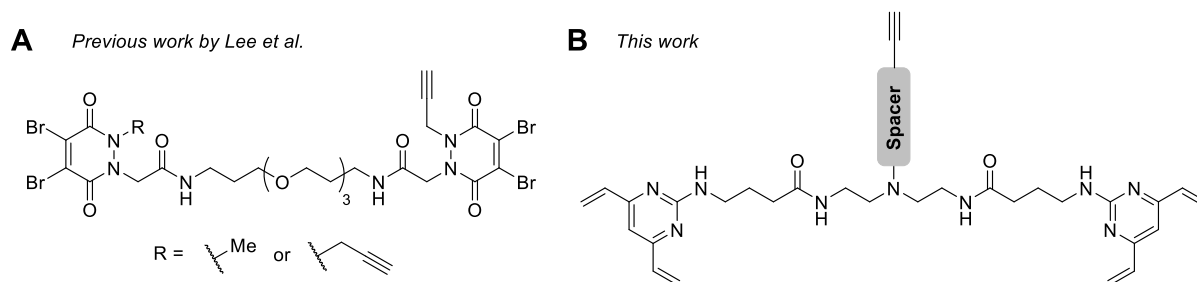
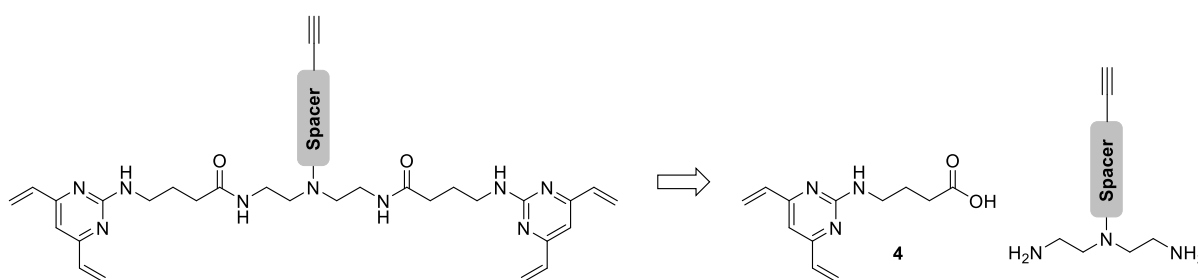


Figure 21: Structures of disulfide rebridging linkers for the rebridging of four cysteine residues. (A) Bis-diBrPD linkers developed by Lee *et al.*¹⁸⁸ (B) General structure of the proposed BisDVP linker.

Inspired by the positive results obtained by Lee *et al.*, the development of a Bis-divinylpyrimidine (BisDVP) linker was proposed to further investigate the potential of cysteine-reactive linkers that can react with four cysteine residues for the generation of homogenous ADCs (Figure 21B).

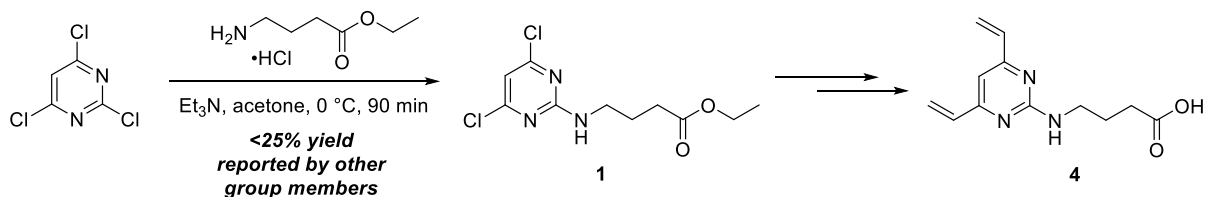
The design of the BisDVP linker was guided by several factors. Firstly, to enable the functional rebridging of four cysteine residues and subsequent payload attachment, the linker must contain two DVP motifs and one or multiple payload attachment handles. A payload attachment handle can be any functional group capable of undergoing a bioorthogonal reaction (e.g. CuAAC, SPAAC) to attach a payload molecule. For the initial BisDVP design, an alkyne group was chosen for payload attachment *via* CuAAC as alkyne attachment handles are known to have high stability and synthetic tractability. Secondly, the two DVP motifs must be separated by a sufficiently long spacer to reach across multiple disulfide bonds in an IgG1 antibody. Guided by structural data of IgG1 molecules for which crystal structures have been obtained,¹⁹³ it was estimated that the maximum distance between any two interchain disulfides is approximately 20 Å. This distance requirement was taken into consideration during linker design. Lastly, the linker should be synthetically tractable, which was deemed achievable through disconnection of the linker into a symmetrical core scaffold and a known DVP building block *via* amide coupling (Scheme 1).



Scheme 1: Retrosynthetic disconnection of the proposed BisDVP linker.

3.2 Divinylpyrimidine (DVP) Linker Synthesis

To synthesise the desired BisDVP linker, initial efforts focused on the synthesis of DVP building block **4**. The compound had previously been synthesised in the group *via* a three-step procedure involving a nucleophilic aromatic substitution (S_NAr) reaction on 2,4,6-trichloropyrimidine, followed by a Suzuki cross-coupling and ester hydrolysis (Scheme 2).¹⁰¹ However, the yield of the first step is known to be low yielding, with an average yield of <25% reported by previous group members. Since a sizable quantity of **4** was thought to be required for this project, it was desirable to optimise the synthetic procedure and improve the yield of the S_NAr reaction.

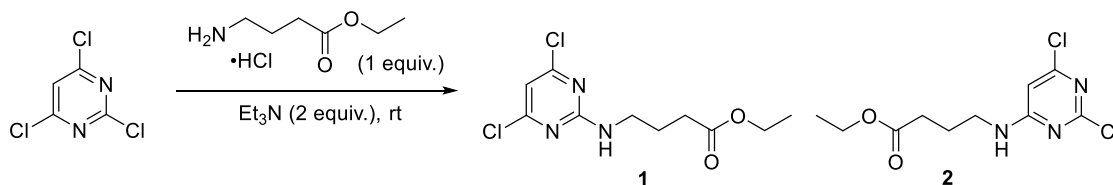


Scheme 2: Previously developed synthesis of DVP building block **4** via $\text{S}_{\text{N}}\text{Ar}$ reaction.

Synthesis of 2-aminopyrimidines from 2,4-dichloropyrimidine or 2,4,6-trichloropyrimidine is generally low yielding due to the preference of amine nucleophiles to substitute at the 4-carbon position of the substrate. Thus, the undesired 4-aminopyrimidine product is usually the major isomer. While slight modifications of reaction conditions are unlikely to overturn the regioselectivity of the reaction, it has been shown that changes in product ratios can be achieved with the aid of computational models.¹⁹⁴ It was thus proposed that the synthesis of 2-aminopyrimidine **1** may be optimised by a combination of traditional ‘one factor at a time’ optimisation and Design of Experiments (DoE).

To enable accurate reaction monitoring by nuclear magnetic resonance (NMR) spectroscopy, it was deemed important to first find a solvent system in which all reaction components are completely soluble. Accordingly, a solvent screen for the reaction of 2,4,6-trichloropyrimidine with ethyl 4-aminobutyrate hydrochloride was conducted. It was found that acetone – the solvent previously used by other group members for this reaction – resulted in poor dissolution of both the reaction mixture and the amine component on its own (Table 1, Entry 2). Other aprotic solvents such as chloroform and acetonitrile yielded similar results (Table 1, Entries 4-5). Dimethylsulfoxide (DMSO) provided good dissolution of the amine starting material; however, upon addition of base and trichloropyrimidine, precipitation was observed (Table 1, Entry 1). Finally, methanol resulted in complete dissolution of both the reaction mixture and the amine starting material on its own (Table 1, Entry 3). Therefore, methanol was selected as the solvent of choice for further reaction optimisation.

Table 1: Optimisation of the reaction of 2,4,6-trichloropyrimidine and ethyl 4-aminobutyrate hydrochloride by solvent screening.



Entry	Solvent	Solubility		
		Amine (200 mM)	Amine + base (200 mM)	Amine + base + pyrimidine (100 mM)
1	DMSO	good	moderate	moderate
2	Acetone	poor	poor	poor
3	MeOH	good	good	good
4	CHCl ₃	poor	poor	poor
5	MeCN	poor	poor	poor

Following the establishment of a suitable solvent system, optimisation of reagent stoichiometry and reaction temperature was carried out using DoE. DoE is a statistical technique for planning experiments and analysing the obtained information in a systematic manner. Given a set of experimental variables, DoE can be used to determine the minimum set of experiments that need to be conducted to ascertain 1) the impact of each variable on product formation and 2) how different variables interact with one another. Based on the data obtained from these experiments, a mathematical model is then created to aid the selection of the optimal reaction conditions.^{195,196} DoE is often considered superior to traditional 'one factor at a time' optimisation methods as the latter rarely consider interactions between different reaction variables.

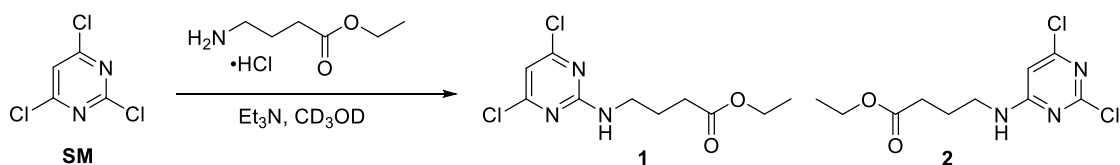
For the DoE optimisation of the S_NAr reaction of 2,4,6-trichloropyrimidine and ethyl 4-aminobutyrate hydrochloride, the following reaction parameters were chosen:

- Temperature range: 0-50 °C
- Amine equivalents: 1.0-2.0
- Base equivalents: 2.0-5.0

Given these parameters and using a 'Central Composite Face' design, which allows for determination of all variable interactions and squared terms, a set of 17 experiments was

designed and carried out (Table 2). The experiments were conducted in deuterated methanol to allow for reaction monitoring and determination of product ratios by ^1H NMR.

Table 2: Optimisation of reaction temperature and reagent stoichiometry for the reaction of 2,4,6-trichloropyrimidine and ethyl 4-aminobutyrate hydrochloride by DoE. Starting material and product ratios were determined by integration of ^1H NMR spectra of crude reaction mixtures.



Exp. #	Temp. / °C	Amine Equiv.	Base Equiv.	Composition / %		
				SM	1	2
1	50	1	2	15	35	50
2	0	1	2	50	25	25
3*	25	1.5	3.5	0	47	53
4	25	1	3.5	7	44	49
5	0	1.5	3.5	7	46	47
6*	25	1.5	3.5	0	47	53
7	0	1	5	14	43	43
8	50	1.5	3.5	0	44	56
9	0	2	5	1	48	51
10	0	2	2	27	36	37
11	25	2	3.5	0	47	53
12	50	1	5	0	45	55
13	50	2	2	15	42	43
14	25	1.5	5	0	47	53
15	50	2	5	0	49	51
16	25	1.5	2	33	31	36
17*	25	1.5	3.5	0	46	54

* Experiments 3, 6 and 17 are the centre points for the design and provide a measure of reproducibility.

Using the data displayed in Table 2, a model for the reaction was generated by Connor J. Taylor using MODDE software. This model was used to produce 4D contour plots displaying the disappearance of starting material and appearance of products in response to the three variables selected for investigation (Figure 22). These plots show that the three variables – temperature, amine equivalents and base equivalents – indeed interact with one another. For example, the effect of temperature on the formation of the undesired 4-substituted product isomer **2** is more pronounced if fewer equivalents of amine are used and vice versa. Generally, the formation of the desired isomer **1** appears to be optimal at medium to high amine

equivalents (1.5-2.0 equiv.) and medium base equivalents (3.5 equiv.), along with medium to high temperature (25-50 °C).

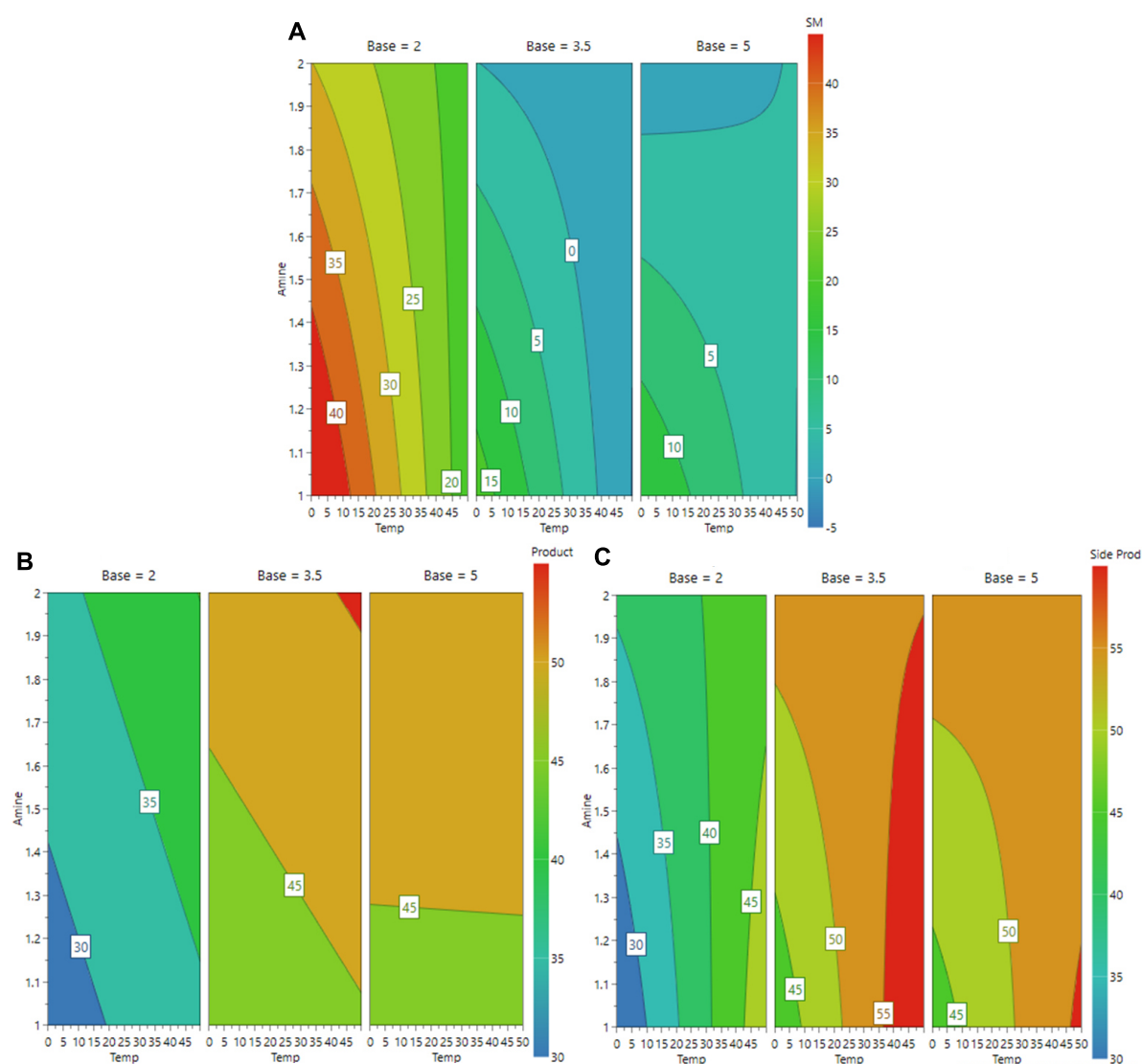
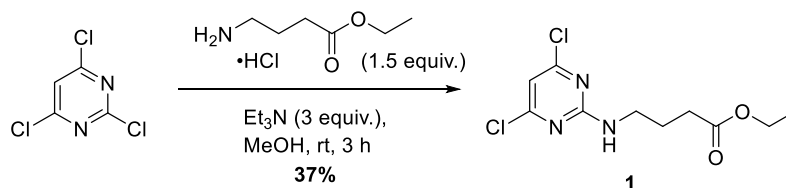


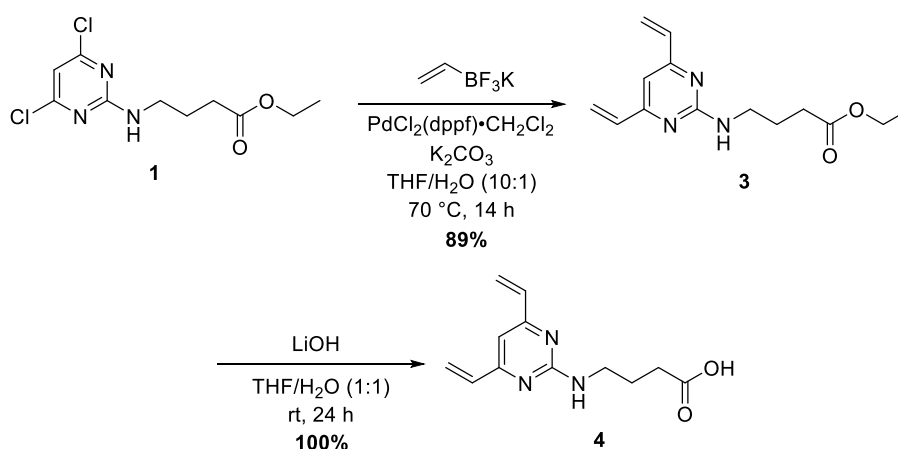
Figure 22: 4D contour plots for the (A) disappearance of 2,4,6-dichloropyrimidine, (B) appearance of desired product isomer **1** and (C) appearance of undesired product isomer **2** in response to variable reaction conditions. Plots were generated by Connor J. Taylor using MODDE software.

Using the data obtained from the DoE optimisation, the S_NAr reaction of 2,4,6-trichloropyrimidine with ethyl 4-aminobutyrate hydrochloride was optimised to give the desired product **1** in 37% yield (Scheme 3), representing an increase in product output by nearly 50%. Additionally, the data presented here later contributed to the development of a novel automated computational approach to kinetic model identification.¹⁹⁷



Scheme 3: Optimised reaction of 2,4,6-trichloropyrimidine with ethyl 4-aminobutyrate hydrochloride.

Having synthesised a sufficient quantity of intermediate **1**, Suzuki cross-coupling with potassium vinyltrifluoroborate was undertaken to produce DVP ester **3** in 89% yield. Finally, intermediate **3** was subjected to base-mediated ester hydrolysis to generate DVP acid **4** in quantitative yield, thus concluding the synthesis of the desired DVP building block (Scheme 4).

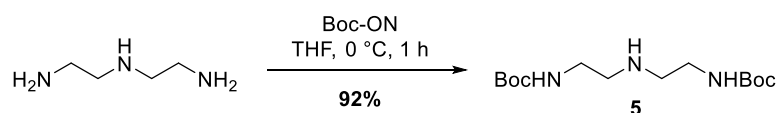


Scheme 4: Synthesis of DVP **4** from dichloropyrimidine intermediate **1**.

3.3 BisDVP Linker Synthesis

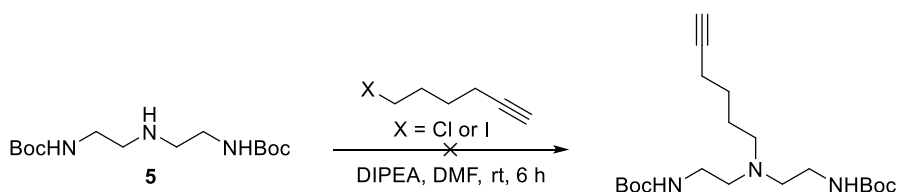
Following the successful synthesis of DVP building block **4**, the synthesis of the alkyne-containing core scaffold (shown in Scheme 1) was investigated. It was proposed that this scaffold could be accessed by alkylation of the secondary amine of diethylenetriamine with an alkyne-functionalised electrophile.

To enable selective alkylation at this position, it was deemed prudent to initially block the primary amines of diethylenetriamine using protecting group chemistry. As such, diethylenetriamine was reacted with 2-(tert-butoxycarbonyloxymino)-2-phenylacetonitrile (Boc-ON) in line with the published procedure by Pittelkow *et al.*,¹⁹⁸ to achieve selective Boc protection of the primary amines, affording intermediate **5** in 92% yield (Scheme 5). The reaction was found to be very robust with no decrease in yield observed on multi-gram (>5.5 g product) scale.



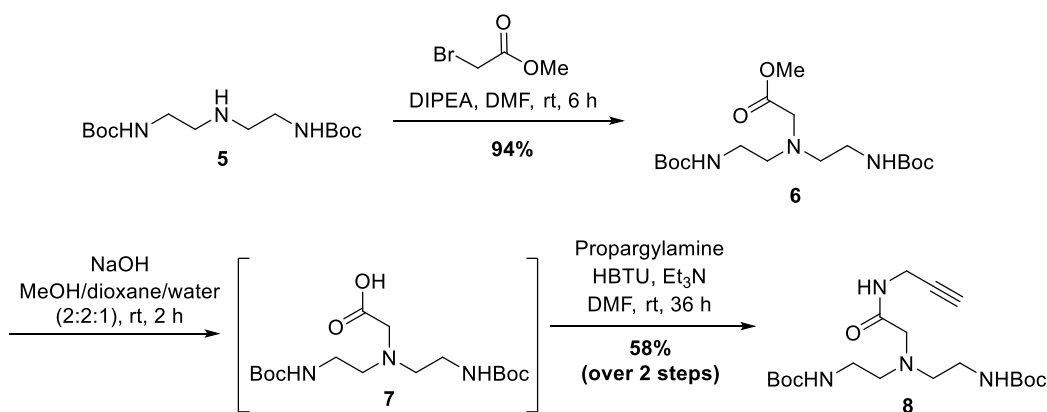
Scheme 5: Boc protection of diethylene triamine using Boc-ON.

With intermediate **5** in hand, installation of the alkyne handle was attempted *via* alkylation of the secondary amine. However, initial attempts at direct alkylation of polyamine **5** with 6-chlorohex-1-yne or 6-iodohex-1-yne did not result in any notable product formation (Scheme 6).



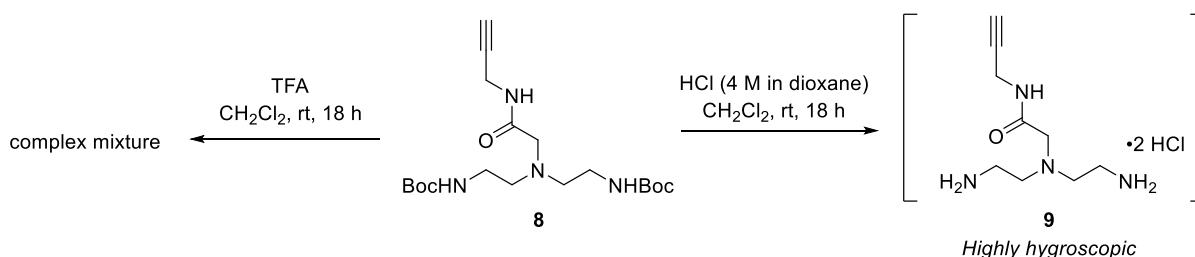
Scheme 6: Attempted modification of polyamine **5** with 6-chlorohex-1-yne or 6-iodohex-1-yne.

Therefore, a three-step procedure was employed to introduce the alkyne handle, involving initial reaction of intermediate **5** with methyl 2-bromoacetate, followed by ester hydrolysis and amide coupling with propargylamine (Scheme 7). Due to the electron-withdrawing properties of the methyl ester, methyl 2-bromoacetate could be alkylated easily, yielding the desired product **6** in 94% yield. Similar to the synthesis of polyamine **5**, the generation of methyl ester **6** was found to be highly scalable and could be used to generate >6.5 g of product in a single batch. Ester hydrolysis of **6** under basic conditions proceeded with full conversion in less than 2 hours as determined by thin-layer chromatography (TLC). Following work-up, the resulting carboxylic acid intermediate **7** was directly used in the next reaction without further purification. Amide coupling of **7** with propargylamine in the presence of triethylamine and hexafluorophosphate benzotriazole tetramethyl uronium (HBTU) gave the desired alkyne-containing core scaffold **8** in 58% yield over two steps.



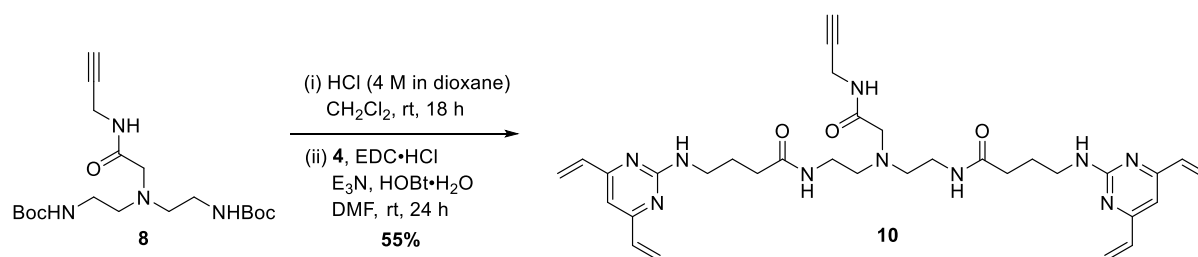
Scheme 7: Modification of polyamine **5** with methyl 2-bromoacetate, followed by ester hydrolysis and installation of the alkyne *via* amide coupling with propargylamine.

Having synthesised all the required building blocks, efforts commenced to assemble the final BisDVP linker. As such, potential conditions for the Boc deprotection of scaffold **8** were investigated. Initial treatment of di-Boc scaffold **8** with trifluoroacetic acid (TFA) in CH_2Cl_2 yielded a complex mixture of products (Scheme 8). However, Boc deprotection with HCl in dioxane/ CH_2Cl_2 succeeded in generating a single product (**9**) which precipitated out of the reaction mixture as a white solid. Hydrochloride salt **9** was found to be highly hygroscopic and turn into a sticky orange oil after exposure to air for approximately 30 minutes. Attempts to use this ‘wet’ hydrochloride salt in an amide coupling did not result in any product formation, indicating that exposure to air renders the compound inert to further modification. Therefore, compound **9** was re-synthesised and used in the next reaction immediately, taking care to limit air exposure to <2 minutes.



Scheme 8: Investigation of reaction conditions for the Boc deprotection of intermediate **8**.

In the final step of the BisDVP synthesis, intermediate **8** was deprotected using the optimised conditions and subsequently coupled to DVP building block **4** in the presence of 1-ethyl-3-(3-dimethylaminopropyl) carbodiimide (EDC) hydrochloride, hydroxybenzotriazole (HOBt) monohydrate and triethylamine to produce BisDVP linker **10** in 55% yield (Scheme 9).



Scheme 9: Synthesis of BisDVP linker **10** from intermediate **8**.

3.3 Trastuzumab Bioconjugation

To evaluate the bioconjugation potential of DVP **4** and BisDVP **10**, the linkers were reacted with the anti-HER2 antibody trastuzumab. Trastuzumab is a humanised IgG1 and a constituent of the FDA-approved ADCs Kadcyla® and Enhertu® – both of which are approved for the treatment of HER2-positive breast cancer – thus making it a model system of clinical relevance. Accordingly, interchain disulfide bonds in trastuzumab were reduced with TCEP in tris-buffered saline (TBS) for one hour at 37 °C, followed by addition of **4** or **10** and incubation at 37 °C in 10% DMSO/TBS (pH 8) for four hours to yield antibody-linker conjugates (ALCs) **11** and **12** (Figure 23A).

To gain a qualitative[†] understanding of the products formed in the reactions, ALCs **11** and **12** were initially analysed by liquid chromatography-mass spectrometry (LC-MS). LC-MS showed that DVP conjugate **11** comprised four DVP linkers bound to each antibody and consisted primarily of half antibody species with only a minor amount of the full antibody observed (Figure 23B). This is consistent with prior observations made within the Spring group.^{101,183,184} Similarly, BisDVP conjugate **12** also comprised a mixture of full and half antibody species; however, only two linkers were bound to each antibody molecule, indicating that BisDVP linkers are indeed capable of rebridging two disulfides per linker molecule as intended (Figure 23C).

[†] Under electrospray ionisation (ESI), different polypeptides ionise differently. Therefore, peak intensities in LC-MS cannot be used as a quantitative measure of product ratios and should be used for qualitative assessment only.

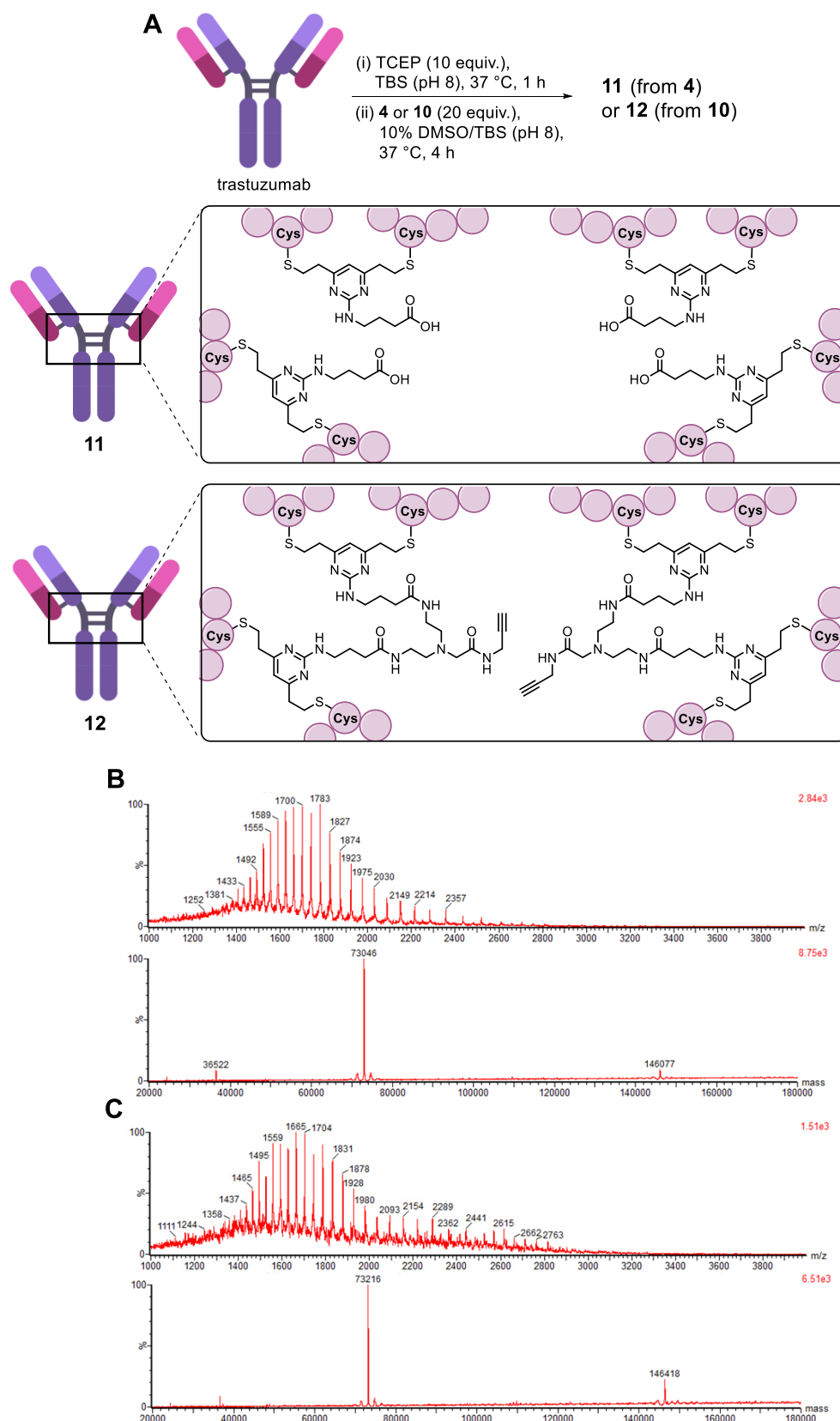


Figure 23: Reaction of trastuzumab with DVP and BisDVP linkers. (A) Reaction conditions. (B) Analysis of conjugate **11** by LC-MS. Top = non-deconvoluted MS. Bottom = deconvoluted MS; expected 73,061 Da (half antibody) and 146,123 Da (full antibody), observed 73,046 and 146,077 Da. (C) Analysis of conjugate **12** by LC-MS. Top = non-deconvoluted MS. Bottom = deconvoluted MS; expected 73,224 Da (half antibody) and 146,448 Da (full antibody), observed 73,216 and 146,418 Da.

To obtain a comparative measure of the relative ratios of full and half antibody species found in each of the conjugates, conjugates **11** and **12** were analysed by sodium dodecyl sulfate polyacrylamide gel electrophoresis (SDS-PAGE). SDS-PAGE analysis revealed that the BisDVP conjugate displayed a reduced amount of half antibody species compared to the DVP conjugate. While the reaction with DVP **4** predominantly yielded the half antibody product, analysis of BisDVP conjugate **12** showed the full antibody product to be the main component (Figure 24). Additionally, conjugate **12** displayed a lower abundance of other side products, such as heavy chain dimers (HH) compared to conjugate **11**. These results indicate that the rebridging of multiple disulfides by a single linker molecule indeed increases the probability of reforming the covalent linkages between the four antibody chains, thus validating the hypothesis that linkers containing multiple DVP motifs may be used for the synthesis of ADCs with improved homogeneity.

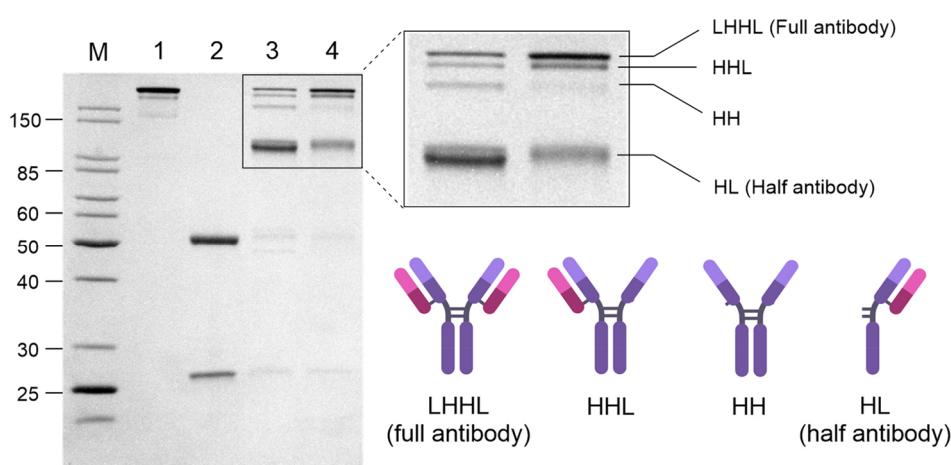


Figure 24: SDS-PAGE analysis of conjugates on 12% polyacrylamide gel with Coomassie staining. Lanes: M = molecular weight marker, 1 = trastuzumab, 2 = reduced trastuzumab, 3 = **11**, 4 = **12**.

3.4 Functionalisation with AlexaFluor™ 488

Having successfully established the ability of BisDVP linkers to modify IgG1 antibodies such as trastuzumab, the ability of the resulting ALCs to undergo CuAAC for the attachment of functional payloads was explored. For this purpose, AlexaFluor™ 488 azide was chosen as a model payload. AlexaFluor™ 488 is a fluorophore with strong absorbance at 495 nm, which allows for facile analysis of its corresponding antibody-fluorophore conjugates (AFCs) by UV-vis spectrophotometry.

AFCs are invaluable tool compounds used in chemical and molecular biology for the detection and/or localisation of antigens. For example, AFCs can be used for fluorescence-based imaging and temporal tracking of antigens in cells and tissues or facilitate fluorescence-activated cell sorting (FACS) to separate antigen-positive from antigen-negative cells.^{199,200} AFCs are also routinely used in the diagnosis of diseases – particularly viral infections – through visualisation of disease-associated markers in patient samples.^{201,202}

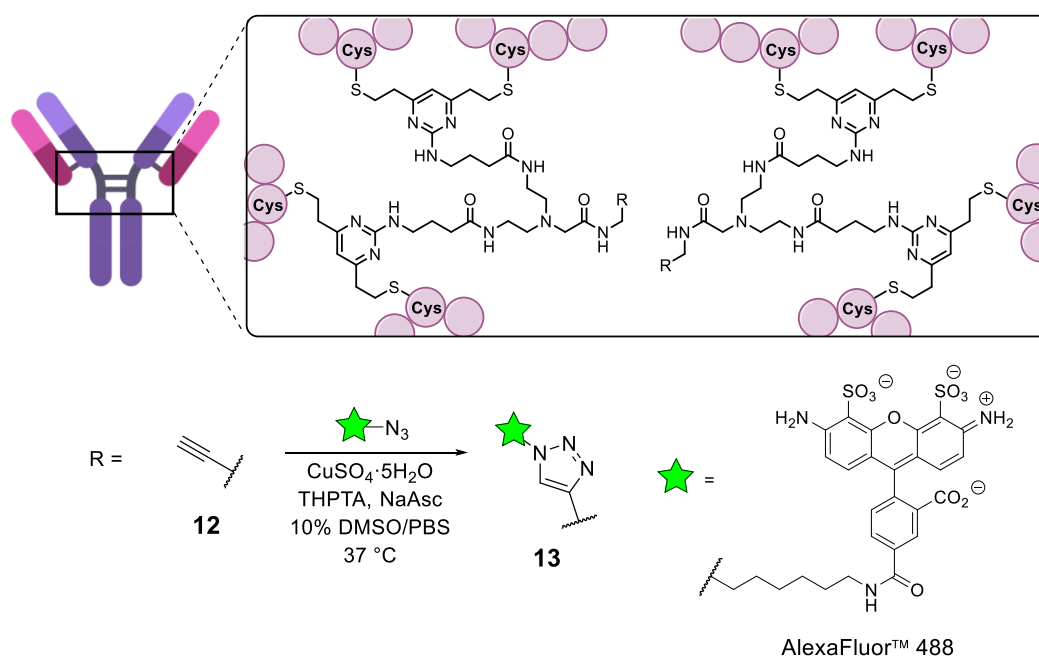
Since BisDVP conjugate **12** contains two alkyne handles, the CuAAC with AlexaFluor™ 488 azide should yield an AFC with a fluorophore-to-antibody ratio (FAR) of 2. Accordingly, conjugate **12** was reacted with 6 equivalents of AlexaFluor™ 488 azide in the presence of CuSO₄·5H₂O (10 equiv.), tris(benzyltriazolylmethyl)amine (THPTA, 50 equiv.) and sodium ascorbate (75 equiv.) in 10% DMSO/PBS at 37 °C for 2 hours (Table 3, Entry 1) and then analysed by UV-vis spectrophotometry. To minimise the risk of photobleaching, this reaction and all subsequent reactions with AlexaFluor™ 488 azide were conducted in the dark. Using Equation 1, the FAR was determined to be 0.7, indicating <50% conversion.

$$FAR = \frac{Abs_{495}/\epsilon_{495}}{(Abs_{280} - 0.11 \times Abs_{495})/\epsilon_{280}}$$

Equation 1: Determination of fluorophore-to-antibody ratios (FAR) by UV-vis spectroscopy. Sample buffer was used as blank for baseline correction with extinction coefficients $\epsilon_{280} = 215,380 \text{ M}^{-1} \text{ cm}^{-1}$ for trastuzumab and $\epsilon_{495} = 71,000 \text{ M}^{-1} \text{ cm}^{-1}$ for AlexaFluor™ 488. The correction factor for absorbance of AlexaFluor™ 488 at 280 nm is 0.11.

To improve conversion, the CuAAC reaction was repeated with increased reagent stoichiometry with regards to AlexaFluor™ 488 azide, CuSO₄·5H₂O, THPTA and sodium ascorbate and a prolonged reaction time of 16 hours. These conditions successfully led to the generation of AFC **13** with a FAR of 2.0 (Table 3, Entry 2 and Figure 25A).

Table 3: Optimisation of CuAAC between BisDVP conjugate **12** and AlexaFluor™ 488 azide.



Entry	Reagents (equivalents)	Reaction time / h	FAR
1	AlexaFluor™ 488 azide (6) CuSO ₄ ·5H ₂ O (10) THPTA (50) NaAsc (75)	2	0.7
2	AlexaFluor™ 488 azide (12) CuSO ₄ ·5H ₂ O (20) THPTA (100) NaAsc (150)	16	2.0

To verify that the observed absorbance is indeed a sign of covalent attachment of the fluorophore to the antibody and does not originate from small molecule contaminants, AFC **13** was analysed by LC-MS and SDS-PAGE with in-gel fluorescence. The resolution of the LC-MS traces was slightly decreased compared to that of the precursor ALC **12**, indicating that the charged nature of the AlexaFluor™ 488 molecules may be interfering with protein ionisation and detection. Nonetheless, the expected masses of both the full and half antibody species of AFC **13** could be detected, indicating that covalent attachment had indeed taken place (Figure 25C). SDS-PAGE analysis further substantiated this claim by showing the presence of two fluorescent bands corresponding to the full and half antibody species of AFC **13** (Figure 25B). These results verify that BisDVP linkers can be utilised for the construction of functional antibody conjugates with a cargo loading of two.

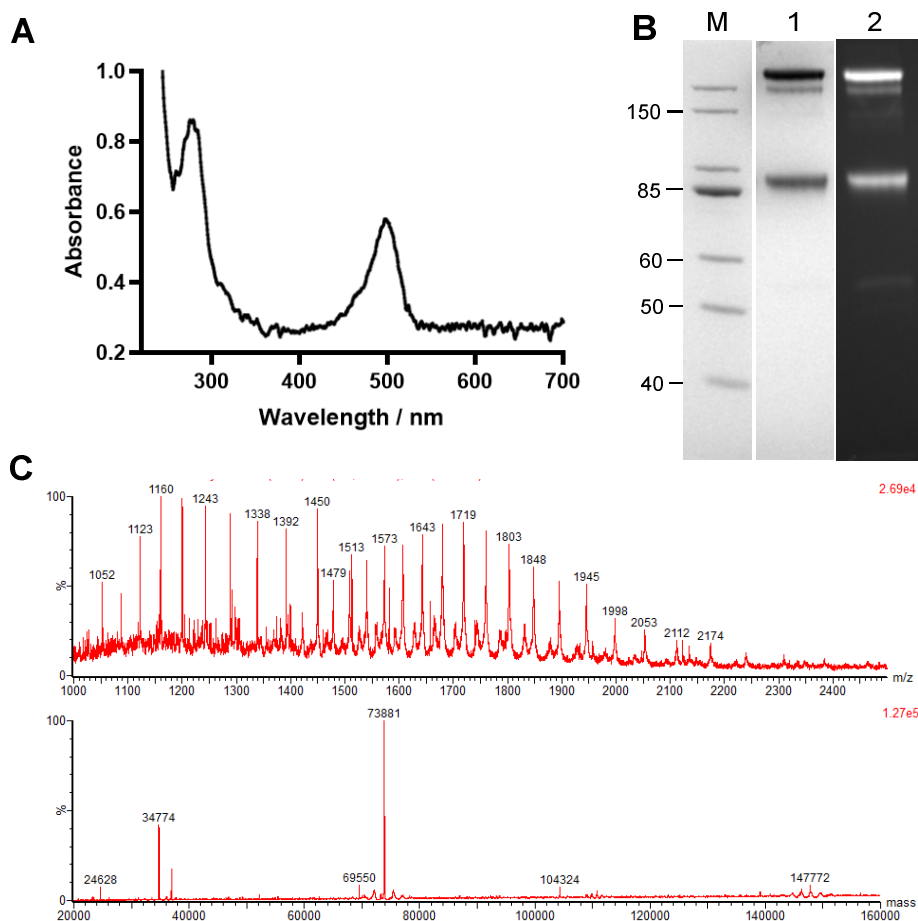


Figure 25: Analysis of AFC **13** by UV-vis spectroscopy, LC-MS and SDS-PAGE. (A) UV-vis spectrum of AFC **13**. (B) Analysis of **13** by SDS-PAGE on 8% polyacrylamide gel. Lanes were loaded with 3 μ g of sample. Lanes: M = molecular weight marker, 1 = **13** (Coomassie staining), 2 = **13** (in-gel fluorescence). (C) Analysis of AFC **13** by LC-MS. Top = non-deconvoluted MS. Bottom = deconvoluted MS; expected 73,881 Da (half antibody) and 147,762 Da (full antibody), observed 73,881 Da and 146,772 Da. The peak at 34,774 Da corresponds to PNGase F.

3.5 Conclusions

In this chapter, the synthesis of a BisDVP linker and its application for the functional modification of IgG1 antibodies were described. It was shown that BisDVP linkers can modify antibodies and generate ALCs with linker-to-antibody ratios of two through the functional rebridging of two disulfide bonds per linker molecule. Furthermore, these ALCs could be further modified through CuAAC to generate a fluorescent conjugate with a FAR of two.

The rebridging of two disulfides per linker molecule was shown to decrease the formation of half antibodies and other side products compared to the synthesis of ALCs using DVP linkers which only rebridge one disulfide per linker molecule. However, despite these improvements, the formation of half antibody species was not fully eradicated, indicating that further linker optimisation is required to achieve the generation of fully homogenous antibody conjugates.

Chapter 4 – TetraDVP Disulfide Rebridging Linkers

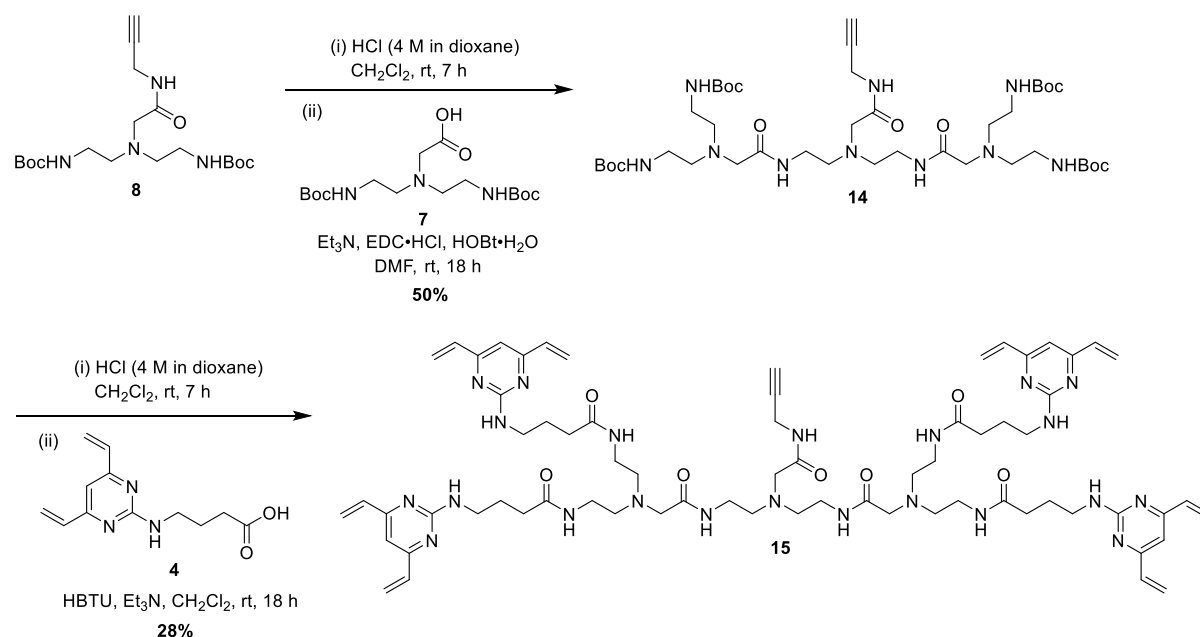
4.1 Introduction

Initial investigations into BisDVP linkers suggested that disulfide rebridging reagents capable of bridging multiple disulfides have the potential to fulfil the primary aims of this work, i.e. the generation of antibody conjugates with modular DAR and reduced half antibody content. However, it was demonstrated that the rebridging of two disulfides with one linker is not sufficient to fully prevent half antibody formation. Furthermore, although BisDVPs carry the potential to access a wider range of DAR values than classical disulfide rebridging reagents (multiples of two vs. multiples of four), the development of methods that enable access to the full scope of integer DAR values ≥ 1 is desirable.

It was proposed that the desired improvements in DAR modularity and half antibody prevention could be achieved by the design of a linker capable of rebridging eight cysteine residues, and thus interconnecting all four interchain disulfides in an IgG1 antibody. Such an ‘all-in-one’ rebridging approach should be able to prevent the loss of covalent linkages between the antibody polypeptide chains. Furthermore, modification of the antibody with the linker in a 1:1 ratio should facilitate access to a wider range of DAR values, including odd values (e.g. 1, 3, etc.) which are extremely challenging to achieve by other site-selective bioconjugation methods.

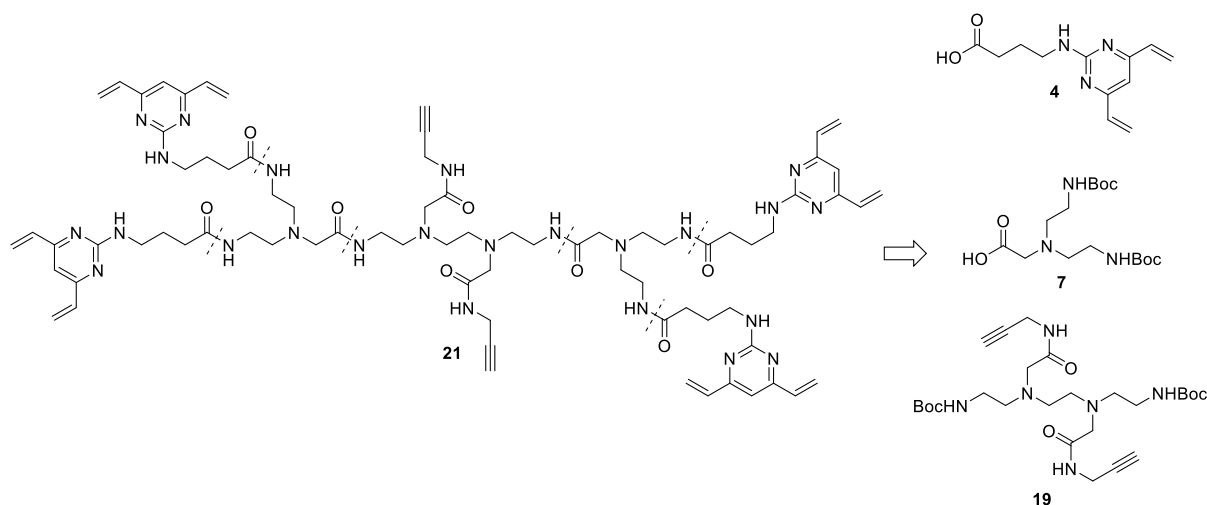
To this end, a series of tetra-divinylpyrimidine (TetraDVP) linkers was designed (Figure 26). The proposed structure encompasses four DVP units to enable reaction with eight cysteine residues, and a variable number of alkyne motifs to facilitate payload attachment *via* CuAAC. Apart from these factors, the general design emulates that of BisDVP **10** to aid synthetic tractability.

HCl and coupled to four equivalents of DVP **4** in the presence of triethylamine and HBTU to produce TetraDVP linker **15** in a moderate 28% yield.



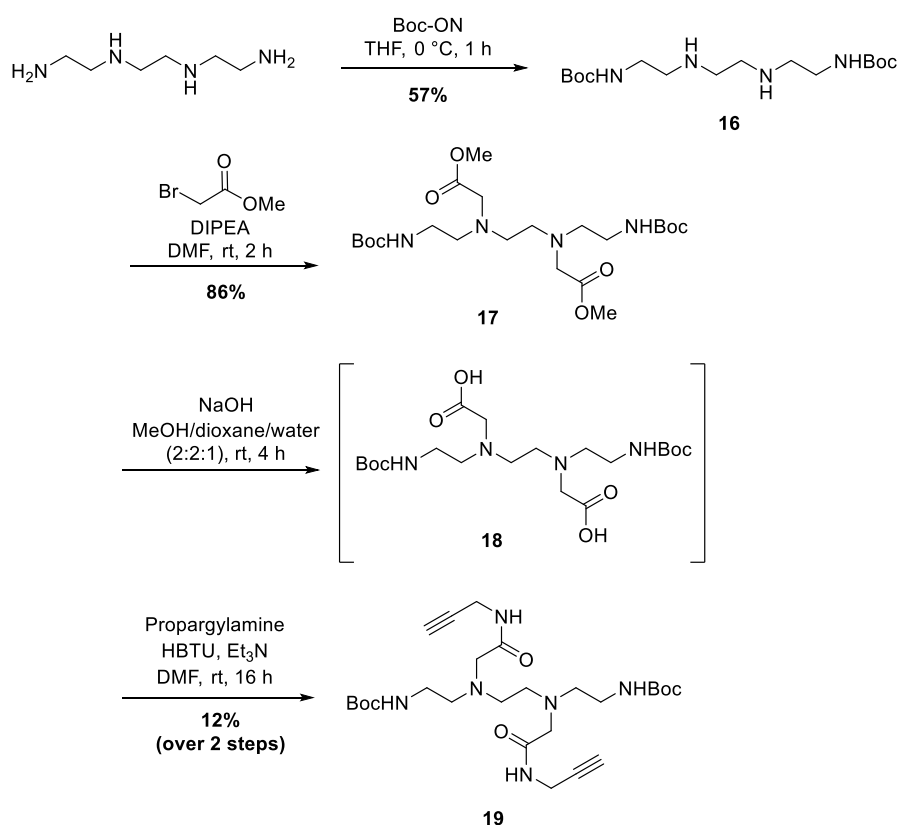
Scheme 11: Synthesis of TetraDVP **15** from di-*N*-Boc building block **8**.

TetraDVP **15** contains one alkyne group; therefore, if the linker is indeed capable of modifying an antibody in a 1:1 ratio, it would enable the attachment of a single payload molecule *via* CuAAC to generate a DAR 1 ADC. To broaden the scope of attainable DAR values beyond DAR 1, a second TetraDVP was designed. This linker – TetraDVP **21** – was designed to include two alkyne groups, thus theoretically enabling the synthesis of DAR 2 ADCs. It was envisioned that TetraDVP **21** could be synthesised *via* a route analogous to the synthesis of TetraDVP **15** in which the alkyne precursor **8** was replaced by bis-alkyne **19** (Scheme 12).



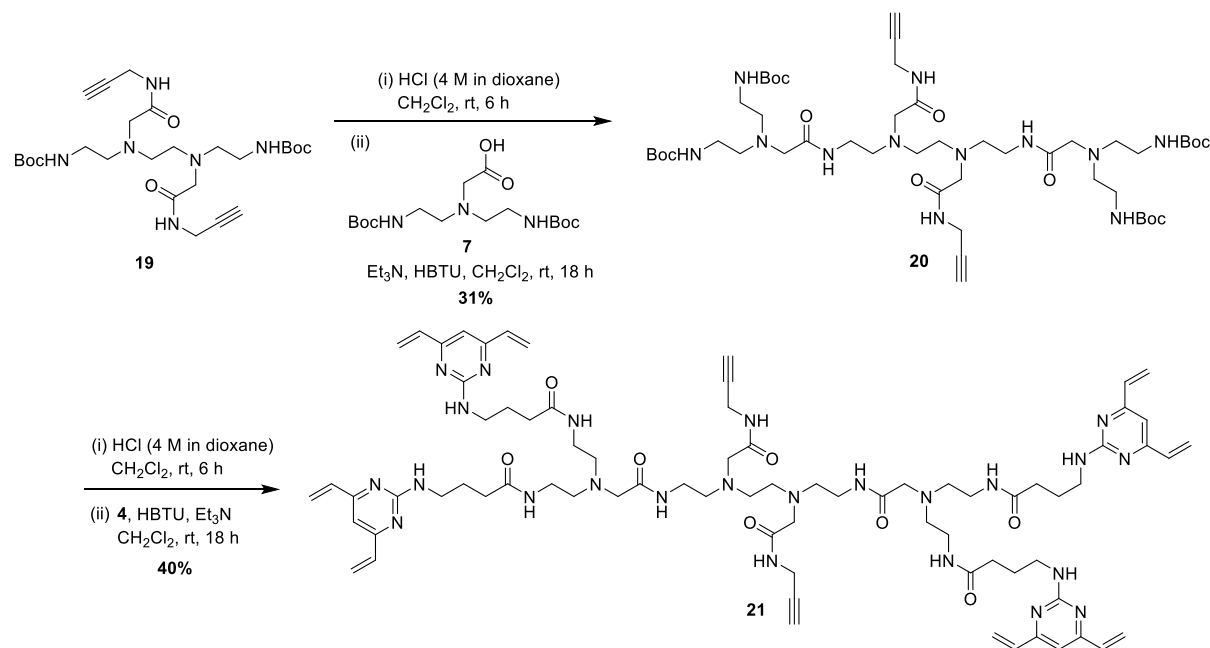
Scheme 12: Retrosynthetic analysis of TetraDVP **21**.

The bis-alkyne building block **19** was synthesised from triethylenetetramine using a synthetic approach similar to that applied for the synthesis of mono-alkyne building block **8**, which was described in Chapter 3.3. Accordingly, triethylenetetramine was reacted with Boc-ON to generate Boc-protected polyamine **16**. Subsequently, polyamine **16** was alkylated with methyl bromoacetate to produce di-ester **17** in good yield. Ester hydrolysis of di-ester **17** led to the formation of carboxylic acid intermediate **18**. Following work-up, the carboxylic acid intermediate was immediately used in the next reaction, consisting of an amide coupling with propargylamine in the presence of HBTU and triethylamine to generate bis-alkyne building block **19** in 12% yield over two steps (Scheme 13). The low yield of bis-alkyne **19** can be explained by a combination of factors, including incomplete conversion during amide coupling and complications during purification, which were caused by the high polarity of the compound (R_f 0.07 in 80% EtOAc/petroleum ether (PE)). Similarly, the reduced yield of di-Boc-tetramine **16** compared to di-Boc-triamine **5** (57% vs 92% yield) was caused by the high polarity of compound **16**, which resulted in a challenging purification process.



Scheme 13: Synthesis of bis-alkyne building block **19** from triethylenetetramine *via* Boc protection, alkylation with methyl bromoacetate, ester hydrolysis and amide coupling to propargylamine.

With bis-alkyne **19** in hand, the assembly of TetraDVP **21** commenced. Accordingly, bis-alkyne **19** was deprotected using HCl, followed by amide coupling with two equivalents of carboxylic acid intermediate **7** in the presence of triethylamine and HBTU to give the tetra-*N*-Boc core scaffold **20** in moderate yield (Scheme 14). Subsequently, the core scaffold was deprotected with HCl and coupled to four equivalents of DVP **4** in the presence of triethylamine and HBTU to produce TetraDVP **21** in 40% yield.

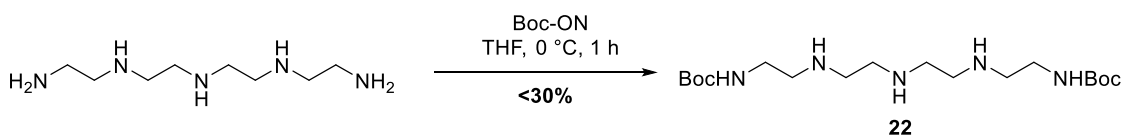


Scheme 14: Synthesis of TetraDVP **21** from bis-alkyne building block **19**.

4.2.2 Synthesis of a TetraDVP with three alkyne groups

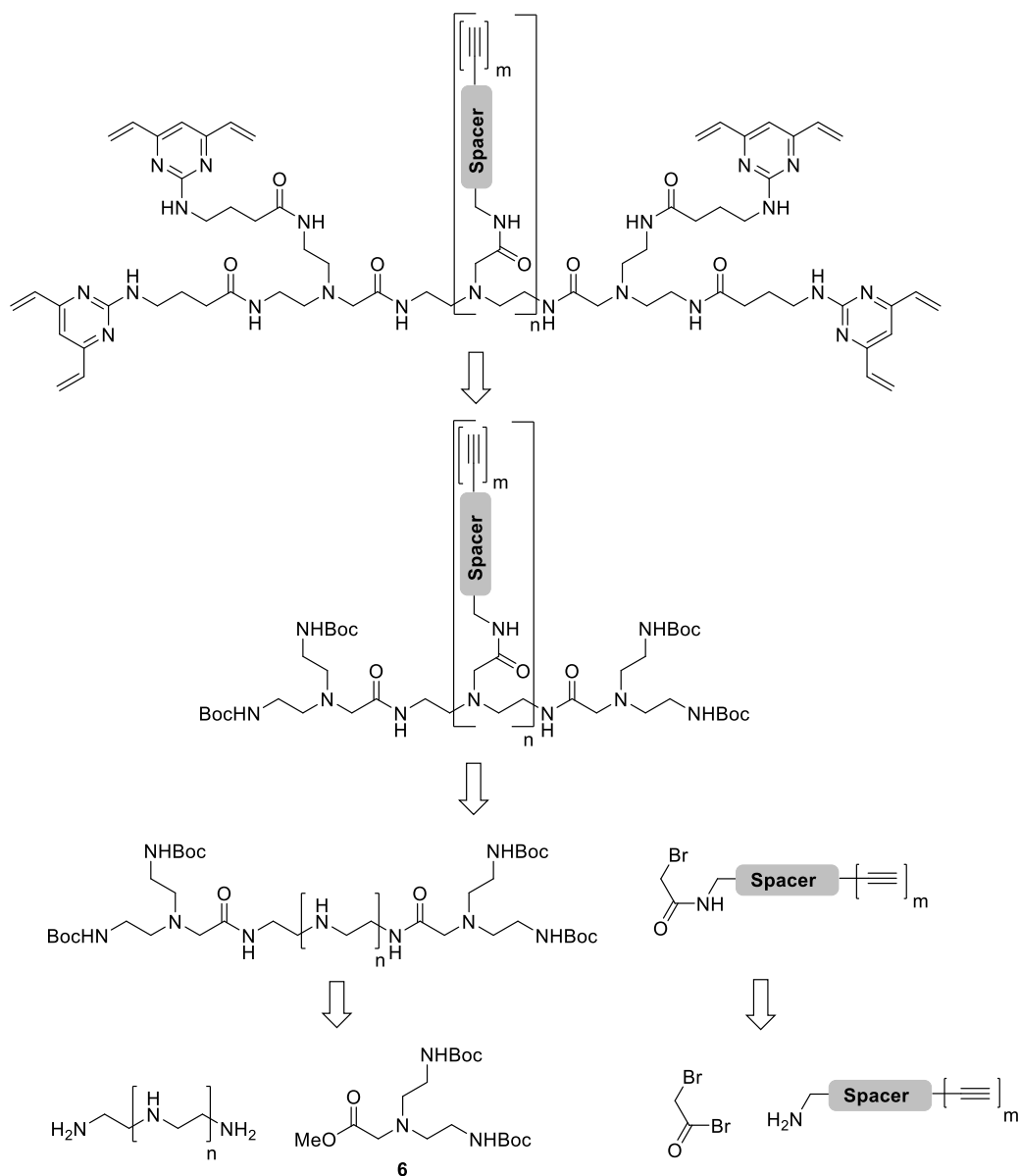
While the original synthetic strategy described in Chapter 4.2.1 did lead to the successful generation of two TetraDVP linkers – and thus proved that this class of linkers is synthetically tractable – the route suffered from a number of drawbacks. For one, the need for elaborate building blocks such as di-Boc alkyne **8** and di-Boc bis-alkyne **19** – which each needed to be synthesised in 4 steps – and the excessive use of protecting group chemistry render the route reasonably lengthy and complex. Furthermore, an attempt to apply the existing route to longer polyamines, such as tetraethylenepentamine, proved extremely challenging as the increasingly high polarity of the starting material and early intermediates made purification increasingly challenging. Indeed, when the Boc protection of tetraethylenepentamine with Boc-ON was attempted, the desired product **22** was isolated in <30% yield (Scheme 15). Further elaboration of di-Boc pentamine **22** to the tris-alkyne scaffold *via* alkylation with

methyl bromoacetate, ester hydrolysis and amide coupling with propargylamine did not result in any product formation.



Scheme 15: Attempted Boc protection of tetraethylenepentamine.

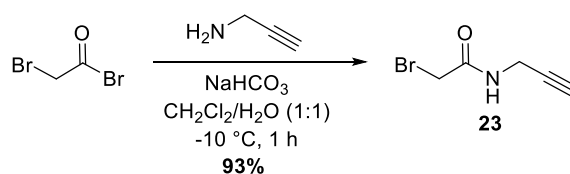
Accordingly, an alternative synthetic route towards TetraDVP linkers was devised by Dr Anders Højgaard Hansen from the Technical University of Denmark (DTU) (Scheme 16).



Scheme 16: Revised disconnection of the TetraDVP linker for the synthesis of linkers with ≥ 3 alkyne groups.

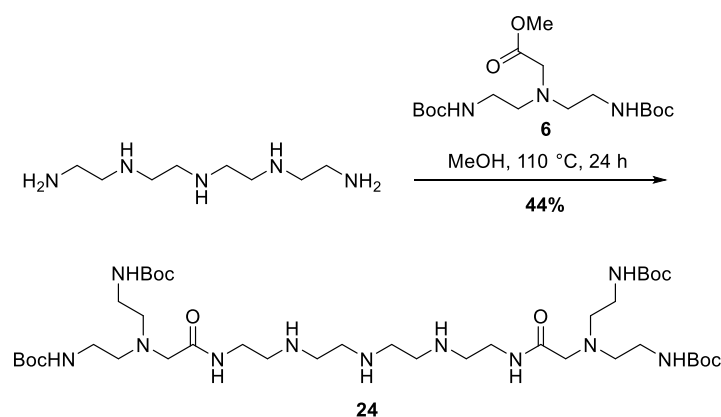
The revised route involves disconnection of the TetraDVP linker to give an alkyne-containing tetra-*N*-Boc intermediate as before; however, in contrast to the previous route, this intermediate is further disconnected to give an alkyne-containing α -bromo carbonyl compound and a tetra-*N*-Boc intermediate containing one or multiple reactive secondary amines. Thus, fewer Boc deprotection steps are required to reach the final target and introduction of the alkyne is achieved at a later stage, enabling the synthesis of analogues with different payload attachment handles in fewer steps. The tetra-*N*-Boc intermediate can be further disconnected into a commercially available polyamine and the previously synthesised building block **6**, allowing for simple derivatisation of linker length and number of payload attachment handles. Crucially, this approach also removes the need for the generation of exceedingly polar Boc-polyamine intermediates such as pentamine **22**. Finally, the alkyne-containing α -bromo carbonyl compound can be disconnected into bromoacetyl bromide and an alkyne-containing amine which may or may not be commercially available, depending on the complexity of the desired spacer unit.

To test the feasibility of this new synthetic strategy, the revised route was initially used to synthesise a TetraDVP with three alkyne groups. This synthesis was carried out Dr Anders Højgaard Hansen. Accordingly, bromoacetyl bromide was first reacted with propargylamine in line with the published procedure by Goswami *et al.*²⁰³ to give alkyne-containing α -bromo carbonyl compound **23** in 93% yield (Scheme 17).



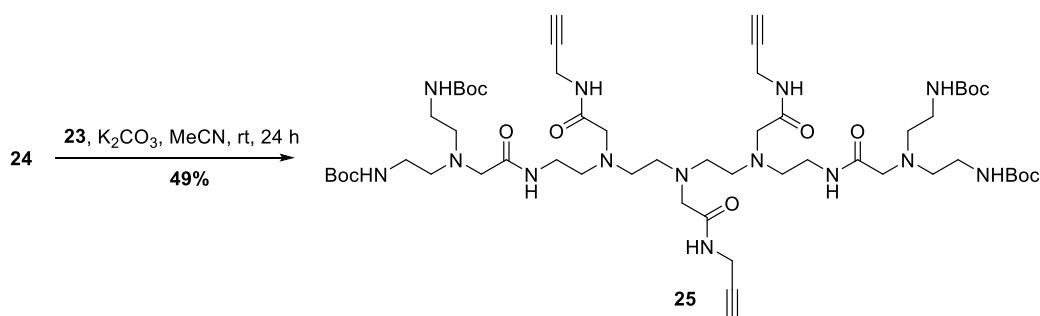
Scheme 17: Reaction of bromoacetyl bromide with propargylamine to yield α -bromo carbonyl **23**.

Following this promising result, synthesis of the tetra-*N*-Boc core scaffold **24** was attempted *via* direct amidation of tetraethylenepentamine with methyl ester **6**. It was found that high reaction temperatures (110 °C) and an excess of compound **6** (>5 equivalents) were necessary to achieve adequate conversion. However, the use of these forcing conditions was deemed acceptable as most of the excess reagent **6** could be recovered during column chromatography. Thus, scaffold **24** was generated in 44% yield (Scheme 18).



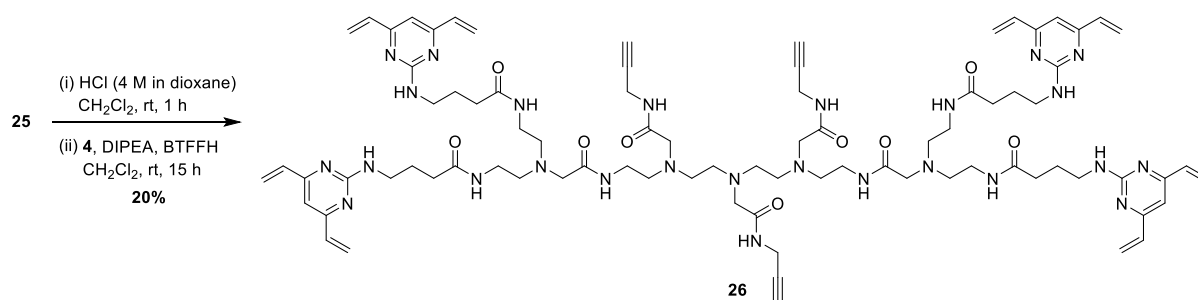
Scheme 18: Synthesis of tetra-*N*-Boc scaffold **24** from tetraethylenepentamine.

With alkyne **23** and polyamine scaffold **24** in hand, the two building blocks were reacted under basic conditions to give the alkyne-containing core scaffold **25** in 49% yield (Scheme 19).



Scheme 19: Synthesis of tris-alkyne scaffold **25** from precursors **23** and **24**.

Following the successful synthesis of tetra-*N*-Boc scaffold **25**, the assembly of tris-alkyne TetraDVP **26** was attempted. Accordingly, scaffold **25** was deprotected using HCl and subsequently reacted with DVP **4**. However, in contrast to the synthesis of linkers **15** and **21**, which proceeded efficiently in the presence of triethylamine and HBTU, the reaction of deprotected tris-alkyne scaffold **25** with DVP **4** under these conditions yielded only trace amounts of the desired linker **26**. To overcome this reactivity issue, fluoro-dipyrrolidinocarbenium hexafluorophosphate (BTFFH) was added dropwise to a mixture of DVP **4** and the deprotected tris-alkyne scaffold to activate the carboxylic acid by acid fluoride formation *in situ*. This approach led to the generation of TetraDVP **26** in 20% yield (Scheme 20).



Scheme 20: Synthesis of TetraDVP **26** via Boc deprotection of tris-alkyne scaffold **25** and subsequent coupling to DVP **4**.

4.2.3 Synthesis of TetraDVPs with one or two alkyne groups (revisited)

In light of the promising results obtained by Anders Højgaard Hansen regarding the synthesis of a TetraDVP **26**, it was postulated that the new synthetic strategy might also improve the synthetic tractability and overall yield of TetraDVPs **15** and **21**. Accordingly, the synthesis of these linkers was revisited.

Initially, diethylenetriamine and triethylenetetramine were reacted with methyl ester **6** to generate tetra-*N*-Boc scaffolds **27** and **28** in 78% and 49% yield, respectively (Scheme 21). The two scaffolds were subsequently alkylated using α -bromo carbonyl **23** to produce mono-alkyne scaffold **14** and bis-alkyne scaffold **20** in good yield. Finally, the two alkyne-containing tetra-*N*-Boc scaffolds were deprotected with HCl and coupled to DVP **4** as before to yield TetraDVP linkers **15** and **21**.

4.2.4 Synthesis of TetraDVPs with four alkyne groups

Following the successful synthesis of TetraDVP linkers containing one, two or three alkyne groups, the synthesis of a TetraDVP linker with four alkynes was attempted, to enable the generation of ADCs with DARs of 1, 2, 3 or 4. However, application of the synthetic route established in Chapter 4.2.2 for this purpose proved challenging, as the required polyamine starting material – pentaethylenehexamine – could not be procured in sufficiently pure form. Therefore, an alternative linker design needed to be devised.

It was proposed that an alternative tetra-alkyne scaffold could be accessed from intermediate **28** *via* alkylation with a branched α -bromo carbonyl compound containing two alkyne groups. Accordingly, two potential linker structures – **35** and **36** – were designed. In TetraDVP **35** (designed by Dr Anders Højgaard Hansen), the alkyne handles branch off an amide nitrogen close to the backbone of the scaffold (Figure 27). While this design was thought to be the most synthetically tractable, there were concerns about the close proximity of the branching point to the backbone introducing steric hindrance around the alkyne functionality which might inhibit attachment of payloads *via* CuAAC. Therefore, a second linker – TetraDVP **36** – was designed to include an additional spacer between the alkynes and the linear backbone of the linker.

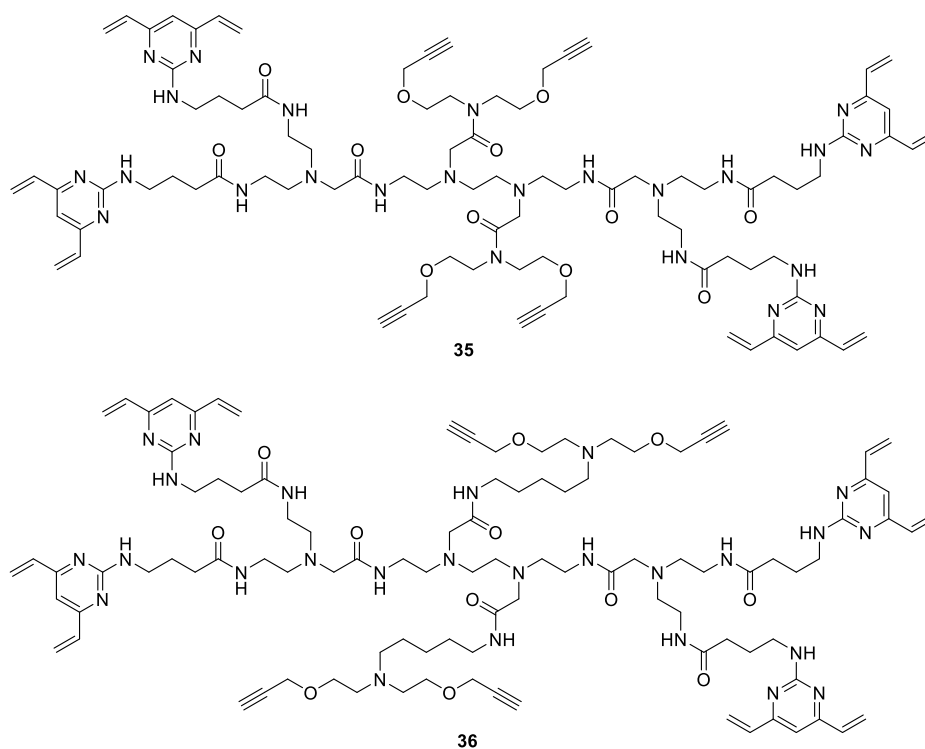
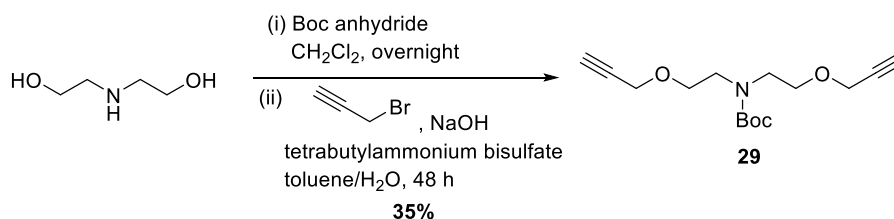


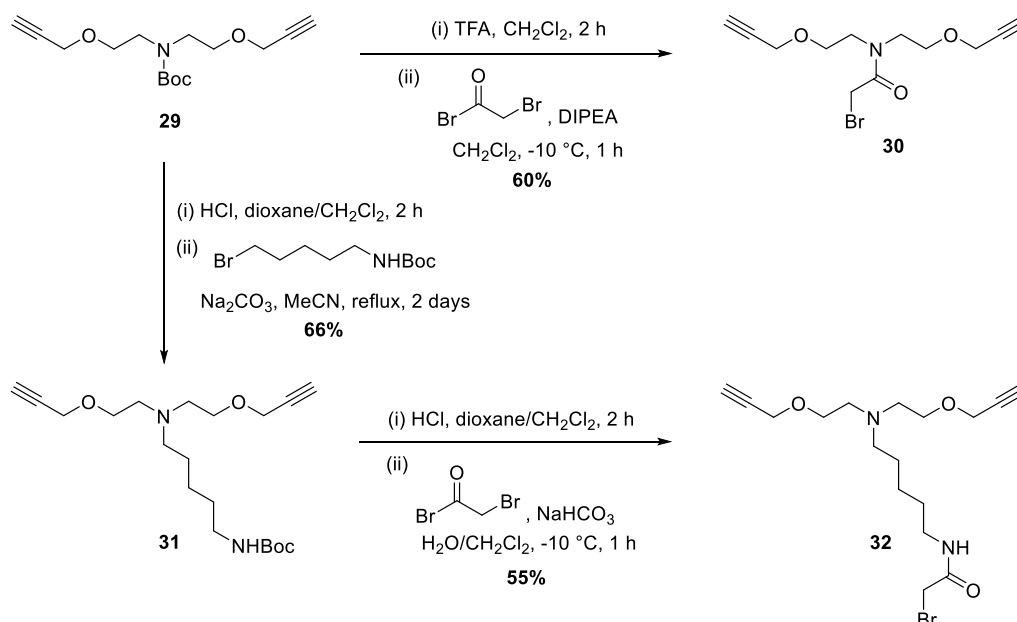
Figure 27: Proposed TetraDVP structures with four alkyne groups.

The first step in the synthesis of both linkers was the generation of bis-alkyne intermediate **29** from 2,2'-azanediybis(ethan-1-ol) *via* Boc protection and subsequent alkylation with propargyl bromide. This protocol was carried out by Dr Anders Højgaard Hansen and yielded the desired bis-alkyne **29** in 35% yield over two steps (Scheme 24).



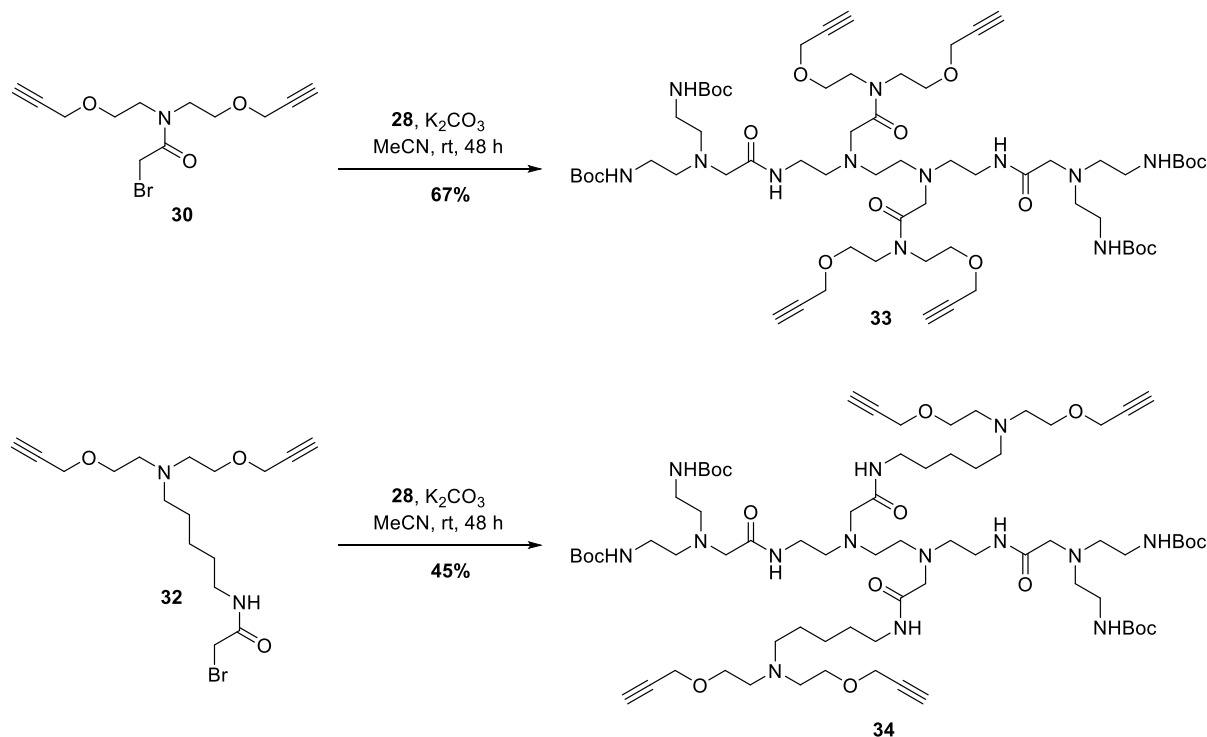
Scheme 24: Synthesis of bis-alkyne intermediate **29**.

Bis-alkyne **29** was subsequently used in the synthesis of two different α -bromo carbonyl compounds. For the first linker, Boc-amine **29** was deprotected using TFA and reacted with bromoacetyl bromide to give α -bromo carbonyl **30** in 60% yield over two steps. This synthesis was performed by Dr Anders Højgaard Hansen. For the second linker, bis-alkyne **29** was deprotected using HCl and alkylated with *tert*-butyl (5-bromopentyl)carbamate to afford tertiary amine **31** in good yield. Intermediate **31** was then further elaborated *via* Boc deprotection and reaction with bromoacetyl bromide to give α -bromo carbonyl **32** in 55% yield over two steps (Scheme 25).



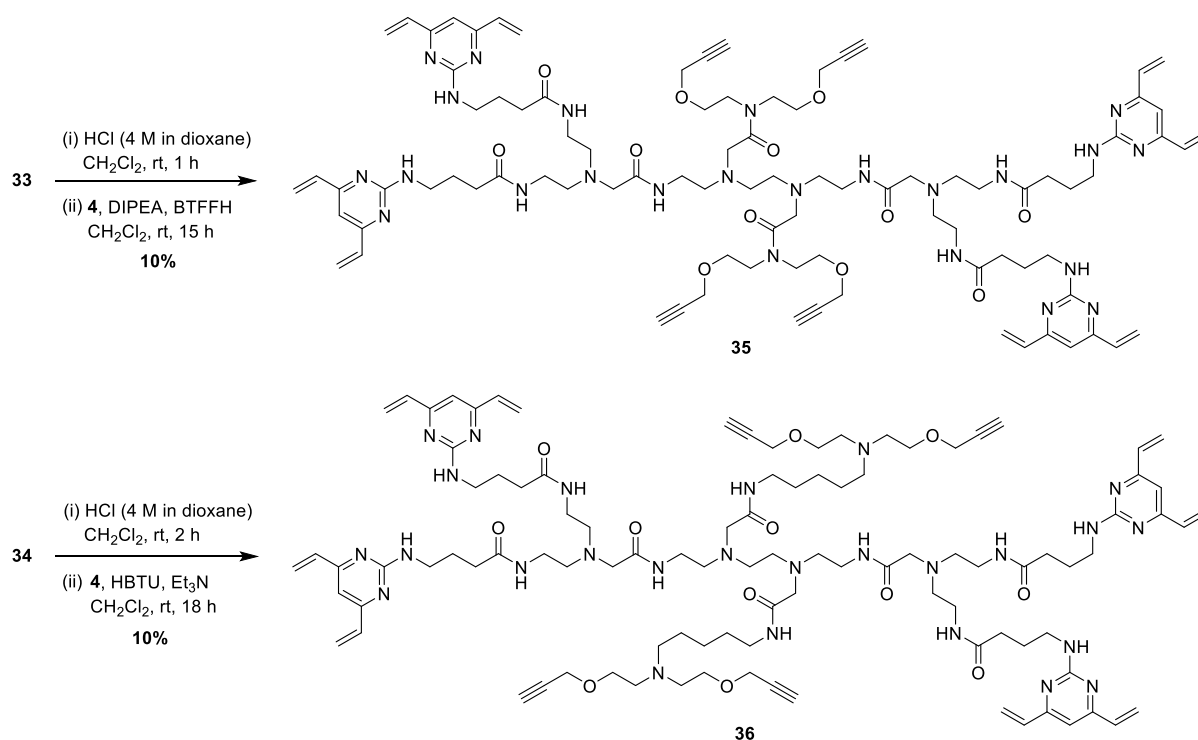
Scheme 25: Synthesis of α -bromo carbonyl compounds **30** and **32** from bis-alkyne **29**.

With all required building blocks in hand, the assembly of TetraDVPs **35** and **36** commenced. Accordingly, α -bromo carbonyl compounds **30** and **32** were each reacted with tetra-*N*-Boc scaffold **28** to afford tetra-alkyne tetra-*N*-Boc intermediates **33** and **34** in 67% and 45% yield, respectively (Scheme 26). The synthesis of compound **33** carried out by Dr Anders Højgaard Hansen.



Scheme 26: Generation of tetra-alkyne tetra-*N*-Boc scaffolds **33** and **34**.

Finally, tetra-*N*-Boc amines **33** and **34** were deprotected using HCl and coupled to DVP **4** to afford TetraDVP linkers **35** and **36** in 10% yield over two steps (Scheme 27), thus successfully concluding the generation of a panel of TetraDVP linkers with one, two, three or four alkyne handles. The reason for the low yield in the final step is unclear but may be related to the increased complexity and polarity of the linkers, which made purification challenging.



Scheme 27: Synthesis of TetraDVP linkers **35** and **36** from intermediates **33** and **34**.

4.3 Trastuzumab Bioconjugation

Following the successful synthesis of five TetraDVP linkers, the bioconjugation potential of this class of linkers was investigated. If the linkers work as designed, each TetraDVP linker should be capable of rebridging all four interchain disulfides in an IgG1 antibody and thus facilitate efficient linking of the four polypeptide chains with minimal half antibody formation.

Initial investigation into the bioconjugation potential of TetraDVP linkers focused on TetraDVP **15**, containing a single alkyne handle. Accordingly, the anti-HER2 antibody trastuzumab was reduced with TCEP at 37 °C for one hour, followed by incubation with 2 equivalents of **15** in 10% DMSO/TBS (pH 8) at 37 °C for 4 hours (Figure 28A). LC-MS analysis of the reaction mixture showed complete conversion to an ALC (**37**) containing a single linker molecule (Figure 28B), showcasing that the TetraDVP linker is capable of reacting with the antibody in a 1:1 ratio. To probe if all eight of the cysteine-reactive vinyl groups of the linker had reacted with the antibody, ALC **37** was incubated with an excess of cysteine (>1000 equiv.) for 2 hours and re-analysed by LC-MS. No change in the mass of ALC **37** was observed by LC-MS, indicating that no unreacted vinyl groups are present in the molecule. These results confirm that TetraDVP

linkers are indeed capable of rebridging all of the eight reactive cysteine residues of a reduced IgG1 antibody.

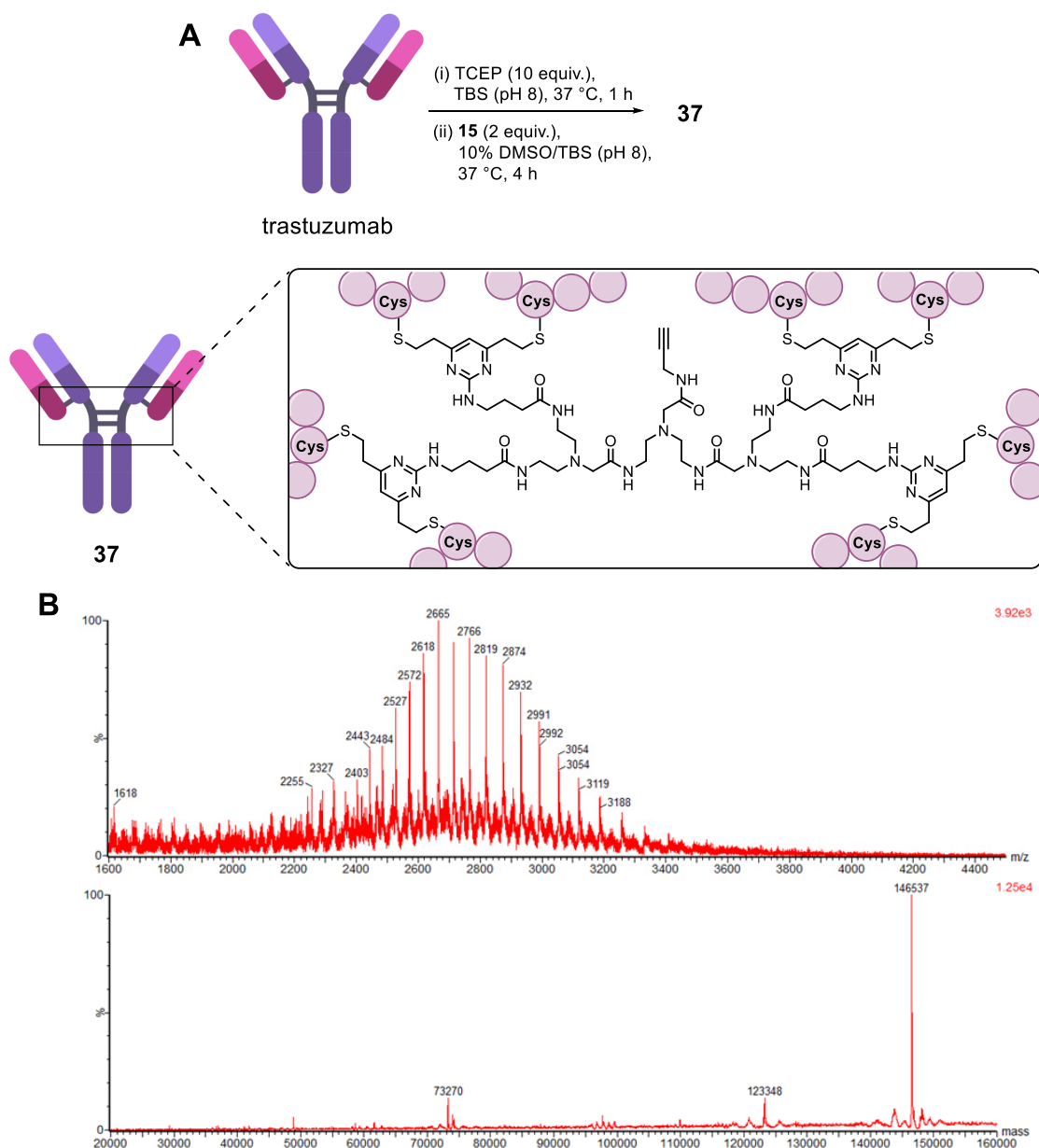


Figure 28: Reaction of trastuzumab with TetraDVP linker **15**. (A) Reaction conditions. (B) Analysis of the reaction between trastuzumab and **15** by LC-MS. Top = non-deconvoluted MS. Bottom = deconvoluted MS; expected 146,536 Da, observed 146,537 Da.

To establish if the rebridging of four disulfides translates to a reduction in half antibody formation as intended, TetraDVP conjugate **37** was analysed by SDS-PAGE alongside the previously synthesised DVP-trastuzumab conjugate **11** and BisDVP-trastuzumab conjugate **12**. Gratifyingly, SDS-PAGE analysis revealed that – unlike conjugates **11** and **12** – TetraDVP conjugate **37** comprised only trace amounts of half antibody (Figure 29). In fact, the only

observable side-product of the reaction was a minor amount of a HHL species in which only one of the light chains is covalently attached to the rest of the antibody. This analysis suggests that TetraDVP reagents significantly reduce the amount of half antibody formed during reaction.

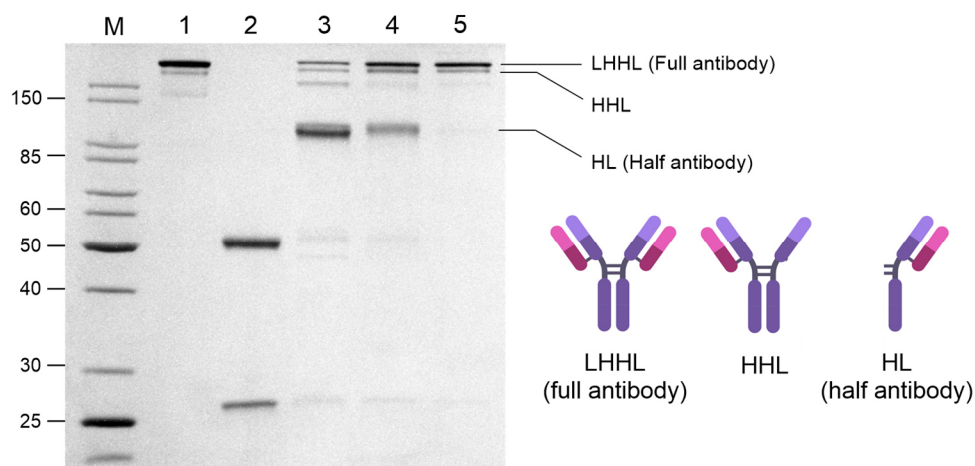


Figure 29: SDS-PAGE analysis of conjugates on 12% polyacrylamide gel with Coomassie staining. Lanes: M = molecular weight marker, 1 = trastuzumab, 2 = reduced trastuzumab, 3 = **11**, 4 = **12**, 5 = **37**. Lane 1 was run under non-reducing conditions, lanes 2-5 were run under reducing conditions.

To explore the robustness of the bioconjugation reaction and discover if a reduction in the presence of the HHL species may be achieved by optimisation of the reaction conditions, the reaction of trastuzumab with TetraDVP **15** was repeated under a range of different conditions (Figure 30). It was found that the reaction could be conducted with as little as 2.5% (v/v) of organic co-solvent and proceeded efficiently at protein concentrations between 1 – 5 mg/mL and temperatures of 4 – 37 °C, although a slight decrease in reactivity was observed at lower temperatures. Furthermore, it was observed that the order of addition of TCEP and linker had little impact on the outcome of the reaction, indicating that the two reagents do not interfere with one another. Across all experiments, the relative amounts of full antibody and HHL stayed consistent. Lastly, scale-up of the reaction showed that the bioconjugation could produce 1.4 milligrams of conjugate in a single batch while maintaining excellent product homogeneity and >90% protein recovery after removal of unreacted small molecule reagents. These results demonstrate that the TetraDVP reaction is both robust and scalable.

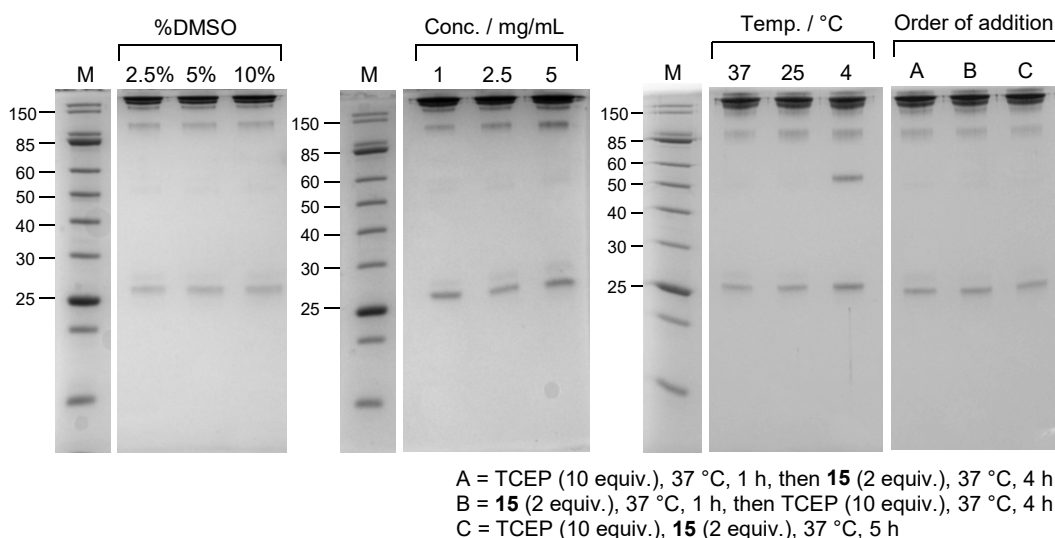


Figure 30: Optimisation of bioconjugation conditions for the reaction of trastuzumab with TetraDVP **15**. Analysis was carried out by reducing SDS-PAGE on 12% polyacrylamide gels with Coomassie staining. Lanes were loaded with 5 µg of protein. Lanes: M = molecular weight marker. Reaction conditions are displayed above the corresponding lane.

Having established the bioconjugation ability of TetraDVP **15**, the reactivity of the remaining linkers was investigated. As such, trastuzumab was reduced with TCEP at 37 °C for one hour, followed by incubation with 2 equivalents of **21**, **26**, **35** or **36** in 10% DMSO/TBS (pH 8) at 37 °C for 4 hours to yield ALCs **38**, **39**, **40** and **41** (Figure 31).

Despite slight variations in linker length, all four linkers displayed comparable reactivity to linker **15** and generated conjugates with outstanding homogeneity, as determined by LC-MS (Figure 32) and SDS-PAGE (Figure 33). These results show that the all-in-one rebridging approach is not restricted to a single linker scaffold and small variations in linker length and flexibility are well tolerated. This suggests that TetraDVPs have potential for modulating the drug loading of antibody conjugates.

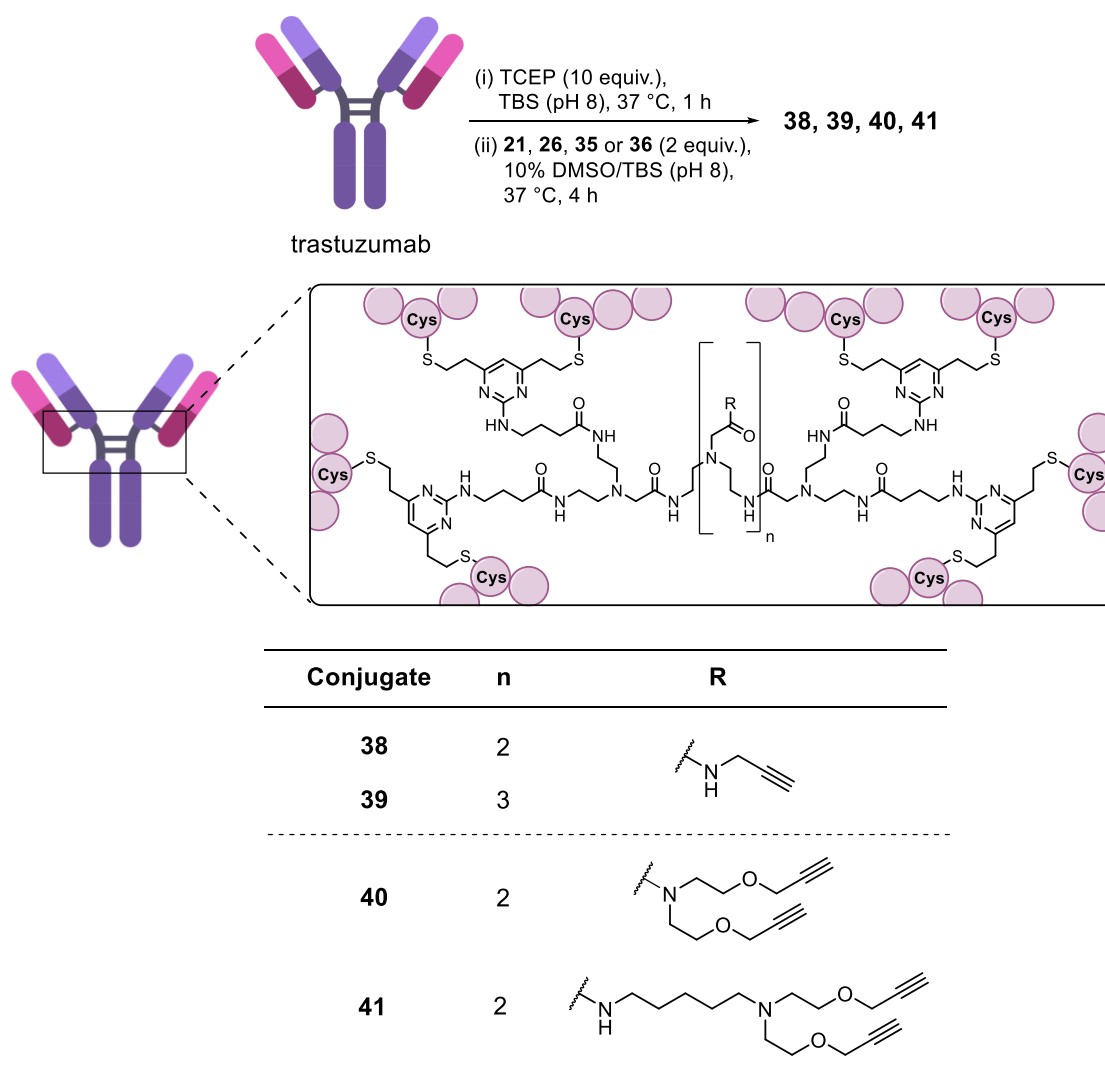


Figure 31: Reaction of trastuzumab with TetraDVP linkers **21**, **26**, **35** and **36**.

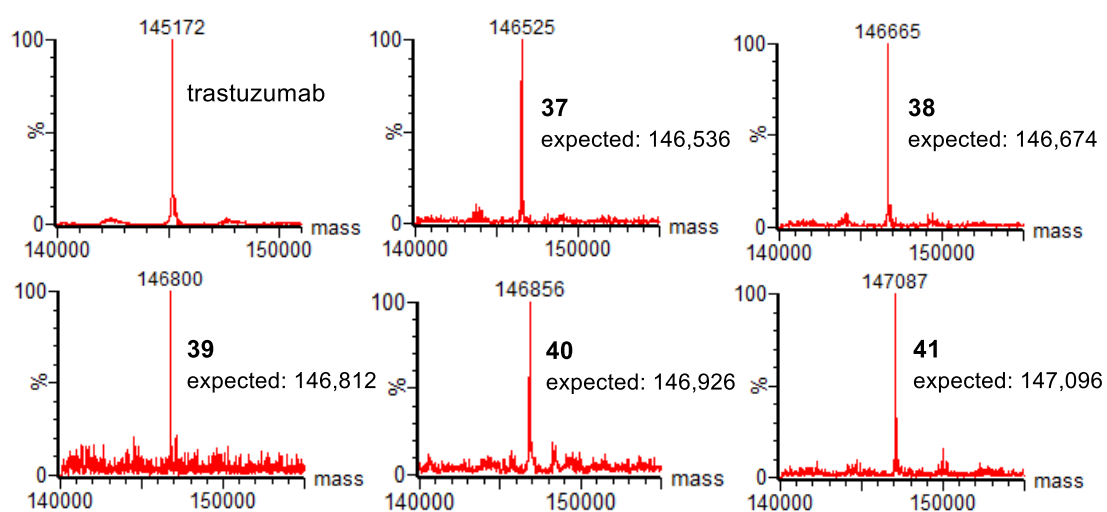


Figure 32: Analysis of trastuzumab and TetraDVP conjugates by LC-MS.

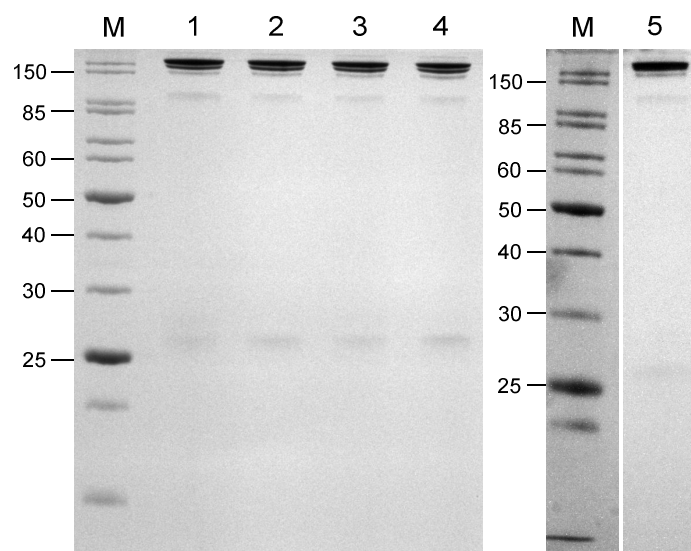


Figure 33: SDS-PAGE analysis of TetraDVP conjugates. Analysis was carried out by reducing SDS-PAGE on 12% polyacrylamide gels with Coomassie staining. Lanes: M = molecular weight marker, 1 = **37**, 2 = **38**, 3 = **39**, 4 = **40**, 5 = **41**.

4.4 Functionalisation with AlexaFluor™ 488

Having established the ability of TetraDVP linkers to generate highly homogenous antibody conjugates with different numbers of alkyne handles, the potential for further functionalisation of the TetraDVP conjugates *via* CuAAC was investigated. For this purpose, the reaction of TetraDVP conjugates **37-41** with AlexaFluor™ 488 azide was studied initially.

Accordingly, TetraDVP conjugates **37-41** were reacted with AlexaFluor™ 488 azide in the presence of CuSO₄·5H₂O, THPTA and sodium ascorbate in 10% DMSO/PBS at 37 °C, and then analysed by UV-vis spectrophotometry.

Reaction of ALC **37** – containing one alkyne handle – with 12 equivalents of AlexaFluor™ 488 azide for 6 hours successfully yielded AFC **42** with a FAR of 1.0 (Table 5, Entry 1 and Figure 34). Similarly, reaction of ALC **38** and **39** – containing two or three alkyne handles – successfully generated AFCs **43** and **44** with FARs of 2.0 and 2.9, respectively (Table 5, Entries 2-3 and Figure 34). However, reaction of ALC **40** – containing four alkynes – did not yield an AFC with a fluorophore loading of four, but rather stalled at a FAR of 1.9 (Table 5, Entry 4). Increasing reagent stoichiometry or reaction time did not result in increased conversion (Table 5, Entries 5-6).

Table 5: CuAAC reactions of TetraDVP ALCs with AlexaFluor™ 488 azide.

Entry	ALC	Reagents (equivalents)	Reaction time / h	Product	FAR
1	37	AlexaFluor™ 488 azide (12) CuSO ₄ •5H ₂ O (20) THPTA (100) NaAsc (150)	6	42	1.0
2	38	AlexaFluor™ 488 azide (24) CuSO ₄ •5H ₂ O (40) THPTA (200) NaAsc (300)	6	43	2.0
3	39	AlexaFluor™ 488 azide (36) CuSO ₄ •5H ₂ O (60) THPTA (300) NaAsc (450)	6	44	2.9
4	40	AlexaFluor™ 488 azide (48) CuSO ₄ •5H ₂ O (80) THPTA (400) NaAsc (600)	4	45	1.9
5	40	AlexaFluor™ 488 azide (240) CuSO ₄ •5H ₂ O (400) THPTA (2000) NaAsc (3000)	4	45	1.9
6	40	AlexaFluor™ 488 azide (48) CuSO ₄ •5H ₂ O (80) THPTA (400) NaAsc (600)	16	45	2.0
7	41	AlexaFluor™ 488 azide (48) CuSO ₄ •5H ₂ O (80) THPTA (400) NaAsc (600)	6	46	4.0

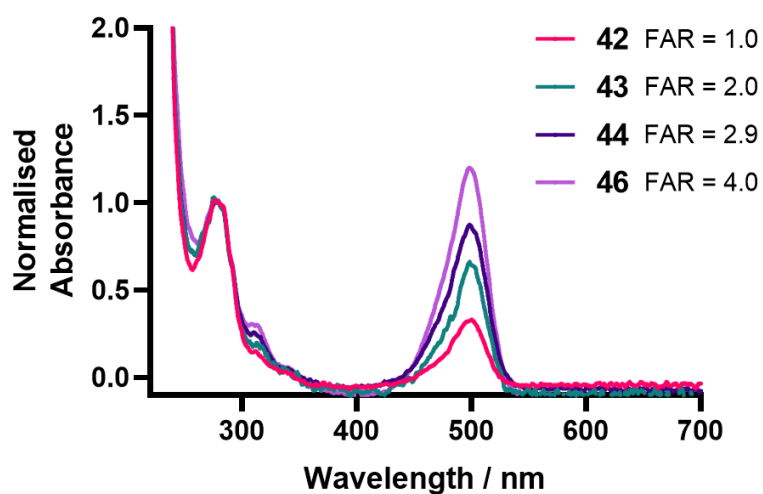


Figure 34: Analysis of AFCs by UV-vis spectroscopy.

The poor reactivity of ALC **40** may be due to conformational rigidity effected by the tertiary amide functionality of its constituent linker **35** (Figure 35). These amides display restricted bond rotation, as evidenced by the ^1H and ^{13}C NMR of TetraDVP **35** and its precursors **30** and **33**, which all appear as a mixture of rotamers. It is possible that this lack of conformational flexibility restricts access to two of the four alkyne handles, thus causing the CuAAC with AlexaFluor™ 488 azide to stall after attachment of the first two fluorophore molecules. This hypothesis is further supported by the fact that the reaction of AlexaFluor™ 488 azide with ALC **41** – which does not contain any tertiary amides – successfully generated an AFC (**42**) with a FAR of 4.0 (Table 5, Entry 7 and Figure 34). These results indicate that TetraDVP linkers must possess a certain degree of conformational flexibility to enable efficient post-conjugation functionalisation with azide-containing payloads.

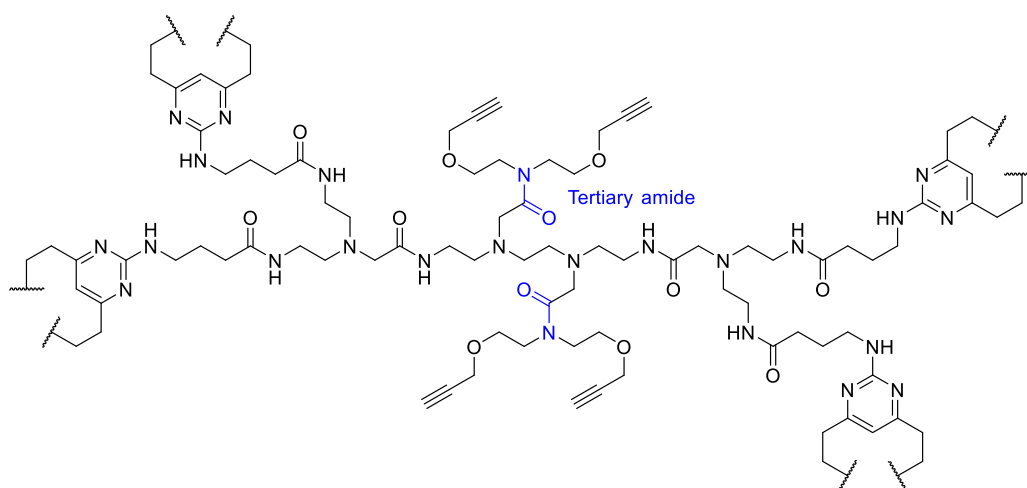


Figure 35: The conformational rigidity caused by the tertiary amides (shown in blue) of ALC **40** may be the cause of poor CuAAC reactivity.

To verify that the observed absorbance of AFCs **42-46** is indeed caused by covalent attachment of the fluorophore to the antibody, AFCs **42**, **43**, **44** and **46** were analysed by SDS-PAGE with in-gel fluorescence (Figure 36). The resulting images not only confirm the covalent attachment of the fluorophore to the antibody but display an increase in fluorescence intensity correlating with the number of alkyne moieties in the ALC precursor, indicating increased fluorophore loading. These observations showcase the viability of TetraDVPs for the construction of antibody conjugates with modular cargo loading and furthermore highlight the utility of this method for imaging applications where AFCs with precisely tuned fluorescence intensity may be required.

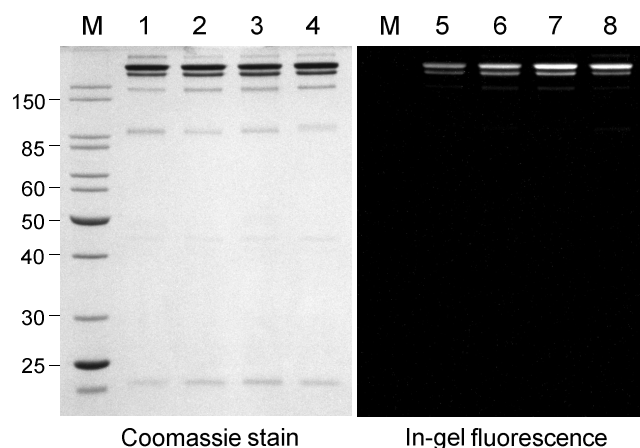


Figure 36: SDS-PAGE analysis of AFCs. Analysis was carried out by reducing SDS-PAGE on 12% polyacrylamide gels. Lanes were loaded with 4 μ g of sample and visualised by in-gel fluorescence (lanes 5-8), followed by Coomassie staining (lanes 1-4). Lanes: M = molecular weight marker, 1 and 5 = **42**, 2 and 6 = **43**, 3 and 7 = **44**, 4 and 8 = **46**.

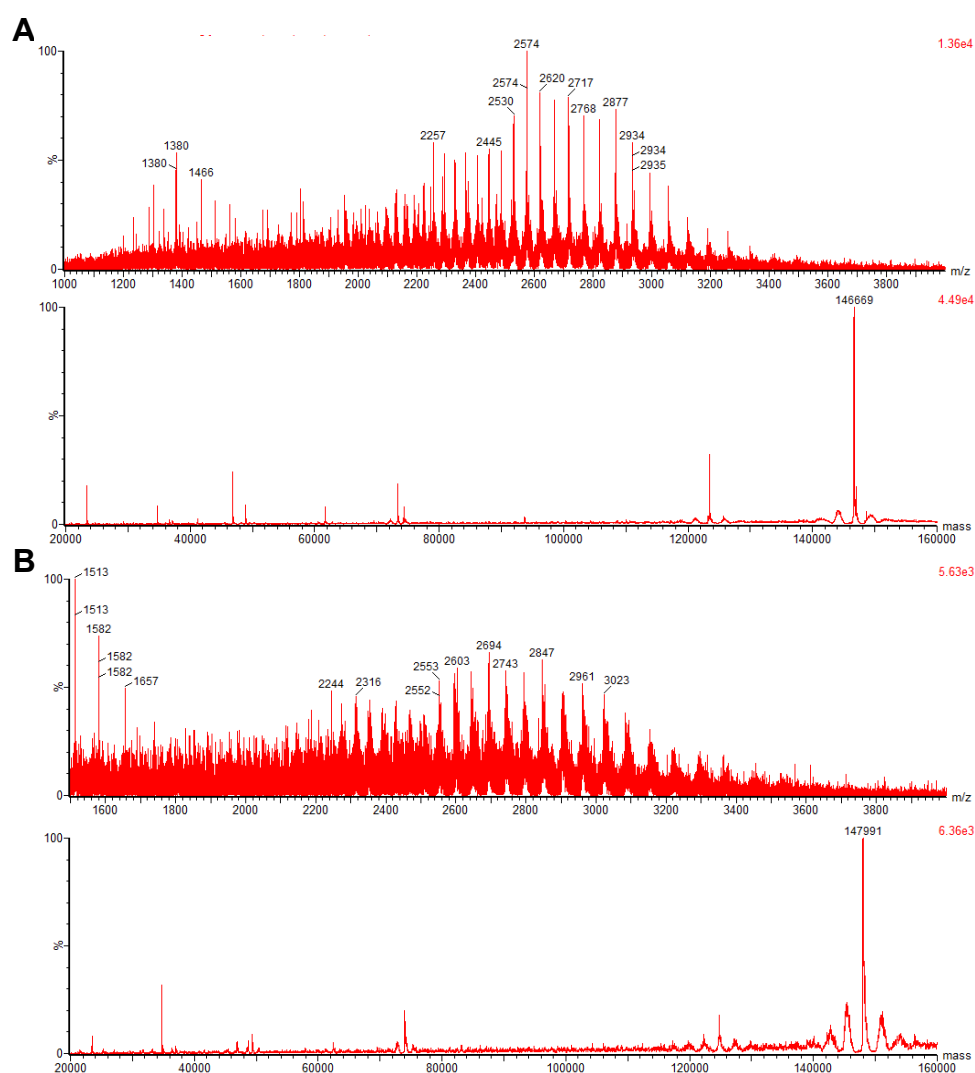


Figure 37: Analysis of the reaction between ALC **38** and AlexaFluor™ 488 azide by LC-MS. (A) Analysis of ALC **38**. Top = non-deconvoluted MS. Bottom = deconvoluted MS; expected 146,674 Da, observed 146,669 Da. (B) Analysis of AFC **43**. Top = non-deconvoluted MS. Bottom = deconvoluted MS; expected 147,988 Da, observed 147,991 Da.

Finally, mass spectrometry was used to unambiguously show covalent attachment of AlexaFluor™ 488 to the TetraDVP conjugates. As such, AFC **43** was analysed by LC-MS (Figure 37). The LC-MS trace confirmed covalent attachment of two molecules of AlexaFluor™ 488 azide to the antibody as expected. This result corroborates the results of the UV-vis analysis (i.e. that AFC **43** has a FAR of 2), and furthermore shows that the measured FAR is a *precise* FAR and not merely an average value produced by a mixture of AFC populations with varying fluorophore loading. These observations showcase the ability of TetraDVPs to facilitate the construction of homogenous antibody conjugates with precise cargo loading in a modular fashion.

4.5 Biological Evaluation

One of the most important features of a successful bioconjugation method is that it does not interfere with the intended biological function of the protein. In the case of an antibody, it is paramount that antigen binding affinity and cellular selectivity are not negatively affected. Additionally, in the case of an ADC, it is critical that the linkage between the antibody and the payload is stable in circulation to prevent premature payload release. Accordingly, a series of assays were carried out to investigate the effect of TetraDVP modification on antigen binding and examine the stability of the linkage under physiological conditions.

4.5.1 Stability

The first priority was to ascertain the stability of the TetraDVP linkage to the antibody. Maleimides – the most commonly employed cysteine bioconjugation reagents in approved and clinical-stage ADCs – are known to generate semi-stable conjugates which have been shown to transfer their payloads to plasma proteins such as serum albumin after just 1-2 days of incubation in blood plasma.^{128,130,132} This instability can be detrimental for drug development, as cytotoxic molecules which are released from the antibody prematurely have the potential to non-selectively harm healthy tissues and cause serious adverse events in patients.

In contrast to the thiosuccinimide linkage generated from maleimides, the thioether linkage created from vinylpyrimidines has been shown to be highly stable under physiological conditions. Indeed, AFCs made *via* monovinylpyrimidine or DVP conjugation have proven to be stable in human plasma for at least 7 or 14 days, respectively.^{132,183} Due to both the

inherent stability of the thioether linkage and the attachment of the payload to the antibody through eight covalent bonds, TetraDVP conjugates are also expected to be stable in human plasma for a minimum of 14 days.

To verify this, a stability assay involving incubation of AFC **42** in human plasma was carried out. Human plasma contains a large number of proteins, the most abundant of which is HSA. HSA is present in human plasma at a concentration of approximately 600 μ M. Approximately 75% of plasma HSA contains a single reduced cysteine residue (Cys34).⁹⁴ This thiol is known to be modifiable by cysteine-reactive linkers;^{132,204,205} thus, if any of the AlexaFluor™ 488 payload of AFC **42** was released during incubation in human plasma, it would likely react with HSA. Due to the fluorescent nature of the payload and the distinctive size of HSA (~66.5 kDa), this transfer would be observable by SDS-PAGE. Accordingly, AFC **42** was incubated in human plasma at 37 °C for 14 days. Throughout the incubation period, aliquots were taken every two days and stored at -80 °C before analysis by SDS-PAGE with in-gel fluorescence detection. Gratifyingly, no transfer of fluorescence to HSA or any other plasma proteins was observed over the entire duration of the study (Figure 38), indicating that the TetraDVP linkage is stable in human plasma.

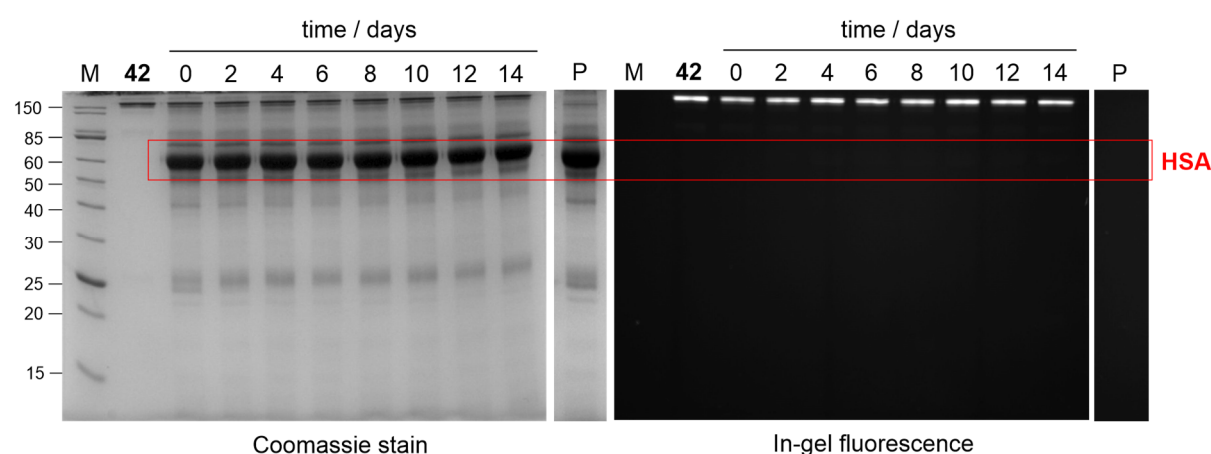


Figure 38: Stability analysis of AFC **42** in human plasma by SDS-PAGE. Lanes: M = molecular weight marker, P = human plasma, days of incubation are depicted above the representative lane. Left gel is after Coomassie staining, right gel is in-gel fluorescence measured before staining. No transfer of AlexaFluor™ 488 to human serum albumin (66.5 kDa, indicated by the red box) or any other plasma proteins was observed over the 14-day incubation period.

To gather additional evidence for the stability of TetraDVP conjugates, AFCs **43**, **44** and **46** were subjected to the same conditions. All conjugates yielded comparable results, with no fluorescence transfer observed over 14 days of incubation in human plasma (Figure 39).

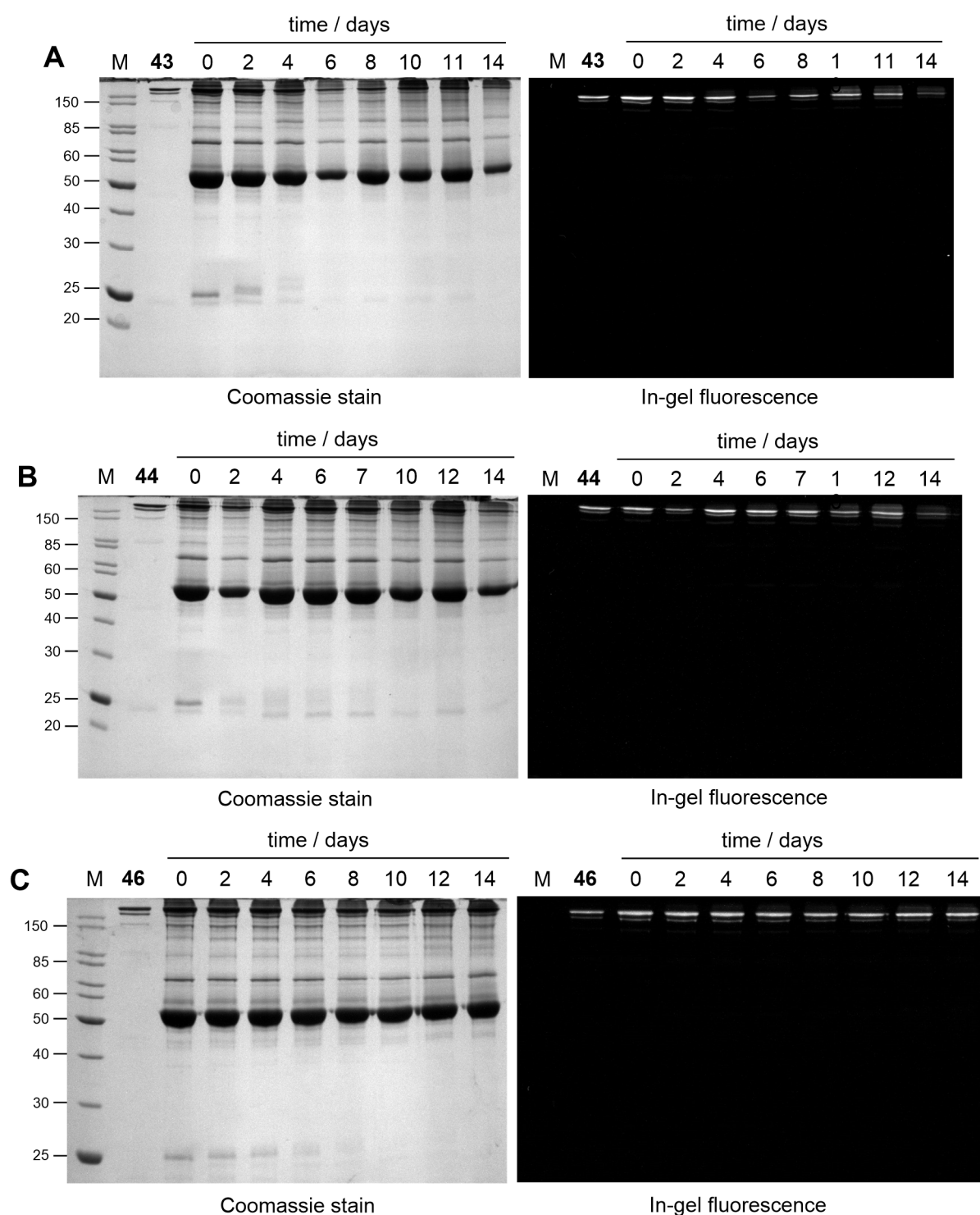


Figure 39: Stability analysis of AFCs (A) **43**, (B) **44** and (C) **46** in human plasma by SDS-PAGE. Lanes: M = molecular weight marker, days of incubation are depicted above the representative lane. Left gel is after Coomassie staining, right gel is in-gel fluorescence measured before staining. No transfer of AlexaFluor™ 488 to human serum albumin or any other plasma proteins was observed over the 14-day incubation period.

These results confirm the exquisite stability of the TetraDVP linker system and inspired further investigations into the biological profile of TetraDVP conjugates.

4.5.2 Aggregation

Modification of antibodies with hydrophobic entities – such as ADC linkers and payloads – has the potential to induce aggregation. This can be detrimental to clinical ADC development, as the presence of aggregates not only reduces the antibody's half-life and biological activity, but may also cause an immunogenic response in patients.^{89,206} Thus, the effect of TetraDVP linkers on aggregation was investigated.

Size-exclusion chromatography (SEC) – also known as gel filtration – is a commonly used method for the quantification of protein aggregates. SEC separates molecules by differences in size as they pass through a resin packed in a column, thus allowing the separation of high molecular weight species (HMWS) and monomeric antibody in an antibody conjugate.²⁰⁷

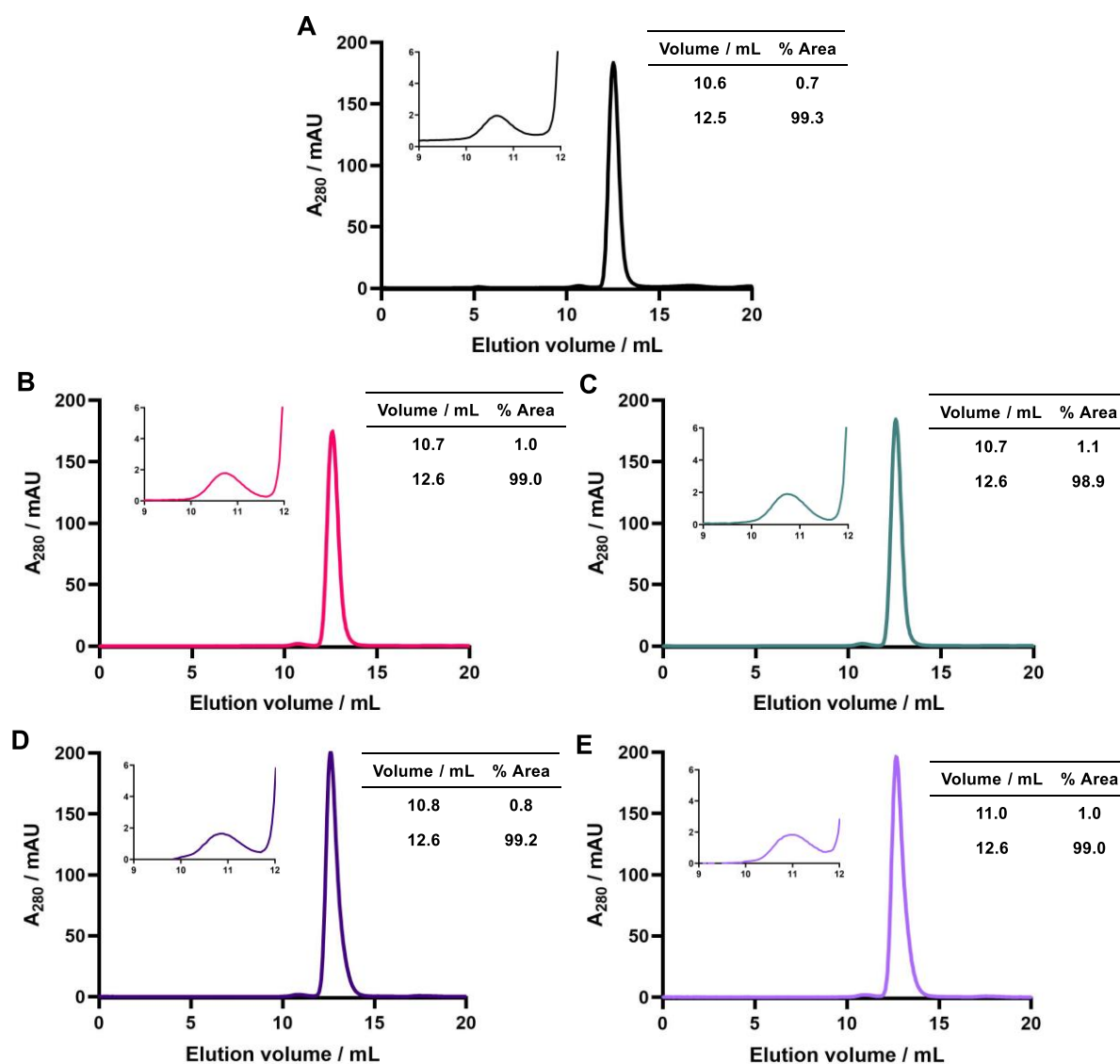


Figure 40: SEC analysis of (A) trastuzumab, (B) ALC 37, (C) ALC 38, (D) ALC 39 and (E) ALC 41.

Accordingly, unmodified trastuzumab and ALCs **37**, **38**, **39** and **41** were analysed by SEC (Figure 40). This analysis was carried out with Teodors Pantelejevs and Matthew Ratcliff. Gratifyingly, all conjugates displayed a comparable level of HMWS (~1%) to native trastuzumab, indicating that TetraDVPs do not induce protein aggregation.

4.5.3 Binding affinity

Having confirmed the exquisite stability and favourable aggregation profile of TetraDVP conjugates, the effect of TetraDVP modification on the binding affinity of trastuzumab for its native antigen – the cell surface receptor HER2 – was investigated.

To determine the binding affinity of TetraDVP conjugates **37**, **38**, **39** and **41** relative to that of the unmodified antibody, an enzyme-linked immunosorbent assay (ELISA) carried out. Encouragingly, no significant difference in HER2 binding affinity was observed between any of the conjugates and unmodified trastuzumab (Figure 41). These results suggest that the modification with TetraDVP linkers does not interfere with antigen recognition.

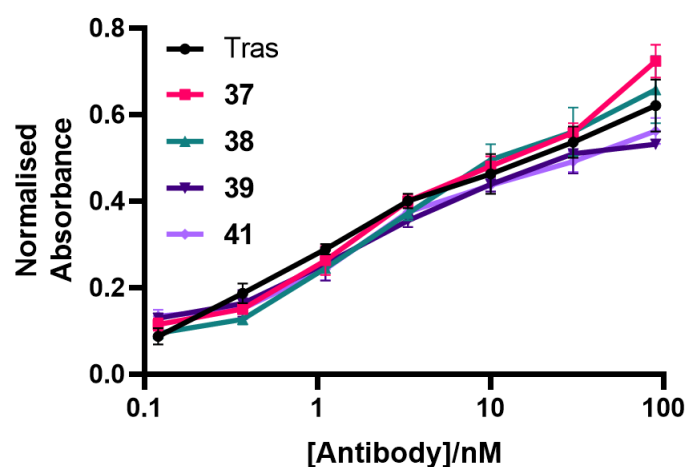


Figure 41: HER2 binding affinity comparison of trastuzumab and ALCs **37**, **38**, **39** and **41** by ELISA. All conjugates display concentration-dependant binding to HER2. Tras = trastuzumab. Error bars represent the standard deviation of biological quadruplicates.

4.5.4 Cellular selectivity

Having confirmed that TetraDVP conjugates retain the antigen binding affinity of the parent antibody, it was investigated if this favourable affinity profile translates to selective targeting of antigen-positive cells *in vitro*. For this purpose, one HER2-positive cell line (SKBR3) and one HER2-negative cell line (MCF7) were chosen. Both SKBR3 and MCF7 are human breast cancer cell lines with widespread use in cancer research.²⁰⁸

To establish if TetraDVP conjugates selectively target the HER2-positive cell line, a live cell microscopy experiment was devised. SKBR3 and MCF7 cells were incubated with fluorescent conjugates **42** or **43**, trastuzumab or vehicle control (PBS) for 1 hour at 4 °C and then washed to remove unbound antibody. The cells were then incubated at 37 °C for a further 3 hours, followed by confocal microscopy imaging. This experiment was carried out with Dr Stephen J. Walsh.

The obtained images revealed high levels of labelling with **42** and **43** in HER2-positive SKBR3 cells. In contrast, no fluorescent signal was observed for the HER2-negative MCF7 cell line (Figure 42), thus confirming the excellent cellular selectivity of TetraDVP conjugates for HER2-positive over HER2-negative cells.

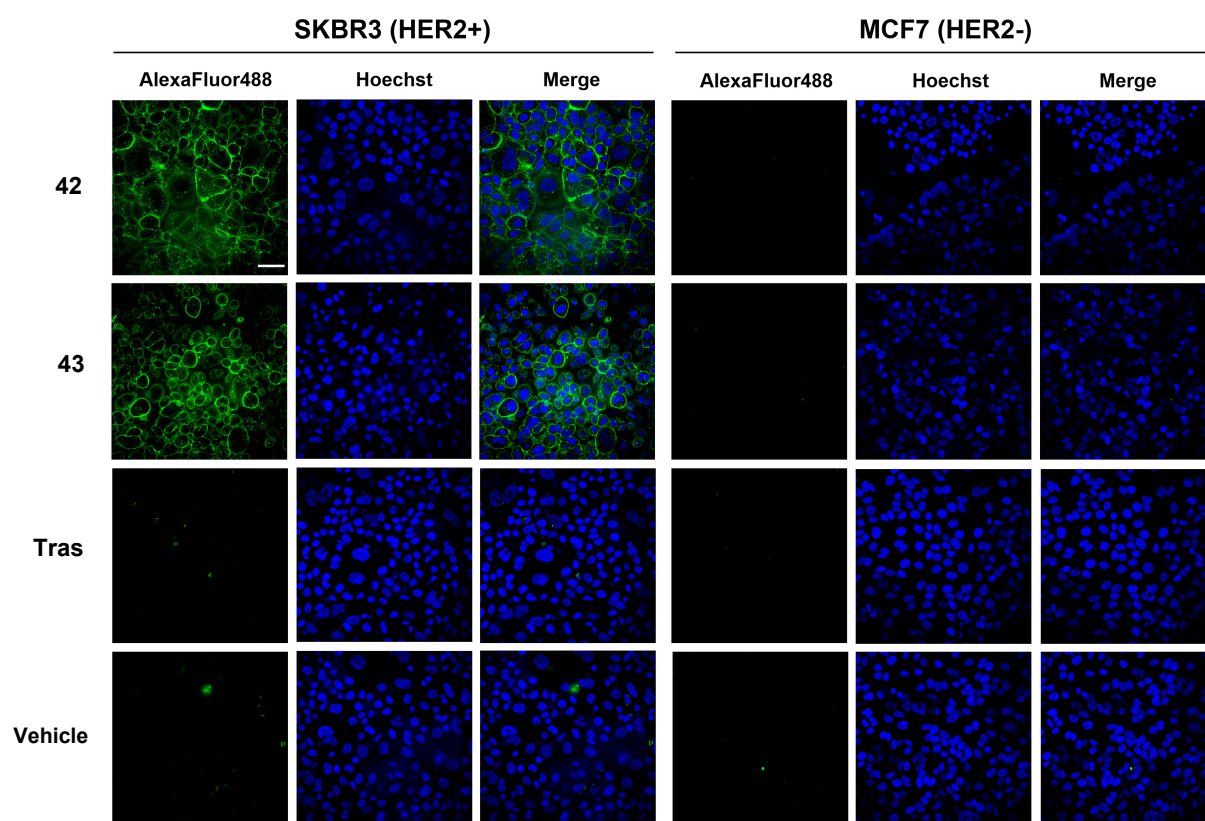


Figure 42: Live cell microscopy images of HER2-positive SKBR3 cells and HER2-negative MCF7 cells after treatment with AFCs **42** or **43**, trastuzumab or vehicle control. Scale bar represents 50 µm.

These results – in combination with the favourable results obtained regarding conjugate stability, aggregation, and binding affinity – provided a strong basis for the investigation of TetraDVPs for the generation of biologically active ADCs.

In the first instance, ALC **37** was reacted with 24 equivalents of payload **47** in the presence of $\text{CuSO}_4 \cdot 5\text{H}_2\text{O}$, THPTA and sodium ascorbate in 10% DMSO/PBS at 37 °C for 6 hours to yield ADC **48**.

Attempts to analyse ADC **48** by LC-MS were unsuccessful due to insufficient resolution. This lack of resolution can likely be attributed to the large size of the conjugate (~148 kDa in deglycosylated form), which approaches the detection limit of the available LC-MS equipment. Therefore, native MS was investigated as an alternative method for ADC analysis. Native MS is a type of mass spectrometry performed under non-denaturing conditions and ideally suited for the analysis of large biomolecules such as ADCs, which may be challenging to analyse using classical denaturing LC-MS techniques.^{125,209} Native MS analysis of ADC **48** revealed the presence of two different antibody species, the masses of which approximated those of the starting material – ALC **37** – and the expected product containing one MMAE payload (Figure 44). The two species appeared to be present in a 1:1 ratio, indicating approximately 50% conversion for the CuAAC reaction.

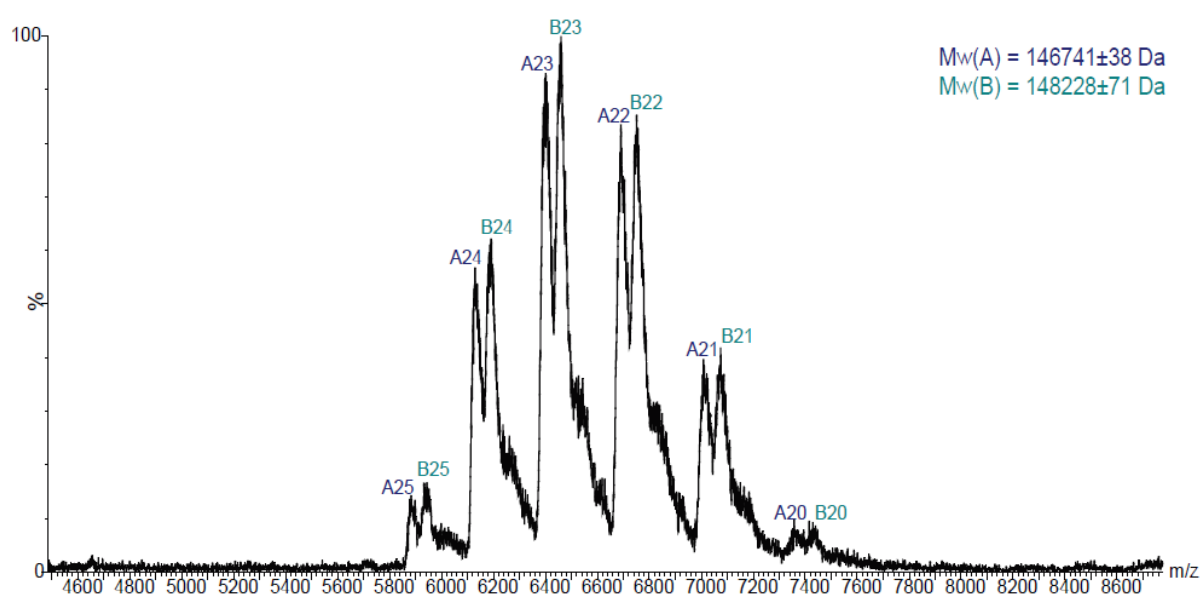


Figure 44: Analysis of the reaction of ALC **37** with payload **47** by native MS. Expected 146,536 Da (starting material) and 147,919 Da (product), observed 146,741 Da and 148,228 Da.

Having ascertained that the initial CuAAC reaction of ALC **37** with payload **47** did not go to completion, it became clear that further reaction optimisation would be required. While native MS gave valuable insight into the composition of ADC **47**, it is a very time-consuming technique, thereby making it unfit for extended optimisation processes. Consequently, an

alternative analytical method based on hydrophobic interaction chromatography (HIC) was devised.

HIC is a chromatographic technique used for the characterisation of ADCs through the separation of different ADC components based on their hydrophobicity. Since most ADC payloads are hydrophobic, their attachment to an antibody increases the hydrophobicity of the latter. This change is proportional to the number of payload molecules attached to the antibody, thus allowing the separation of different ADC populations with varying DAR by HIC.^{210–212} The method by which HIC separates the different ADC species is based on the principle of proteins precipitating in high salt buffers due to the loss of their hydration shell. The precipitated proteins associate with the nonpolar column matrix through non-covalent interactions – the strength of which is proportional to the net hydrophobicity of the protein – and can subsequently be eluted in the order of least hydrophobic to most hydrophobic by treatment with a linear gradient of a low salt buffer.²¹³

Accordingly, HIC analysis of ADC **48** and its precursor ALC **37** was carried out using a linear gradient of solvent B in solvent A, where solvent A is 1.5 M $(\text{NH}_4)_2\text{SO}_4$ in 25 mM NaPi and solvent B is 25% isopropyl alcohol (IPA) in 25 mM NaPi. The HIC trace of ADC **48** confirmed the presence of two distinct antibody species – corresponding to the DAR 0 and DAR 1 conjugates – as previously indicated by native MS analysis (Figure 45). The two species appeared to be present in a 45:55 ratio, corresponding to an average DAR of 0.6 for ADC **48** (Table 6, Entry 1).

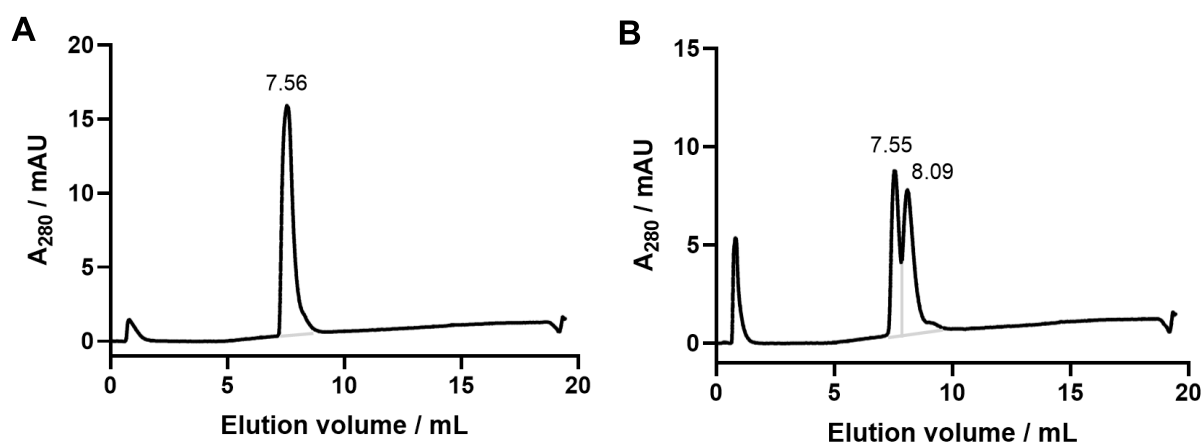


Figure 45: Example HIC traces of (A) ALC **37** and (B) ADC **48** obtained at a 0-100% gradient of Buffer B [25% IPA/NaPi (25 mM, pH 7)] in Buffer A [1.5 M $(\text{NH}_4)_2\text{SO}_4$, 25 mM NaPi (pH 7)].

Having developed a suitable analytical technique to quantify the conversion of post-conjugation CuAAC reactions with MMAE payloads, optimisation of the CuAAC of ALC **37** with payload **47** was attempted by adjustment of reagent stoichiometry (Table 6, Entries 2-3). However, even in the presence of 100 equivalents of azide **47**, no increase in conversion was observed.

Table 6: Optimisation of the CuAAC of ALC **37** with N₃-PEG₄-Val-Cit-PABC-MMAE **47**.

Entry	ALC	Reagents (equivalents)	Reaction time / h	Product	DAR
1	37	N ₃ -PEG ₄ -Val-Cit-PABC-MMAE 47 (24) CuSO ₄ •5H ₂ O (40) THPTA (200) NaAsc (300)	6	48	0.6
2	37	N ₃ -PEG ₄ -Val-Cit-PABC-MMAE 47 (48) CuSO ₄ •5H ₂ O (40) THPTA (200) NaAsc (300)	6	48	0.6
3	37	N ₃ -PEG ₄ -Val-Cit-PABC-MMAE 47 (100) CuSO ₄ •5H ₂ O (150) THPTA (600) NaAsc (1000)	7	48	0.6

To ascertain if the observed lack of reactivity regarding the CuAAC with payload **47** is specific to ALC **37**, the modification of ALCs **38**, **39** and **41** was attempted. Accordingly, the ALCs were reacted with 100 equivalents of payload **47** in the presence of CuSO₄•5H₂O, THPTA and sodium ascorbate in 10% DMSO/PBS at 37 °C for 7 hours to yield ADCs **49**, **50** and **51** (Figure 46).

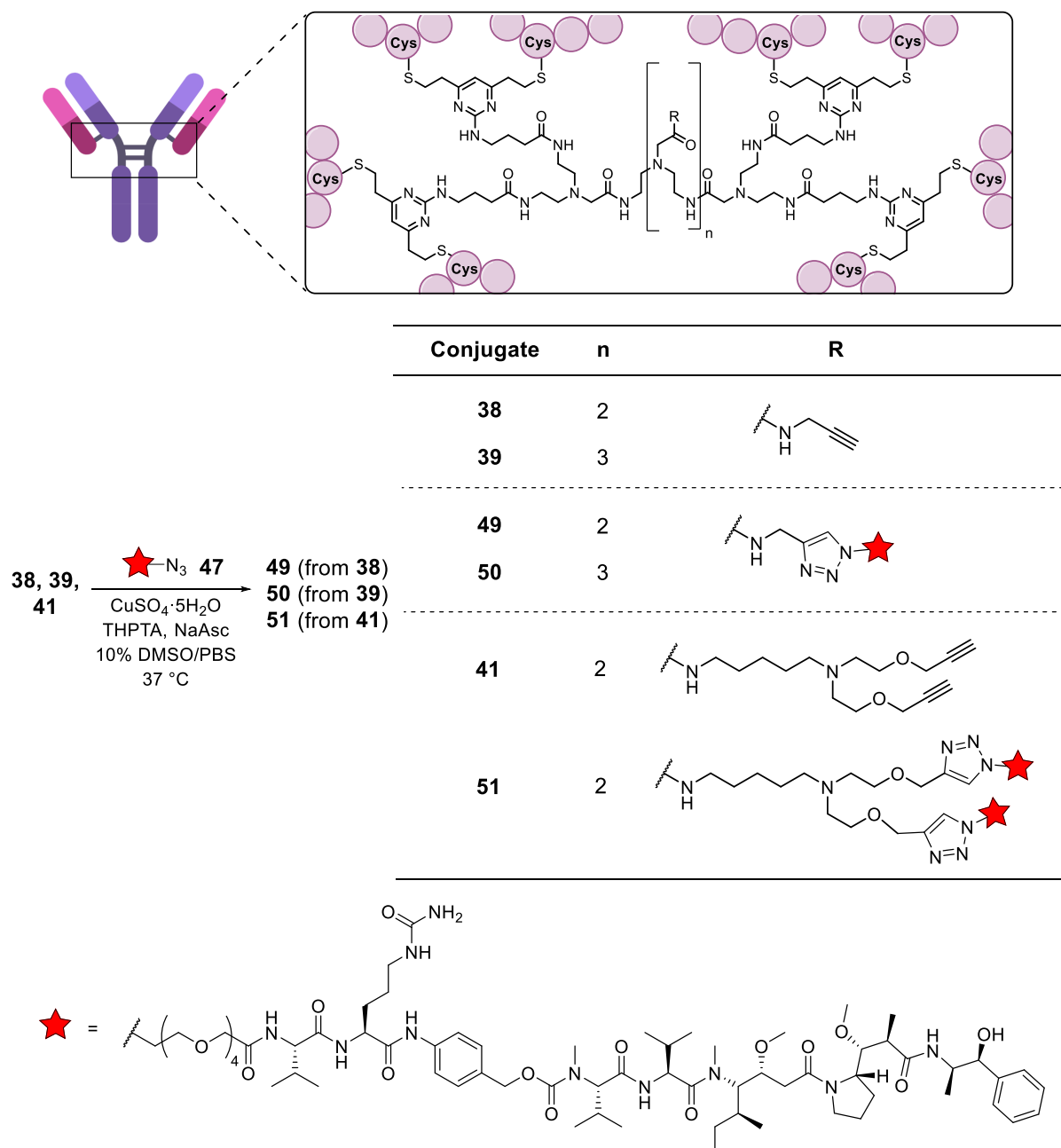


Figure 46: Structures of ALCs **38**, **39** and **41** and ADCs **49-51**.

As ALCs **38**, **39** and **41** contain two, three and four alkyne handles, they should theoretically yield ADCs with DARs of 2.0, 3.0 and 4.0, respectively. However, analysis of the reactions by HIC revealed all three ADCs to be composed of a mixture of ADC populations with varying DAR. This composition resulted in measured average DAR values of 1.0, 1.6 and 2.5 for ADCs **49**, **50** and **51**, respectively (Table 7). In the case of ADC **49**, the desired DAR 2 species accounted for 27% of the total composition, while for ADC **50** the desired DAR 3 species

constituted 16%. For ADC **51**, the desired DAR 4 species accounted for 21% of all antibody species. These results indicate the lack of observed CuAAC reactivity is not specific to ALC **37**.

Table 7: CuAAC reactions of ALCs **38**, **39** and **41** with N₃-PEG₄-Val-Cit-PABC-MMAE **47**.

Entry	ALC	Reagents (equivalents)	Reaction time / h	Product	DAR
1	38	N ₃ -PEG ₄ -Val-Cit-PABC-MMAE 47 (100) CuSO ₄ •5H ₂ O (150) THPTA (600) NaAsc (1000)	7	49	1.0
2	39	N ₃ -PEG ₄ -Val-Cit-PABC-MMAE 47 (100) CuSO ₄ •5H ₂ O (150) THPTA (600) NaAsc (1000)	7	50	1.6
3	41	N ₃ -PEG ₄ -Val-Cit-PABC-MMAE 47 (100) CuSO ₄ •5H ₂ O (150) THPTA (600) NaAsc (1000)	7	51	2.5

Considering that all four TetraDVP ALCs (**37**, **38**, **39** and **41**) displayed excellent reactivity in the CuAAC with AlexaFluor™ 488 azide, it was hypothesised that the poor reactivity observed for the functionalisation with MMAE may be due to the nature of the selected payload **47**. Therefore, a number of alternative payloads were investigated. The following chapters contain an overview of these investigations.

4.6.1.2 N₃-PEG₂₄-Val-Cit-PABC-MMAE

It was hypothesised that the poor reactivity of N₃-PEG₄-Val-Cit-PABC-MMAE **47** may be due to insufficient aqueous solubility, as precipitation was observed in all reactions carried out with this payload. Therefore, it was speculated that the use of a payload with improved solubility might increase the conversion of the CuAAC reaction.

A common way of increasing the aqueous solubility of ADC linker-payloads is the incorporation of extended PEG chains.^{179,214} Accordingly, N₃-PEG₂₄-Val-Cit-PABC-MMAE **52** – containing 20 additional PEG spacers relative to payload **47** – was investigated as an alternative payload for the functionalisation of TetraDVP conjugates. Accordingly, ALCs **37** and **38** were reacted with 100 equivalents of N₃-PEG₂₄-Val-Cit-PABC-MMAE **52** (synthesised by Dr Stephen J. Walsh) in the presence of CuSO₄•5H₂O, THPTA and sodium ascorbate to yield ADCs **53** and **54** (Figure 47).

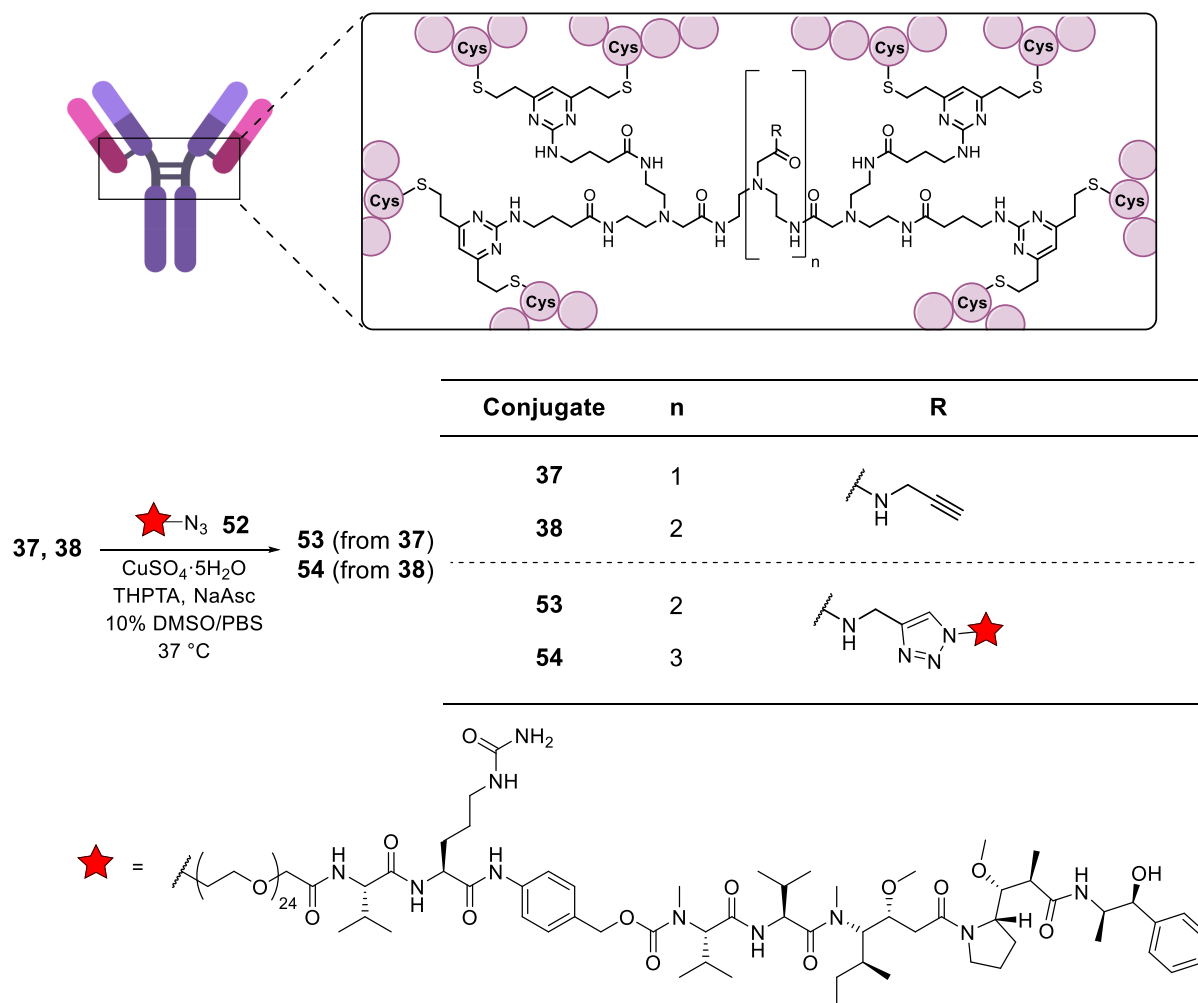


Figure 47: Reaction of ALCs **37** and **38** with N₃-PEG₂₄-Val-Cit-PABC-MMAE **52** to yield ADCs **53** and **54**.

The additional PEG spacers indeed appeared to improve the aqueous solubility of the payload as observed by lower levels of payload precipitation in 10% DMSO/PBS. However, despite this, poor conversion was observed. In fact, the reactivity of N₃-PEG₂₄-Val-Cit-PABC-MMAE **52** appeared to be lower than that of N₃-PEG₄-Val-Cit-PABC-MMAE **47**, with DAR values of 0.1 and 0.3 measured for ADCs **53** and **54** (Table 8).

Table 8: Reaction conditions for CuAAC reactions of ALCs **37** and **38** with N₃-PEG₂₄-Val-Cit-PABC-MMAE **52**.

Entry	ALC	Reagents (equivalents)	Reaction time / h	Product	DAR
1	37	N ₃ -PEG ₂₄ -Val-Cit-PABC-MMAE 52 (100) CuSO ₄ ·5H ₂ O (150) THPTA (600) NaAsc (1000)	7	53	0.1
2	38	N ₃ -PEG ₂₄ -Val-Cit-PABC-MMAE 52 (100) CuSO ₄ ·5H ₂ O (150) THPTA (600) NaAsc (1000)	7	54	0.3

It is possible that the extended PEG chain component of payload **52** increases steric hindrance around the azide group, thus restricting its participation in CuAAC reactions.

4.6.1.3 *N₃-PEG₄-Glu₂-PEG₂-Val-Cit-PABC-MMAE*

In addition to PEGylation, strategies for improving aqueous solubility of ADC linkers commonly involve the incorporation of anionic functional groups, such as carboxylic acids, sulfites or phosphate groups.^{102,215,216} Therefore, *N₃-PEG₄-Glu₂-PEG₂-Val-Cit-PABC-MMAE* **55** was investigated as an alternative payload for the functionalisation of TetraDVP ALCs. Payload **55** (synthesised by Dr Stephen J. Walsh) contains two glutamate residues, which are negatively charged at physiological pH, thus improving the overall aqueous solubility of the payload.

Reaction of 100 equivalents of *N₃-PEG₄-Glu₂-PEG₂-Val-Cit-PABC-MMAE* **55** with ALCs **37**, **38**, **39** and **41** was carried out in the presence of CuSO₄·5H₂O, THPTA and sodium ascorbate to yield ADCs **56-59** (Figure 48).

The ADCs were analysed by HIC, revealing average DAR values of 0.7, 1.6, 1.9 and 3.0 for ADCs **56**, **57**, **58** and **59**, respectively (Table 9, Entries 1-4). These results show that an improvement in CuAAC conversion can be attained by using *N₃-PEG₄-Glu₂-PEG₂-Val-Cit-PABC-MMAE* **55** instead of the original payload, *N₃-PEG₄-Val-Cit-PABC-MMAE* **47**, thus confirming that improvements in payload solubility have the potential to improve CuAAC reactivity. Nonetheless, none of the reactions with payload **55** went to competition, suggesting that further optimisation is required.

To assess if adjustments of reagent stoichiometry could push the reaction to competition, ALCs **39** and **41** were reacted with 200 equivalents of *N₃-PEG₄-Glu₂-PEG₂-Val-Cit-PABC-MMAE* **55** in the presence of CuSO₄·5H₂O, THPTA and sodium ascorbate. The reaction of ALC **39** with payload **55** yielded an ADC with an increased DAR of 2.3, indicating that increasingly forcing conditions can indeed lead to improved CuAAC conversion (Table 9, Entry 5). In contrast, the reaction of ALC **41** with 200 equivalents of payload **55** did not result in an increase in DAR compared to the previous reaction with 100 equivalents of payload **55** (Table 9, Entry 6). These results indicate that forcing conditions are not beneficial in all cases, and that further linker and/or payload optimisation will be required to achieve consistently good conversion in the CuAAC reaction.

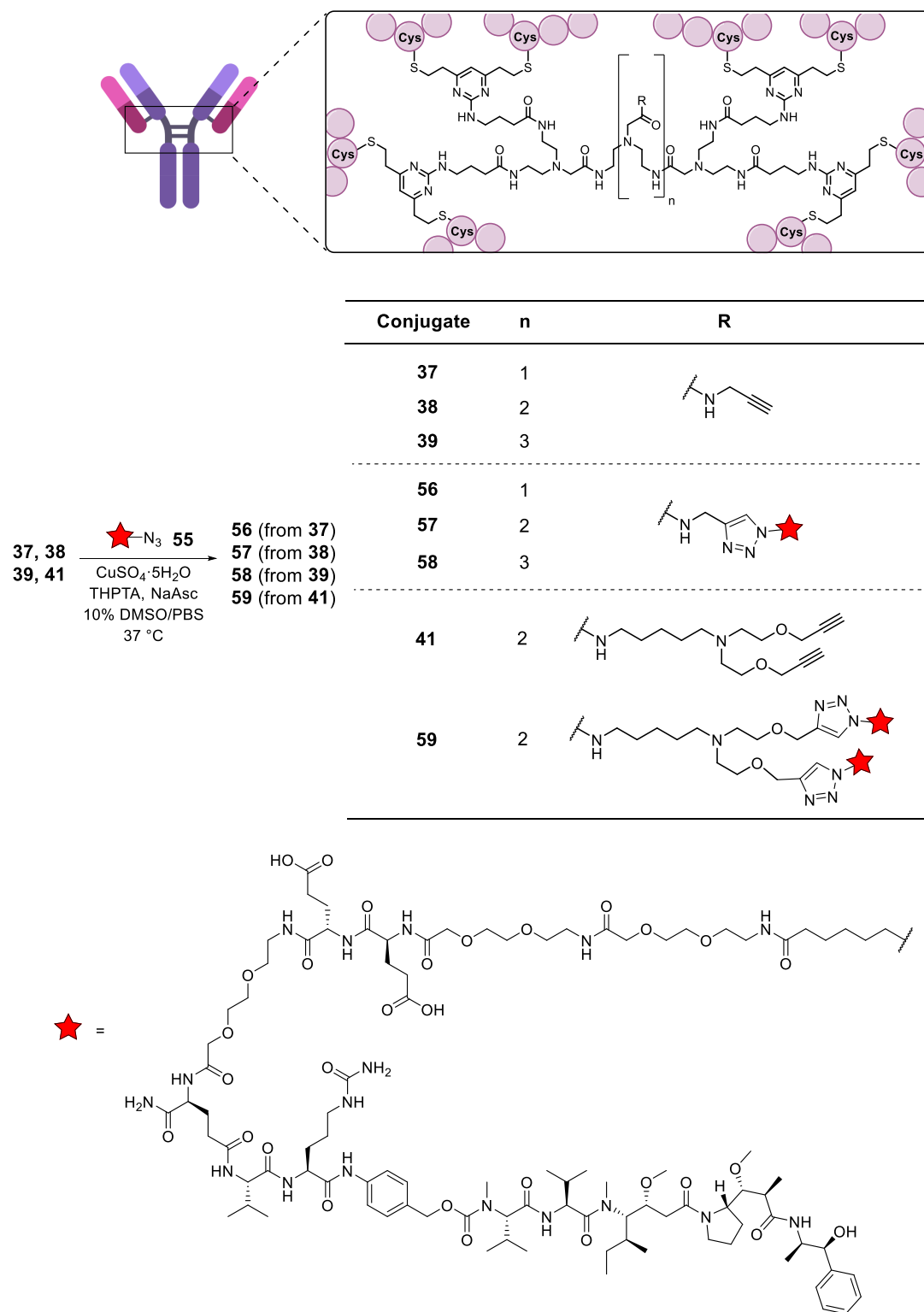


Figure 48: Reaction of TetraDVP ALCs **37**, **38**, **39** and **41** with N₃-PEG₄-Glu₂-PEG₂-Val-Cit-PABC-MMAE **55**.

Table 9: Reaction conditions and outcomes of CuAAC reactions of ALCs **37**, **38**, **39** and **41** with N₃-PEG₄-Glu₂-PEG₂-Val-Cit-PABC-MMAE **55**.

Entry	ALC	Reagents (equivalents)	Reaction time / h	Product	DAR
1	37	N ₃ -PEG ₄ -Glu ₂ -PEG ₂ -Val-Cit-PABC-MMAE 55 (100) CuSO ₄ •5H ₂ O (150) THPTA (600) NaAsc (1000)	7	56	0.7
2	38	N ₃ -PEG ₄ -Glu ₂ -PEG ₂ -Val-Cit-PABC-MMAE 55 (100) CuSO ₄ •5H ₂ O (150) THPTA (600) NaAsc (1000)	7	57	1.6
3	39	N ₃ -PEG ₄ -Glu ₂ -PEG ₂ -Val-Cit-PABC-MMAE 55 (100) CuSO ₄ •5H ₂ O (150) THPTA (600) NaAsc (1000)	7	58	1.9
4	41	N ₃ -PEG ₄ -Glu ₂ -PEG ₂ -Val-Cit-PABC-MMAE 55 (100) CuSO ₄ •5H ₂ O (150) THPTA (600) NaAsc (1000)	7	59	3.0
5	39	N ₃ -PEG ₄ -Glu ₂ -PEG ₂ -Val-Cit-PABC-MMAE 55 (200) CuSO ₄ •5H ₂ O (300) THPTA (1200) NaAsc (2000)	7	58	2.3
6	41	N ₃ -PEG ₄ -Glu ₂ -PEG ₂ -Val-Cit-PABC-MMAE 55 (200) CuSO ₄ •5H ₂ O (300) THPTA (1200) NaAsc (2000)	7	59	3.0

4.6.1.4 N₃-PEG₄-MMAE

In light of the dissatisfactory results obtained for the CuAAC of TetraDVP ALCs with cathepsin-cleavable Val-Cit-PABC-MMAE payloads **47**, **52** and **55**, the functionalisation of TetraDVP conjugates with a non-cleavable MMAE payload was attempted. N₃-PEG₄-MMAE **60** was chosen as a suitable payload for this purpose. The cleavable Val-Cit motif is one of primary causes of the low aqueous solubility of cathepsin-cleavable MMAE payloads.^{41,217} Therefore, it was postulated that the removal of this functionality should yield a payload with improved solubility, even without the addition of extended PEG chains or anionic functional groups. Furthermore, it was hypothesised that the smaller size of the payload compared to cleavable payloads **47**, **52** and **55** might alleviate issues with steric hindrance.

Reaction of 100 equivalents of N₃-PEG₄-MMAE **60** (synthesised by Dr Stephen J. Walsh) with ALCs **37**, **38**, **39** and **41** was carried out in the presence of CuSO₄·5H₂O, THPTA and sodium ascorbate to yield ADCs **61-64** (Figure 49).

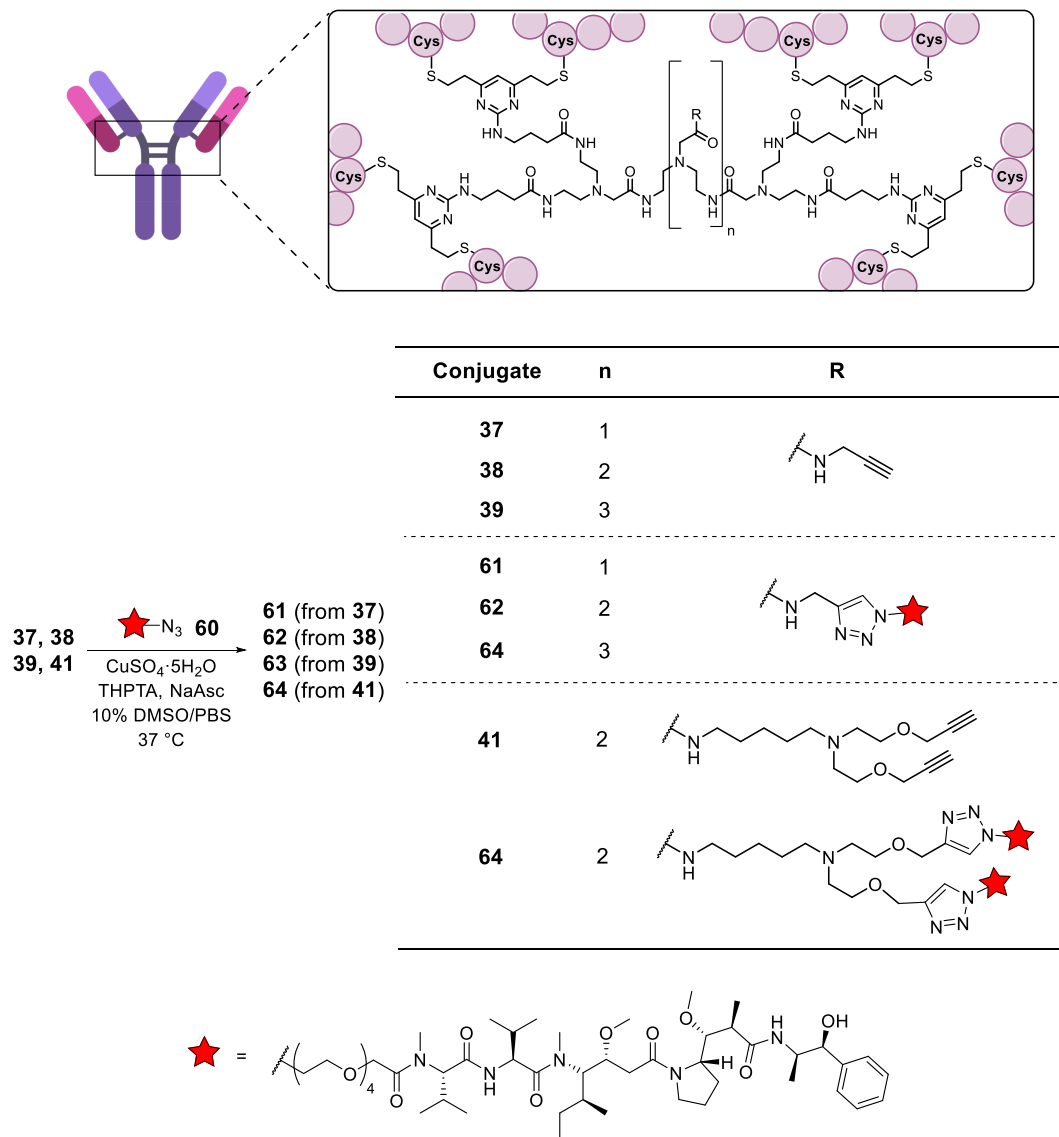


Figure 49: Reaction of TetraDVP ALCs **37**, **38**, **39** and **41** with N₃-PEG₄-MMAE **60**.

HIC analysis enabled the measurement of average DAR values of 0.8, 1.6, 2.1 and 2.8 for ADCs **61**, **62**, **63** and **64**, respectively (Table 10). These results represent an improvement over the conversion achieved with N₃-PEG₄-Val-Cit-PABC-MMAE **47**, but no significant improvement over N₃-PEG₄-Glu₂-PEG₂-Val-Cit-PABC-MMAE **55**.

Table 10: Reaction conditions and outcomes of CuAAC reactions of ALCs **37**, **38**, **39** and **41** with N₃-PEG₄-MMAE **60**.

Entry	ALC	Reagents (equivalents)	Reaction time / h	Product	DAR
1	37	N ₃ -PEG ₄ -MMAE 60 (100) CuSO ₄ •5H ₂ O (150) THPTA (600) NaAsc (1000)	7	61	0.8
2	38	N ₃ -PEG ₄ -MMAE 60 (100) CuSO ₄ •5H ₂ O (150) THPTA (600) NaAsc (1000)	7	62	1.6
3	39	N ₃ -PEG ₄ -MMAE 60 (100) CuSO ₄ •5H ₂ O (150) THPTA (600) NaAsc (1000)	7	63	2.1
4	41	N ₃ -PEG ₄ -MMAE 60 (100) CuSO ₄ •5H ₂ O (150) THPTA (600) NaAsc (1000)	7	64	2.8

The results presented herein show that the functionalisation of TetraDVP conjugates with cleavable and non-cleavable MMAE payloads is possible, and that the DAR of the resulting ADCs correlates with the number of alkyne moieties introduced onto the antibody. However, further optimisation is required to achieve complete conversion for the post-conjugation CuAAC reaction and generate fully homogenous ADCs. Changes in the size and/or solubility of the MMAE payload were shown to affect CuAAC conversion to a certain degree but are unlikely to be sufficient to achieve full conversion. Therefore, to meet the objective of generating fully homogenous ADCs using TetraDVPs, more significant adjustments of the methodology may be required.

4.6.2 Post-conjugation functionalisation with SN-38

Considering the moderate conversion observed regarding the generation of TetraDVP ADCs with MMAE payloads, the use of an alternative payload was investigated. For this purpose, the topoisomerase inhibitor 7-ethyl-10-hydroxycamptothecin – more commonly known as SN-38 – was chosen.

SN-38 is a synthetic analogue of the natural product camptothecin and has found extensive use in ADC development in recent years – most notably as the payload of the FDA-approved ADC Trodelvy®. Compared to MMAE, SN-38 is approximately 100-times less potent. Thus, the

preferred DAR for ADCs containing SN-38 is deemed to be around eight.²¹⁸ The reason why SN-38 was chosen as an alternative payload for the functionalisation of TetraDVP conjugates is because of its small size: SN-38 has the lowest molecular weight of all FDA-approved ADC payloads. It was hoped that the compact size of SN-38 might alleviate issues with steric hindrance in the CuAAC reaction.

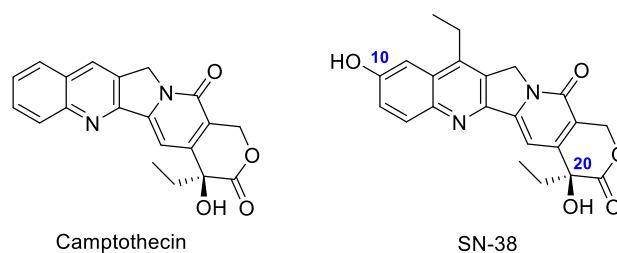
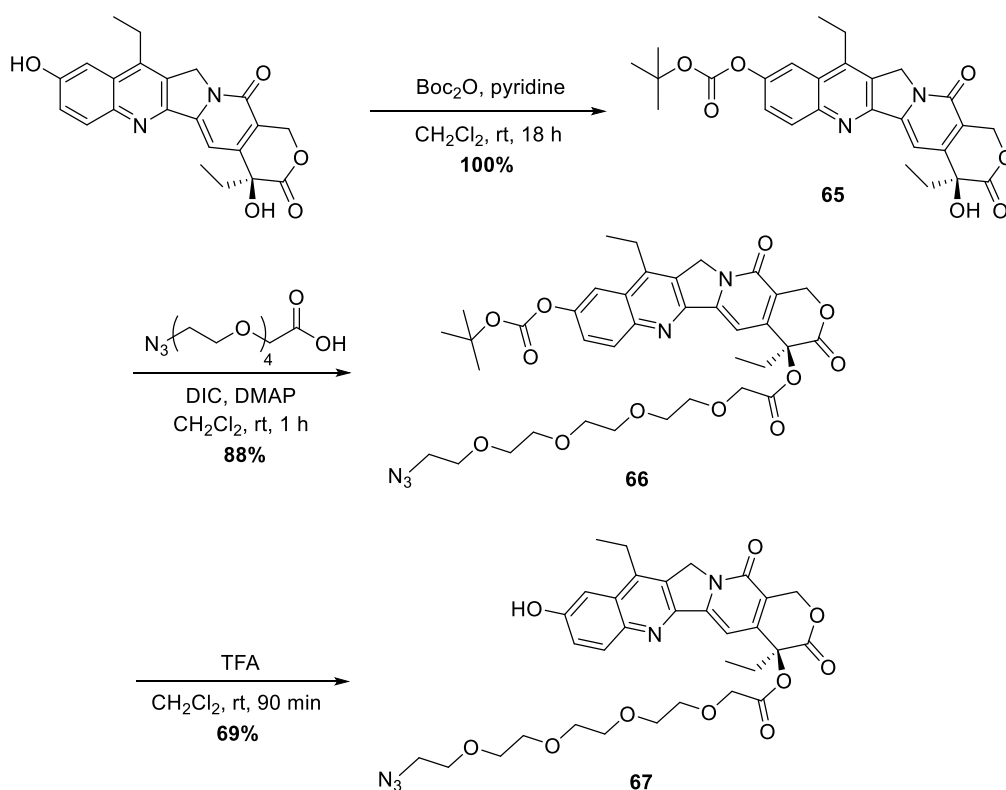


Figure 50: Structures of camptothecin and SN-38. The labelled carbon atoms in SN-38 represent the two most common linker attachment points.

To investigate the modification of TetraDVP conjugates with SN-38, an azide-functionalised analogue of SN-38 needed to be synthesised. Past studies have investigated the functionalisation of SN-38 through the two alcohol groups at C10 and C20 *via* carbonate or ester formation.^{93,219,220} It was found that the phenolic alcohol at C10 is the more reactive of the two alcohols; however, linker attachment at the C20 position is preferable from a pharmacological standpoint, as the resulting linkage is more stable. Furthermore, linker attachment at the C20 position prevents opening of the lactone ring to the inactive carboxylate form. Unmodified SN-38 exists in an pH-dependent equilibrium between the active lactone form and the inactive carboxylate form, the latter of which constitutes approximately 30-40% of the total composition of unmodified SN-38.²²¹ Modification of the C20 position with carbonates or esters significantly reduces the presence of the inactive carboxylate form.²²² Indeed, Trodelvy® is synthesised *via* linker attachment to the C20 position of SN-38.

Based on these findings and a need for high synthetic tractability, azide-functionalised SN-38 **67** was designed and synthesised. Initially, SN-38 was reacted with Boc anhydride to block the C10 position and generate intermediate **65** in quantitative yield. Subsequently, the Boc-protected intermediate was reacted with 14-azido-3,6,9,12-tetraoxatetradecanoic acid (N₃-PEG₃-CO₂H) in the presence of *N,N'*-diisopropylcarbodiimide (DIC) and 4-dimethylaminopyridine (DMAP) to produce azide **66** in good yield. Lastly, *O*-Boc azide **66**

was deprotected using TFA to restore the free alcohol and deliver the azide-functionalised SN-38 payload **67** in 69% yield (Scheme 28).



Scheme 28: Synthesis of azide-functionalised SN-38 payload **67** from SN-38 via Boc protection, ester formation and Boc deprotection.

With the desired payload in hand, the post-conjugation CuAAC with TetraDVP ALCs was attempted. Accordingly, TetraDVP-trastuzumab conjugates **37**, **38**, **39** and **41** were reacted with payload **67** in the presence of $\text{CuSO}_4 \cdot 5\text{H}_2\text{O}$, THPTA and sodium ascorbate to yield ADCs **68-71** (Figure 51).

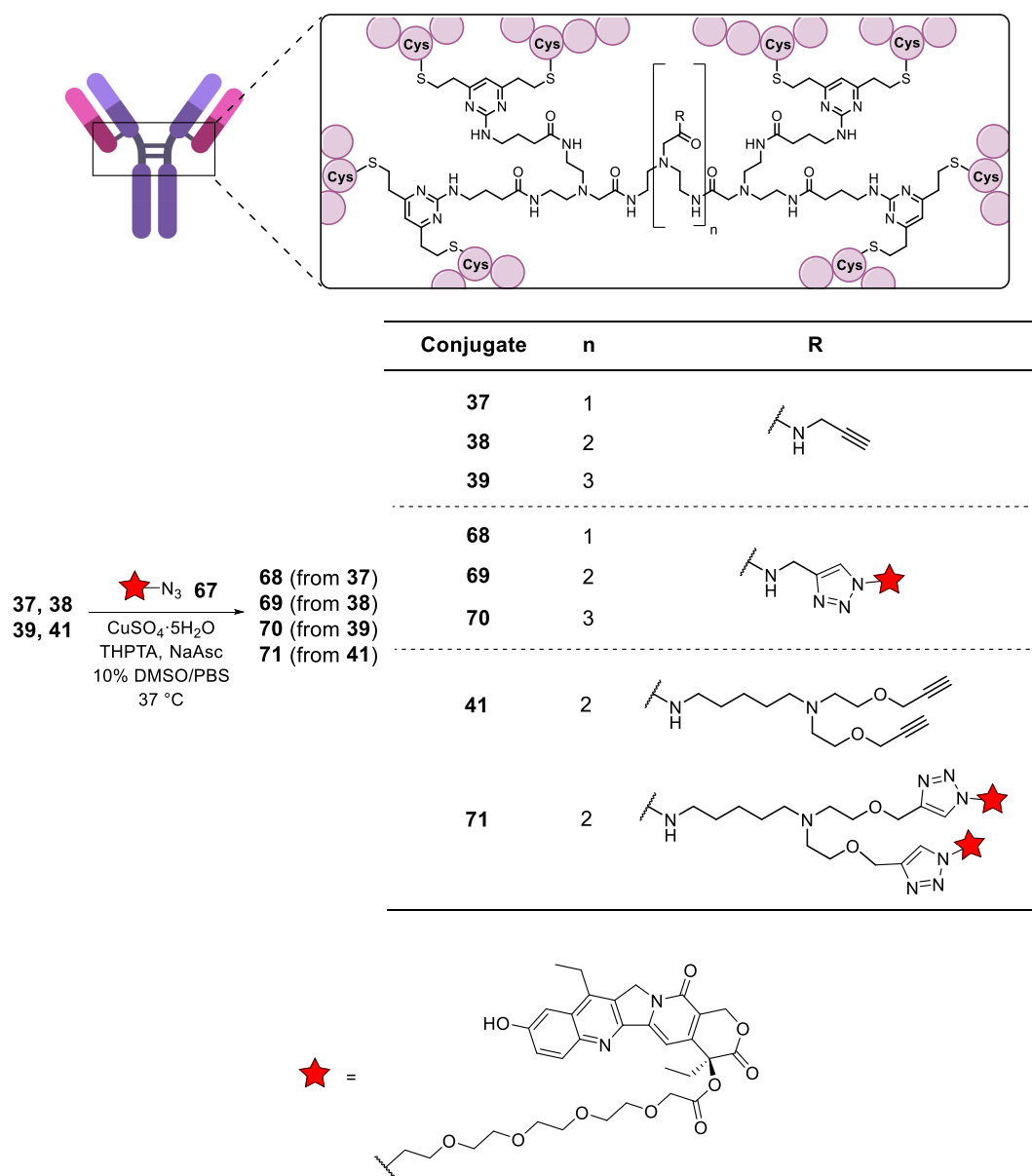


Figure 51: CuAAC reaction of ALCs **37**, **38**, **39** and **41** with SN-38 payload **67**.

To determine the degree of conversion, the ADCs were analysed by HIC. However, accurate DAR values could not be determined due to significant peak overlap (Figure 52). The increased peak broadening and delayed elution time of ADCs **68-71** with respect to their ALC precursors indicates that a reaction has taken place; however, the degree of conversion is unknown.

Despite extensive screening of different buffer systems and gradients, no improvement in peak resolution could be achieved. This suggests that SN-38 payload **67** may not be sufficiently hydrophobic to allow reaction monitoring by HIC.

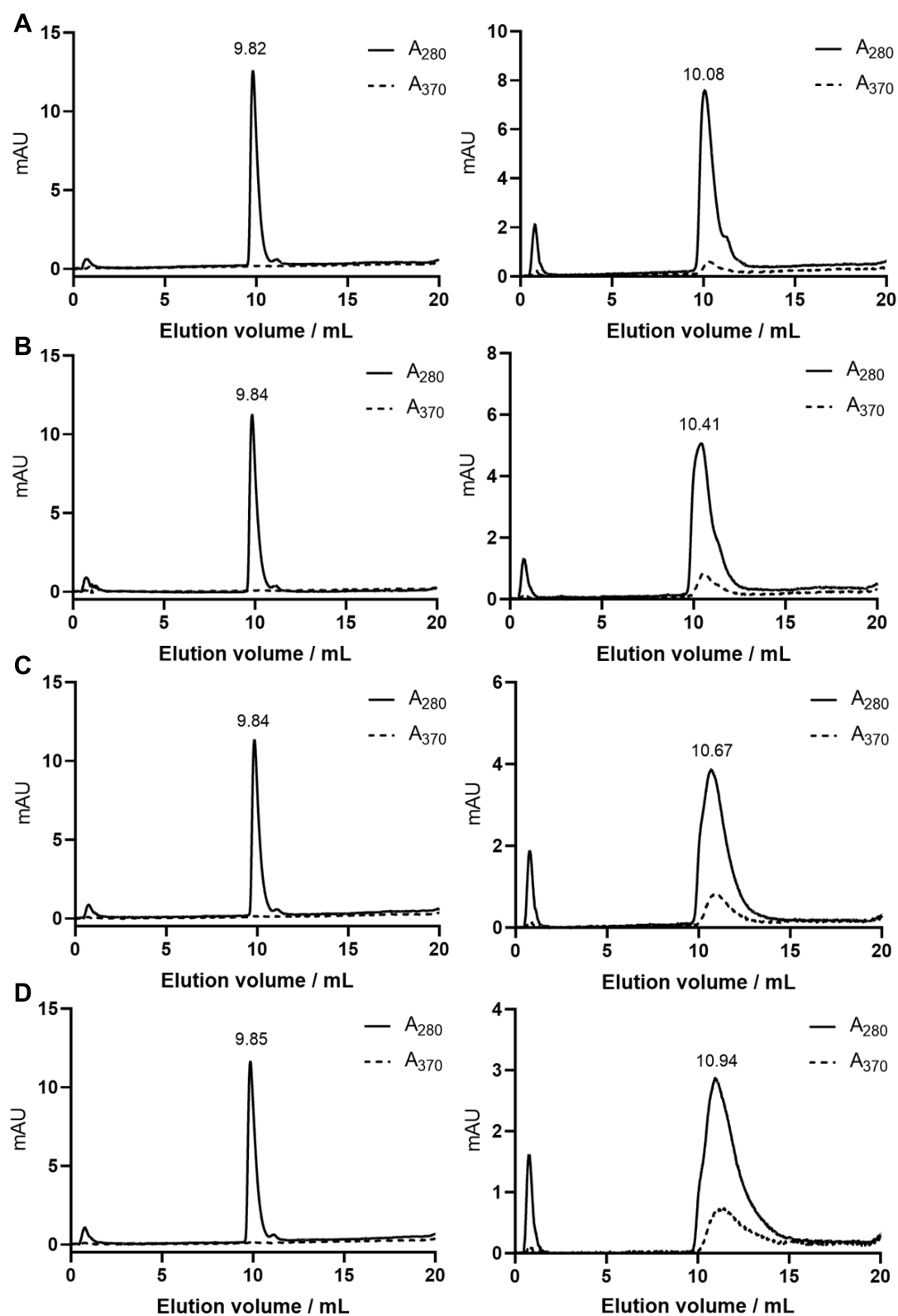


Figure 52: HIC analysis of CuAAC of TetraDVP ALCs with SN-38 **67**. Left panels = ALC starting material. Right panels = Reaction product. (A) Reaction of **67** with ALC **37**. (B) Reaction of **67** with ALC **38**. (C) Reaction of **67** with ALC **39**. (D) Reaction of **67** with ALC **41**.

SN-38 and its analogues are known to weakly absorb light at 370 nm.⁹³ Indeed, multi-wavelength HIC analysis shows absorbance at 370 nm for ADCs **68-71** but not for their precursor ALCs **37, 38, 39** and **41** (Figure 52). Therefore, the use of UV-vis spectrophotometry was investigated as an alternative means of DAR determination.

Encouragingly, UV-vis analysis of ADCs **68-71** showed an increase in the ratio of A_{370} over A_{280} proportional to the number of alkyne handles in the precursor ALC (Figure 53). This indicates that an increased number of alkynes in the precursor ALC does indeed lead to an increased SN-38 loading in the final ADC, as intended.

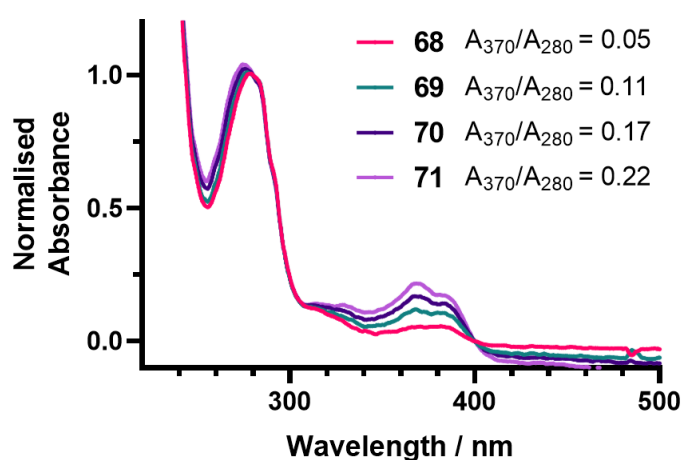


Figure 53: Analysis of SN-38 ADCs by UV-vis spectroscopy.

To accurately determine an average DAR for each ADC from its UV-vis spectrum, an extinction coefficient for SN-38 absorbance at 370 nm and a correction factor for SN-38 absorbance at 280 nm is required. Determination of these factors was attempted by measuring the absorbance of a dilution series of SN-38 in MeCN/H₂O. However, due to the poor aqueous solubility of SN-38, the highest attainable concentration of SN-38 in 20% MeCN/H₂O was 1 mM. Considering the weak absorbance of SN-38, this concentration maximum was insufficiently high to accurately determine an extinction coefficient or a correction factor.

An attempt to assess the composition of ADCs **68-71** by LC-MS proved equally unsuccessful due to insufficient resolution.

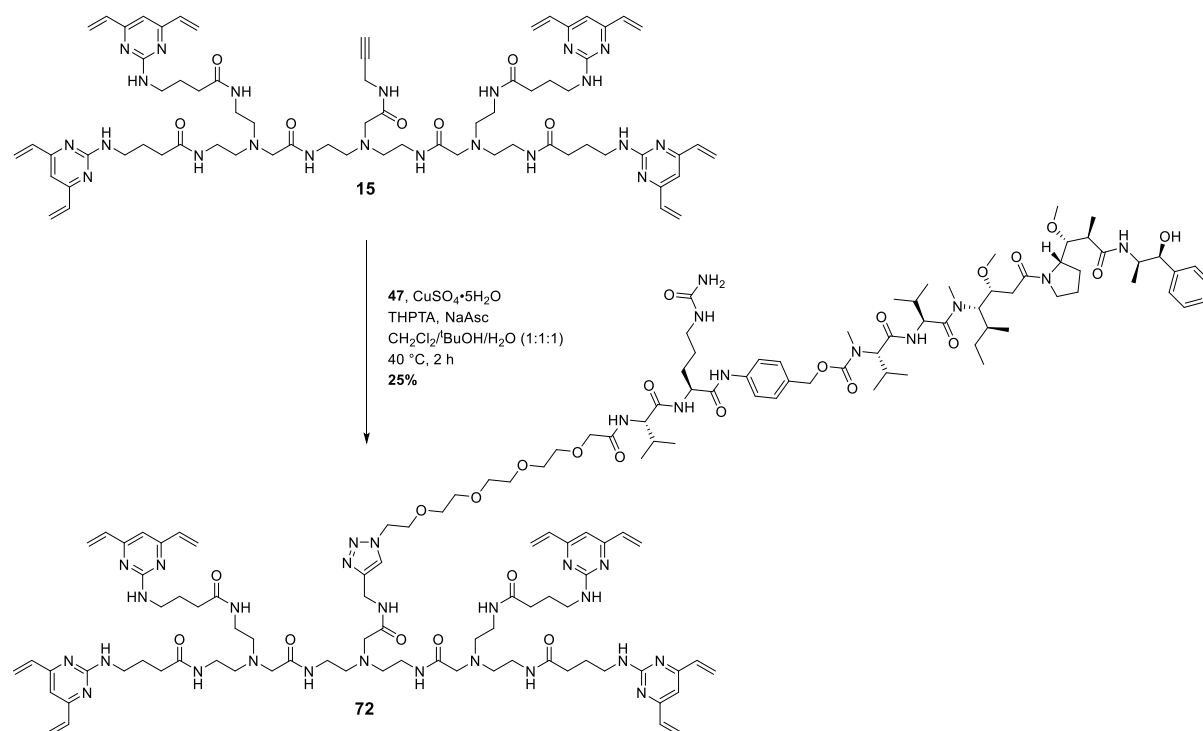
These results show that TetraDVP conjugates have the potential for functionalisation with SN-38 payloads. However, the selected SN-38 payload **67** is not ideal for this purpose as

reactions with this payload are difficult to monitor by any of the established analytical techniques.

4.6.3 Pre-conjugation functionalisation with MMAE

Considering the dissatisfactory conversion obtained for the post-conjugation functionalisation of TetraDVP ALCs with ADC payloads, an attempt was made to change the order of the rebridging and CuAAC steps in a bid to generate fully homogenous TetraDVP ADCs. The conjugation of TetraDVP linkers to trastuzumab generates steric hindrance around the alkyne functionality of the linker, which is likely to be a contributing factor to the poor conversion observed for the post-conjugation CuAAC. Performing the CuAAC reaction prior to bioconjugation may therefore improve reactivity.

Accordingly, TetraDVP **15** – containing a single alkyne handle – was reacted with N₃-PEG₄-Val-Cit-PABC-MMAE **47** in the presence of CuSO₄·5H₂O, THPTA and sodium ascorbate for 2 hours to yield TetraDVP-MMAE linker-payload **72** in 25% yield (Scheme 29). Analysis of the crude reaction mixture by LC-MS showed >90% conversion to the desired product; therefore, the low isolated yield of **72** can likely be attributed to complications during purification.



Scheme 29: CuAAC reaction of TetraDVP **15** with N₃-PEG₄-Val-Cit-PABC-MMAE **47** to generate linker-payload **72**.

Next, the reaction of TetraDVP-MMAE linker-payload **72** with trastuzumab was attempted. Trastuzumab was reduced with TCEP at 37 °C for 1 hour, followed by incubation with 2 or 10 equivalents of TetraDVP **72** in 5% DMSO/TBS at 37 °C for 4 hours (Figure 54A). Analysis of the reactions by SDS-PAGE revealed incomplete conversion in both cases, as evidenced by the presence of significant amounts of unreacted heavy and light chains (Figure 54B).

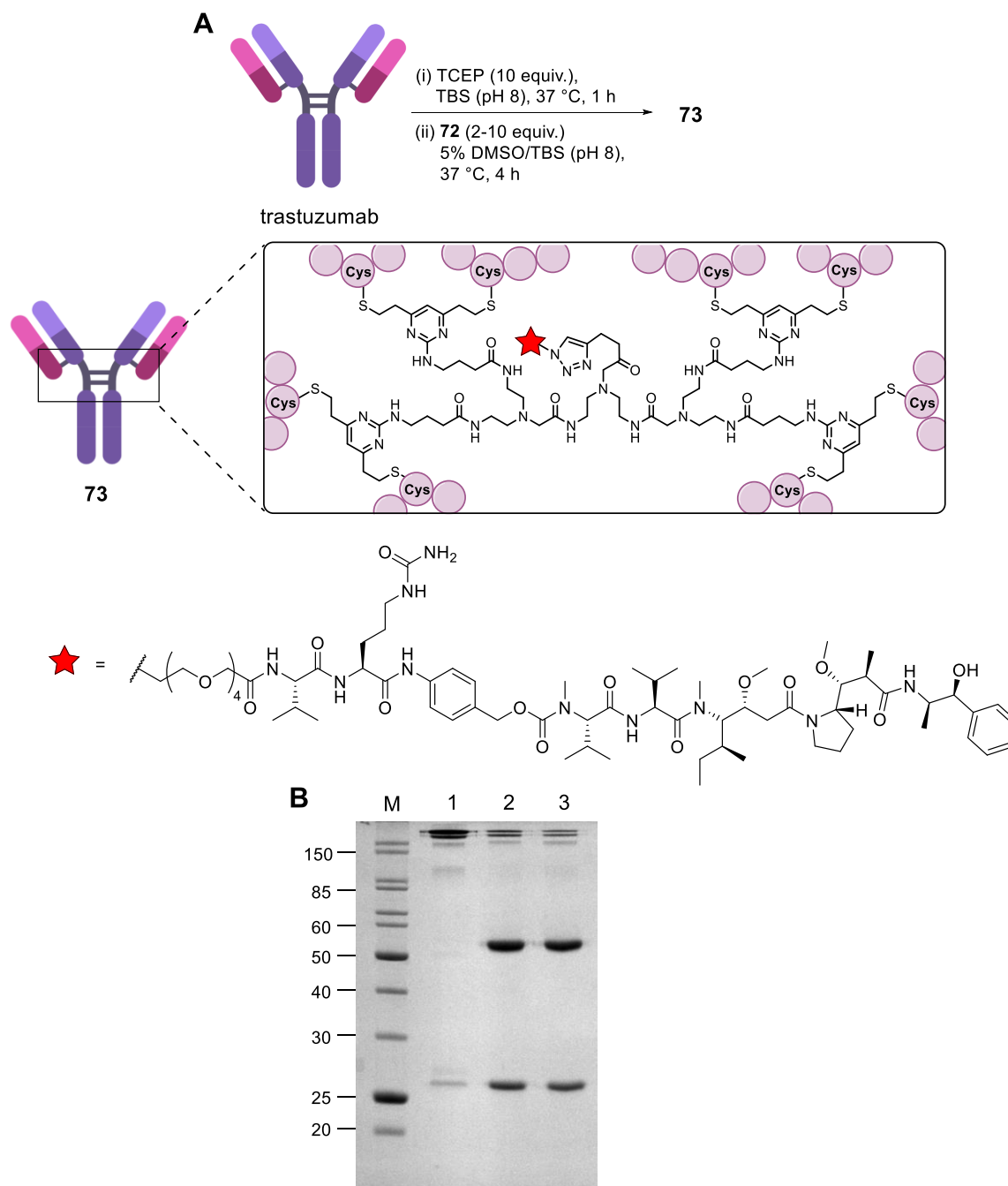


Figure 54: Reaction of trastuzumab with TetraDVP-MMAE linker-payload **72**. (A) Reaction conditions. (B) SDS-PAGE analysis of TetraDVP conjugates. Analysis was carried out by reducing SDS-PAGE on 12% polyacrylamide gels with Coomassie staining. Lanes: M = molecular weight marker, 1 = Reaction of trastuzumab with 2 equiv. of TetraDVP **15**, 2 = Reaction of trastuzumab with 2 equiv. of TetraDVP **72**, 3 = Reaction of trastuzumab with 10 equiv. of TetraDVP **72**.

To establish if the poor rebridging efficiency might be caused by insufficient reaction time or a lack of linker-payload solubility in the selected buffer system, a number of different reaction conditions were screened. Accordingly, reduced trastuzumab was reacted with linker-payload **72** in TBS with 5, 10 or 15% organic co-solvent at 37 °C for 4 or 24 hours (Figure 55A). Analysis of the reactions by SDS-PAGE showed that an increase in DMSO content from 5% to 10% indeed resulted in a slight increase in the amount of fully rebridged antibodies produced by the reaction (Figure 55B). However, a significant amount of unreacted light and heavy chain was still seen to be present. Further increasing the DMSO content from 10% to 15% did not appear to have a significant impact on the outcome of the reaction. An increase in reaction time from 4 to 24 hours also appeared to result in a slight increase in conversion.

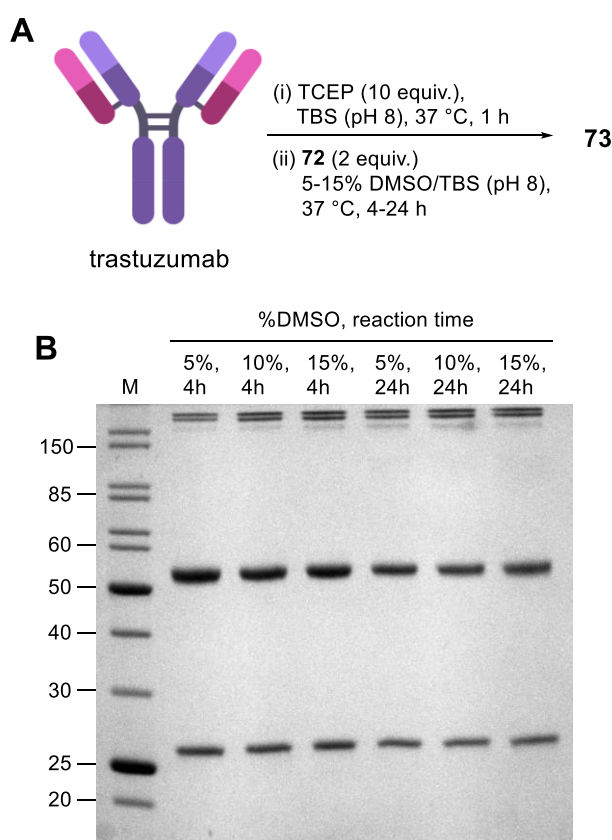


Figure 55: Optimisation of the reaction of TetraDVP linker-payload **72** with trastuzumab. (A) Reaction conditions. (B) Reducing SDS-PAGE analysis of reactions on 12% polyacrylamide gel with Coomassie staining. Lanes: M = molecular weight marker, reaction conditions displayed above the corresponding lane.

These results suggest that the poor rebridging efficiency observed for the reaction of trastuzumab with TetraDVP **72** may be caused by factors other than insufficient solubility and reaction time. It is possible that the appended PEG₄-Val-Cit-PABC-MMAE payload of TetraDVP **72** generates steric hindrance around the cysteine-reactive DVP groups, thus impeding their

reaction with cysteine residues in trastuzumab. As such, the results obtained from the reaction of trastuzumab with linker-payload **72** showcase that the generation of ADCs *via* rebridging with TetraDVP-MMAE linker-payloads is possible, but optimisation of linker-payload structure will likely be necessary to achieve satisfactory conversion.

4.7 Cytotoxicity

To assess the cytotoxic potential of TetraDVP ADCs, several cell viability assays were carried out using the ADCs described in Chapter 4.6.1.

4.7.1 Cleavable MMAE ADCs

Initially the cytotoxic potential of cathepsin-cleavable PEG₄-Val-Cit-MMAE ADCs **48-51** was assessed. Accordingly, two HER2-positive cell lines (SKBR3 and BT474) and two HER2-negative cell lines (MCF7 and MDA-MB-468) were treated with varying concentrations of ADCs **48-51** or trastuzumab. After 96 hours of incubation, a CellTiter-Glo® assay was used to measure the number of viable cells present for each concentration of the different compounds tested. These experiments were carried out with Dr Stephen J. Walsh.

Pleasingly, all ADCs displayed a significant increase in concentration-dependent cytotoxicity in HER2-positive cells compared to trastuzumab alone (Figure 56). In contrast, the proliferation of HER2-negative cells was not significantly affected compared to vehicle control, thus confirming the selectivity for HER2-positive cells. Notably, the antiproliferative effect of the ADCs on HER2-positive cells correlated with DAR. As such, ADCs **48-51** – for which average DARs of 0.6, 1.0, 1.6 and 2.5 were measured by HIC (see Chapter 4.6.1.1 for details) – had IC₅₀ values of 157 pM, 98.5 pM, 40.6 pM and 29.1 pM against SKBR3 cells and 464 pM, 276 pM, 139 pM and 93.4 pM against BT474 cells.

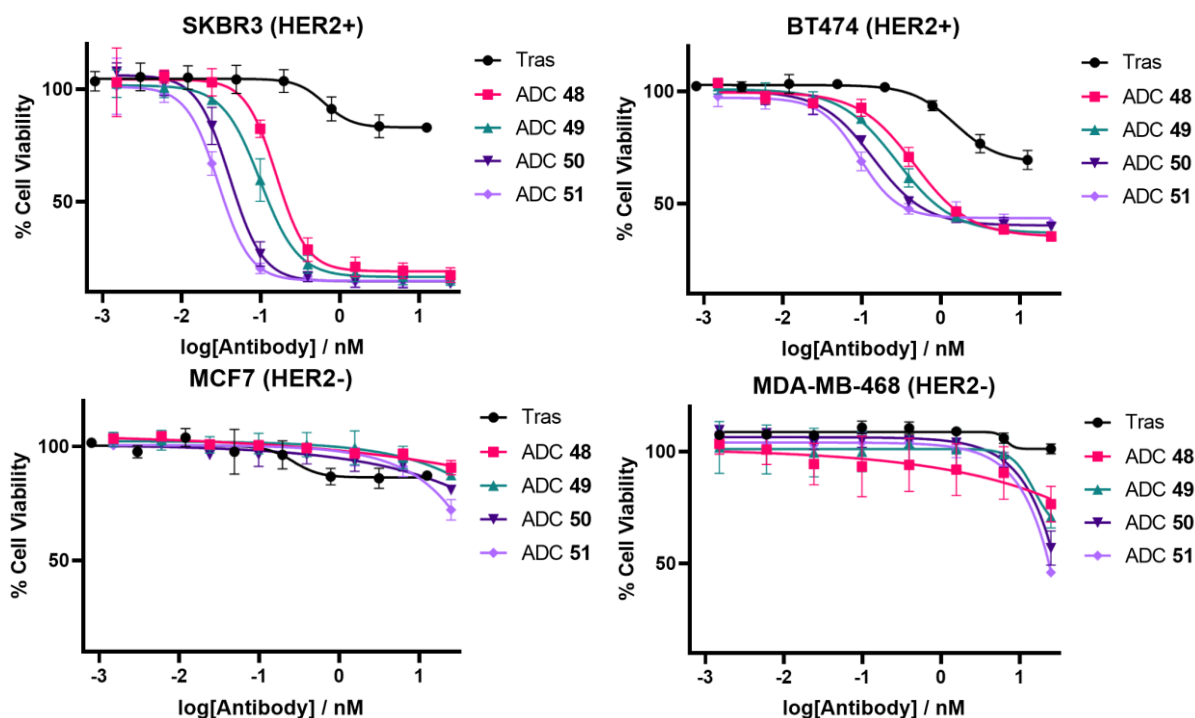


Figure 56: Cytotoxicity of TetraDVP ADCs **48-51** in HER2-positive (SKBR3 and BT474) and HER2-negative (MCF7 and MDA-MB-468) cell lines. Viability data shows the mean of three independent experiments and error bars represent the standard error of the mean (SEM).

These results demonstrate that increased steric bulk with increasing DAR does not impede payload release. Furthermore, the IC_{50} values measured for ADCs **48-51** showcase how even minor differences in DAR (± 0.5) can have a noticeable effect on the biological activity of an ADC, thus providing further evidence of the benefits of antibody modification methods which offer DAR tunability.

4.7.2 Non-cleavable MMAE ADCs

Having demonstrated the excellent potency and selectivity of enzyme-cleavable TetraDVP ADCs, non-cleavable MMAE ADCs **61-64** were assessed. As described in Chapter 1.5.1.2, non-cleavable ADCs lack specific payload release mechanisms. Instead, the drug is released upon lysosomal degradation of the antibody into its constituent amino acids. This mechanism releases the payload with the linker and point-of-attachment amino acid appendage still attached. In the case of a non-cleavable TetraDVP ADC such as **61**, this mechanism may result in the release of a payload like the one shown in Figure 57.

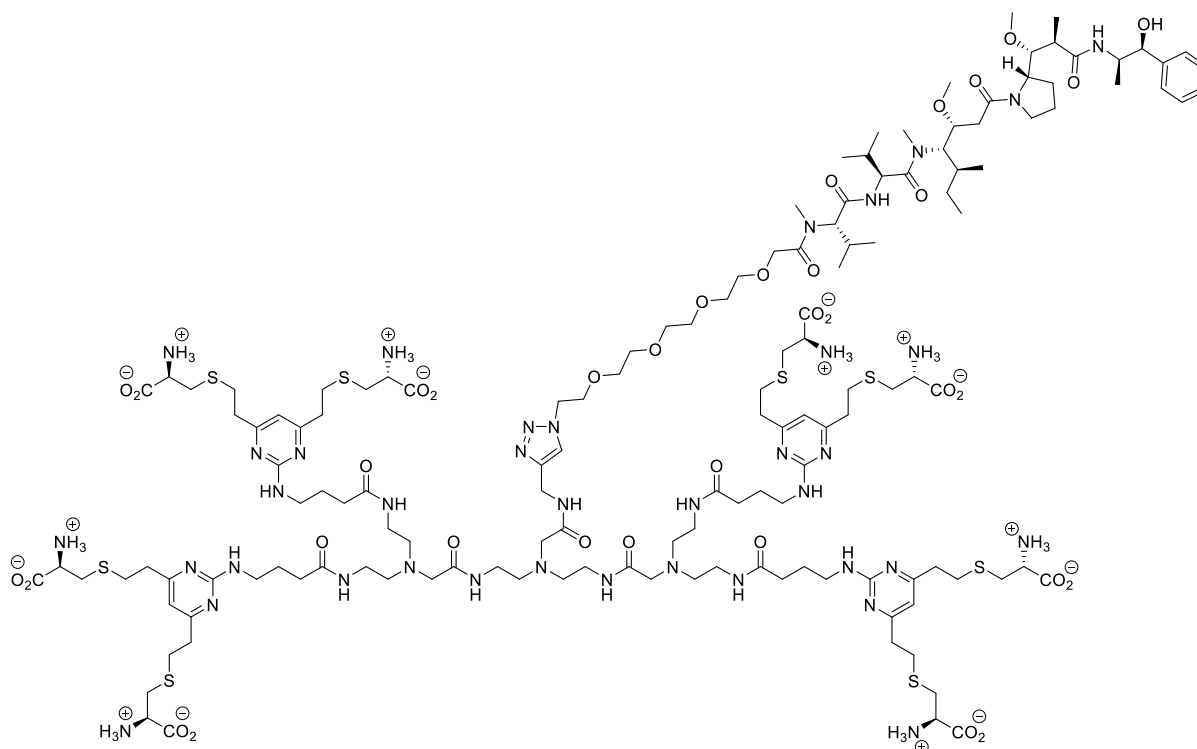


Figure 57: Possible structure of the payload released by lysosomal degradation of ADC **61**.

To assess the cytotoxic potential of ADCs **61-64**, SKBR3 and MCF7 cells were treated with varying concentrations of ADCs or trastuzumab, incubated for 96 hours, and analysed using a CellTiter-Glo® assay. Interestingly, the ADCs showed no significant effect on either the HER2-positive or the HER2-negative cell lines up to a concentration of 200 nM (Figure 58).

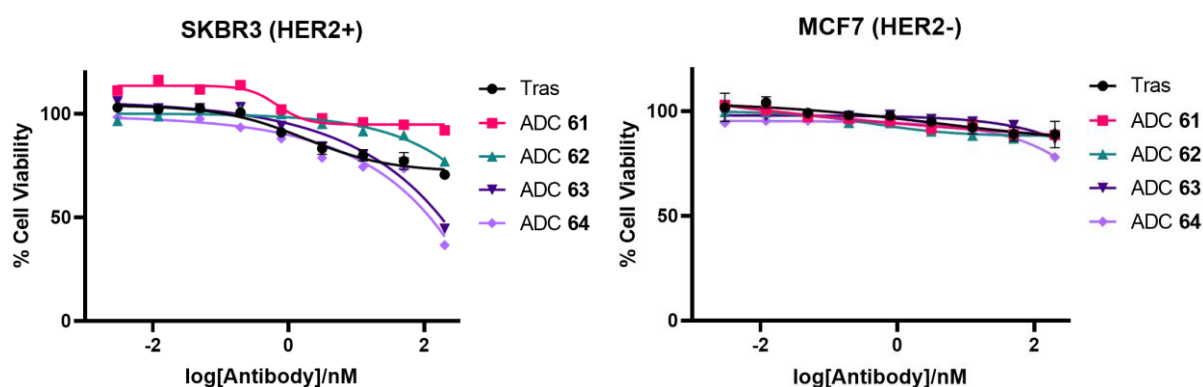


Figure 58: Cytotoxicity of TetraDVP ADCs **61-64** in HER2-positive (SKBR3) and HER2-negative (MCF7) cell lines. Viability data for trastuzumab shows the mean of two independent experiments and error bars represent the standard error of the mean (SEM).

These results suggest that the appendage of the TetraDVP linker and the eight attached cysteine residues might be interfering with the MoA of MMAE. In previous studies by Walsh *et al.* non-cleavable DVP-MMAE ADCs were shown to exert potent antiproliferative effects

against antigen-positive cells,¹⁸³ indicating that small DVP-based appendages do not interfere with the MoA of MMAE. However, the TetraDVP-(cysteine)₈ appendages generated *via* lysosomal degradation of ADCs **61-64** are significantly larger than the DVP-(cysteine)₂ appendage generated from the ADC by Walsh and co-workers. It is possible that the large size of the TetraDVP-(cysteine)₈ appendage creates steric hindrance around the MMAE payload which prevents it from binding to its cellular target, tubulin. Therefore, TetraDVP linkers may not be suitable bioconjugation reagents in combination with non-cleavable MMAE payloads.

4.8 PEGylated TetraDVP Linker

The results obtained regarding the functionalisation of TetraDVP conjugates **37**, **38**, **39** and **41** with cytotoxic payloads (see Chapter 4.6) have made it evident that the TetraDVP linker structure needs to be modified to achieve full conversion in CuAAC reaction and realise the synthesis of fully homogenous ADCs. It was hypothesised that the incorporation of an extended spacer unit between the DVP motifs and the alkyne(s) might be beneficial, as it might reduce steric hindrance around the alkyne(s) and thus enable improved CuAAC conversion. To test this hypothesis, TetraDVP **76** was designed. TetraDVP **76** is an analogue of TetraDVP **15** with an additional PEG₂ spacer unit incorporated between the alkyne and the linear backbone of the scaffold (Figure 59).

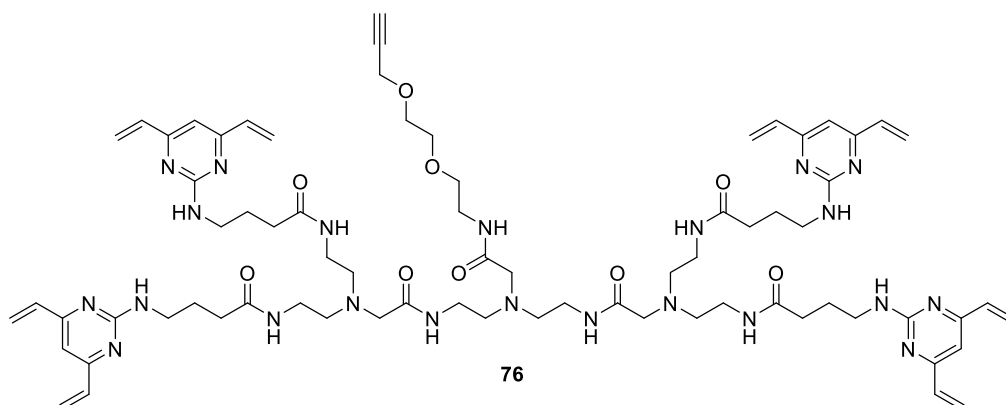
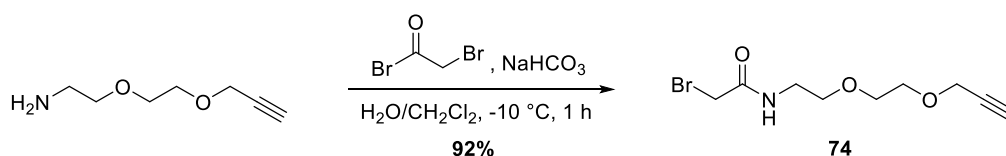


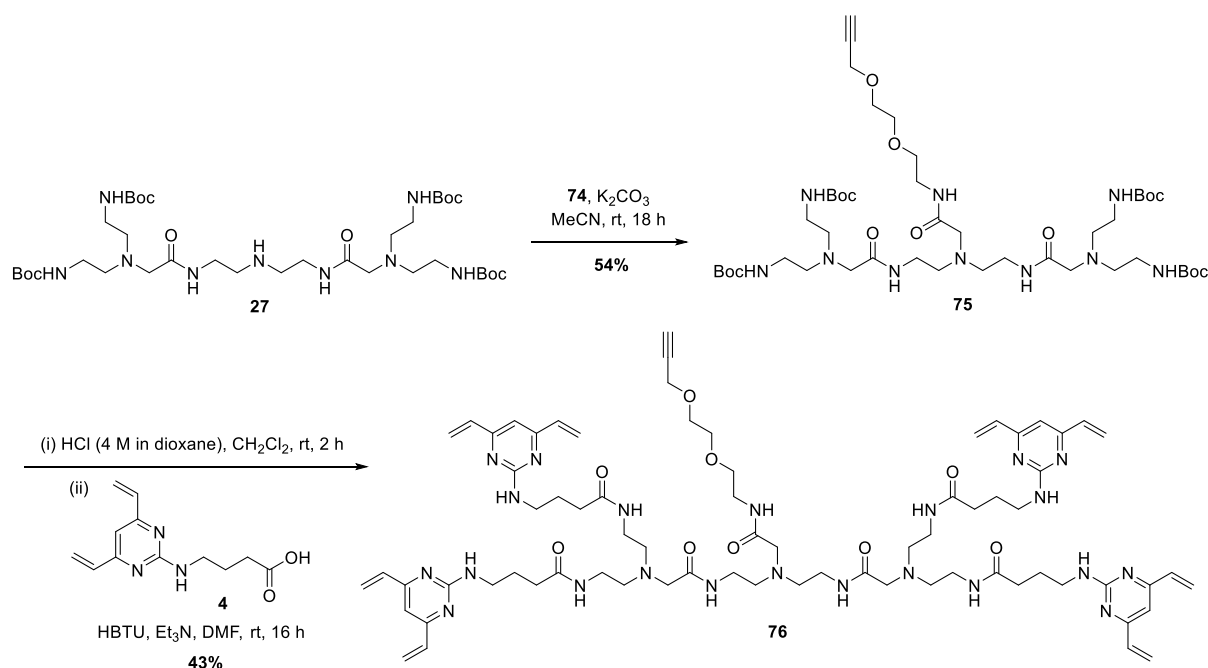
Figure 59: Structure of PEGylated TetraDVP **76**.

To commence the synthesis of TetraDVP **76**, propargyl-PEG₂-amine was reacted with bromoacetyl bromide to yield α -bromo carbonyl **74** in 92% yield (Scheme 30).



Scheme 30: Synthesis of α -bromo carbonyl **74**.

Alkyne **74** was subsequently reacted with tetra-*N*-Boc scaffold **27** to generate tetra-*N*-Boc alkyne **75** in moderate yield. Finally, tetra-*N*-Boc amine **75** was deprotected with HCl and then coupled to DVP **4** in the presence of HBTU and triethylamine to form TetraDVP **76** in 43% yield, over two steps (Scheme 31).



Scheme 31: Synthesis of TetraDVP **76** from tetra-*N*-Boc scaffold **27** via alkylation, Boc deprotection and amide coupling to DVP building block **4**.

With TetraDVP **76** in hand, the modification of trastuzumab was attempted. Accordingly, interchain disulfides in trastuzumab were reduced with TCEP at 37 °C for one hour, followed by incubation with TetraDVP **76** at 37 °C for four hours. Analysis of the reaction by LC-MS and SDS-PAGE showed excellent conversion to the desired TetraDVP conjugate **77** (Figure 60).

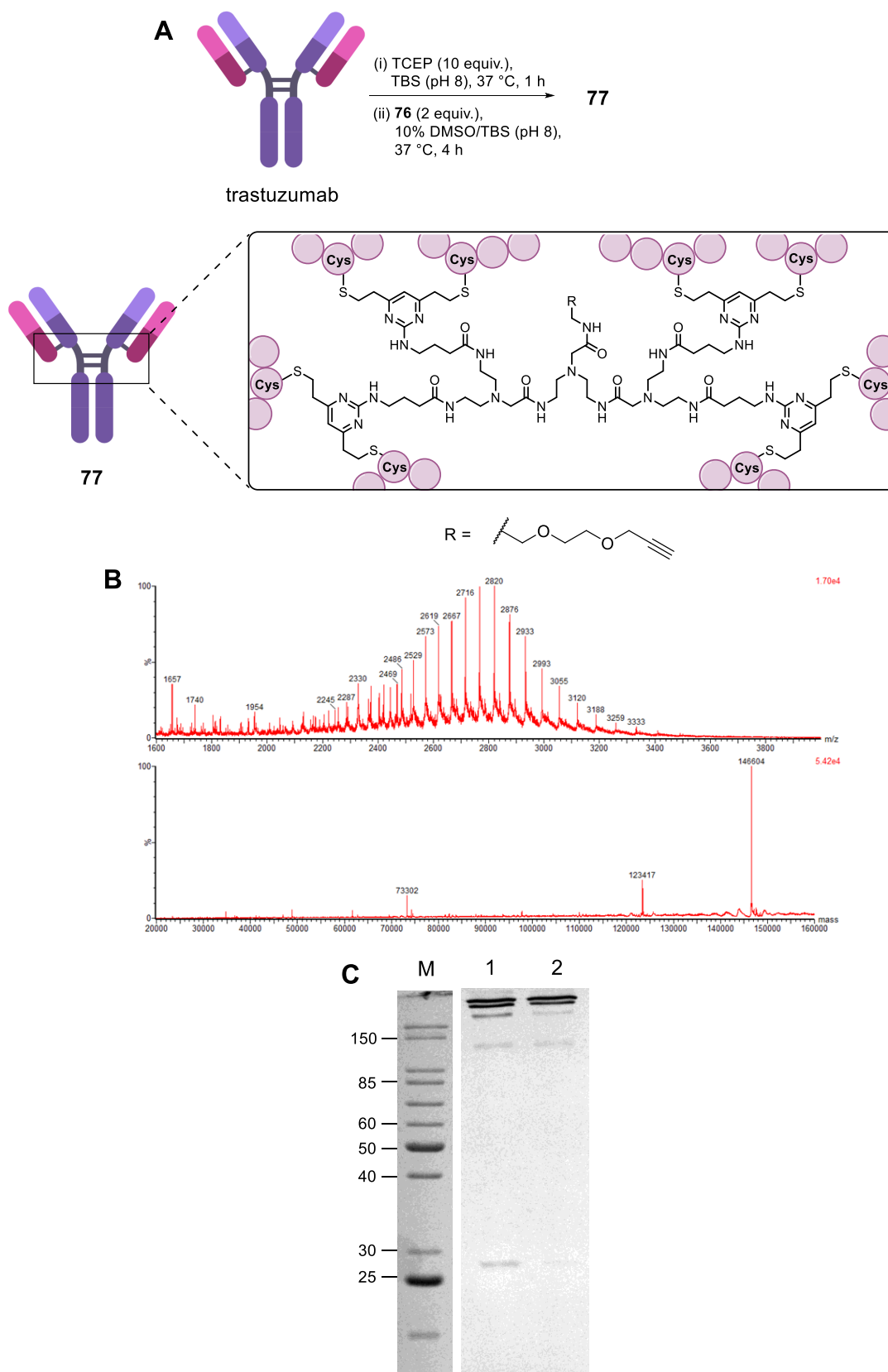


Figure 60: Reaction of trastuzumab with TetraDVP **76**. (A) Reaction conditions. (B) Analysis of the reaction between trastuzumab and **76** by LC-MS. Top = non-deconvoluted MS. Bottom = deconvoluted MS; expected 146,624 Da, observed 146,604 Da. (C) Reducing SDS-PAGE analysis of reactions on 12% polyacrylamide gel with Coomassie staining. Lanes: M = molecular weight marker, 1 = ALC **37** (from TetraDVP **15**), 2 = ALC **77** (from TetraDVP **76**).

To investigate if the additional PEG spacer of ALC **77** has a positive effect on post-conjugation CuAAC efficiency, ALC **77** was reacted with three different azide-functionalised payloads – N₃-PEG₂₄-Val-Cit-PABC-MMAE **52**, N₃-PEG₄-Glu₂-PEG₂-Val-Cit-PABC-MMAE **55** and N₃-PEG₄-MMAE **60** – in the presence of CuSO₄·5H₂O, THPTA and sodium ascorbate. In parallel, a series of control reaction using non-PEGylated mono-alkyne ALC **37** was carried out. In all cases, the reaction with the PEGylated ALC **77** displayed slightly higher conversion than the control reaction with non-PEGylated ALC **37** (Table 11). Despite this, none of the reactions reached full conversion.

Table 11: Reaction conditions and outcomes of the reactions of TetraDVP ALCs **37** and **77** with MMAE payloads.

Entry	ALC	Reagents (equivalents)	Reaction time / h	Product	DAR
1	37	N ₃ -PEG ₂₄ -Val-Cit-PABC-MMAE 52 (100) CuSO ₄ ·5H ₂ O (150) THPTA (600) NaAsc (1000)	6	53	0.5
2	77	N ₃ -PEG ₂₄ -Val-Cit-PABC-MMAE 52 (100) CuSO ₄ ·5H ₂ O (150) THPTA (600) NaAsc (1000)	6	78	0.6
3	37	N ₃ -PEG ₄ -Glu ₂ -PEG ₂ -Val-Cit-PABC-MMAE 55 (100) CuSO ₄ ·5H ₂ O (150) THPTA (600) NaAsc (1000)	6	56	0.7
4	77	N ₃ -PEG ₄ -Glu ₂ -PEG ₂ -Val-Cit-PABC-MMAE 55 (100) CuSO ₄ ·5H ₂ O (150) THPTA (600) NaAsc (1000)	6	79	0.8
5	37	N ₃ -PEG ₄ -MMAE 60 (100) CuSO ₄ ·5H ₂ O (150) THPTA (600) NaAsc (1000)	6	61	0.6
6	77	N ₃ -PEG ₄ -MMAE 60 (100) CuSO ₄ ·5H ₂ O (150) THPTA (600) NaAsc (1000)	6	80	0.7

These results indicate that the incorporation of an additional spacer unit between the TetraDVP backbone and the alkyne functionality indeed increases the reactivity of the alkyne. However, a short PEG₂ spacer may not be sufficient to enable complete conversion. Future development of TetraDVP linkers should therefore focus on linker structures containing longer spacers.

4.9 Conclusions

In this chapter, the development of a TetraDVP linker platform for the modification of IgG1 antibodies was described.

Initially, synthetic procedures for the production of a series of TetraDVP reagents containing four cysteine-reactive DVP units alongside one, two, three or four alkyne handles were developed. Subsequently, these reagents were utilised for the modification of trastuzumab. The TetraDVP reagents were shown to efficiently rebridge all four interchain disulfides in trastuzumab to yield ALCs with a linker-to-antibody ratio of one and minimal half antibody formation.

Further modification of the TetraDVP-trastuzumab conjugates with AlexaFluor™ 488 azide yielded a series AFCs with precise FARs of 1, 2, 3 and 4 depending on the number of alkyne moieties in the linker. Assessment of these AFCs in a number of stability and cellular selectivity assays demonstrated that TetraDVP linkages are stable in human plasma for multiple weeks and do not interfere with trastuzumab's ability to recognise its target antigen HER2.

Modification of TetraDVP-trastuzumab conjugates with different azide-functionalised payloads yielded a series of ADCs with variable DAR values. Unlike the reactions with AlexaFluor™ 488 azide, these reactions did not reach completion, thereby generating mixtures of ADC populations with different DARs. Investigations into a TetraDVP linker with an additional spacer unit between the alkyne moiety and the linker backbone suggested that this reactivity problem may be overcome by further optimisation of the TetraDVP linker scaffold.

Finally, the generated TetraDVP ADCs were assessed in multiple *in vitro* cell viability assays, which demonstrated the excellent potency and cell selectivity of cleavable TetraDVP ADCs. This collective data highlights the utility of the TetraDVP linker platform to generate functional antibody conjugates *via* cysteine rebridging.

Chapter 5 – Conclusions and future work

5.1 Conclusions

An outstanding problem in the ADC field is a lack of robust methods that allow the synthesis of stable and homogenous ADCs with modular DAR. While numerous contemporary bioconjugation methods allow alterations of the number of drugs attached to each antibody, many of these methods require major modifications to the native antibody structure, which typically require extensive case-by-case optimisation. Disulfide rebridging reagents have emerged as an attractive universal strategy to facilitate the synthesis of homogenous ADCs from native antibodies. However, this approach is currently limited by the formation of half antibody species during rebridging. Therefore, the establishment of new approaches towards the synthesis of homogenous ADCs from native antibodies is desirable.

This thesis describes the development of a novel method for the production of antibody conjugates *via* the rebridging of multiple disulfides with a single linker molecule. The primary objective throughout this work was the development of a methodology that avoids half antibody formation and simultaneously enables DAR modulation in integer increments to facilitate access to an increased scope of integer DAR values compared to those obtainable using classical disulfide rebridging techniques.

Preliminary studies in this area, described in Chapter 3, focused on a bis-divinylpyrimidine (BisDVP) scaffold, containing four cysteine-reactive vinyl groups. This linker was found to be synthetically tractable and enabled the functional rebridging of two disulfide bonds in trastuzumab to generate antibody conjugates with a linker-to-antibody ratio of two. This strategy was found to result in reduced half antibody formation compared to the reaction with a classical DVP rebridging linker. However, despite these improvements, the formation of half antibody species was not fully eradicated.

It was postulated that increasing the number of cysteine-reactive groups in the linker might reduce the risk of half antibody formation. Therefore, further studies, which are detailed in Chapter 4, centred around tetra-divinylpyrimidine (TetraDVP) linkers containing eight cysteine-reactive groups. Accordingly, a series of TetraDVP linkers with variable backbone structures was designed and synthesised. Subsequently, these reagents were utilised for the

modification of trastuzumab, which revealed their ability to efficiently rebridge all four interchain disulfides to yield conjugates with a linker-to-antibody ratio of one and minimal half antibody formation. Furthermore, the incorporation of varying numbers of alkyne groups into the TetraDVP structure enabled functional modification of the TetraDVP-trastuzumab conjugates with different numbers of payloads *via* post-conjugation CuAAC. While satisfactory conversion was only achieved in a limited number of cases, these results showcase the potential of TetraDVPs to facilitate the generation of homogenous ADCs with different DARs *via* a modular strategy. Biological evaluation of the TetraDVP conjugates demonstrated their exquisite plasma stability, aggregation profile and antigen binding affinity. Moreover, *in vitro* assessment of a panel of TetraDVP-trastuzumab ADCs containing cathepsin-cleavable MMAE payloads showed that these conjugates possess excellent cellular selectivity and potency against HER2-positive cell lines.

Overall, this work describes the development of a novel method for the site-selective modification of antibodies *via* disulfide rebridging with minimal half antibody formation and the potential to modulate DAR in integer increments.

5.2 Future work

5.2.1 Improving post-conjugation payload attachment

The primary obstacle encountered with TetraDVP-mediated ADC synthesis were the low levels of conversion observed in the post-conjugation CuAAC reaction used to attach cytotoxic payloads to the antibody-linker conjugates. While the resulting ADCs displayed favourable selectivity and activity *in vitro*, the lack of homogeneity with respect to DAR caused by low CuAAC conversion undermines the utility of the method for DAR modulation and necessitates further optimisation of the linker scaffolds.

One possible approach might include the incorporation of additional spacer units in between the core TetraDVP scaffold and the alkyne handles to reduce steric hindrance around the latter (Figure 61A). The potential of this approach is supported by the results obtained with the PEGylated TetraDVP linker described in Chapter 4.8.

Alternatively, the conversion of post-conjugation payload attachment may be improved by employing a different type of bioorthogonal reaction. Suitable linkers may include azides or strained alkynes to enable SPAAC chemistry or tetrazines to enable inverse electron demand Diels-Alder (iEDDA) reactions (Figure 61B).^{223,224} In addition to increasing the rate of post-conjugation functionalisation, the use of these metal-free attachment chemistries would remove the need to use a copper catalyst for payload attachment. Prolonged exposure to copper can have detrimental effects on protein stability and residual metal contaminants present in the final ADCs may cause undesired off-target toxicity. Therefore, the removal of copper from the synthetic process is desirable.

A specific approach centred around SPAAC chemistry is currently being developed by Dr Stephen J. Walsh and Thomas A. King of the Spring group.

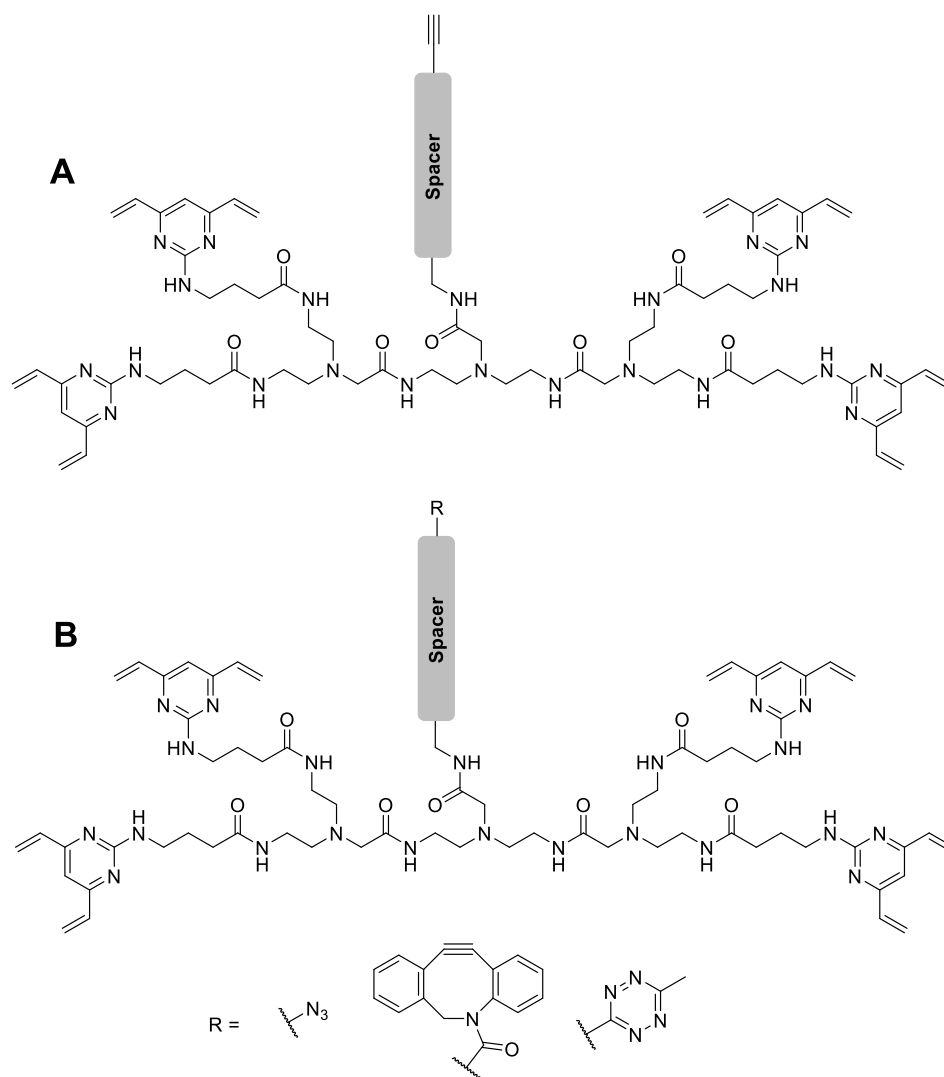


Figure 61: Potential TetraDVP linker structures to be explored in the future.

5.2.2 *In vivo* evaluation of ADCs

The work described in this thesis demonstrated that TetraDVP conjugates possess high stability, selectivity, and activity through a variety of *in vitro* assays. However, to fully understand the pharmacological profile of TetraDVP ADCs and ascertain their potential for further development, *in vivo* assessment is required. To achieve this, antigen-positive mouse xenograft models (cell lines or patient-derived) could be employed for further investigation of ADC efficacy, tolerability, and pharmacokinetic behaviour.

5.2.3 Structural investigations

One of the main objectives of BisDVP and TetraDVP development was the prevention of half antibody formation because the associated loss of covalent linkages between the antibody chains has been implicated with reduced stability.¹²⁷ To investigate if TetraDVP and BisDVP conjugates indeed possess increased structural stability compared to DVP conjugates and explore how their stability compares to unmodified trastuzumab, a number of biophysical assays could be employed. Such assays could include differential scanning calorimetry (DSC) to compare the melting temperatures of the different conjugates and chemical denaturation experiments such as those reported by Orozco *et al.* to measure the unfolding kinetics of the individual antibody domains.²²⁵ Any observed differences in structure and/or conformational dynamics could then be further investigated using hydrogen-deuterium exchange mass spectrometry (HDX-MS) to pinpoint which regions of the antibody are most affected.

5.2.4 Fc fusion compounds

Many small and medium sized biotherapeutics (such as peptides and small proteins) suffer from short circulation half-lives which limit their therapeutic potential. A common half-life extension strategy for such biomolecules is their fusion to the Fc fragment of an antibody.²²⁶ This fusion is usually achieved *via* recombinant methods and expression of the genetically engineered fusion proteins in mammalian host cells. However, this approach suffers from several limitations, including incompatibility with unnatural amino acids, cyclic peptides, or non-peptidic modalities such as oligonucleotides.²²⁷ To overcome these limitations, several synthetic and semisynthetic methods for the generation of Fc fusion compounds have been developed, including the use of chemical ligation,²²⁸ N-terminal extension reactions (NEXT-A),²²⁹ trans-splicing²³⁰ or host-guest chemistry²³¹ to attach the biotherapeutic to the Fc. However, these methods generally suffer from long reaction times (20+ hours) and/or require additional amino acid residues to be engineered into the Fc structure. Therefore, the development of novel methods for the synthetic generation of Fc fusion compounds is desirable.

BisDVP linkers may serve as a valuable tool in this context. While the reaction of BisDVP linkers with full-length antibodies containing four interchain disulfide bonds yielded conjugates of

moderate homogeneity in terms of half antibody formation, they may be able to yield fully homogenous conjugates in conjunction with Fc fragments containing only two disulfides. As such, BisDVPs may enable the modification of Fc fragments with therapeutic peptides and oligonucleotides in a quick and simple manner to furnish highly homogenous Fc fusion compounds without the need for antibody engineering (Figure 62).

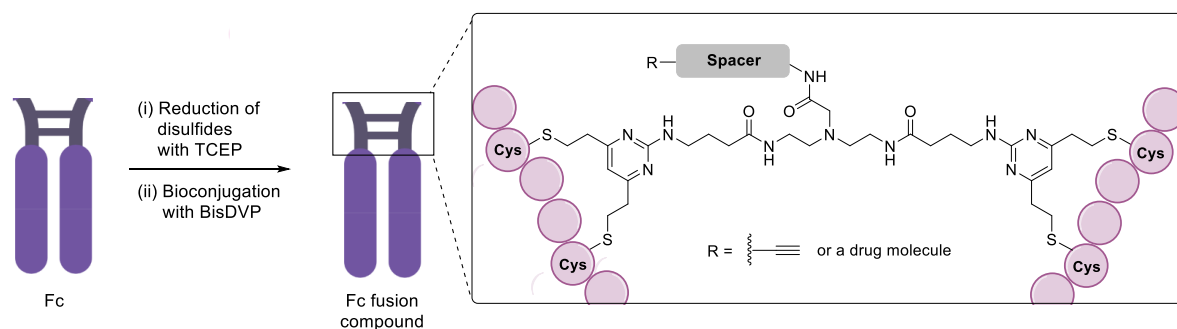


Figure 62: Proposed construction of Fc fusion compounds using BisDVP linkers.

Chapter 6 - Experimental

6.1 General Experimental

All solvents and reagents were used as received unless otherwise stated. Ethyl acetate, methanol, dichloromethane, acetonitrile and toluene were distilled from calcium hydride. Diethyl ether was distilled from a mixture of lithium aluminium hydride and calcium hydride. Petroleum ether (PE) refers to the fraction between 40-60 °C upon distillation. Tetrahydrofuran was dried using Na wire and distilled from a mixture of lithium aluminium hydride and calcium hydride with triphenylmethane as indicator.

Non-aqueous reactions were conducted under a stream of dry nitrogen using oven-dried glassware. Temperatures of 0 °C were maintained using an ice-water bath. Room temperature (rt) refers to ambient temperature.

Yields refer to spectroscopically and chromatographically pure compounds unless otherwise stated. Reactions were monitored by thin layer chromatography (TLC) or liquid chromatography mass spectrometry (LC-MS). TLC was performed using glass plates pre-coated with Merck silica gel 60 F₂₅₄ and visualised by quenching of UV fluorescence (λ_{max} = 254 nm) or by staining with potassium permanganate. Retention factors (R_f) are quoted to two decimal places. LC-MS was carried out using a Waters ACQUITY H-Class UPLC with an ESCi Multi-Mode Ionisation Waters SQ Detector 2 spectrometer using MassLynx 4.1 or MassLynx 4.2 software; ESI refers to the electrospray ionisation technique; LC system: solvent A: 2 mM NH₄OAc in H₂O/MeCN (95:5); solvent B: MeCN; solvent C: 2% formic acid; column: ACQUITY UPLC® CSH C18 (2.1 mm × 50 mm, 1.7 μ m, 130 Å) at 40 °C; gradient: 5-95 % B with constant 5 % C over 1 min at flow rate of 0.6 mL/min; detector: PDA e λ Detector 220-800 nm, interval 1.2 nm.

Flash column chromatography was carried out using slurry-packed Merck 9385 Kieselgel 60 SiO₂ (230-400 mesh) or a Combiflash Rf200 automated chromatography system with Redisep® reverse-phase C18-silica flash columns (20-40 μ m).

Analytical high performance liquid chromatography (HPLC) was performed on an Agilent 1260 Infinity machine, using a Supelcosil™ ABZ+PLUS column (150 mm × 4.6 mm, 3 μ m) with a

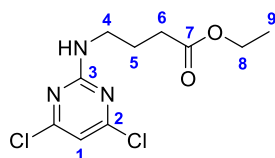
linear gradient system (solvent A: 0.05% (v/v) TFA in H₂O; solvent B: 0.05% (v/v) TFA in MeCN) over 20 min at a flow rate of 1 mL/min, and UV detection (λ_{max} = 220 – 254 nm).

Infrared (IR) spectra were recorded neat on a Perkin-Elmer Spectrum One spectrometer with internal referencing. Selected absorption maxima (ν_{max}) are reported in wavenumbers (cm⁻¹) with peak intensity reported as follows: w = weak; m = medium; s = strong.

¹H and ¹³C nuclear magnetic resonance (NMR) were recorded using an internal deuterium lock on Bruker DPX-400 (400 MHz, 101 MHz), Bruker Avance 400 QNP (400 MHz, 101 MHz) and Bruker Avance 500 Cryo Ultrashield (500 MHz, 126 MHz). In ¹H NMR, chemical shifts (δ_{H}) are reported in parts per million (ppm), to the nearest 0.01 ppm and are referenced to the residual non-deuterated solvent peak (CDCl₃: 7.26, CD₃OD: 3.31). Coupling constants (*J*) are reported in Hertz (Hz) to the nearest 0.1 Hz. Data are reported as follows: chemical shift, multiplicity (s = singlet; br s = broad singlet; d = doublet; t = triplet; q = quartet; qn = quintet; m = multiplet; or as a combination of these, e.g. dd, dt etc.), integration and coupling constant(s). In ¹³C NMR, chemical shifts (δ_{C}) are quoted in ppm, to the nearest 0.1 ppm, and are referenced to the residual non-deuterated solvent peak (CDCl₃: 77.16, CD₃OD: 49.00).

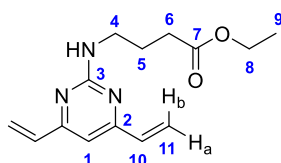
High resolution mass spectrometry (HRMS) measurements were recorded with a Micromass Q-TOF mass spectrometer or a Waters LCT Premier Time of Flight mass spectrometer. Mass values are reported within the error limits of ± 5 ppm mass units. ESI refers to the electrospray ionisation technique.

6.2 Synthetic procedures



Ethyl 4-((4,6-dichloropyrimidin-2-yl)amino)butanoate (1) To a solution of 4-aminobutyric acid ethyl ester hydrochloride (2.01 g, 12.0 mmol) and triethylamine (4.18 mL, 30.0 mmol) in methanol (100 mL) was added dropwise 2,4,6-trichloropyrimidine (1.15 mL, 10.0 mmol). After addition, the reaction mixture was stirred at rt for 3 h before being concentrated *in vacuo*. The residue was purified by column chromatography (0-20% EtOAc/PE) to provide the title compound as a white crystalline solid (1.02 g, 3.67 mmol, 37%). R_f 0.55 (SiO₂, 30% EtOAc/PE); ν_{\max} (neat/cm⁻¹) 1747 (s, C=O), 1562 (m, C=C); δ_H (400 MHz, CD₃OD) 6.66 (s, 1H, H1), 4.12 (q, 2H, J = 7.1 Hz, H8), 3.40 (t, 2H, J = 6.8 Hz, H4), 2.38 (t, 2H, J = 7.3 Hz, H6), 1.88 (qn, 2H, J = 7.1 Hz, H5), 1.24 (t, 3H, J = 7.1 Hz, H9); δ_C (101 MHz, CD₃OD) 175.1 (C7), 163.4 (C3), 162.8 (C2), 108.8 (C1), 61.6 (C8), 41.5 (C4), 32.3 (C6), 25.5 (C5), 14.5 (C9); **LRMS** (ESI) m/z found [M+H]⁺ 278.4, C₁₀H₁₄O₂N₃Cl₂⁺ required 278.0.

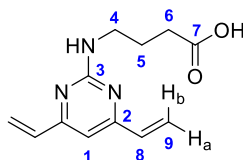
These data are consistent with those previously reported.¹⁰¹



Ethyl 4-((4,6-divinylpyrimidin-2-yl)amino)butanoate (3) A mixture of ethyl 4-((4,6-dichloropyrimidin-2-yl)amino)butanoate **1** (757 mg, 2.72 mmol), potassium vinyltrifluoroborate (1.09 g, 8.16 mmol), PdCl₂(dppf)·CH₂Cl₂ (333 mg, 0.408 mmol) and K₂CO₃ (1.13 g, 8.16 mmol) in THF (33 mL) and H₂O (3.3 mL) was heated to 70 °C under nitrogen for 14 h. The reaction mixture was cooled to rt, filtered through Celite®, and concentrated *in vacuo*. The residue was purified by column chromatography (0-20% EtOAc/PE) to yield the product as a colourless oil (630 mg, 2.41 mmol, 89%). R_f 0.32 (SiO₂, 20% EtOAc/PE); ν_{\max} (neat/cm⁻¹) 1743 (s, C=O), 1562 (m, C=C); δ_H (400 MHz, CDCl₃) 6.57 (dd, 2H, J = 10.6, 17.3 Hz, H10), 6.52 (s, 1H, H1), 6.35 (d, 2H, J = 17.3 Hz, H11b), 5.55 (dd, 2H, J = 1.5, 10.6 Hz, H11a), 5.16 (t, 1H, J = 5.4 Hz, NH), 4.12 (q, 2H, J = 7.1 Hz, H8), 3.52 (q, 2H, J = 6.6 Hz, H4), 2.40 (t, 2H, J = 7.4 Hz, H6), 1.95 (qn, 2H, J = 7.1 Hz, H5), 1.23 (t, 3H, J = 7.1 Hz, H9); δ_C (101 MHz, CDCl₃)

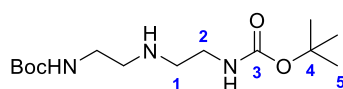
173.6 (C7), 163.8 (C3), 162.8 (C2), 136.0 (C10), 121.5 (C11), 105.9 (C1), 60.5 (C8), 40.8 (C4), 31.9 (C6), 25.2 (C5), 14.3 (C9); **LRMS** (ESI) m/z found $[M+H]^+$ 262.6, $C_{14}H_{20}O_2N_3^+$ required 262.2.

These data are consistent with those previously reported.¹⁰¹



4-((4,6-divinylpyrimidin-2-yl)amino)butanoic acid (4) To a solution of ethyl 4-((4,6-divinylpyrimidin-2-yl)amino)butanoate **3** (345 mg, 1.32 mmol) in THF (12 mL) and H_2O (12 mL) at 0 °C was added $LiOH \cdot H_2O$ (55.6 mg, 1.32 mmol). The mixture was stirred at room temperature for 24 h, and then diluted with H_2O (30 mL) and washed with Et_2O (30 mL). The aqueous layer was adjusted to pH 4 using 1 M HCl and then extracted with CH_2Cl_2 (5 x 30 mL). The organic layer was dried over Na_2SO_4 , filtered, and concentrated *in vacuo* to yield the product as a white solid (307 mg, 1.32 mmol, 100%). ν_{max} (neat/ cm^{-1}) 3277 (m, O-H), 1702 (s, C=O), 1562 (m, C=C); δ_H (600 MHz, CD_3OD) 6.70 (s, 1H, H1), 6.61 (dd, 2H, $J = 10.7, 17.4$ Hz, H8), 6.37 (d, 2H, $J = 17.4$ Hz, H9b), 5.57 (dd, 2H, $J = 1.4, 10.7$ Hz, H9a), 3.48 (t, 2H, $J = 6.9$ Hz, H4), 2.38 (t, 2H, $J = 7.4$ Hz, H6), 1.92 (qn, 2H, $J = 7.1$ Hz, H5); δ_C (101 MHz, CD_3OD) 177.4 (C7), 165.4 (C2), 164.1 (C3), 137.0 (C8), 122.1 (C9), 105.7 (C1), 41.5 (C4), 32.4 (C6), 26.2 (C5); **LRMS** (ESI) m/z found $[M+H]^+$ 234.4, $C_{12}H_{16}O_2N_3^+$ required 234.1.

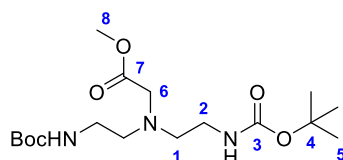
These data are consistent with those previously reported.¹⁰¹



Di-tert-butyl (azanediylbis(ethane-2,1-diyl))dicarbamate (5) To a solution of diethylenetriamine (2.16 mL, 20.0 mmol) in THF (25 mL) at 0 °C was slowly added a solution of Boc-ON (9.92 g, 40.0 mmol) in THF (25 mL). The reaction was stirred at 0 °C under nitrogen for 1 h and then concentrated *in vacuo*. The crude yellow oil was dissolved in CH_2Cl_2 and sequentially washed with 10% aq. NaOH, water and brine. The organic phase was dried over Na_2SO_4 and concentrated *in vacuo*. Purification by column chromatography (10% MeOH/ CH_2Cl_2) yielded the product as a colourless oil (5.61 g, 18.5 mmol, 92%). R_f 0.08 (SiO_2 , 10% MeOH/ CH_2Cl_2); ν_{max} (neat/ cm^{-1}) 3336 (m, N-H), 2975 (m, C-H), 1687 (s, C=O); δ_H (400

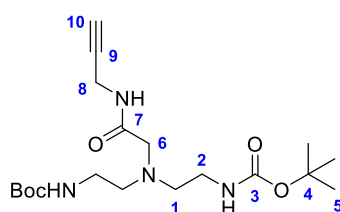
MHz, CDCl₃) 4.93 (br s, 2H, NH), 3.24-3.19 (m, 4H, H₂), 2.73 (t, 4H, *J* = 5.7 Hz, H₁), 1.44 (s, 18H, H₅); δ_c (101 MHz, CDCl₃) 156.3 (C₃), 79.4 (C₄), 49.0 (C₁), 40.4 (C₂), 28.6 (C₅); **HRMS** (ESI) *m/z* found [M+H]⁺ 304.2221, C₁₄H₃₀O₄N₃⁺ required 304.2231.

These data are consistent with those previously reported.¹⁹⁸



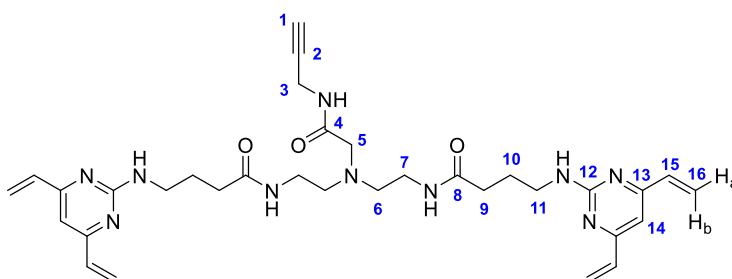
Methyl bis(2-((tert-butoxycarbonyl)amino)ethyl)glycinate (6) To a solution of di-*tert*-butyl (azanediylbis(ethane-2,1-diyl))dicarbamate **5** (5.61 g, 18.5 mmol) in DMF (80 mL) were added DIPEA (3.86 mL, 22.2 mmol) and methyl bromoacetate (2.61 mL, 27.8 mmol). The reaction was stirred at rt for 6 h and then concentrated under a stream of nitrogen. The crude residue was purified by column chromatography (40-50% EtOAc/PE) yielding the product as a colourless oil (6.56 g, 17.5 mmol, 94%). *R*_f 0.28 (SiO₂, 50% EtOAc/PE); *v*_{max} (neat/cm⁻¹) 3345 (m, N-H), 2979 (m, C-H), 1740 (s, C=O), 1688 (s, C=O); δ_H (400 MHz, CDCl₃) 5.13 (br s, 2H, NH), 3.70 (s, 3H, H₈), 3.37 (s, 2H, H₆), 3.15 (q, 4H, *J* = 5.6 Hz, H₂), 2.72 (t, 4H, *J* = 5.9 Hz, H₁), 1.44 (s, 18H, H₅); δ_c (101 MHz, CDCl₃) 172.3 (C₇), 156.3 (C₃), 79.3 (C₄), 55.1 (C₆), 54.3 (C₁), 51.8 (C₈), 38.7 (C₂), 28.6 (C₅); **LRMS** (ESI) *m/z* found [M+H]⁺ 376.5, C₁₇H₃₄O₆N₃⁺ required 376.2.

These data are consistent with those previously reported.²³²



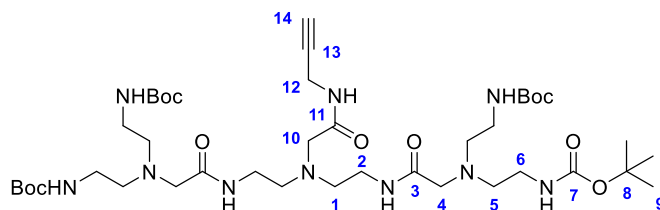
Di-*tert*-butyl ((2-oxo-2-(prop-2-yn-1-ylamino)ethyl)azanediyl)bis(ethane-2,1-diyl) dicarbamate (8) To a solution of methyl bis(2-((tert-butoxycarbonyl)amino)ethyl)glycinate **6** (2.00 g, 5.33 mmol) in MeOH (21.6 mL) and 1,4-dioxane (21.6 mL) was added aqueous NaOH (1 M, 10.8 mL). The reaction mixture was stirred at rt for 2 h and then concentrated *in vacuo*. The resulting residue was re-dissolved in MeOH, filtered, and concentrated again. The residue was then dissolved in DMF (40 mL), followed by addition of *N*-propargylamine (1.02 mL, 16.0 mmol), triethylamine (2.23 mL, 16.0 mmol) and HBTU (3.03 g, 8.00 mmol). After stirring at rt for 36 h, the reaction mixture was diluted with brine (40 mL) and extracted with EtOAc (3 x 40 mL). The

combined organic layers were washed with 1 M HCl (40 mL), saturated NaHCO₃ (40 mL) and water (40 mL). The organic phase was dried over Na₂SO₄ and concentrated *in vacuo*. Purification by column chromatography (50-100% EtOAc/PE) yielded the product as a pale orange oil (1.24 g, 3.10 mmol, 58%). **R_f** 0.19 (SiO₂, 80% EtOAc/PE); **v_{max}** (neat/cm⁻¹) 3290 (m, N-H), 2978 (m, C-H), 2112 (m, C≡C), 1657 (s, C=O); **δ_H** (600 MHz, CD₃OD) 4.01 (d, 2H, *J* = 2.5 Hz, H8), 3.19 (s, 2H, H6), 3.13 (t, 4H, *J* = 6.2 Hz, H2), 2.60 (t, 4H, *J* = 5.8 Hz, H1), 2.58 (t, 1H, *J* = 2.5 Hz, H10), 1.45 (s, 18H, H5); **δ_C** (101 MHz, CD₃OD) 173.9 (C7), 158.6 (C3), 80.6 (C9), 80.2 (C4), 72.2 (C10), 59.7 (C6), 56.3 (C1), 39.5 (C2), 29.2 (C8), 28.9 (C5); **HRMS** (ESI) *m/z* found [M+H]⁺ 399.2593, C₁₉H₃₅O₅N₄⁺ required 399.2607.



***N,N'*-(((2-oxo-2-(prop-2-yn-1-ylamino)ethyl)azanediyl)bis(ethane-2,1-diyl))bis(4-((4,6-divinylpyrimidin-2-yl)amino)butanamide) (10)** To a solution of **8** (50.0 mg, 0.125 mmol) in CH₂Cl₂ (0.35 mL) at 0 °C was added HCl (4 M in dioxane, 0.85 mL). The reaction was stirred under nitrogen for 6 h and then concentrated *in vacuo* to yield the desired amine hydrochloride salt as a white solid. The amine hydrochloride salt was re-dissolved in DMF (2 mL) and cooled to 0 °C. A solution of 4-((4,6-divinylpyrimidin-2-yl)amino)butanoic acid **4** (58.0 mg, 0.250 mmol), triethylamine (174 μL, 1.25 mmol), EDC·HCl (96.0 mg, 0.500 mmol) and HOBt monohydrate (77.0 mg, 0.500 mmol) in DMF (4 mL) at 0 °C was added. The reaction was stirred under nitrogen for 18 h and then diluted with EtOAc (20 mL), washed with brine (20 mL), dried over Na₂SO₄, and concentrated *in vacuo*. Purification by column chromatography (0-10% MeOH/EtOAc) yielded the product as a colourless oil (43.3 mg, 69.0 μmol, 55%). **R_f** 0.17 (SiO₂, 10% MeOH/CH₂Cl₂); **v_{max}** (neat/cm⁻¹) 3291 (m, N-H), 2934 (m, C-H), 2147 (w, C≡C), 1631 (s, C=O), 1539 (s, C=C); **δ_H** (600 MHz, CD₃OD) 6.68 (s, 2H, H14), 6.60 (dd, 4H, *J* = 10.7, 17.4 Hz, H15), 6.36 (d, 4H, *J* = 17.4 Hz, H16b), 5.56 (dd, 4H, *J* = 1.4, 10.7 Hz, H16a), 3.97 (d, 2H, *J* = 2.5 Hz, H3), 3.46 (t, 4H, *J* = 6.8 Hz, H11), 3.24 (t, 4H, *J* = 6.2 Hz, H7), 3.18 (s, 2H, H5), 2.61 (t, 4H, *J* = 6.2 Hz, H6), 2.58 (t, 1H, *J* = 2.5 Hz, H1), 2.31 (t, 4H, *J* = 7.5 Hz, H9), 1.92 (qn, 4H, *J* = 7.1 Hz, H10); **δ_C** (101 MHz, CD₃OD) 176.1 (C8), 173.7 (C4), 165.3 (C13), 164.0

(C12), 137.1 (C15), 122.1 (C16), 105.8 (C14), 80.6 (C2), 72.4 (C1), 59.4 (C5), 55.8 (C6), 41.7 (C11), 38.6 (C7), 34.7 (C9), 29.3 (C3), 27.0 (C10); **HRMS** (ESI) m/z found $[M+H]^+$ 629.3658, $C_{33}H_{45}O_3N_{10}^+$ required 629.3676.



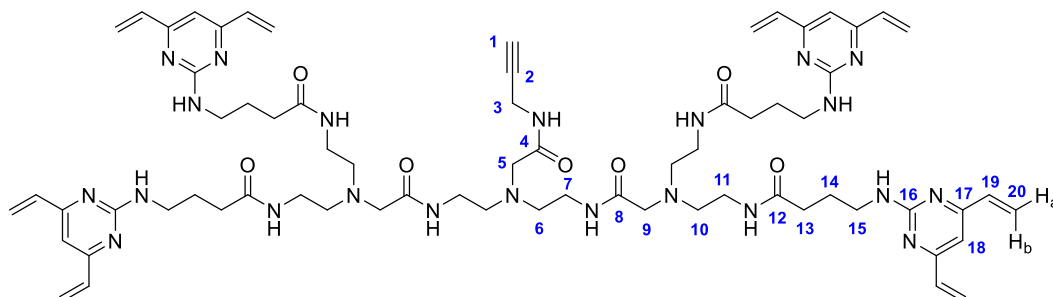
Tetra-*N*-Boc-amine backbone, (alkyne)₁ (**14**)

Method A: To a solution of methyl bis(2-((*tert*-butoxycarbonyl)amino)ethyl)glycinate **6** (200 mg, 0.533 mmol) in MeOH (2.16 mL) and 1,4-dioxane (2.16 mL) was added aqueous NaOH (1 M, 1.08 mL). The reaction mixture was stirred at rt for 2 h and then concentrated *in vacuo*. The resulting residue was re-dissolved in MeOH, filtered, and concentrated again to yield the desired carboxylic acid intermediate. Concurrently, a solution of **8** (106 mg, 0.265 mmol) in CH₂Cl₂ (0.7 mL) at 0 °C was treated with HCl (4 M in dioxane, 1.7 mL). The reaction was stirred under nitrogen for 6 h and then concentrated *in vacuo* to yield the desired amine hydrochloride salt as a white solid. The carboxylic acid and the amine hydrochloride salt were combined, dissolved in DMF (10 mL) and cooled to 0 °C before addition of triethylamine (369 μ L, 2.65 mmol), EDC·HCl (203 mg, 1.06 mmol) and HOBt monohydrate (162 mg, 1.06 mmol). The reaction was stirred under nitrogen at rt for 18 h and then diluted with EtOAc (30 mL), washed with sat. NaHCO₃ (20 mL) and brine (20 mL), dried over Na₂SO₄, and concentrated *in vacuo*. Purification by column chromatography (0-5% MeOH/CH₂Cl₂) yielded the product as a white solid (118 mg, 0.133 mmol, 50%).

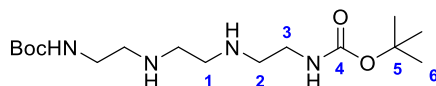
Method B: A suspension of tetra-*N*-Boc backbone **27** (59.3 mg, 75.0 μ mol) and K₂CO₃ (20.7 mg, 0.150 mmol) in MeCN (0.15 mL) was cooled to 0 °C. A solution of 2-bromo-*N*-(prop-2-yn-1-yl)acetamide **23** (16.5 mg, 94.0 μ mol) in MeCN (0.5 mL) was slowly added to the stirring suspension, after which the reaction was brought to rt and stirred overnight under nitrogen. The reaction mixture was concentrated and purified by column chromatography (0-10% MeOH/CH₂Cl₂) to give the title compound as a white solid (35.9 mg, 41.0 μ mol, 54%).

R_f 0.30 (SiO₂, 10% MeOH/CH₂Cl₂); **v_{max}** (neat/cm⁻¹) 3359 (m, N-H), 2985 (m, C-H), 2101 (m, C \equiv C), 1724 (s, C=O); **δ_H** (600 MHz, CDCl₃) 7.79 (br s, 2H, NH), 5.70 (s, 4H, NH), 4.04 (dd, 2H, J =

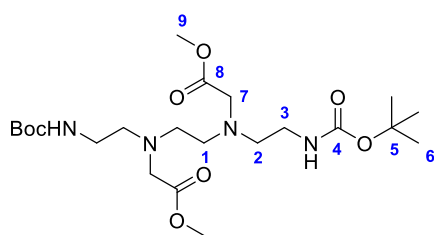
2.4, 5.4 Hz, H12), 3.37-3.32 (m, 4H, H2), 3.24 (s, 2H, H10), 3.20-3.14 (m, 8H, H6), 3.14 (s, 4H, H4), 2.75-2.70 (m, 4H, H1), 2.60-2.55 (m, 8H, H5), 2.25-2.22 (m, 1H, H14), 2.10 (s, 1H, NH), 1.42 (s, 36H, H9); δ_c (101 MHz, CDCl₃) 172.2 (C11), 171.5 (C3), 156.7 (C7), 80.0 (C13), 79.4 (C8), 71.5 (C14), 59.5 (C10/C4), 55.8 (C1/C5), 38.8 (C2), 37.9 (C6), 29.0 (C12), 28.6 (C9); **HRMS** (ESI) m/z found [M+H]⁺ 885.5760, C₄₁H₇₇O₁₁N₁₀⁺ required 885.5768.



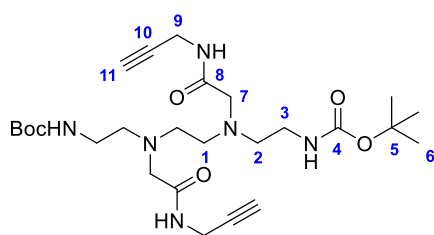
TetraDVP-alkyne₁ (15) To a solution of **14** (69.0 mg, 78.0 μ mol) in CH₂Cl₂ (0.5 mL) at 0 °C was added HCl (4 M in dioxane, 1.0 mL). The reaction was stirred under nitrogen for 6 h and then concentrated *in vacuo* to yield the desired amine hydrochloride salt as a white solid. The amine hydrochloride salt was re-dissolved in CH₂Cl₂ (1 mL) and cooled to 0 °C. To this solution, a solution of 4-((4,6-divinylpyrimidin-2-yl)amino)butanoic acid **4** (72.8 mg, 0.312 mmol), triethylamine (217 μ L, 1.56 mmol) and HBTU (118 mg, 0.312 mmol) in CH₂Cl₂ (2 mL) at 0 °C was added. The reaction was stirred under nitrogen for 18 h and then concentrated *in vacuo*. Purification by column chromatography (2.5-10% MeOH/CH₂Cl₂) yielded the product as a colourless oil (29.6 mg, 22.0 μ mol, 28%). R_f 0.15 (SiO₂, 10% MeOH/CH₂Cl₂); ν_{max} (neat/cm⁻¹) 3290 (m, N-H), 2944 (m, C-H), 2187 (m, C \equiv C), 1633 (s, C=O); δ_H (600 MHz, CD₃OD) 6.67 (s, 4H, H18), 6.59 (dd, 8H, J = 10.7, 17.4 Hz, H19), 6.35 (d, 8H, J = 17.4 Hz, H20b), 5.55 (dd, 8H, J = 1.5, 10.7 Hz, H20a), 3.97 (d, 2H, J = 2.5 Hz, H3), 3.45 (t, 8H, J = 6.8 Hz, H15), 3.27 (t, 4H, J = 6.5 Hz, H7), 3.24 (t, 8H, J = 6.3 Hz, H11), 3.21 (s, 2H, H5), 3.18 (s, 4H, H9), 2.65 (t, 4H, J = 6.4 Hz, H6), 2.62-2.59 (m, 1H, H1), 2.60 (t, 8H, J = 6.2 Hz, H10), 2.28 (t, 8H, J = 7.5 Hz, H13), 1.90 (qn, 8H, J = 7.2 Hz, H14); δ_c (101 MHz, CD₃OD) 175.9 (C12), 174.1 (C4), 173.7 (C8), 165.3 (C17), 164.0 (C16), 137.1 (C19), 122.1 (C20), 105.8 (C18), 80.8 (C2), 72.5 (C1), 59.7 (C9), 59.3 (C5), 55.9 (C10), 55.8 (C6), 41.7 (C15), 38.7 (C11), 38.5 (C7), 34.7 (C13), 29.4 (C3), 27.0 (C14); **HRMS** (ESI) m/z found [M+H]⁺ 1345.7930, C₆₉H₉₇O₇N₂₂⁺ required 1345.7905.



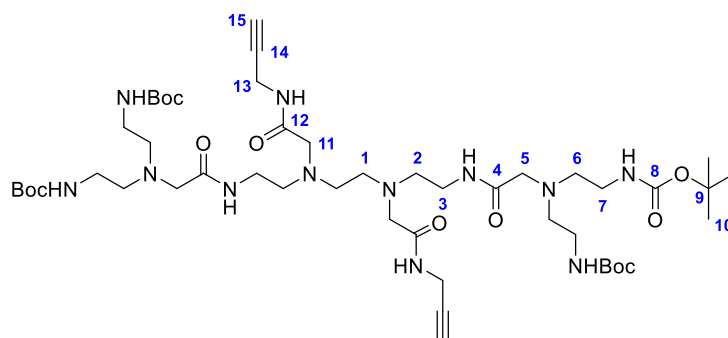
Di-tert-butyl ((ethane-1,2-diylbis(azanediyl))bis(ethane-2,1-diyl))dicarbamate (16) To a solution of triethylenetetramine (745 μL , 5.00 mmol) in THF (5 mL) at 0 $^{\circ}\text{C}$ was slowly added a solution of Boc-ON (2.46 g, 10.0 mmol) in THF (7.5 mL). The reaction was stirred at 0 $^{\circ}\text{C}$ under nitrogen for 1 h and then concentrated *in vacuo*. The crude yellow oil was dissolved in CH_2Cl_2 and sequentially washed with 10% aq. NaOH, water and brine. The organic phase was dried over Na_2SO_4 and concentrated *in vacuo*. Purification by column chromatography (0-10% MeOH/ CH_2Cl_2) yielded the product as a colourless oil (981 mg, 2.83 mmol, 57%). R_f 0.04 (SiO_2 , 10% MeOH/ CH_2Cl_2); ν_{max} (neat/ cm^{-1}) 3328 (m, N-H), 2976 (m, C-H), 1688 (s, C=O); δ_{H} (400 MHz, CDCl_3) 5.04 (br s, 2H, NH), 3.25-3.18 (m, 4H, H3), 2.75-2.70 (m, 4H, H2), 2.71 (s, 4H, H1), 1.44 (s, 18H, H6); δ_{C} (101 MHz, CDCl_3) 156.3 (C4), 79.3 (C5), 49.2 (C1), 49.0 (C2), 40.4 (C3), 28.6 (C6); **LRMS** (ESI) m/z found $[\text{M}+\text{H}]^+$ 347.5, $\text{C}_{16}\text{H}_{35}\text{O}_4\text{N}_4^+$ required 347.3.



Methyl 11-(2-((tert-butoxycarbonyl)amino)ethyl)-8-(2-methoxy-2-oxoethyl)-2,2-dimethyl-4-oxo-3-oxa-5,8,11-triazatridecan-13-oate (17) To a solution of di-tert-butyl ((ethane-1,2-diylbis(azanediyl))bis(ethane-2,1-diyl))dicarbamate **16** (970 mg, 2.80 mmol) in DMF (12.5 mL) were added DIPEA (1.17 mL, 6.72 mmol) and methyl bromoacetate (795 μL , 8.40 mmol). The reaction was stirred at rt for 2 h and then concentrated under a stream of nitrogen. The crude residue was purified by column chromatography (50-70% EtOAc/PE) yielding the product as a colourless oil (1.19 g, 2.42 mmol, 86%). R_f 0.10 (SiO_2 , 50% EtOAc/PE); ν_{max} (neat/ cm^{-1}) 3363 (m, N-H), 2974 (m, C-H), 1737 (s, C=O), 1707 (s, C=O); δ_{H} (400 MHz, CDCl_3) 5.73 (br s, 2H, NH), 3.69 (s, 6H, H9), 3.43 (s, 4H, H7), 3.20-3.12 (m, 4H, H3), 2.77-2.72 (m, 4H, H2), 2.76 (s, 4H, H1), 1.44 (s, 18H, H6); δ_{C} (101 MHz, CDCl_3) 171.9 (C8), 156.2 (C4), 79.1 (C5), 54.5 (C7), 52.4 (C1), 52.0 (C2), 51.6 (C9), 38.7 (C3), 28.6 (C6); **HRMS** (ESI) m/z found $[\text{M}+\text{H}]^+$ 491.3071, $\text{C}_{22}\text{H}_{43}\text{O}_8\text{N}_4^+$ required 491.3081.



Di-tert-butyl ((5,12-dioxo-4,7,10,13-tetraazahexadeca-1,15-diyne-7,10-diyl)bis(ethane-2,1-diyl))dicarbamate (19) To a solution of methyl 11-(2-((tert-butoxycarbonyl)amino)ethyl)-8-(2-methoxy-2-oxoethyl)-2,2-dimethyl-4-oxo-3-oxa-5,8,11-triazatridecan-13-oate **17** (1.18 g, 2.40 mmol) in MeOH (9.78 mL) and 1,4-dioxane (9.78 mL) was added aqueous NaOH (1 M, 4.89 mL). The reaction mixture was stirred at rt for 4 h and then concentrated *in vacuo*. The resulting residue was re-dissolved in MeOH, filtered, and concentrated again. The residue was then dissolved in DMF (20 mL), followed by addition of *N*-propargylamine (922 μ L, 14.4 mmol), triethylamine (2.01 mL, 14.4 mmol) and HBTU (2.73 g, 7.20 mmol). After stirring at rt for 16 h, the reaction mixture was diluted with EtOAc and washed with brine, 1 M HCl, brine, saturated NaHCO₃ and water. The organic phase was dried over Na₂SO₄ and concentrated *in vacuo*. Purification by column chromatography (EtOAc) yielded the product as an orange oil (151 mg, 0.282 mmol, 12%). **R_f** 0.07 (SiO₂, 80% EtOAc/PE); **v_{max}** (neat/cm⁻¹) 3288 (m, N-H), 2977 (m, C-H), 2151 (m, C≡C), 1661 (s, C=O); **δ _H** (600 MHz, CD₃OD) 4.02 (d, 4H, *J* = 2.5 Hz, H9), 3.19 (s, 4H, H7), 3.14 (t, 4H, *J* = 6.2 Hz, H3), 2.64 (s, 4H, H1), 2.63-2.58 (m, 4H, H2), 2.58 (t, 2H, *J* = 2.5 Hz, H11), 1.45 (s, 18H, H6); **δ _C** (101 MHz, CD₃OD) 173.8 (C8), 158.6 (C4), 80.8 (C10), 80.1 (C5), 72.2 (C11), 59.7 (C7), 56.5 (C1), 54.5 (C2), 38.9 (C3), 29.2 (C9), 28.8 (C6); **HRMS** (ESI) *m/z* found [M+H]⁺ 537.3400, C₂₆H₄₅O₆N₆⁺ required 537.3401.



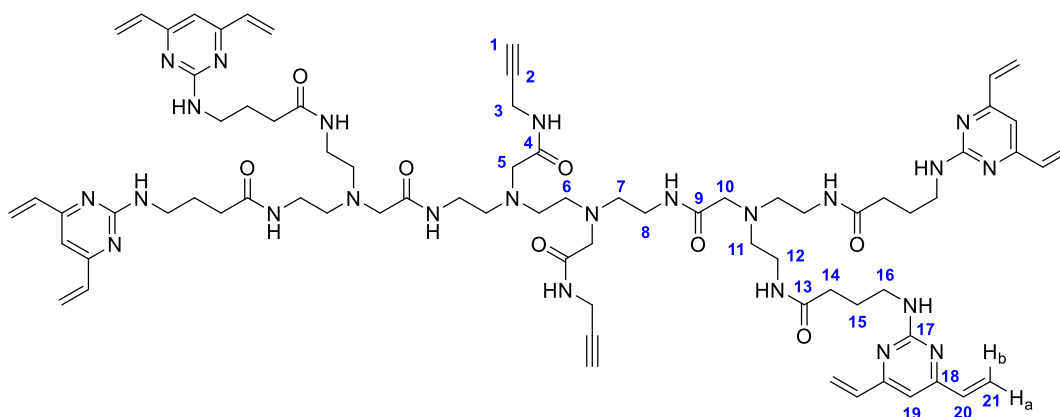
Tetra-*N*-Boc-amine backbone, (alkyne)₂ (**20**)

Method A: To a solution of methyl bis(2-((tert-butoxycarbonyl)amino)ethyl)glycinate **6** (190 mg, 0.506 mmol) in MeOH (2.16 mL) and 1,4-dioxane (2.16 mL) was added aqueous NaOH (1 M,

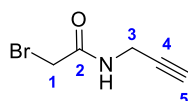
1.08 mL). The reaction mixture was stirred at rt for 4 h and then concentrated *in vacuo*. The resulting residue was re-dissolved in MeOH, filtered, and concentrated again to yield the desired carboxylic acid intermediate. Concurrently, a solution of **19** (136 mg, 0.253 mmol) in CH₂Cl₂ (0.7 mL) at 0 °C was treated with HCl (4 M in dioxane, 1.7 mL). The reaction was stirred under nitrogen for 6 h and then concentrated *in vacuo* to yield the desired amine hydrochloride salt as a white solid. The carboxylic acid and the amine hydrochloride salt were combined, dissolved in CH₂Cl₂ (10 mL) and cooled to 0 °C before addition of triethylamine (352 µL, 2.53 mmol) and HBTU (240 mg, 0.633 mmol). The reaction was stirred under nitrogen at rt for 18 h and then diluted with EtOAc (30 mL), washed with sat. NaHCO₃ (20 mL) and brine (20 mL), dried over Na₂SO₄, and concentrated *in vacuo*. Purification by column chromatography (0-10% MeOH/CH₂Cl₂) yielded the product as a white solid (80.8 mg, 79.0 µmol, 31%).

Method B: A suspension of tetra-*N*-Boc scaffold **28** (39.2 mg, 47.0 µmol) and K₂CO₃ (26.0 mg, 0.188 mmol) in MeCN (0.1 mL) was cooled to 0 °C. A solution of 2-bromo-*N*-(prop-2-yn-1-yl)acetamide **23** (20.8 mg, 0.118 mmol) in MeCN (0.4 mL) was slowly added to the stirring suspension, after which the reaction was brought to rt and stirred overnight under nitrogen. The reaction mixture was concentrated and purified by column chromatography (0-10% MeOH/CH₂Cl₂) to give the title compound as a white solid (30.0 mg, 29.0 µmol, 62%).

R_f 0.18 (SiO₂, 10% MeOH/CH₂Cl₂); **v_{max}** (neat/cm⁻¹) 3296 (m, N-H), 2978 (m, C-H), 2157 (m, C≡C), 1654 (s, C=O); **δ_H** (600 MHz, CD₃OD) 4.20 (s, 4H, H11), 4.08 (d, 4H, *J* = 2.5 Hz, H13), 3.80 (s, 4H, H5), 3.57 (t, 4H, *J* = 6.0 Hz, H3), 3.51-3.44 (m, 16H, H6/7), 3.27 (s, 4H, H1), 3.21-3.17 (m, 4H, H2), 2.72 (t, 2H, *J* = 2.5 Hz, H15), 1.47 (s, 36H, H10); **δ_C** (101 MHz, CD₃OD) 169.8 (C12), 166.3 (C4), 159.1 (C8), 81.3 (C14), 80.3 (C9), 73.2 (C15), 57.0 (C5), 56.1 (C11), 56.0 (C2), 55.9 (C6), 53.3 (C1), 37.0 (C3), 36.7 (C7), 30.0 (C13), 28.8 (C10); **HRMS** (ESI) *m/z* found [M+H]⁺ 1023.6547, C₄₈H₈₇O₁₂N₁₂⁺ required 1023.6566.



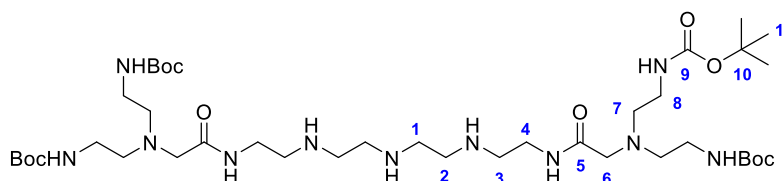
TetraDVP-alkyne 21 To a solution of **20** (79.8 mg, 78.0 μmol) in CH_2Cl_2 (0.5 mL) at 0 °C was added HCl (4 M in dioxane, 1.0 mL). The reaction was stirred under nitrogen for 6 h and then concentrated *in vacuo* to yield the desired amine hydrochloride salt as a white solid. The amine hydrochloride salt was re-dissolved in CH_2Cl_2 (1 mL) and cooled to 0 °C. To this solution was added a solution of 4-((4,6-divinylpyrimidin-2-yl)amino)butanoic acid **4** (72.8 mg, 0.312 mmol), triethylamine (217 μL , 1.56 mmol) and HBTU (118 mg, 0.312 mmol) in CH_2Cl_2 (2 mL) at 0 °C. The reaction was stirred under nitrogen for 18 h and then concentrated *in vacuo*. Purification by reverse phase flash column chromatography (35-70% solvent B in solvent A. Solvent A: 100 mM NH_4OH (aq). Solvent B: MeCN) and lyophilisation yielded the product as a colourless oil (46.1 mg, 31.0 μmol , 40%). ν_{max} (neat/ cm^{-1}) 3289 (m, N-H), 2938 (m, C-H), 2186 (m, $\text{C}\equiv\text{C}$), 1637 (s, $\text{C}=\text{O}$); δ_{H} (600 MHz, CD_3OD) 6.67 (s, 4H, H19), 6.59 (dd, 8H, J = 10.6, 17.4 Hz, H20), 6.35 (d, 8H, J = 17.3 Hz, H21b), 5.56 (dd, 8H, J = 1.2, 10.7 Hz, H21a), 3.98 (d, 4H, J = 2.3, H3), 3.45 (t, 8H, J = 6.7 Hz, H16), 3.27 (t, 4H, J = 6.8 Hz, H8), 3.24 (t, 8H, J = 6.4 Hz, H12), 3.18 (s, 4H, H5), 3.17 (s, 4H, H10), 2.64-2.57 (m, 4H, H7), 2.64-2.57 (m, 2H, H1), 2.64-2.57 (m, 8H, H11), 2.60 (s, 4H, H6), 2.29 (t, 8H, J = 7.5 Hz, H14), 1.91 (qn, 8H, J = 7.1 Hz, H15); δ_{C} (101 MHz, CD_3OD) 175.9 (C13), 174.1 (C4), 173.7 (C9), 165.3 (C18), 164.0 (C17), 137.1 (C20), 122.1 (C21), 105.8 (C19), 80.9 (C2), 72.4 (C1), 59.7 (C10), 59.3 (C5), 55.8 (C7), 55.8 (C11), 54.4 (C6), 41.7 (C16), 38.7 (C12), 38.4 (C8), 34.7 (C14), 29.4 (C3), 27.0 (C15); **HRMS** (ESI) m/z found $[\text{M}+\text{H}]^+$ 1483.8687, $\text{C}_{76}\text{H}_{107}\text{O}_8\text{N}_{24}^+$ required 1483.8698.



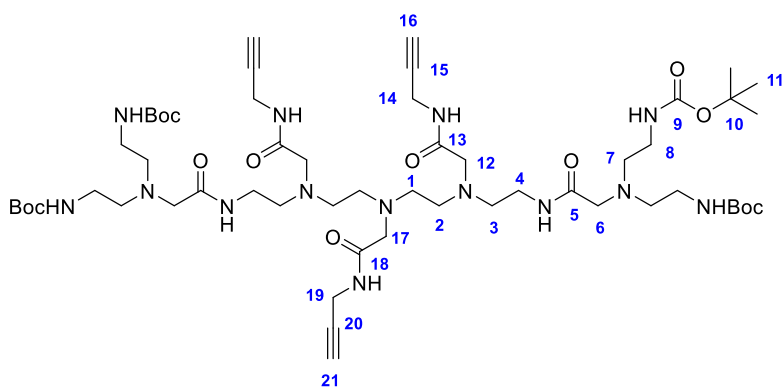
2-bromo-N-(prop-2-yn-1-yl)acetamide (23) A solution of propargylamine (1.16 mL, 18.2 mmol) in CH_2Cl_2 (33 mL) and sat. NaHCO_3 (33 mL) was cooled to -10 °C and 2-bromoacetyl

bromide (2.42 mL, 27.2 mmol) was added dropwise over 15 min with vigorous stirring. The reaction mixture was allowed to warm to rt and stirred for a further 45 min. Following addition of water (30 mL), the aqueous solution was extracted with EtOAc (2 x 80 mL), and the combined organic extracts were washed with sat. NaHCO₃ (30 mL), 5% HCl (30 mL) and brine (30 mL). Combined organic extracts were dried over Na₂SO₄ and concentrated *in vacuo* to give the title compound as a pale yellow solid (2.97 g, 16.9 mmol, 93%). **R_f** 0.69 (SiO₂, 20% MeOH/CH₂Cl₂); **v_{max}** (neat/cm⁻¹) 3289 (m, N-H), 3071 (m, C-H), 2120 (w, C≡C), 1645 (s, C=O); **δ_H** (400 MHz, CDCl₃) 6.68 (s, 1H, NH), 4.09 (dd, 2H, *J* = 5.3, 2.6 Hz, H3), 3.90 (s, 2H, H1), 2.28 (t, 1H, *J* = 2.6 Hz, H5); **δ_C** (100 MHz, CDCl₃) 165.3 (C2), 78.6 (C4), 72.4 (C5), 30.1 (C3), 28.8 (C1); **LRMS** (ESI) *m/z* found [M+H]⁺ 178.0, C₅H₇ONBr⁺ required 178.0.

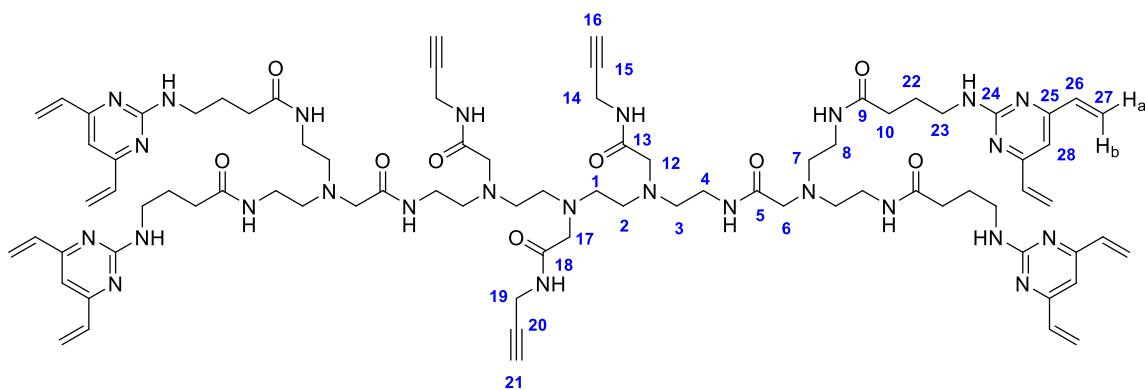
These data are consistent with those previously reported.²⁰³



Tetra-*N*-Boc-amine backbone, (NH)₃ (24) To a pre-dried microwave vial containing methyl bis(2-((*tert*-butoxycarbonyl)amino)ethyl)glycinate **6** (964 mg, 2.57 mmol) dissolved in dry MeOH (1 mL) was added tetraethylenepentamine (90.0 μL, 0.475 mmol). The vial was capped, flushed with nitrogen, and stirred overnight at 110 °C. The reaction mixture was concentrated, re-dissolved in CH₂Cl₂, and purified by column chromatography (0-20% MeOH/CH₂Cl₂) to give the desired compound as a white foam (184 mg, 0.210 mmol, 44%). **R_f** 0.06 (BuOH:H₂O:MeCN, 8:1:1); **v_{max}** (neat/cm⁻¹) 3330 (m, N-H), 2980 (m, C-H), 1689 (s, C=O); **δ_H** (400 MHz, CDCl₃) 7.63 (br s, 1H, NH), 6.21 (br s, 2H, NH), 3.40-3.30 (m, 4H, H4), 3.16-3.09 (m, 8H, H8), 3.06 (s, 4H, H6), 2.83-2.66 (m, 12H, H1/2/3), 2.60-2.52 (m, 8H, H7), 1.40 (s, 36H, H11); **δ_C** (100 MHz, CDCl₃) 171.5 (C5), 156.6 (C9), 79.2 (C10), 59.2 (C6), 55.3 (C7), 48.6 (C3), 48.5 (C2), 48.4 (C1), 38.7 (C8), 38.6 (C4), 28.6 (C11); **HRMS** (ESI) *m/z* found [M+H]⁺ 876.6284, C₄₀H₈₂N₁₁NaO₁₀⁺ required 876.6246.

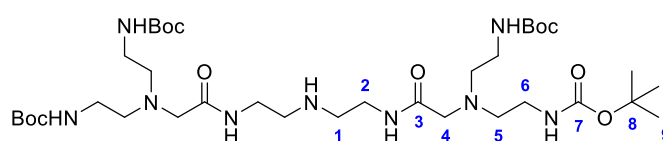


Tetra-*N*-Boc-amine backbone, (alkyne)₃ (25) A suspension of **24** (184 mg, 0.210 mmol) and K₂CO₃ (174 mg, 1.26 mmol) in MeCN (0.26 mL) was cooled to 0 °C. A solution of **23** (MeCN, 0.5 M, 1.58 mL) was slowly added to the stirring suspension, after which the reaction was brought to rt and stirred overnight. The reaction mixture was concentrated, re-dissolved in CH₂Cl₂ (40 mL), washed with water (2 x 10 mL) and brine (20 mL), dried over Na₂SO₄, and purified by column chromatography (5-10% MeOH/CH₂Cl₂) to give the title compound as a white foam (119 mg, 0.102 mmol, 49%). *R*_f 0.50 (SiO₂, 20% MeOH/CH₂Cl₂); *v*_{max} (neat/cm⁻¹) 3309 (m, N-H), 2928 (m, C-H), 2158 (m, C≡C), 1658 (s, C=O); *δ*_H (400 MHz, CD₃OD) 4.05 (d, 4H, *J* = 2.6 Hz, H14), 4.03 (d, 2H, *J* = 2.5 Hz, H19), 3.35-3.30 (m, 7H, H4), 3.25 (s, 4H, H12), 3.23 (s, 2H, H17), 3.18 (s, 4H, H6), 3.14 (t, 8H, *J* = 6.0 Hz, H8), 2.74-2.65 (m, 12H, H3/7), 3.64 (t, 2H, *J* = 2.3 Hz, H16), 2.62-2.58 (m, 9H, H1/2/21), 1.44 (s, 36H, H11); *δ*_C (100 MHz, CD₃OD) 174.3 (C13), 173.8 (C5), 173.6 (C18), 158.4 (C9), 80.9 (C20), 80.8 (C15), 80.1 (C10), 72.6 (C16), 72.3 (C21), 60.2 (C6), 59.3 (C17), 59.2 (C12), 56.5 (C7), 55.7 (C3), 54.4 (C2), 54.3 (C1), 39.7 (C8), 38.5 (C4), 29.5 (C14), 29.3 (C19), 28.9 (C11); **HRMS** (ESI) *m/z* found [M+H]⁺ 1161.7365, C₅₅H₉₇O₁₃N₁₄⁺ required 1161.7360.



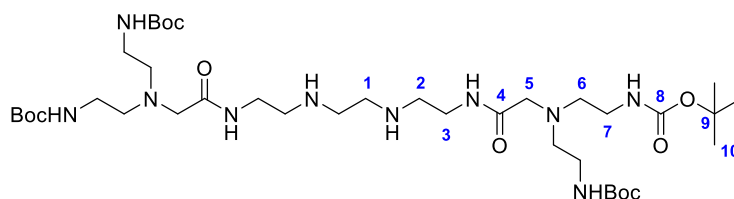
TetraDVP-alkyne₃ (26) To a solution of **25** (25.0 mg, 22.0 μmol) in CH₂Cl₂ (150 μL) at 0 °C was added HCl (4 M in dioxane, 270 μL). The reaction was brought to rt and stirred for 1 h. The

reaction mixture was concentrated to give the desired amine hydrochloride salt as a white solid. The amine hydrochloride salt was re-suspended in CH₂Cl₂ (150 μ L) and cooled to 0 $^{\circ}$ C, followed by addition of DIPEA (74.0 μ L, 0.420 mmol) and 4-((4,6-divinylpyrimidin-2-yl)amino)butanoic acid **4** (25.0 mg, 0.110 mmol). The solution was stirred at rt for 10 min, after which a solution of BTFFH in CH₂Cl₂ (0.6 M, 205 μ L) was added dropwise over 3 h with maximum stirring. After complete addition of BTFFH the reaction was stirred for an additional 12 h, concentrated, and then purified by reverse phase flash column chromatography (35-70% solvent B in solvent A. Solvent A: 100 mM NH₄OH (aq). Solvent B: MeCN) to yield the product after lyophilisation as a pale yellow solid (6.70 mg, 41.4 μ mol, 20%). ν_{max} (neat/cm⁻¹) 3305 (m, N-H), 2970 (m, C-H), 2156 (m, C \equiv C), 1637 (s, C=O); δ_{H} (400 MHz, CD₃OD) 6.68 (s, 4H, H28), 6.60 (dd, 8H, J = 17.4, 10.7 Hz, H26), 6.36 (d, 8H, J = 17.3 Hz, H27b), 5.56 (dd, 8H, J = 10.6, 1.6 Hz, H27a), 3.99 (t, 6H, J = 2.8 Hz, H14/19), 3.45 (t, 8H, J = 6.8 Hz, H23), 3.28 (t, 4H, J = 6.5 Hz, H4), 3.25 (t, 8H, J = 6.3 Hz, H8), 3.19 (s, 4H, H6), 3.18 (s, 4H, H12), 3.16 (s, 2H, H17), 2.65-2.58 (m, 23H, H1/2/3/7/16/21), 2.29 (t, 8H, J = 7.5 Hz, H10), 1.91 (qn, 8H, J = 7.0 Hz, H22); δ_{C} (126 MHz, CD₃OD) 175.9 (C9), 174.1 (C5), 173.8 (C13), 173.7 (C18), 165.3 (C25), 164.0 (C24), 137.2 (C26), 122.1 (C27), 105.8 (C28), 81.0 (C20), 81.0 (C15), 72.5 (C16), 72.4 (C21), 59.8 (C6), 59.4 (C12), 59.3 (C17), 55.9 (C3), 55.8 (C7), 54.5 (C1), 54.3 (C2), 41.7 (C23), 38.7 (C8), 38.4 (C4), 34.7 (C10), 29.4 (C14), 29.3 (C19), 27.0 (C22); **HRMS** (ESI) m/z found [M+H]⁺ 1621.9491, C₈₃H₁₁₇N₂₆O₉⁺ required 1621.9497.

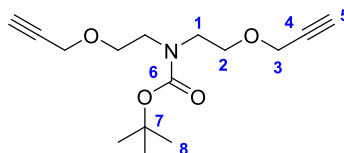


Tetra-N-Boc-amine backbone, (NH)₁ (27) In a pre-dried microwave vial containing methyl bis(2-((*tert*-butoxycarbonyl)amino)ethyl)glycinate **6** (200 mg, 0.530 mmol) dissolved in dry MeOH (0.3 mL) was added diethylenetriamine (10.7 μ L, 98.0 μ mol). The vial was capped, flushed with nitrogen, and stirred overnight at 110 $^{\circ}$ C. The reaction mixture was concentrated and purified by column chromatography (0-10% MeOH/CH₂Cl₂) to give the product as a colourless oil (60.6 mg, 77.0 μ mol, 78%). R_f 0.14 (SiO₂, 10% MeOH/CH₂Cl₂); ν_{max} (neat/cm⁻¹) 3316 (m, N-H), 2974 (m, C-H), 1687 (s, C=O); δ_{H} (400 MHz, CD₃OD) 3.48 (t, 4H, J = 5.8 Hz, H2), 3.21 (s, 4H, H4), 3.14 (t, 8H, J = 6.3 Hz, H6), 3.06 (t, 4H, J = 5.7 Hz, H1), 2.61 (t, 8H, J = 6.3 Hz, H5), 1.45 (s, 36H, H9); δ_{C} (101 MHz, CD₃OD) 175.6 (C3), 158.6 (C7), 80.2 (C8), 59.9 (C4), 56.4

(C5), 49.5 (C1), 39.7 (C2), 38.4 (C6), 28.9 (C9); **HRMS** (ESI) m/z found $[M+H]^+$ 790.5425, $C_{36}H_{72}O_{10}N_9^+$ required 790.5402.



Tetra-*N*-Boc-amine backbone, (NH)₂ (28) In a pre-dried microwave vial containing methyl bis(2-((*tert*-butoxycarbonyl)amino)ethyl)glycinate **6** (203 mg, 0.540 mmol) dissolved in dry MeOH (0.3 mL) was added triethylenetetramine (14.9 μ L, 0.100 mmol). The vial was capped, flushed with nitrogen, and stirred overnight at 110 °C. The reaction mixture was concentrated and purified by column chromatography (0-20% MeOH/ CH_2Cl_2) to give the product as a colourless oil (40.8 mg, 49.0 μ mol, 49%). R_f 0.38 (SiO₂, 20% MeOH/ CH_2Cl_2); ν_{max} (neat/ cm^{-1}) 3335 (m, N-H), 2980 (m, C-H), 1690 (s, C=O); δ_H (600 MHz, CD₃OD) 3.38 (t, 4H, J = 6.3 Hz, H3), 3.17 (s, 4H, H5), 3.13 (t, 8H, J = 6.1 Hz, H7), 2.80-2.77 (m, 4H, H2), 2.76 (s, 4H, H1), 2.60 (t, 8H, J = 5.7 Hz, H6), 1.45 (s, 36H, H10); δ_C (101 MHz, CD₃OD) 174.5 (C4), 158.6 (C8), 80.2 (C9), 60.1 (C5), 56.4 (C6), 49.7 (C1), 49.4 (C2), 39.7 (C3), 39.7 (C7), 28.9 (C10); **HRMS** (ESI) m/z found $[M+H]^+$ 833.5843, $C_{38}H_{77}O_{10}N_{10}^+$ required 833.5824.

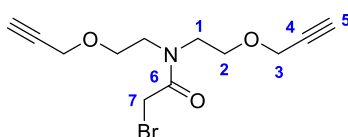


***tert*-butyl bis(2-(prop-2-yn-1-yloxy)ethyl)carbamate (29)** A solution of diethanolamine (2.44 g, 23.0 mmol) in CH_2Cl_2 (25 mL) was cooled to 0 °C and a solution of di-*tert*-butyl dicarbonate (6.33 g, 29.0 mmol) in CH_2Cl_2 (5 mL) as slowly added. The reaction was stirred for 12 h at rt, diluted in CH_2Cl_2 (40 mL) and washed with water (40 mL). The aqueous phase was extracted with CH_2Cl_2 (2 x 20 mL). The combined organic extracts were washed with brine, dried over Na₂SO₄, and concentrated to give *tert*-butyl bis(2-hydroxyethyl)carbamate as a clear oil, which was used directly in the next step without further purification.

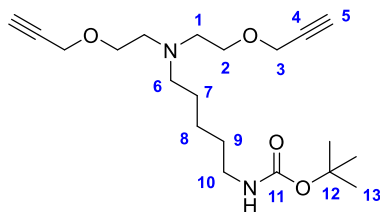
To a 50% NaOH_(aq) solution (11 mL) was sequentially added *tert*-butyl bis(2-hydroxyethyl)carbamate in toluene (11 mL), tetrabutylammonium bisulfate (16.0 mg, 47.0 μ mol), and propargyl bromide (80% in toluene, 8.70 mL, 78.0 mmol), and the reaction

was stirred at rt for 48 h. The organic layer was isolated, concentrated, and purified by column chromatography (50% EtOAc/hexane) to give the title compound as a yellow viscous oil (2.30 g, 7.57 mmol, 35%). R_f 0.60 (SiO₂, 50% EtOAc/hexane); ν_{\max} (neat/cm⁻¹) 2975 (m, C-H), 2117 (m, C≡C), 1686 (s, C=O); δ_H (400 MHz, CDCl₃) 4.13 (d, 4H, J = 2.4 Hz, H3), 3.66-3.57 (m, 4H, H2), 3.52-3.38 (m, 4H, H1), 2.41 (t, 2H, J = 2.4 Hz, H5), 1.45 (s, 9H, H8); δ_C (100 MHz, CDCl₃) 155.6 (C6), 79.9 (C7), 79.8 (C4), 74.5 (C5), 68.7 (C2), 58.3 (C3), 47.9 (C1), 28.6 (C8); **LRMS** (ESI) m/z found $[M+Na]^+$ 304.2, C₁₅H₂₃N₂O₄Na⁺ required 304.2.

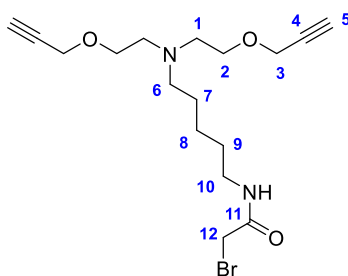
These data are consistent with those previously reported.^{233,234}



2-bromo-*N,N*-bis(2-(prop-2-yn-1-yloxy)ethyl)acetamide (30) A solution of **29** (0.570 g, 2.03 mmol) in CH₂Cl₂ (3 mL) was treated with TFA (1 mL) and the reaction was stirred at rt for 2 h. The reaction mixture was concentrated to remove excess TFA and a light yellow solid was obtained, which was used directly in the next step without any further purification. The solid was suspended in CH₂Cl₂ (8 mL) and cooled to 0 °C, followed by addition of DIPEA (1.40 mL, 8.10 mmol) and bromoacetyl bromide (0.350 mL, 4.05 mmol). The reaction was stirred at rt for 1 h. The reaction mixture was diluted with CH₂Cl₂ (20 mL), cooled to 0 °C, sat. NaHCO₃ (15 mL) added, and the resulting suspension was stirred vigorously for 5 min. The reaction mixture was concentrated and water (10 mL) and EtOAc (20 mL) added. The aqueous phase was extracted with EtOAc (2 x 20 mL), the combined organic layers washed with sat. NaHCO₃ (20 mL), 1 M HCl (2 x 10 mL), and brine (20 mL). The organic layer was dried over Na₂SO₄ and concentrated *in vacuo*. Purification by column chromatography (25% EtOAc/hexane) yielded the title compound as a light yellow oil (0.360 g, 1.20 mmol, 60%). R_f 0.55 (SiO₂, 50% EtOAc/hexane); ν_{\max} (neat/cm⁻¹) 2865 (m, C-H), 2114 (m, C≡C), 1638 (s, C=O); δ_H (400 MHz, CDCl₃) 4.08 (d, 2H, J = 2.4 Hz, H3), 4.06* (d, 2H, J = 2.4 Hz, H3), 3.93 (s, 2H, H7), 3.64-3.60 (m, 6H, H1/2), 3.53-3.48* (m, 2H, H1), 2.42 (t, 1H, J = 2.4 Hz, H5), 2.40* (t, 1H, J = 2.4 Hz, H5); δ_C (100 MHz, CDCl₃) 167.6 (C6), 79.5 (C4), 79.1* (C4), 75.0 (C5), 74.7* (C5), 68.1 (C2), 67.5* (C2), 58.5 (C3), 58.3* (C3), 49.9 (C1), 46.8* (C1), 27.1 (C7); **HRMS** (ESI) m/z found $[M+H]^+$ 302.0388, C₁₂H₁₇O₃NBr⁺ required 302.0392. *Rotamer

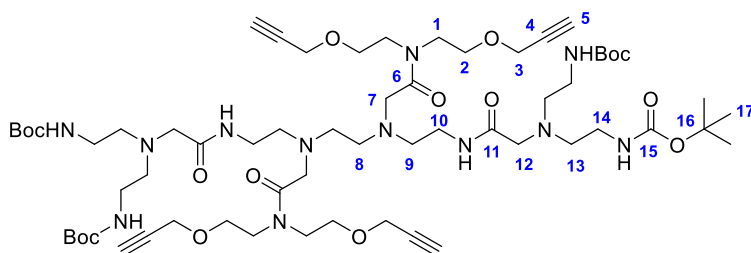


tert-butyl (5-(bis(2-(prop-2-yn-1-yloxy)ethyl)amino)pentyl)carbamate (31) A solution of **29** (281 mg, 1.00 mmol) in CH₂Cl₂ (1.5 mL) was cooled to 0 °C, followed by addition of HCl (4 M in dioxane, 3 mL). The reaction was brought to rt and stirred for 2 h. The reaction mixture was concentrated to give the desired amine hydrochloride salt as a white solid. The solid was re-suspended in MeCN (10 mL). Sodium carbonate (1.06 g, 10.0 mmol) was added. After stirring for 5 min, a solution of *tert*-butyl (5-bromopentyl)carbamate (399 mg, 1.50 mmol) in MeCN (2 mL) was added. The reaction mixture was then refluxed at 70 °C for 48 h. Subsequently, the reaction mixture was diluted with brine (30 mL) and extracted with EtOAc (3 x 20 mL). The combined organic layers were dried over Na₂SO₄, concentrated *in vacuo*, and purified by column chromatography (30-50% EtOAc/PE) to give the title compound as a pale yellow oil (242 mg, 0.661 mmol, 66%). *R*_f 0.21 (SiO₂, 80% EtOAc/PE); *v*_{max} (neat/cm⁻¹) 3342 (m, N-H), 2938 (m, C-H), 2111 (m, C≡C), 1676 (s, C=O); *δ*_H (400 MHz, CDCl₃) 4.54 (br s, 1H, NH), 4.16 (d, 4H, *J* = 2.3 Hz, H3), 3.60 (t, 4H, *J* = 6.0 Hz, H2), 3.14-3.06 (m, 2H, H10), 2.73 (t, 4H, *J* = 6.0 Hz, H1), 2.55-2.49 (m, 2H, H6), 2.42 (t, 2H, *J* = 2.2 Hz, H5), 1.51-1.42 (m, 4H, H7/9), 1.44 (s, 9H, H13), 1.30 (qn, 2H, *J* = 7.6 Hz, H8); *δ*_C (100 MHz, CDCl₃) 156.0 (C11), 79.9 (C12), 79.0 (C4), 74.3 (C5), 68.3 (C2), 58.2 (C3), 55.0 (C6), 53.8 (C1), 40.5 (C10), 29.9 (C9), 28.4 (C13), 26.7 (C7), 24.5 (C8); **HRMS** (ESI) *m/z* found [M+H]⁺ 367.2587, C₂₀H₃₄O₄N₂⁺ required 367.2597.

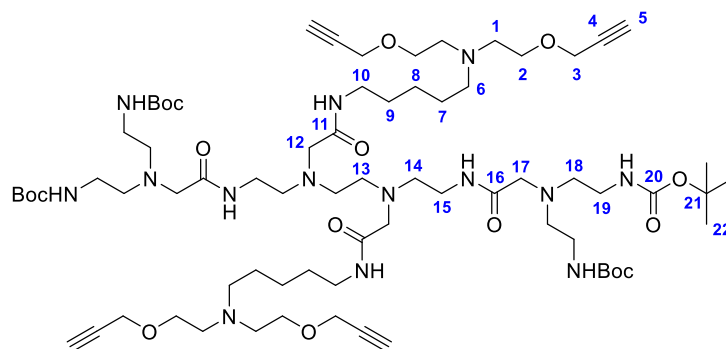


***N*-(5-(bis(2-(prop-2-yn-1-yloxy)ethyl)amino)pentyl)-2-bromoacetamide (32)** To a solution of *tert*-butyl (5-(bis(2-(prop-2-yn-1-yloxy)ethyl)amino)pentyl)carbamate **31** (100 mg, 0.270 mmol) in CH₂Cl₂ (0.5 mL) at 0 °C was added HCl (4 M in dioxane, 1 mL). The reaction was stirred under nitrogen for 2 h and then concentrated *in vacuo* to yield the desired amine hydrochloride salt as a white solid. The hydrochloride salt was re-dissolved in a mixture of

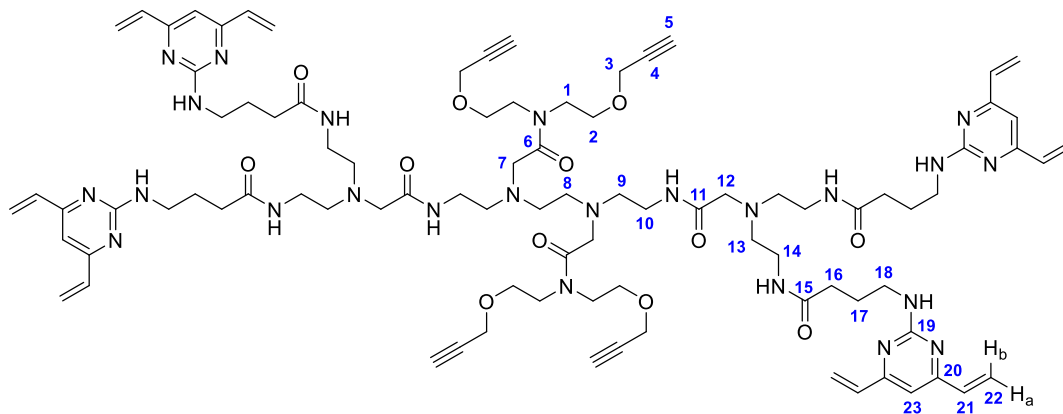
CH₂Cl₂ (1 mL) and sat. NaHCO₃ (1 mL) and cooled to -10 °C, followed by dropwise addition of 2-bromoacetyl bromide (35.3 μL, 0.405 mmol). The reaction mixture was stirred for 1 h, and then diluted with brine and extracted with CH₂Cl₂ (3 x 10 mL). Combined organic phases were dried over Na₂SO₄ and concentrated *in vacuo*. Purification by column chromatography (0-5% MeOH/CH₂Cl₂) yielded the title compound as a pale yellow oil (57.3 mg, 0.148 mmol, 55%). **R_f** 0.41 (SiO₂, 10% MeOH/CH₂Cl₂); **v_{max}** (neat/cm⁻¹) 3219 (m, N-H), 2928 (m, C-H), 2111 (m, C≡C), 1672 (s, C=O); **δ_H** (400 MHz, CDCl₃) 6.55 (br s, 1H, NH), 4.15 (d, 4H, *J* = 2.4 Hz, H3), 3.87 (s, 2H, H12), 3.62 (t, 4H, *J* = 5.5 Hz, H2), 3.27 (q, 2H, *J* = 6.7 Hz, H10), 2.78-2.75 (m, 4H, H1), 2.58-2.54 (m, 2H, H6), 2.43 (t, 2H, *J* = 2.4 Hz, H5), 1.55 (qn, 2H, *J* = 7.4 Hz, H7), 1.50 (qn, 2H, *J* = 7.4 Hz, H9), 1.33 (qn, 2H, *J* = 7.6 Hz, H8); **δ_C** (100 MHz, CDCl₃) 165.5 (C11), 79.7 (C4), 74.8 (C5), 67.8 (C2), 58.4 (C3), 55.0 (C6), 53.9 (C1), 40.2 (C10), 29.8 (C9), 29.5 (C12), 29.1 (C7), 24.5 (C8); **HRMS** (ESI) *m/z* found [M+H]⁺ 387.1273, C₁₇H₂₈O₃N₂Br⁺ required 387.1283.



Tetra-*N*-Boc-amine backbone, ((alkyne)₂)₂ (33) To a solution of tetra-*N*-Boc backbone **28** (55.0 mg, 66.0 μmol) in MeCN (0.2 mL) was added K₂CO₃ (51.0 mg, 0.370 mmol), followed by a solution of 2-bromo-*N,N*-bis(2-(prop-2-yn-1-yloxy)ethyl)acetamide **30** (49.7 mg, 165 μmol) in MeCN (0.5 mL). The reaction was stirred at rt for 48 h. The reaction mixture was concentrated, and the desired compound was purified by column chromatography (5-10% MeOH/CH₂Cl₂) to give the title compound as a clear oil (56.0 mg, 43.9 μmol, 67%). **R_f** 0.34 (10% MeOH/CH₂Cl₂); **v_{max}** (neat/cm⁻¹) 3296 (m, N-H), 2969 (m, C-H), 2493 (m, C≡C), 1654 (s, C=O); **δ_H** (400 MHz, CD₃OD) 4.21 (d, 4H, *J* = 2.3 Hz, H3), 4.18* (d, 4H, *J* = 2.3 Hz, H3), 3.76-3.60 (m, 20H, H1/2/7), 3.35-3.27 (m, 4H, H10), 3.21-3.14 (m, 12H, H12/14), 2.92 (t, 2H, *J* = 2.1 Hz, H5), 2.88* (t, 2H, *J* = 2.4 Hz, H5), 2.81-2.73 (m, 8H, H8/9), 2.65 (t, 8H, *J* = 6.1 Hz, H13), 1.46 (s, 36H, H17); **δ_C** (126 MHz, CD₃OD) 174.2 (C11), 173.6 (C6), 158.4 (C15), 80.7 (C4), 80.6* (C4), 80.1 (C16), 76.4 (C5), 76.2* (C5), 68.9 (C2), 68.8* (C2), 60.3 (C12), 59.3 (C3), 59.0* (C3), 57.1 (C7), 56.7 (C13), 55.4 (C9), 53.8 (C8), 47.4 (C1), 39.9 (C14), 38.4 (C10), 29.0 (C17); **HRMS** (ESI) *m/z* found [M+H]⁺ 1275.7987, C₆₂H₁₀₇N₁₂O₁₆⁺ required 1275.7928. *Rotamer

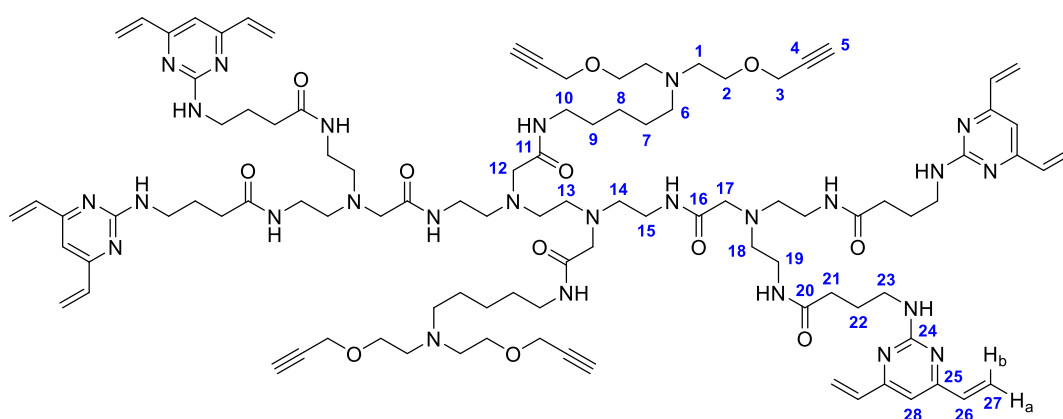


Tetra-*N*-Boc-amine backbone, (pentane-(alkyne)₂)₂ (34) To a solution of tetra-*N*-Boc backbone **28** (49.3 mg, 59.2 μ mol) in MeCN (1 mL) was added K₂CO₃ (32.7 mg, 237 μ mol), followed by a solution of *N*-(5-(bis(2-(prop-2-yn-1-yloxy)ethyl)amino)pentyl)-2-bromoacetamide **32** (57.3 mg, 148 μ mol) in MeCN (0.5 mL). The reaction was stirred at rt for 48 h. The reaction mixture was concentrated, and the desired compound purified by column chromatography (0-15% MeOH/CH₂Cl₂) to give the title compound as a clear oil (38.8 mg, 26.6 μ mol, 45%). *R*_f 0.35 (15% MeOH/CH₂Cl₂); *v*_{max} (neat/cm⁻¹) 3283 (m, N-H), 2936 (m, C-H), 2155 (m, C≡C), 1654 (s, C=O); δ _H (400 MHz, CD₃OD) 4.17 (s, 4H, H3), 3.66 (t, 8H, *J* = 5.5 Hz, H2), 3.32-3.29 (m, 8H, H5/15), 3.26-3.21 (m, 4H, H10), 3.20 (s, 4H, H12), 3.16 (s, 4H, H17), 3.13 (t, 8H, *J* = 5.8 Hz, H19), 2.89-2.84 (m, 8H, H1), 2.70-2.65 (m, 12H, H6/13/14), 2.59 (t, 8H, *J* = 5.7 Hz, H18), 1.61-1.50 (m, 8H, H7/9), 1.44 (s, 36H, H22), 1.38-1.30 (m, 4H, H8); δ _C (126 MHz, CD₃OD) 174.3 (C11), 173.8 (C16), 158.5 (C20), 80.7 (C4), 80.2 (C21), 76.2 (C5), 68.3 (C2), 60.2 (C12), 59.6 (C17), 59.0 (C3), 56.5 (C14/18), 56.0 (C6/13), 54.6 (C1), 40.3 (C10), 39.7 (C15), 38.6 (C19), 30.5 (C9), 29.0 (C22), 26.8 (C7), 25.8 (C8); **HRMS** (ESI) *m/z* found [M+H]⁺ 1445.9692, C₇₂H₁₂₉N₁₄O₁₆⁺ required 1445.9711.



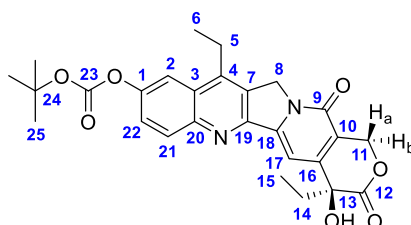
TetraDVP-((alkyne)₂)₂ (35) A solution of tetra-*N*-Boc backbone **33** (38.0 mg, 30.0 μ mol) in CH₂Cl₂ (210 μ L) was cooled to 0 °C and HCl (4 M in dioxane, 370 μ L) was added. The reaction

was brought to rt and stirred for 1 h. The reaction mixture was concentrated *in vacuo* to give the desired amine hydrochloride salt as a white solid. The amine hydrochloride salt was re-suspended in CH₂Cl₂ (210 μ L) and cooled to 0 °C. DIPEA (105 μ L, 0.600 mmol) was added, followed by 4-((4,6-divinylpyrimidin-2-yl)amino)butanoic acid **4** (35.0 mg, 0.150 mmol). The solution was stirred at rt for 10 min, after which a solution of BTFFH in CH₂Cl₂ (0.6 M, 290 μ L) was added dropwise over 3 h during maximum stirring. After complete addition of BTFFH the reaction was stirred for an additional 12 h at rt, concentrated, and purified by reverse phase flash column chromatography (35-70% solvent B in solvent A; Solvent A: 100 mM NH₄OH (aq). Solvent B: MeCN) to yield the desired product after lyophilisation as a clear oil (5.00 mg, 2.88 μ mol, 10%). ν_{max} (neat/cm⁻¹) 3335 (m, N-H), 2928 (m, C-H), 2336 (m, C \equiv C), 1636 (s, C=O); δ_{H} (400 MHz, CD₃OD) 6.68 (s, 4H, H23), 6.60 (dd, 8H, *J* = 17.4, 10.6 Hz, H21), 6.36 (d, 8H, *J* = 17.4 Hz, H22b), 5.56 (dd, 8H, *J* = 10.6, 1.5 Hz, H22a), 4.15 (d, 4H, *J* = 2.3 Hz, H3), 4.11* (d, 4H, *J* = 2.3 Hz, H3), 3.67-3.54 (m, 16H, H1/2), 3.53 (s, 4H, H7), 3.45 (t, 8H, *J* = 6.8 Hz, H18), 3.28-3.22 (m, 12H, H10/14), 3.18 (s, 4H, H12), 2.89 (t, 2H, *J* = 2.3 Hz, H5), 2.84* (t, 2H, *J* = 2.4 Hz, H5), 2.68 (s, 4H, H8), 2.66-2.59 (m, 12H, H9/13), 2.28 (t, 8H, *J* = 7.5 Hz, H16), 1.91 (qn, 8H, *J* = 7.1 Hz, H17); δ_{C} (126 MHz, CD₃OD) 175.8 (C15), 173.9 (C6), 173.9 (C11), 165.3 (C20), 164.0 (C19), 137.2 (C21), 122.1 (C22), 105.9 (C23), 80.7 (C4), 80.7* (C4), 76.4 (C5), 76.2* (C5), 68.8 (C2), 68.8* (C2), 59.8 (C12), 59.3 (C3), 59.0* (C3), 57.1 (C7), 55.8 (C13), 55.4 (C9), 54.2 (C8), 47.2 (C1), 41.8 (C18), 38.7 (C14), 38.6 (C10), 34.7 (C16), 27.0 (C17); **HRMS** (ESI) *m/z* found [M+H]⁺ 1736.0099, C₉₀H₁₂₇N₂₄O₁₂⁺ required 1736.0060. *Rotamer



TetraDVP-(pentane-(alkyne)₂)₂ (36) To a solution of tetra-*N*-Boc backbone **34** (13.0 mg, 8.99 μ mol) in CH₂Cl₂ (0.25 mL) at 0 °C was added HCl (4 M in dioxane, 0.5 mL). The reaction was stirred under nitrogen for 2 h and then concentrated *in vacuo* to yield the desired amine hydrochloride salt as a white solid. The amine hydrochloride salt was re-dissolved in CH₂Cl₂

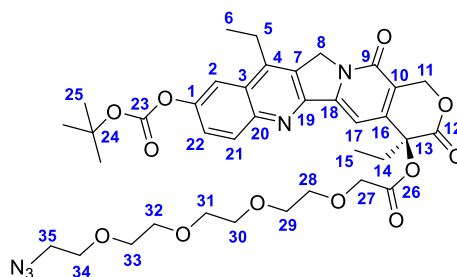
(0.25 mL) and cooled to 0 °C. To this solution was added a solution of 4-((4,6-divinylpyrimidin-2-yl)amino)butanoic acid **4** (12.6 mg, 53.9 μ mol), triethylamine (25 μ L, 180 μ mol) and HBTU (20.5 mg, 53.9 μ mol) in CH₂Cl₂ (0.25 mL) at 0 °C. The reaction was stirred under nitrogen for 18 h and then concentrated *in vacuo*. Purification by reverse phase flash column chromatography (35-70% solvent B in solvent A. Solvent A: 100 mM NH₄OH (aq). Solvent B: MeCN) and lyophilisation yielded the product as a white solid (1.80 mg, 0.940 μ mol, 10%). ν_{max} (neat/cm⁻¹) 3299 (m, N-H), 2928 (m, C-H), 2153 (m, C \equiv C), 1645 (s, C=O); δ_{H} (400 MHz, CD₃OD) 6.69 (s, 4H, H28), 6.60 (dd, 8H, *J* = 17.4, 10.7 Hz, H26), 6.36 (d, 8H, *J* = 17.3 Hz, H27b), 5.57 (dd, 8H, *J* = 10.7, 1.5 Hz, H27a), 4.23 (d, 8H, *J* = 2.4 Hz, H3), 3.83 (t, 8H, *J* = 4.9 Hz, H2), 3.45 (t, 8H, *J* = 6.8 Hz, H23), 3.30-3.15 (m, 32H, H1/10/12/15/17/19), 3.00 (t, 4H, *J* = 2.3 Hz, H5), 2.65-2.60 (m, 24H, H6/13/14/18), 2.29 (t, 8H, *J* = 7.5 Hz, H21), 1.91 (qn, 8H, *J* = 7.1 Hz, H22), 1.56 (qn, 4H, *J* = 7.5 Hz, H9), 1.39-1.30 (m, 8H, H7/8); δ_{C} (126 MHz, CD₃OD) 175.9 (C20), 174.2 (C11/16), 165.3 (C25), 164.0 (C24), 137.2 (C26), 122.2 (C27), 105.9 (C28), 89.9 (C4), 77.2 (C5), 68.8 (C2), 59.9 (C12/17), 59.2 (C3), 56.1 (C14), 56.0 (C6), 55.3 (C18), 54.0 (C13), 47.1 (C1), 41.8 (C23), 40.4 (C10), 38.8 (C15/19), 34.7 (C21), 30.2 (C9), 26.8 (C7), 27.1 (C22), 25.0 (C8); **HRMS** (ESI) *m/z* found [M+H]⁺ 1906.1851, C₁₀₀H₁₄₉N₂₆O₁₂⁺ required 1906.1848.



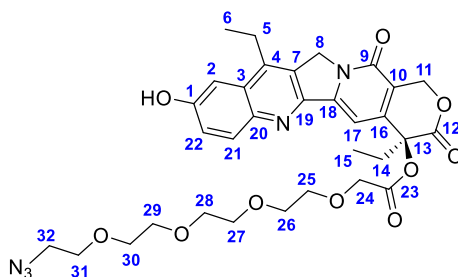
SN-38-Boc (65) To a suspension of SN-38 (20.0 mg, 50.0 μ mol) in CH₂Cl₂ (2 mL) were added pyridine (140 μ L) and Boc anhydride (16.4 mg, 75.0 μ mol). The reaction was stirred at rt under nitrogen for 1 h and then washed with 0.5 M HCl (3 x 5 mL) and sat. NaHCO₃ (5 mL). The organic phase was dried over Na₂SO₄ and concentrated *in vacuo* to yield the product as a white solid (24.6 mg, 50.0 μ mol, 100%). δ_{H} (400 MHz, CDCl₃) 8.26 (d, 1H, *J* = 9.2 Hz, H21), 7.90 (d, 1H, *J* = 2.5 Hz, H2), 7.69 (s, 1H, H17), 7.67 (dd, 1H, *J* = 9.2, 2.5 Hz, H22), 5.75 (d, 1H, *J* = 16.3 Hz, H11), 5.31 (d, 1H, *J* = 16.3 Hz, H11), 5.26 (s, 2H, H8), 3.80 (br s, 1H, OH), 3.16 (q, 2H, *J* = 7.7 Hz, H5), 1.96-1.83 (m, 2H, H14), 1.61 (s, 9H, H25), 1.40 (t, 3H, *J* = 7.7 Hz, H6), 1.04 (t, 3H, *J* = 7.4 Hz, H15); δ_{C} (101 MHz, CDCl₃) 174.0 (C12), 157.8 (C9), 151.9 (C1), 151.6 (C23), 150.3 (C19), 150.2 (C16), 147.2 (C18), 146.8 (C20), 145.8 (C4), 132.0 (C21), 127.6 (C7), 127.5 (C3), 125.5 (C22), 118.8 (C10), 114.3 (C2), 98.4 (C17), 84.6 (C24), 72.9 (C13), 66.5 (C11), 49.6 (C8), 31.8

(C14), 27.9 (C25), 23.4 (C5), 14.1 (C6), 8.0 (C15); **LRMS** (ESI) m/z found $[M+H]^+$ 493.2, $C_{27}H_{29}N_2O_7^+$ required 493.2.

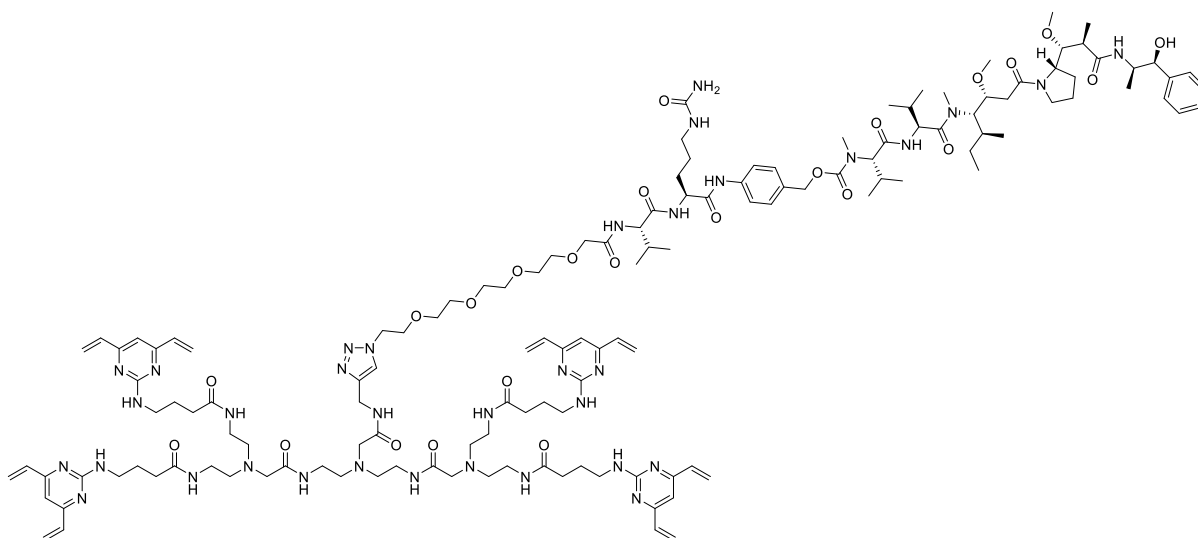
These data are consistent with those previously reported.^{219,235}



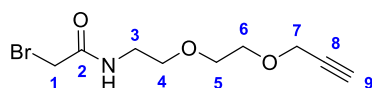
SN-38-Boc-azide (66) To a solution of SN-38-Boc **65** (24.6 mg, 50.0 μ mol) and 14-azido-3,6,9,12-tetraoxatetradecanoic acid (0.5M in TBME, 200 μ L, 100 μ mol) in CH_2Cl_2 (2 mL) were added EDC·HCl (19.2 mg, 100 μ mol) and DMAP (3.05 mg, 25.0 μ mol). The reaction was stirred at rt under nitrogen for 2 h and then sequentially washed with 0.5M HCl, sat. $NaHCO_3$, and water. The organic phase was dried over Na_2SO_4 and concentrated *in vacuo*. Purification by column chromatography (0-5% MeOH/ CH_2Cl_2) yielded the product as a white solid (33.0 mg, 44.0 μ mol, 88%). R_f 0.38 (SiO_2 , 5% MeOH/ CH_2Cl_2); δ_H (400 MHz, $CDCl_3$) 8.25 (d, 1H, J = 9.2 Hz, H21), 7.91 (d, 1H, J = 2.5 Hz, H2), 7.69 (dd, 1H, J = 9.2, 2.5 Hz, H22), 7.22 (s, 1H, H17), 5.69 (d, 1H, J = 17.2 Hz, H11), 5.42 (d, 1H, J = 17.2 Hz, H11), 5.25 (d, 2H, J = 1.8 Hz, H8), 4.36 (s, 1H, H27), 4.34 (s, 1H, H27), 3.67-3.62 (m, 12H, H28/29/30/31/32/33), 3.36 (t, 2H, J = 5.1 Hz, H34), 3.16 (q, 2H, J = 7.7 Hz, H5), 2.37-2.11 (m, 2H, H14), 1.61 (s, 9H, H25), 1.40 (t, 3H, J = 7.5 Hz, H6), 1.22-1.18 (m, 2H, H35), 0.97 (t, 3H, J = 7.5 Hz, H15); δ_C (101 MHz, $CDCl_3$) 169.8 (C26), 167.3 (C12), 157.4 (C9), 151.6 (C1), 151.5 (C23), 150.2 (C19), 146.5 (C18), 146.2 (C16/20), 145.6 (C4), 131.6 (C21), 127.7 (C7), 127.4 (C3), 125.7 (C22), 120.6 (C10), 114.4 (C2), 96.5 (C17), 84.6 (C24), 76.5 (C13), 71.2/70.9/70.8/70.8/70.7 (C29/30/31/32/33), 70.6 (C34), 70.1 (C28), 68.3 (C27), 67.3 (C11), 50.8 (C35), 49.5 (C8), 31.9 (C14), 27.9 (C25), 23.4 (C5), 14.1 (C6), 7.7 (C15); **HRMS** (ESI) m/z found $[M+H]^+$ 752.3148, $C_{37}H_{46}O_{12}N_5^+$ required 752.3143.



SN-38-azide (67) To a solution of SN-38-Boc-azide **66** (12.7 mg, 16.9 μmol) in CH_2Cl_2 (0.5 mL) at 0 $^\circ\text{C}$ was added TFA (0.5 mL). The reaction was stirred at 0 $^\circ\text{C}$ for 90 min and then concentrated *in vacuo*. Purification by column chromatography (0-10% MeOH/ CH_2Cl_2) yielded the product as a white solid (7.60 mg, 11.7 μmol , 69%). R_f 0.19 (SiO_2 , 5% MeOH/ CH_2Cl_2); δ_H (400 MHz, CDCl_3) 8.34 (d, 1H, $J = 9.2$ Hz, H21), 7.55 (dd, 1H, $J = 9.2, 2.2$ Hz, H22), 7.50 (s, 1H, H17), 7.40 (d, 1H, $J = 2.2$ Hz, H2), 5.72 (d, 1H, $J = 17.3$ Hz, H11), 5.41 (d, 1H, $J = 17.3$ Hz, H11), 5.19 (s, 2H, H8), 4.50-4.32 (m, 2H, H24), 3.82-3.68 (m, 2H, H5), 3.68-3.59 (m, 12H, H25/26/27/28/29/30), 3.34 (t, 2H, $J = 5.1$ Hz, H31), 3.14-3.04 (m, 2H, H32), 2.30-2.10 (m, 2H, H14), 1.36 (t, 3H, $J = 7.6$ Hz, H6), 1.00 (t, 3H, $J = 7.5$ Hz, H15); δ_C (101 MHz, CDCl_3) 170.5 (C23), 166.9 (C12), 158.7 (C1), 157.0 (C9), 151.8 (C19), 146.4 (C16), 143.9 (C18), 141.8 (C4), 136.9 (C20), 129.5 (C3), 128.2 (C7), 126.4 (C22), 126.1 (C21), 122.0 (C10), 106.3 (C2), 100.7 (C17), 76.6 (C13), 70.8/70.4/70.3/70.3/70.2 (C26/27/28/29/30), 70.1 (C31), 70.0 (C28), 67.9 (C25), 66.8 (C11), 50.7 (C32), 49.8 (C8), 31.4 (C14), 24.2 (C5), 13.6 (C6), 7.6 (C15); **HRMS** (ESI) m/z found $[\text{M}+\text{Na}]^+$ 674.2443, $\text{C}_{32}\text{H}_{37}\text{O}_{10}\text{N}_5\text{Na}^+$ required 674.2433; **HPLC** (5-95% MeCN/ H_2O over 20 min) retention time 9.368 min.

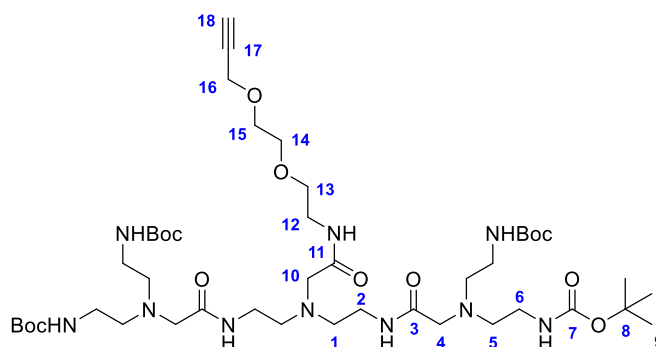


TetraDVP-Val-Cit-PABC-MMAE (72) To a solution of TetraDVP **15** (2.00 mg, 1.49 μmol) and $\text{N}_3\text{-PEG}_4\text{-ValCit-PABC-MMAE}$ (2.06 mg, 1.49 μmol) in CH_2Cl_2 (250 μL) was added a solution of $\text{CuSO}_4 \cdot 5\text{H}_2\text{O}$ (0.450 mg, 1.79 μmol), THPTA (1.29 mg, 2.98 μmol) and sodium ascorbate (1.48 mg, 7.45 μmol) in 1:1 $\text{H}_2\text{O}/t\text{BuOH}$ (500 μL). The reaction was stirred at 40 $^\circ\text{C}$ for 2 h and then purified by reverse phase flash column chromatography (40-70% solvent B in solvent A. Solvent A: 100 mM NH_4OH (aq). Solvent B: MeCN). Lyophilisation yielded the product as a white solid (1.01 mg, 0.370 μmol , 25%). **LRMS** (ESI) m/z found $[\text{M}+\text{H}]^+$ 2729.1 and $[\text{M}+2\text{H}]^{2+}$ 1364.8, $\text{C}_{137}\text{H}_{208}\text{N}_{35}\text{O}_{24}$ required 2727.6; **HPLC** (5-95% MeCN/ H_2O over 20 min) retention time 9.175 min.

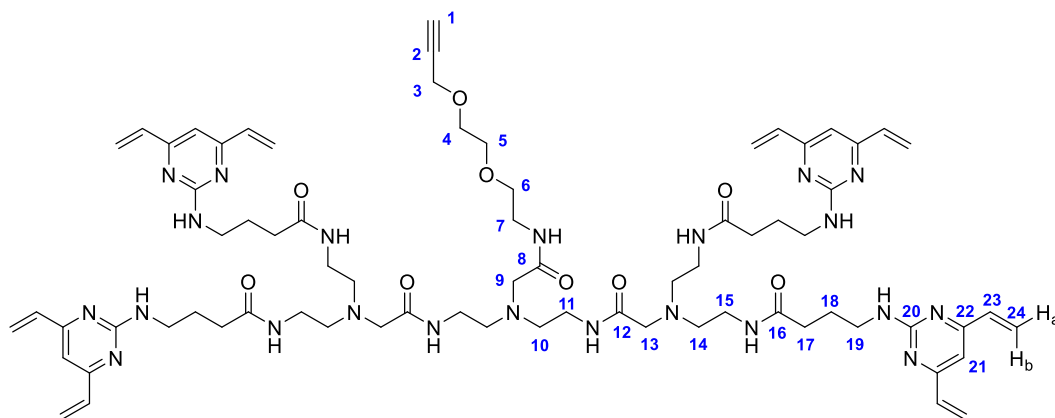


2-bromo-N-(2-(2-(prop-2-yn-1-yloxy)ethoxy)ethyl)acetamide (74) A solution of propargyl-PEG2-amine (70.9 μL , 0.500 mmol) in CH_2Cl_2 (2 mL) and sat. NaHCO_3 (2 mL) was cooled to -10 $^\circ\text{C}$ and 2-bromoacetyl bromide (65.0 μL , 0.750 mmol) was added dropwise. The reaction mixture was allowed to slowly reach rt and stirred for 1 h. The reaction mixture was diluted with water (5 mL) and extracted with CH_2Cl_2 (3 x 10 mL). The combined organic phases were dried over Na_2SO_4 and concentrated *in vacuo* to give the title compound as a pale orange oil (122 mg, 0.462 mmol, 92%). ν_{max} (neat/ cm^{-1}) 3299 (m, N-H), 3873 (m, C-H), 2253 (w, $\text{C}\equiv\text{C}$), 1659 (s, $\text{C}=\text{O}$); δ_{H} (400 MHz, CDCl_3) 6.95 (br s, 1H, NH), 4.18-4.15 (m, 2H, H7), 3.83 (s, 2H, H1), 3.68-3.60 (m, 4H, H5/H6), 3.55 (t, 2H, J = 4.9 Hz, H4), 3.45 (q, 2H, J = 5.0 Hz, H3), 2.45-2.42 (m, 1H, H9); δ_{C} (100 MHz, CDCl_3) 165.7 (C2), 79.5 (C8), 74.8 (C9), 70.1 (C4), 69.4 (C5), 69.0 (C6),

58.5 (C7), 39.9 (C3), 29.1 (C1); **HRMS** (ESI) m/z found $[M+H]^+$ 264.0231, $C_9H_{14}O_3NBr^+$ required 264.0230.



Tetra-*N*-Boc backbone, PEG2-alkyne (75) To a suspension of **27** (79.0 mg, 0.100 mmol) and K_2CO_3 (27.6 mg, 0.200 mmol) in MeCN (0.5 mL) was added a solution of **74** (33.0 mg, 0.125 mmol) in MeCN (0.5 mL). The reaction was stirred under nitrogen for 18 h and then concentrated *in vacuo*. Purification by column chromatography (0-10% MeOH/ CH_2Cl_2) gave the title compound as a white solid (52.6 mg, 54.0 μ mol, 54%). R_f 0.26 (SiO_2 , 10% MeOH/ CH_2Cl_2); ν_{max} (neat/ cm^{-1}) 3309 (m, N-H), 2977 (m, C-H), 2252 (m, $C\equiv C$), 1691 (s, C=O); δ_H (600 MHz, $CDCl_3$) 7.70 (br s, 2H, NH), 5.82 (br s, 4H, NH), 4.20-4.17 (m, 2H, H16), 3.70-3.62 (m, 4H, H14/H15), 3.58 (t, 2H, $J = 4.8$ Hz, H13), 3.47 (q, 2H, $J = 5.0$ Hz, H12), 3.37-3.30 (m, 4H, H2), 3.24 (s, 2H, H10), 3.21-3.11 (m, 8H, H6), 3.12 (s, 4H, H4), 2.76-2.70 (m, 4H, H1), 2.62-2.54 (m, 8H, H5), 2.50-2.47 (m, 1H, H18), 1.87 (s, 1H, NH), 1.43 (s, 36H, H9); δ_C (101 MHz, $CDCl_3$) 171.9 (C11), 171.8 (C3), 156.7 (C7), 79.6 (C17), 79.4 (C8), 75.1 (C18), 70.0 (C13), 69.7 (C14), 69.1 (C15), 59.3 (C16), 59.1 (C10), 59.5 (C4), 55.7 (C5), 55.0 (C1), 39.2 (C12), 38.8 (C6), 37.7 (C2), 28.7 (C9); **HRMS** (ESI) m/z found $[M+H]^+$ 973.6280, $C_{45}H_{85}O_{13}N_{10}^+$ required 973.6292.



TetraDVP-PEG2-alkyne (76) To a solution of tetra-*N*-Boc backbone **75** (45.9 mg, 47.2 μmol) in CH_2Cl_2 (0.5 mL) at 0 $^\circ\text{C}$ was added HCl (4 M in dioxane, 1.0 mL). The reaction was stirred under nitrogen for 2 h and then concentrated *in vacuo* to yield the desired amine hydrochloride salt as a white solid. The amine hydrochloride salt was re-dissolved in DMF (0.5 mL) and cooled to 0 $^\circ\text{C}$. To this solution, a solution of 4-((4,6-divinylpyrimidin-2-yl)amino)butanoic acid **4** (44.1 mg, 0.189 mmol), triethylamine (131 μL , 0.943 mmol) and HBTU (71.7 mg, 0.189 mmol) in DMF (0.5 mL) at 0 $^\circ\text{C}$ was added. The reaction was stirred under nitrogen for 16 h and then purified by reverse phase flash column chromatography (0-100% solvent B in solvent A. Solvent A: 100 mM NH_4OH (aq). Solvent B: MeCN). Lyophilisation yielded the product as a white solid (28.9 mg, 20.2 μmol , 43%). ν_{max} (neat/ cm^{-1}) 3295 (m, N-H), 2933 (m, C-H), 2252 (m, $\text{C}\equiv\text{C}$), 1636 (s, C=O); δ_{H} (600 MHz, CD_3OD) 6.67 (s, 4H, H21), 6.59 (dd, 8H, J = 10.7, 17.4 Hz, H23), 6.35 (d, 8H, J = 17.4 Hz, H24b), 5.56 (dd, 8H, J = 1.4, 10.7 Hz, H24a), 4.15 (d, 2H, J = 2.3, H3), 3.64-3.57 (m, 4H, H4/H5), 3.53 (t, 2H, J = 5.4 Hz, H6), 3.44 (t, 8H, J = 6.8 Hz, H19), 3.39 (t, 2H, J = 5.4 Hz, H7), 3.27 (t, 4H, J = 6.6 Hz, H11), 3.23 (t, 8H, J = 6.3 Hz, H15), 3.19 (s, 2H, H9), 3.17 (s, 4H, H13), 2.86 (t, 1H, J = 2.4 Hz, H1), 2.65 (t, 4H, J = 6.6 Hz, H10), 2.60 (t, 8H, J = 6.3 Hz, H14), 2.28 (t, 8H, J = 7.5 Hz, H17), 1.90 (qn, 8H, J = 7.1 Hz, H18); δ_{C} (101 MHz, CD_3OD) 175.9 (C16), 174.1 (C12), 174.0 (C8), 165.3 (C22), 164.0 (C20), 137.1 (C23), 122.2 (C24), 105.8 (C21), 80.6 (C2), 76.2 (C1), 71.0 (C6), 70.4 (C5), 70.1 (C4), 59.6 (C13), 59.5 (C9), 59.1 (C3), 55.8 (C10), 55.7 (C14), 41.7 (C19), 40.0 (C7), 38.6 (C15), 38.6 (C11), 34.7 (C17), 27.0 (C18); **HRMS** (ESI) m/z found $[\text{M}+\text{H}]^+$ 1433.8401, $\text{C}_{73}\text{H}_{105}\text{O}_9\text{N}_{22}^+$ required 1433.8435.

6.3 Protein Chemistry

SDS-PAGE:

Non-reducing Tris-Glycine SDS-PAGE with 8% or 12% acrylamide with 4% stacking gel was performed as standard. Broad range molecular weight marker (10-200 kDa, New England BioLabs) was run in all gels. Samples (5 μ L, 2.5 μ g unless stated otherwise) were prepared with reducing or non-reducing loading dye (5 μ L, reducing dye contains β -mercaptoethanol) and heated to 90 °C for 5 min before loading. Gels were run at constant voltage (200 V) for 45-60 min in 1 x Laemmli running buffer (LRB). All gels were stained with Coomassie dye and imaged on a Syngene gel imaging system. Gels containing fluorescently labelled samples were imaged for in-gel fluorescence prior to Coomassie staining.

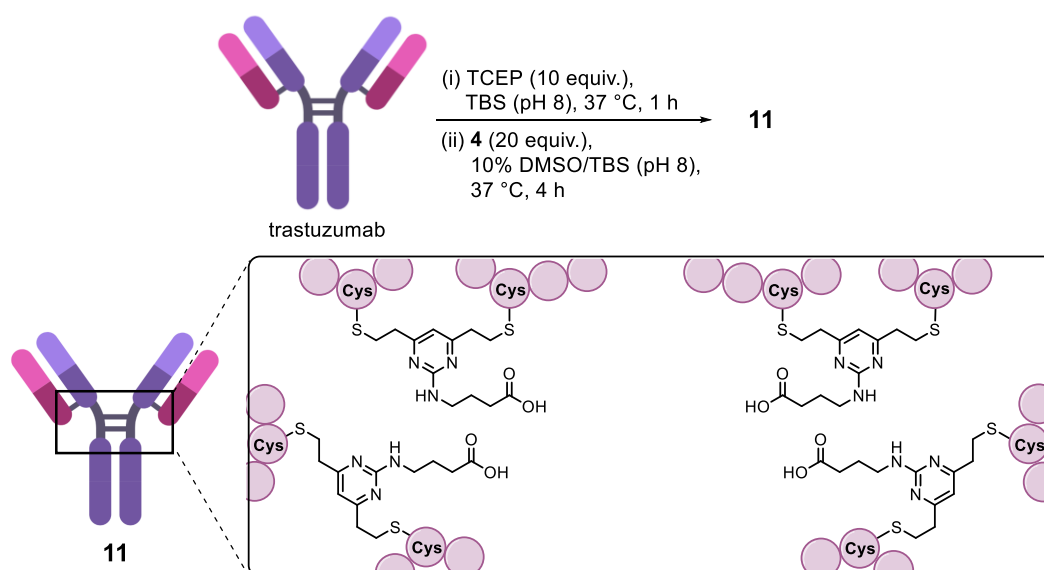
UV-vis spectroscopy:

UV-vis spectroscopy was used to determine protein concentrations and fluorophore-to-antibody ratios (FAR) using a NanoDrop One spectrophotometer. Sample buffer was used as blank for baseline correction with extinction coefficients $\epsilon_{280} = 215,380 \text{ M}^{-1} \text{ cm}^{-1}$ for trastuzumab and $\epsilon_{495} = 71,000 \text{ M}^{-1} \text{ cm}^{-1}$ for AlexaFluor™ 488. The correction factor for AlexaFluor™ 488 absorption at 280 nm is 0.11. FAR was calculated using the following formula:

$$FAR = \frac{Abs_{495}/\epsilon_{495}}{(Abs_{280} - 0.11 \times Abs_{495})/\epsilon_{280}}$$

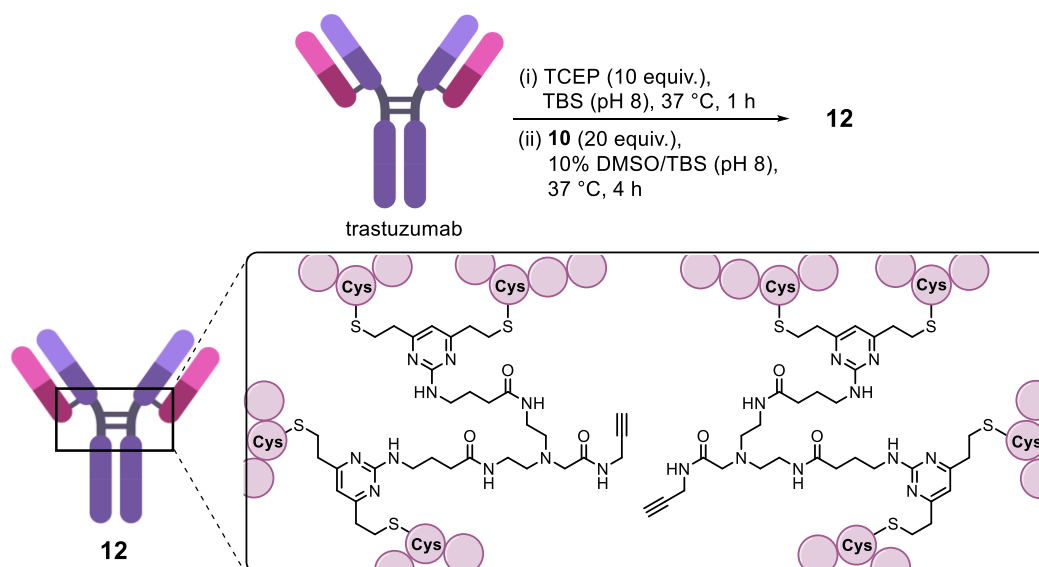
Chapter 3:

Reaction of trastuzumab with DVP 4



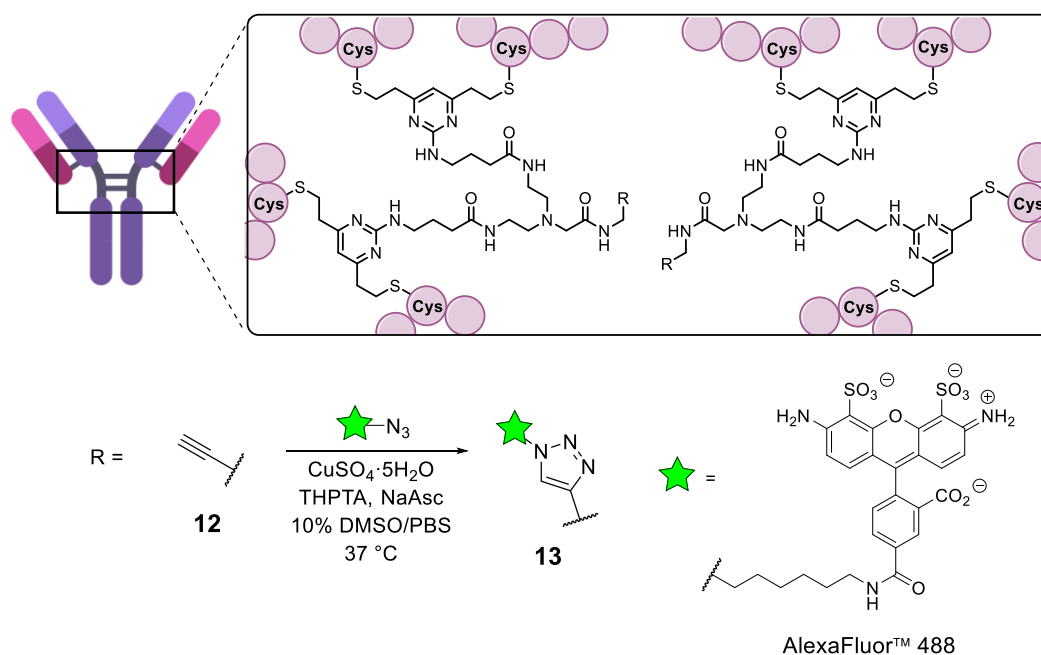
To a solution of trastuzumab (11.9 μL , 17 μM , 2.5 mg/mL) in TBS pH 8 (25 mM Tris HCl, 25 mM NaCl, 0.5 mM EDTA) was added a solution of TCEP·HCl in H₂O (final concentration of 170 μM , 10 equiv.). The mixture was vortexed and incubated at 37 °C for 1 h. A solution of **4** in DMSO was added (final concentration of 340 μM , 20 equiv.) and the reaction mixture incubated at 37 °C for 4 h. The excess reagents were removed by use of a Zeba™ Spin Desalting Column (7,000 molecular weight cut off [MWCO], Thermo Fisher Scientific).

Reaction of trastuzumab with BisDVP 10



To a solution of trastuzumab (198 μ L, 17 μ M, 2.5 mg/mL) in TBS pH 8 (25 mM Tris HCl, 25 mM NaCl, 0.5 mM EDTA) was added a solution of TCEP·HCl in H₂O (final concentration of 170 μ M, 10 equiv.). The mixture was vortexed and incubated at 37 °C for 1 h. A solution of **10** in DMSO was added (final concentration of 340 μ M, 20 equiv.) and the reaction mixture incubated at 37 °C for 4 h. The excess reagents were removed by use of a Zeba™ Spin Desalting Column (7,000 MWCO, Thermo Fisher Scientific), followed by repeated diafiltration into PBS using an Amicon-Ultra centrifugal filter (10,000 MWCO, Merck Millipore).

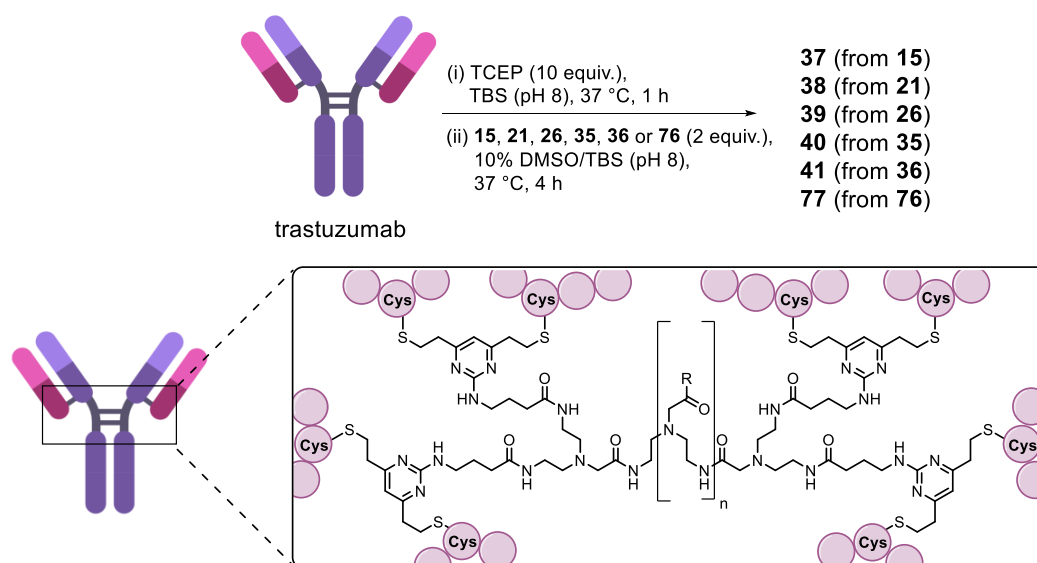
Preparation of BisDVP AlexaFluor™ 488 conjugate



To a solution of BisDVP conjugate **12** in PBS were added $\text{CuSO}_4 \cdot 5\text{H}_2\text{O}$ (20 equiv.), THPTA (100 equiv.), sodium ascorbate (150 equiv.) and AlexaFluor™ 488 Azide (Thermo Fisher Scientific) (5 mM in DMSO, 12 equiv.). The mixture was vortexed and incubated at 37 °C for 16 h. The excess reagents were removed by filtration through two successive Zeba™ Spin Desalting Columns (7,000 MWCO, Thermo Fisher Scientific), followed by repeated diafiltration into PBS using an Amicon-Ultra centrifugal filter (10,000 MWCO, Merck Millipore).

Chapter 4:

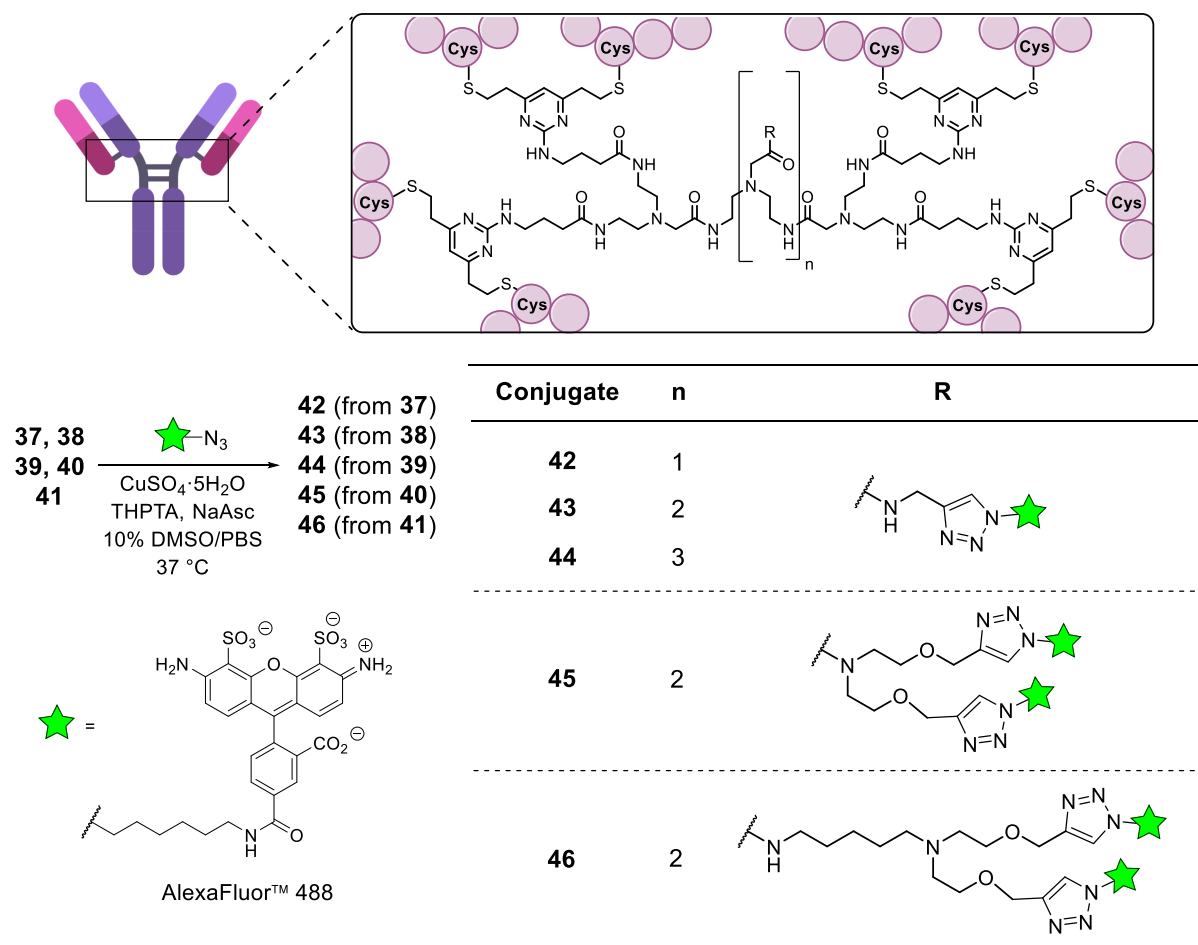
Reaction of trastuzumab with TetraDVPs **15**, **21**, **26**, **35**, **36** or **76**



Conjugate	n	R
37	1	
38	2	
39	3	
40	2	
41	2	
77	1	

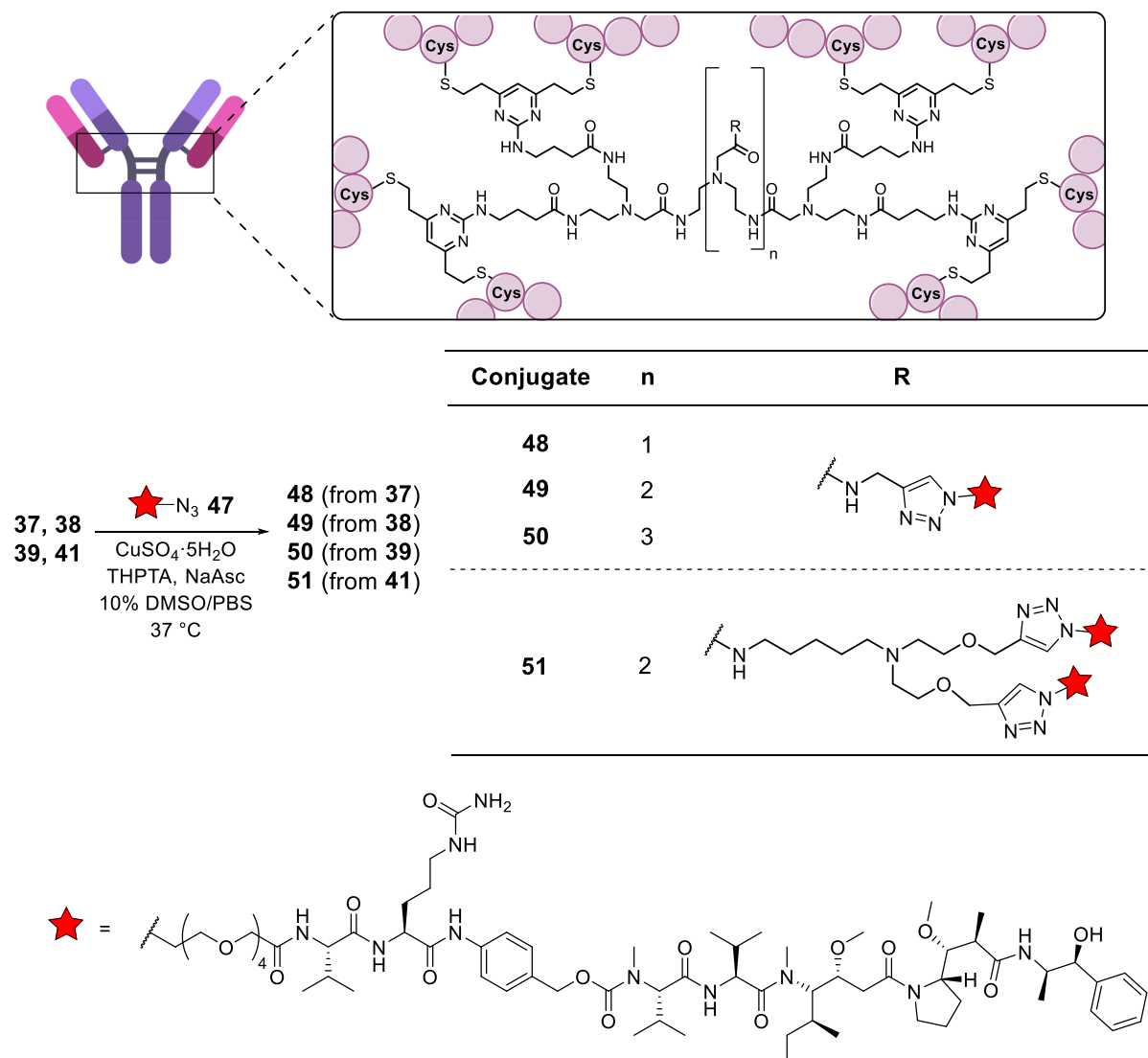
To a solution of trastuzumab (277 μL , 17 μM , 2.5 mg/mL) in TBS pH 8 (25 mM Tris HCl, 25 mM NaCl, 0.5 mM EDTA) was added a solution of TCEP·HCl in H_2O (final concentration of 170 μM , 10 equiv.). The mixture was vortexed and incubated at 37 °C for 1 h. A solution of TetraDVP **15**, **21**, **26**, **35**, **36** or **76** in DMSO was added (final concentration of 34 μM , 2 equiv.) and the reaction mixture incubated at 37 °C for 4 h. The excess reagents were removed by use of a Zeba™ Spin Desalting Column (40,000 MWCO, Thermo Fisher Scientific), followed by repeated diafiltration into PBS using an Amicon-Ultra centrifugal filter (10,000 MWCO, Merck Millipore).

Preparation of TetraDVP AlexaFluor™ 488 conjugates



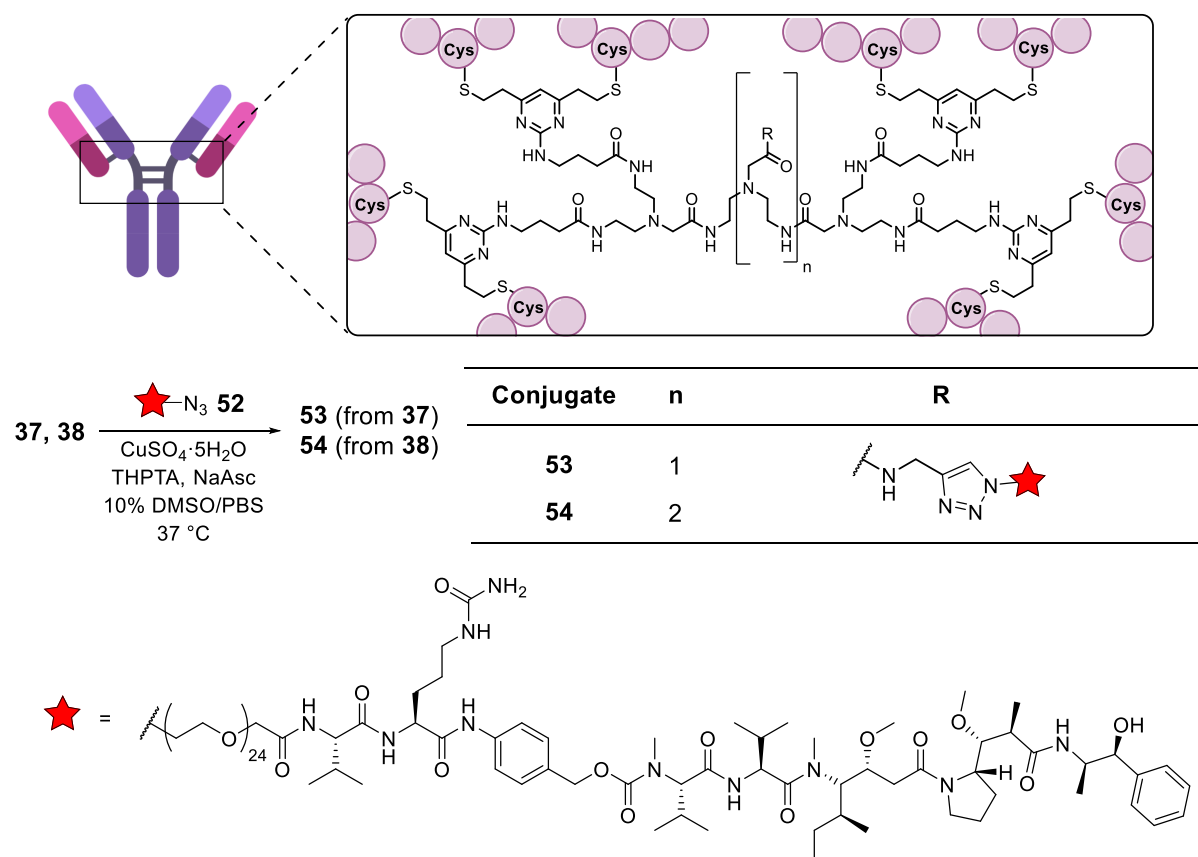
To a solution of TetraDVP conjugate **37, 38, 39, 40** or **41** in PBS were added $\text{CuSO}_4 \cdot 5\text{H}_2\text{O}$ (20 equiv. per alkyne), THPTA (100 equiv. per alkyne), sodium ascorbate (150 equiv. per alkyne) and AlexaFluor™ 488 Azide (Thermo Fisher Scientific) (20 mM in DMSO, 12 equiv. per alkyne). The mixture was vortexed and incubated at 37°C for 6 h. The excess reagents were removed by filtration through two successive Zeba™ Spin Desalting Columns (7,000 MWCO, Thermo Fisher Scientific), followed by repeated diafiltration into PBS using an Amicon-Ultra centrifugal filter (10,000 MWCO, Merck Millipore).

Preparation of TetraDVP ADCs 48-51



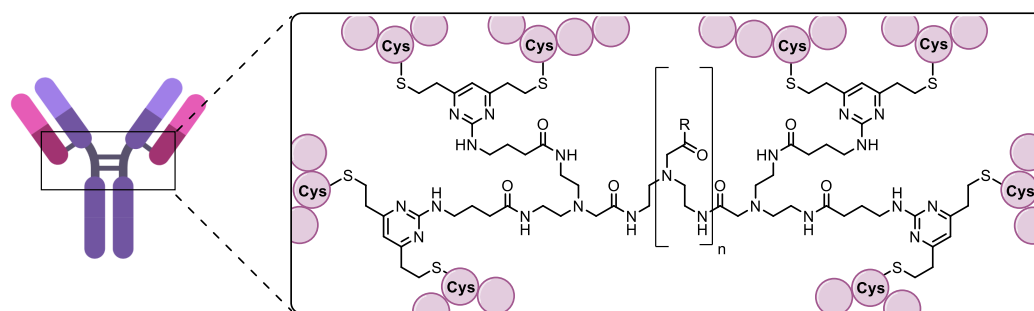
To a solution of TetraDVP conjugate **37**, **38**, **39** or **41** in PBS were added $\text{CuSO}_4 \cdot 5\text{H}_2\text{O}$ (150 equiv.), THPTA (600 equiv.), sodium ascorbate (1000 equiv.) and $\text{N}_3\text{-PEG}_4\text{-Val-Cit-PABC-MMAE}$ **47** (20 mM in DMSO, 100 equiv.). The mixture was vortexed and incubated at 37 °C for 7 h. The reaction was quenched by addition of EDTA, and the excess reagents were removed by filtration through two successive Zeba™ Spin Desalting Columns (40,000 MWCO, Thermo Fisher Scientific), followed by repeated diafiltration into PBS using an Amicon-Ultra centrifugal filter (10,000 MWCO, Merck Millipore).

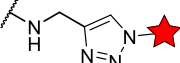
Preparation of TetraDVP ADCs 53-54

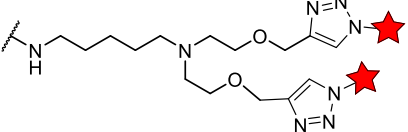


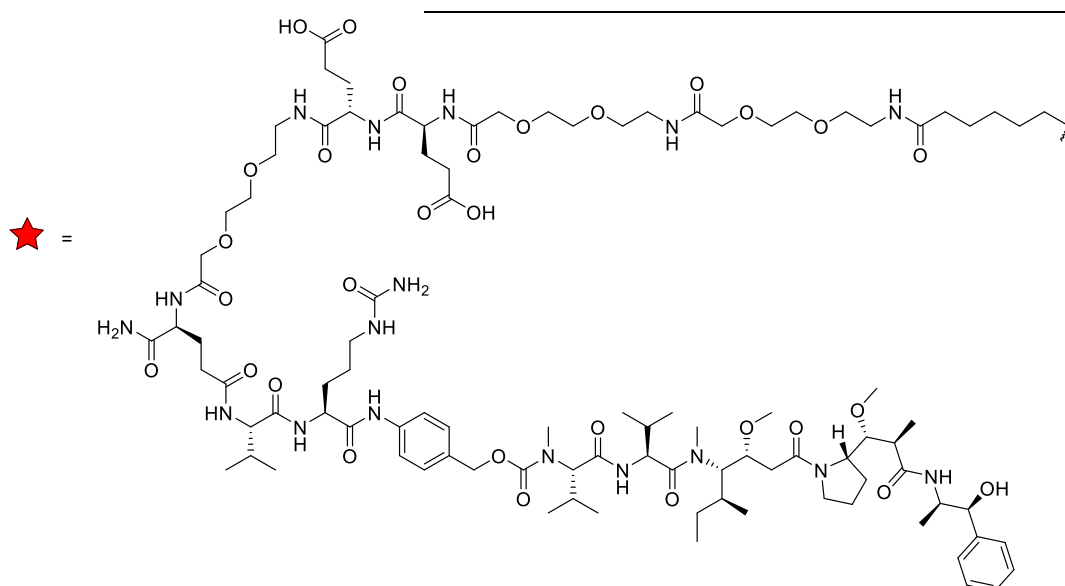
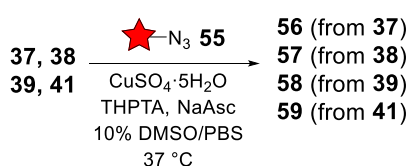
To a solution of TetraDVP conjugate **37** or **38** in PBS were added $\text{CuSO}_4 \cdot 5\text{H}_2\text{O}$ (150 equiv.), THPTA (600 equiv.), sodium ascorbate (1000 equiv.) and N_3 -PEG₂₄-Val-Cit-PABC-MMAE **52** (20 mM in DMSO, 100 equiv.). The mixture was vortexed and incubated at 37 °C for 7 h. The reaction was quenched by addition of EDTA, and the excess reagents were removed by filtration through a Zeba™ Spin Desalting Column (40,000 MWCO, Thermo Fisher Scientific), followed by repeated diafiltration into PBS using an Amicon-Ultra centrifugal filter (10,000 MWCO, Merck Millipore).

Preparation of TetraDVP ADCs 56-59



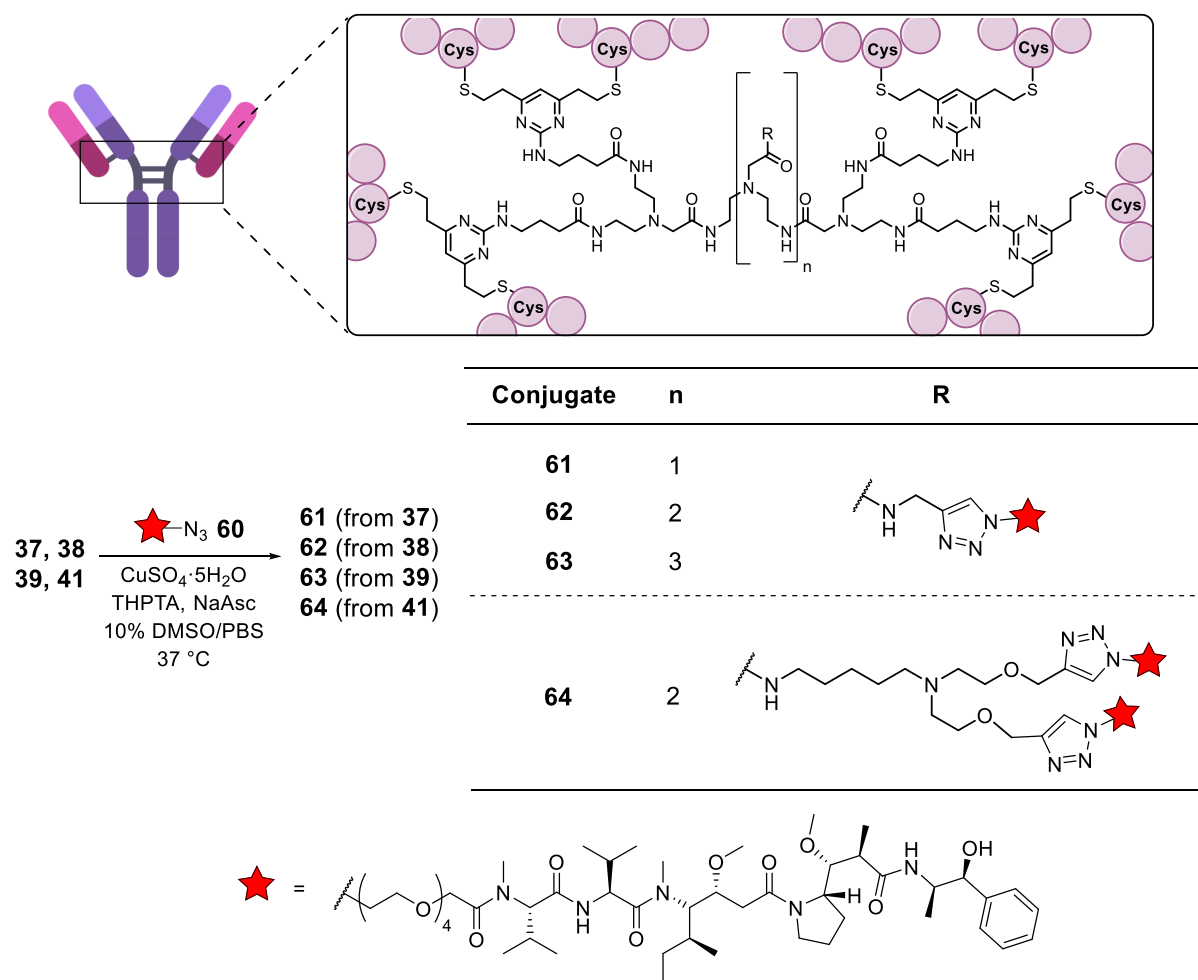
Conjugate	n	R
56	1	
57	2	
58	3	

59	2	
----	---	--



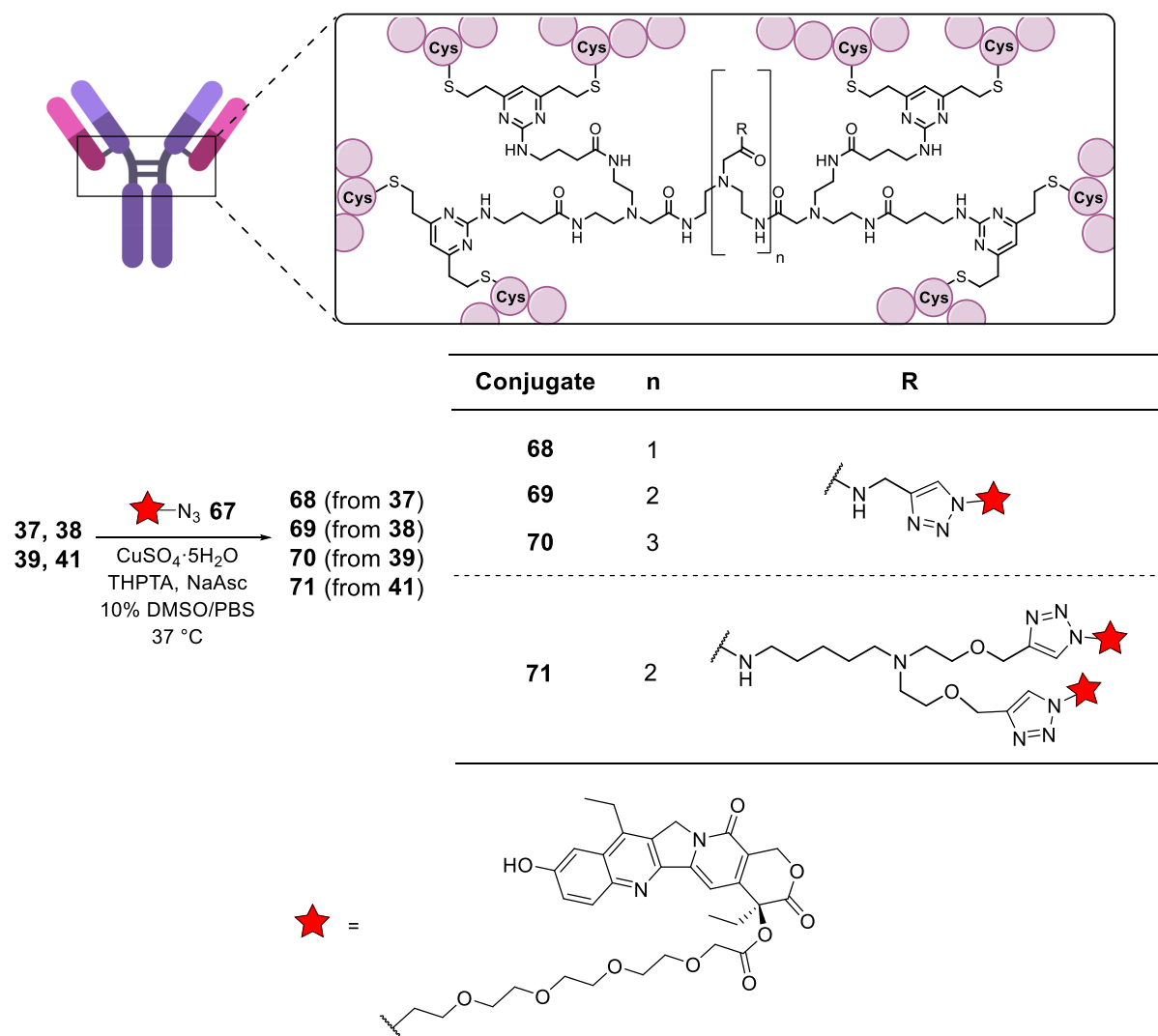
To a solution of TetraDVP conjugate **37**, **38**, **39** or **41** in PBS were added CuSO₄·5H₂O (150 equiv.), THPTA (600 equiv.), sodium ascorbate (1000 equiv.) and N₃-PEG₄-Glu₂-PEG₂-Val-Cit-PABC-MMAE **55** (20 mM in DMSO, 100 equiv.). The mixture was vortexed and incubated at 37 °C for 7 h. The reaction was quenched by addition of EDTA, and the excess reagents were removed by filtration through a Zeba™ Spin Desalting Column (40,000 MWCO, Thermo Fisher Scientific), followed by repeated diafiltration into PBS using an Amicon-Ultra centrifugal filter (10,000 MWCO, Merck Millipore).

Preparation of TetraDVP ADCs 61-64



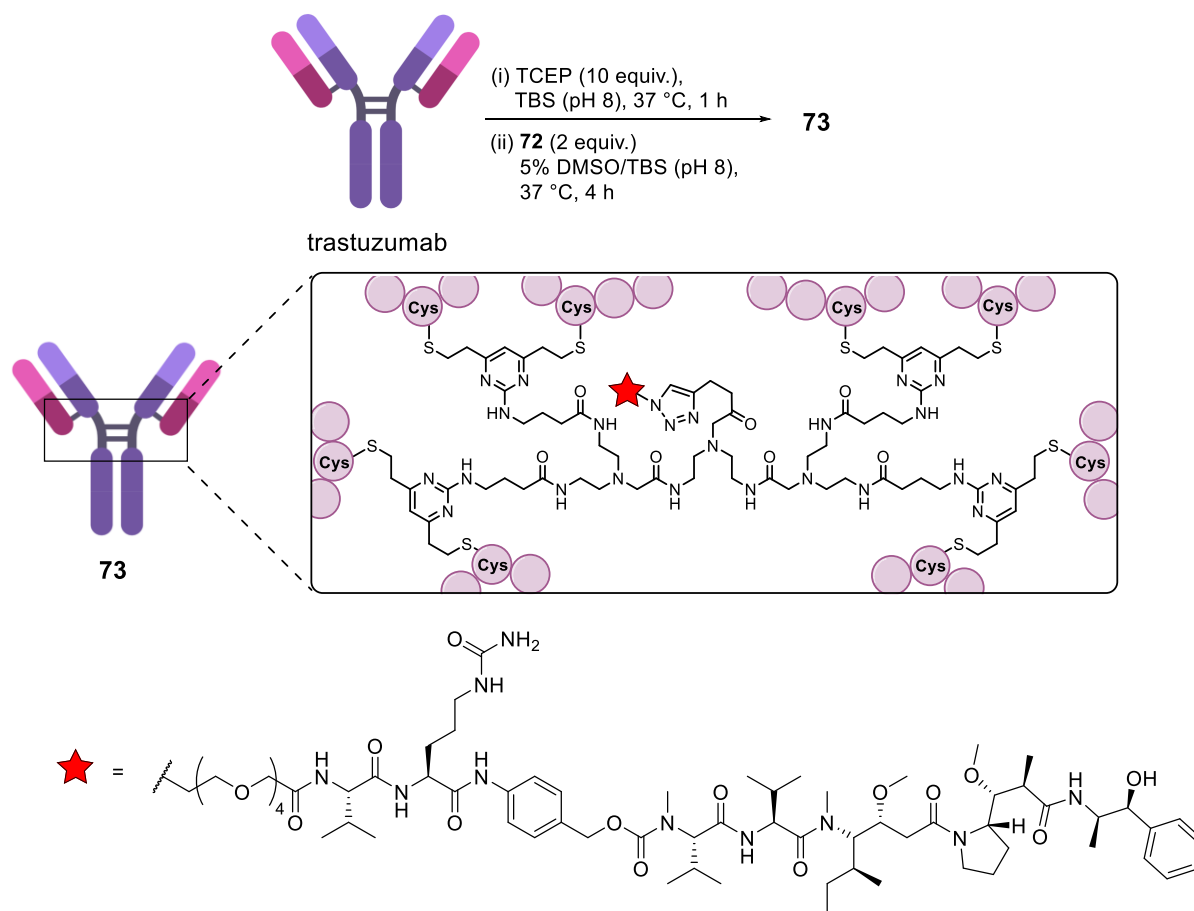
To a solution of TetraDVP conjugate **37**, **38**, **39** or **41** in PBS were added CuSO₄·5H₂O (150 equiv.), THPTA (600 equiv.), sodium ascorbate (1000 equiv.) and N₃-PEG₄-MMAE **60** (20 mM in DMSO, 100 equiv.). The mixture was vortexed and incubated at 37 °C for 7 h. The reaction was quenched by addition of EDTA, and the excess reagents were removed by SEC using a Superdex™ 200 Increase 10/300 GL column with PBS pH 7 elution buffer.

Preparation of TetraDVP ADCs 68-71



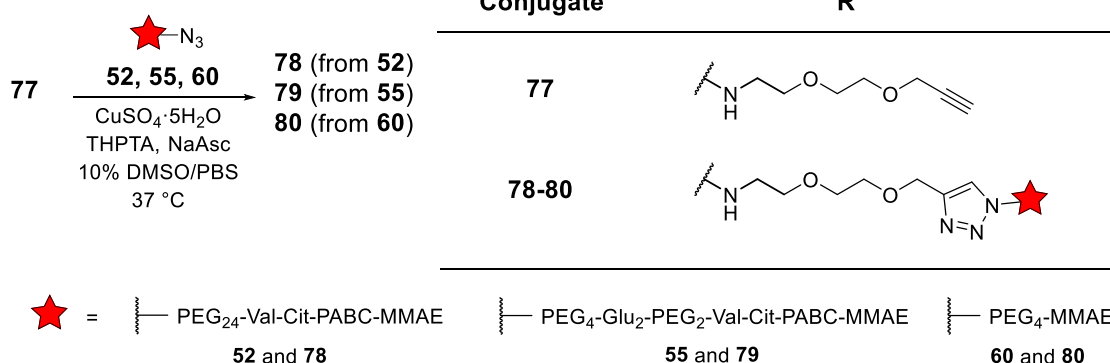
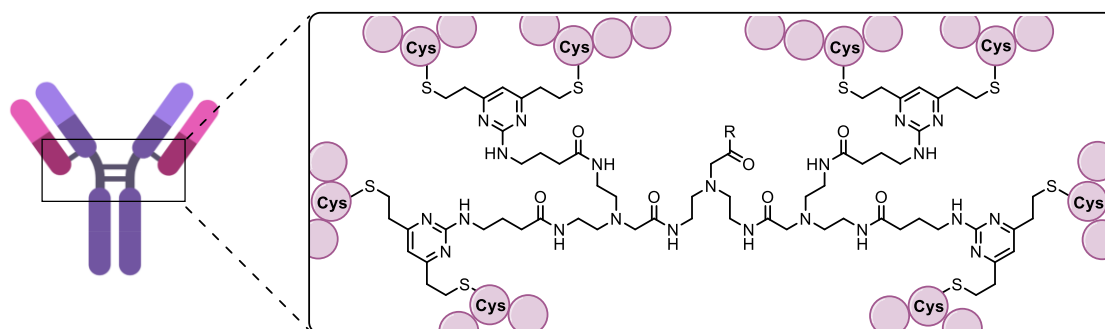
To a solution of TetraDVP conjugate **37**, **38**, **39** or **41** in PBS were added $\text{CuSO}_4 \cdot 5\text{H}_2\text{O}$ (150 equiv.), THPTA (600 equiv.), sodium ascorbate (1000 equiv.) and $\text{N}_3\text{-PEG}_4\text{-SN-38}$ **67** (20 mM in DMSO, 100 equiv.). The mixture was vortexed and incubated at 37 °C for 6 h. The reaction was quenched by addition of EDTA, and the excess reagents were removed by filtration through a Zeba™ Spin Desalting Column (40,000 MWCO, Thermo Fisher Scientific), followed by repeated diafiltration into PBS using an Amicon-Ultra centrifugal filter (10,000 MWCO, Merck Millipore).

Reaction of trastuzumab with TetraDVP-MMAE linker-payload **72**



To a solution of trastuzumab (11.9 μL , 17 μM , 2.5 mg/mL) in TBS pH 8 (25 mM Tris HCl, 25 mM NaCl, 0.5 mM EDTA) was added TCEP (final concentration of 170 μM , 10 equiv.). The mixture was vortexed and incubated at 37 °C for 1 h. A solution of TetraDVP **72** (10 mM in DMSO) was added (final concentration of 34 μM , 2 equiv.) and the reaction mixture incubated at 37 °C for 4 h. The excess reagents were removed by use of a Zeba™ Spin Desalting Column (40,000 MWCO, Thermo Fisher Scientific).

Preparation of TetraDVP ADCs 78-80



To a solution of TetraDVP conjugate **77** in PBS were added $\text{CuSO}_4 \cdot 5\text{H}_2\text{O}$ (150 equiv.), THPTA (600 equiv.), sodium ascorbate (1000 equiv.) and azide **52**, **55** or **60** (20 mM in DMSO, 100 equiv.). The mixture was vortexed and incubated at 37 °C for 6 h. The reaction was quenched by addition of EDTA, and the excess reagents were removed by filtration through a Zeba™ Spin Desalting Column (40,000 MWCO, Thermo Fisher Scientific).

6.4 Biological Evaluation

Stability Analysis:

To a solution of trastuzumab-AlexaFluor™ 488 conjugate **42**, **43**, **44** or **46** (138 µL, 3.75 µM) in PBS were added 12 µL of reconstituted human plasma (Sigma). The mixture was incubated at 37 °C for 14 days. Aliquots were removed after 0, 2, 4, 6, 8, 10, 12 and 14 days, flash frozen and stored at -80 °C until analysis. SDS-PAGE was followed by in-gel fluorescence imaging and Coomassie brilliant blue staining and imaging.

Size Exclusion Chromatography (SEC):

Analytical size-exclusion chromatography (SEC) was carried out on an AKTA pure chromatography system using a Superdex™ 200 Increase 10/300 GL column. Samples were injected at a concentration of 1 mg/mL and eluted with TBS pH 8 (25 mM Tris HCl, 200 mM NaCl, 0.5 mM EDTA) at a flow rate of 0.5 mL/min.

Enzyme-linked immunosorbent assay (ELISA):

A 96-well plate was coated with 100 µL of a 0.25 µg/mL solution of HER2 (Sino Biological, His-tagged) overnight at 4 °C. Coating solutions were removed and each well washed with PBS (2 × 200 µL). Each well was then blocked with 1% BSA in PBS (200 µL) for 1 h at room temperature. The blocking solution was then removed and each well washed with PBS (3 × 200 µL). Wells were treated with a serial dilution of trastuzumab and trastuzumab-TetraDVP conjugates **37**, **38**, **39** and **41** in PBS (100 µL of 90 nM, 30 nM, 10 nM, 3.33 nM, 1.11 nM, 0.37 nM, 0.12 nM, 0 nM) and incubated at room temperature for 2 h. The conjugate solutions were removed, and each well was washed with 0.1% Tween 20 in PBS (2 × 200 µL) followed by PBS (3 × 200 µL). Next, 100 µL of detection antibody (1:500 dilution of a mouse anti-human IgG-HRP, ThermoFisher) in PBS was added to each well and incubated at room temperature for 1 h. Each well was washed with 0.1% Tween 20 in PBS (2 × 200 µL) followed by PBS (3 × 200 µL). Finally, an OPD solution (100 µL of a solution prepared by dissolving 1 capsule in 9 mL H₂O and 1 mL stable peroxide substrate buffer (10×), ThermoFisher) was added to each well. After 15 minutes, 4 M HCl (aq.) (50 µL) was added to each well to quench the reaction. Absorbance at 490 nm and 590 nm was measured using a CLARIOstar Microplate

Reader. Measurements were performed in quadruplicate and three independent repeats were performed.

Cell lines:

HER2-positive SKBR3 and BT474 cells were obtained from the American Type Culture Collection (ATCC) and HER2-negative MCF7 and MDA-MB-468 cells were obtained from the European Collection of Authenticated Cell Cultures (ECACC) and ATCC, respectively. SKBR3 cells were maintained in high glucose McCoy's 5A medium, supplemented with 10% heat-inactivated foetal-bovine serum (FBS), GlutaMAX™, 50 U/mL penicillin and 50 µg/mL streptomycin. MCF7 and MDA-MB-468 cells were maintained in Dulbecco's Modified Eagle Medium (DMEM) supplemented with 10% FBS, 2 mM L-glutamine, 50 U/mL penicillin and 50 µg/mL streptomycin. BT474 cells were maintained in RPMI1640 medium supplemented with 10% FBS, 2 mM L-glutamine, 50 U/mL penicillin and 50 µg/mL streptomycin. All cell lines were incubated at 37 °C with 5% CO₂.

Live cell microscopy:

SKBR3 or MCF7 cells were seeded at 40,000 cells/well in 8-well chambered µ-slide (Ibidi, 80826) for 48 h at 37 °C with 5% CO₂. Slides were then placed on ice and washed with Ham's F12 Nutrient Mix media containing 10% FBS, 2 mM L-glutamine, 50 U/mL penicillin and 50 µg/mL streptomycin (3 × 200 µL). Antibody conjugates **42** and **43** (50 nM), trastuzumab (50 nM) or vehicle (PBS) were added to the cells in complete F12 growth medium and incubated at 4 °C in the dark for 1 h. Cells were placed back on ice and washed with complete F12 growth medium (3 × 200 µL). Complete F12 growth medium (200 µL) was added, and the cells incubated for 3.5 h at 37 °C with 5% CO₂. After 3 h incubation, Hoechst 33342 trihydrochloride trihydrate (1 µg/mL, Invitrogen, H3570) was added. Live cell microscopy was performed on an Operetta CLS confocal microscope (Perkin Elmer) with a 40× water objective. Cells were maintained in a humidified atmosphere at 37 °C and 5% CO₂ throughout analysis. Data analysis was performed using ImageJ (Fiji).

Cell viability:

Cells were seeded in 96-well plates for 24 h at 37 °C with 5% CO₂. SKBR3 cells were seeded at 15,000 cells/well, BT474 cells were seeded at 20,000 cells/well, MCF7 cells were seeded at

7,500 cells/well and MDA-MB-468 cells were seeded at 10,000 cells/well. Serial dilutions of ADCs **48, 49, 50, 51, 61, 62, 63, 64** or trastuzumab were added to the cells in complete growth medium and incubated at 37 °C with 5% CO₂ for 96 h. Cell viability was determined using a CellTiter-Glo viability assay (Promega) according to the manufacturer's instructions. Cell viability was plotted as a percentage of that of untreated cells. Each measurement was taken in triplicate. For ADCs **48, 49, 50, 51** and trastuzumab three independent repeats were performed.

References

- 1 Cancer Research UK, Cancer Statistics for the UK, <https://www.cancerresearchuk.org/health-professional/cancer-statistics-for-the-uk>, (accessed 31 December 2020).
- 2 Cancer Research UK, Cancer survival statistics for all cancers combined | Cancer Research UK, <http://www.cancerresearchuk.org/health-professional/cancer-statistics/survival/all-cancers-combined#heading-Zero>, (accessed 31 December 2020).
- 3 L. S. Goodman, M. M. Wintrobe, W. Dameshek, M. J. Goodman, A. Gilman and M. T. Mclennan, *J. Am. Med. Assoc.*, 1946, **132**, 126–132.
- 4 V. T. DeVita and E. Chu, *Cancer Res.*, 2008, **68**, 8643–8653.
- 5 Cancer Research UK, Cancer diagnosis and treatment statistics | Cancer Research UK, <http://www.cancerresearchuk.org/health-professional/cancer-statistics/diagnosis-and-treatment#heading-Five>, (accessed 31 December 2020).
- 6 R. T. Skeel, in *Handbook of Cancer Chemotherapy*, 8th Edition, LWW, 2011, pp. 1–16.
- 7 S. Dasari and P. Bernard Tchounwou, *Eur. J. Pharmacol.*, 2014, **740**, 364–378.
- 8 I. A. Riddell and S. J. Lippard, in *Metallo-Drugs: Development and action of anticancer agents*, De Gruyter, 2018, pp. 2–43.
- 9 E. A. Perez, *Mol. Cancer Ther.*, 2009, **8**, 2086–2095.
- 10 C. Dumontet and M. A. Jordan, *Nat. Rev. Drug Discov.*, 2010, **9**, 790–803.
- 11 B. A. Weaver, *Mol. Biol. Cell*, 2014, **25**, 2677–2681.
- 12 M. Moudi, R. Go, C. Y. S. Yien and M. Nazre, *Int. J. Prev. Med.*, 2013, **4**, 1131–1135.
- 13 R. T. Skeel, in *Handbook of Cancer Chemotherapy*, 8th Edition, LWW, 2011, pp. 45–62.
- 14 V. Malhotra and M. C. Perry, *Cancer Biol. Ther.*, 2003, **2**, 1–3.
- 15 O. E. Rahma and S. N. Khleif, in *Handbook of Cancer Chemotherapy*, 8th Edition, LWW, 2011, pp. 16–44.
- 16 T. Baudino, *Curr. Drug Discov. Technol.*, 2015, **12**, 3–20.
- 17 T. Sacha, *Mediterr. J. Hematol. Infect. Dis.*, 2014, **6**, 2014007.
- 18 D. C. Allred, P. Brown and D. Medina, *Breast Cancer Res.*, 2004, **6**, 240–245.
- 19 S. J. Johnston and J. S. Carroll, *Biochim. Biophys. Acta - Rev. Cancer*, 2015, **1855**, 183–192.
- 20 H. K. Patel and T. Bihani, *Pharmacol. Ther.*, 2018, **186**, 1–24.
- 21 O. Hantschel, U. Rix and G. Superti-Furga, *Leuk. Lymphoma*, 2008, **49**, 615–619.
- 22 S. J. Lee and J. Y. J. Wang, *J. Biol.*, 2009, **8**, 30.
- 23 S. Yip, Top 10 Best-Selling Drugs of 2019, <https://pharmaintelligence.informa.com/~media/informa-shop-window/pharma/2020/files/reports/top-10-best-selling-drugs-of-2019.pdf>, (accessed 12 January 2021).

- 24 V. R. Gómez Román, J. C. Murray and L. M. Weiner, in *Antibody Fc*, Elsevier, 2014, pp. 1–27.
- 25 M. Suzuki, C. Kato and A. Kato, *J. Toxicol. Pathol.*, 2015, **28**, 133–139.
- 26 G. A. Leget and M. S. Czuczman, *Curr. Opin. Oncol.*, 1998, **10**, 548–551.
- 27 T. Cerny, B. Borisch, M. Introna, P. Johnson and A. L. Rose, *Anticancer Drugs*, 2002, **13**, S3–S10.
- 28 R. M. Lu, Y. C. Hwang, I. J. Liu, C. C. Lee, H. Z. Tsai, H. J. Li and H. C. Wu, *J. Biomed. Sci.*, 2020, **27**, 1–30.
- 29 H. Kaplon, M. Muralidharan, Z. Schneider and J. M. Reichert, *MAbs*, 2020, **12**, 1703531.
- 30 P. J. Kennedy, C. Oliveira, P. L. Granja and B. Sarmento, *Pharmacol. Ther.*, 2017, **177**, 129–145.
- 31 M. B. Schaaf, A. D. Garg and P. Agostinis, *Cell Death Dis.*, 2018, **9**, 115.
- 32 C. Chakraborty, A. R. Sharma, G. Sharma, C. G. P. Doss and S. S. Lee, *Mol. Ther. Nucleic Acids*, 2017, **8**, 132–143.
- 33 X. Shen and D. R. Corey, *Nucleic Acids Res.*, 2018, **46**, 1584–1600.
- 34 B. M. Cooper, J. Iegre, D. H. O'Donovan, M. Ölwegård Halvarsson and D. R. Spring, *Chem. Soc. Rev.*, 2021, **50**, 1480–1494.
- 35 Y. Wang, A. G. Cheetham, G. Angacian, H. Su and L. Xie, *Adv. Drug Deliv. Rev.*, 2017, **110–111**, 112–126.
- 36 V. Prasad, *Nat. Rev. Clin. Oncol.*, 2018, **15**, 11–12.
- 37 A. C. Komor, A. H. Badran and D. R. Liu, *Cell*, 2017, **168**, 20–36.
- 38 C. Fellmann, B. G. Gowen, P. C. Lin, J. A. Doudna and J. E. Corn, *Nat. Rev. Drug Discov.*, 2017, **16**, 89–100.
- 39 H. Kaplon and J. M. Reichert, *MAbs*, 2021, **13**, 1860476.
- 40 S. Sau, H. O. Alsaab, S. K. Kashaw, K. Tatiparti and A. K. Iyer, *Drug Discov. Today*, 2017, **22**, 1547–1556.
- 41 J. D. Bargh, A. Isidro-Llobet, J. S. Parker and D. R. Spring, *Chem. Soc. Rev.*, 2019, **48**, 4361–4374.
- 42 A. H. Staudacher and M. P. Brown, *Br. J. Cancer*, 2017, **117**, 1736–1742.
- 43 G. Mathé, T. Loc and J. Bernard, *C. R. Hebd. Seances Acad. Sci.*, 1958, **246**, 1626–1628.
- 44 P. F. Bross, J. Beitz, G. Chen, X. H. Chen, E. Duffy, L. Kieffer, S. Roy, R. Sridhara, A. Rahman, G. Williams and R. Pazdur, *Clin. Cancer Res.*, 2001, **7**, 1490–1496.
- 45 P. R. Hamann, L. M. Hinman, C. F. Beyer, D. Lindh, J. Upešlācis, D. A. Flowers and I. Bernstein, *Bioconjug. Chem.*, 2002, **13**, 40–46.
- 46 C. D. Godwin, R. P. Gale and R. B. Walter, *Leukemia*, 2017, **31**, 1855–1868.
- 47 A. Younes, N. L. Bartlett, J. P. Leonard, D. A. Kennedy, C. M. Lynch, E. L. Sievers and A. Forero-Torres, *N. Engl. J. Med.*, 2010, **363**, 1812–1821.
- 48 J. C. Villasboas and S. M. Ansell, *F1000Research*, 2016, **5**, 768.

- 49 S. Verma, D. Miles, L. Gianni, I. E. Krop, M. Welslau, J. Baselga, M. Pegram, D.-Y. Oh, V. Diéras, E. Guardino, L. Fang, M. W. Lu, S. Olsen and K. Blackwell, *N. Engl. J. Med.*, 2012, **367**, 1783–1791.
- 50 J. M. Lambert and R. V. J. Chari, *J. Med. Chem.*, 2014, **57**, 6949–6964.
- 51 G. Recondo, M. de la Vega, F. Galanternik, E. Díaz-Cantón, B. A. Leone and J. P. Leone, *Cancer Manag. Res.*, 2016, **8**, 57–65.
- 52 Y. N. Lamb, *Drugs*, 2017, **77**, 1603–1610.
- 53 B. Shor, H.-P. Gerber and P. Sapra, *Mol. Immunol.*, 2015, **67**, 107–116.
- 54 J. F. De Vries, C. M. Zwaan, M. De Bie, J. S. A. Voerman, M. L. Den Boer, J. J. M. Van Dongen and V. H. J. Van Der Velden, *Leukemia*, 2012, **26**, 255–264.
- 55 P. M. Challita-Eid, D. Satpayev, P. Yang, Z. An, K. Morrison, Y. Shostak, A. Raitano, R. Nadell, W. Liu, D. R. Lortie, L. Capo, A. Verlinsky, M. Leavitt, F. Malik, H. Avina, C. I. Guevara, N. Dinh, S. Karki, B. S. Anand, D. S. Pereira, I. B. J. Joseph, F. Donate, K. Morrison and D. R. Stover, *Cancer Res.*, 2016, **76**, 3003–3013.
- 56 S. Modi, C. Saura, T. Yamashita, Y. H. Park, S. B. Kim, K. Tamura, F. Andre, H. Iwata, Y. Ito, J. Tsurutani, J. Sohn, N. Denduluri, C. Perrin, K. Aogi, E. Tokunaga, S. A. Im, K. S. Lee, S. A. Hurvitz, J. Cortes, C. Lee, S. Chen, L. Zhang, J. Shahidi, A. Yver and I. Krop, *N. Engl. J. Med.*, 2020, **382**, 610–621.
- 57 E. D. Deeks, *Drugs*, 2019, **79**, 1467–1475.
- 58 T. N. Iwata, C. Ishii, S. Ishida, Y. Ogitan, T. Wada and T. Agatsuma, *Mol. Cancer Ther.*, 2018, **17**, 1494–1503.
- 59 Y. Y. Syed, *Drugs*, 2020, **80**, 1019–1025.
- 60 A. J. Ocean, A. N. Starodub, A. Bardia, L. T. Vahdat, S. J. Isakoff, M. Guarino, W. A. Messersmith, V. J. Picozzi, I. A. Mayer, W. A. Wegener, P. Maliakal, S. V. Govindan, R. M. Sharkey and D. M. Goldenberg, *Cancer*, 2017, **123**, 3843–3854.
- 61 S. Trudel, N. Lendvai, R. Popat, P. M. Voorhees, B. Reeves, E. N. Libby, P. G. Richardson, A. Hoos, I. Gupta, V. Bragulat, Z. He, J. B. Opalinska and A. D. Cohen, *Blood Cancer J.*, 2019, **9**, 1–10.
- 62 S. Lonial, H. C. Lee, A. Badros, S. Trudel, A. K. Nooka, A. Chari, A. O. Abdallah, N. Callander, N. Lendvai, D. Sborov, A. Suvannasankha, K. Weisel, L. Karlin, E. Libby, B. Arnulf, T. Facon, C. Hulin, K. M. Kortüm, P. Rodríguez-Otero, S. Z. Usmani, P. Hari, R. Baz, H. Quach, P. Moreau, P. M. Voorhees, I. Gupta, A. Hoos, E. Zhi, J. Baron, T. Piontek, E. Lewis, R. C. Jewell, E. J. Dettman, R. Popat, S. D. Esposti, J. Opalinska, P. Richardson and A. D. Cohen, *Lancet Oncol.*, 2020, **21**, 207–221.
- 63 F. Zammarchi, S. Corbett, L. Adams, P. C. Tyrer, K. Kiakos, N. Janghra, T. Marafioti, C. E. Britten, C. E. G. Havenith, S. Chivers, F. D’Hooze, D. G. Williams, A. Tiberghien, P. W. Howard, J. A. Hartley and P. H. Van Berkel, *Blood*, 2018, **131**, 1094–1105.
- 64 A. Beck, L. Goetsch, C. Dumontet and N. Corvaia, *Nat. Rev. Drug Discov.*, 2017, **16**, 315–337.
- 65 C. A. Janeway, P. Travers, M. Walport and M. Shlomchik, *Immunobiology: The Immune System in Health and Disease*, Garland Pub, 5th edn., 2001.
- 66 I. Sela-Culang, V. Kunik and Y. Ofra, *Front. Immunol.*, 2013, **4**, 302.

- 67 G. Vidarsson, G. Dekkers and T. Rispens, *Front. Immunol.*, 2014, **5**, 520.
- 68 M. F. Jennewein and G. Alter, *Trends Immunol.*, 2017, **38**, 358–372.
- 69 R. M. Hoffmann, B. G. T. Coumbe, D. H. Josephs, S. Mele, K. M. Ilieva, A. Cheung, A. N. Tutt, J. F. Spicer, D. E. Thurston, S. Crescioli and S. N. Karagiannis, *Oncoimmunology*, 2018, **7**, e1395127.
- 70 H. Liu and K. May, *MAbs*, 2012, **4**, 17–23.
- 71 Z. B. Dong, G. Manolikakes, L. Shi, P. Knochel and H. Mayr, *Chem. - A Eur. J.*, 2010, **16**, 248–253.
- 72 A. F. Labrijn, A. O. Buijsse, E. T. J. Van Den Bremer, A. Y. W. Verwilligen, W. K. Bleeker, S. J. Thorpe, J. Killestein, C. H. Polman, R. C. Aalberse, J. Schuurman, J. G. J. Van De Winkel and P. W. H. I. Parren, *Nat. Biotechnol.*, 2009, **27**, 767–771.
- 73 C. Peters and S. Brown, *Biosci. Rep.*, 2015, **35**, e00225.
- 74 F. A. Harding, M. M. Stickler, J. Razo and R. B. DuBridge, *MAbs*, 2010, **2**, 256–65.
- 75 G. D. L. Phillips, G. Li, D. L. Dugger, L. M. Crocker, K. L. Parsons, E. Mai, W. A. Blättler, J. M. Lambert, R. V. J. Chari, R. J. Lutz, W. L. T. Wong, F. S. Jacobson, H. Koeppen, R. H. Schwall, S. R. Kenkare-Mitra, S. D. Spencer and M. X. Sliwowski, *Cancer Res.*, 2008, **68**, 9280–9290.
- 76 N. Joubert, C. Denevault-Sabourin, F. Bryden and M. C. Viaud-Massuard, *Eur. J. Med. Chem.*, 2017, **142**, 393–415.
- 77 C. K. Tsui, R. M. Barfield, C. R. Fischer, D. W. Morgens, A. Li, B. A. H. Smith, M. A. Gray, C. R. Bertozzi, D. Rabuka and M. C. Bassik, *Nat. Chem. Biol.*, 2019, **15**, 949–958.
- 78 P. A. Trail, D. Willner, S. J. Lasch, A. J. Henderson, S. Hofstead, A. M. Casazza, R. A. Firestone, I. Hellström and K. E. Hellström, *Science*, 1993, **261**, 212–215.
- 79 A. W. Tolcher, S. Sugarman, K. A. Gelmon, R. Cohen, M. Saleh, C. Isaacs, L. Young, D. Healey, N. Onetto and W. Slichenmyer, *J. Clin. Oncol.*, 1999, **17**, 478–484.
- 80 K. C. Nicolaou and S. Rigol, *Angew. Chemie Int. Ed.*, 2019, **58**, 11206–11241.
- 81 N. Joubert, A. Beck, C. Dumontet and C. Denevault-Sabourin, *Pharmaceuticals*, 2020, **13**, 1–30.
- 82 Y. Kawato, M. Aonuma, Y. Hirota, H. Kuga and K. Sato, *Cancer Res.*, 1991, **51**, 4187–4191.
- 83 F. Li, T. Jiang, Q. Li and X. Ling, *Am. J. Cancer Res.*, 2017, **7**, 2350–2394.
- 84 A. C. Tiberghien, J.-N. Levy, L. A. Masterson, N. V. Patel, L. R. Adams, S. Corbett, D. G. Williams, J. A. Hartley and P. W. Howard, *ACS Med. Chem. Lett.*, 2016, **7**, 983–987.
- 85 J. A. Hartley, M. J. Flynn, J. P. Bingham, S. Corbett, H. Reinert, A. Tiberghien, L. A. Masterson, D. Antonow, L. Adams, S. Chowdhury, D. G. Williams, S. Mao, J. Harper, C. E. G. Havenith, F. Zammarchi, S. Chivers, P. H. Van Berkel and P. W. Howard, *Sci. Rep.*, 2018, **8**, 10479.
- 86 R. C. Elgersma, R. G. E. Coumans, T. Huijbregts, W. M. P. B. Menge, J. A. F. Joosten, H. J. Spijker, F. M. H. de Groot, M. M. C. van der Lee, R. Ubink, D. J. van den Dobbelaar, D. F. Egging, W. H. A. Dokter, G. F. M. Verheijden, J. M. Lemmens, C. M. Timmers and P. H. Beusker, *Mol. Pharm.*, 2015, **12**, 1813–1835.
- 87 P. J. Carter and G. A. Lazar, *Nat. Rev. Drug Discov.*, 2017, **17**, 197–223.

- 88 A. Pahl, C. Lutz and T. Hechler, *Drug Discov. Today Technol.*, 2018, **30**, 85–89.
- 89 A. V. Gandhi, K. J. Arlotta, H. N. Chen, S. C. Owen and J. F. Carpenter, *J. Pharm. Sci.*, 2018, **107**, 1858–1869.
- 90 K. J. Hamblett, P. D. Senter, D. F. Chace, M. M. C. Sun, J. Lenox, C. G. Cervený, K. M. Kissler, S. X. Bernhardt, A. K. Kopcha, R. F. Zabinski, D. L. Meyer and J. A. Francisco, *Clin. Cancer Res.*, 2004, **10**, 7063–7070.
- 91 X. Sun, J. F. Ponte, N. C. Yoder, R. Laleau, J. Coccia, L. Lanieri, Q. Qiu, R. Wu, E. Hong, M. Bogalhas, L. Wang, L. Dong, Y. Setiady, E. K. Maloney, O. Ab, X. Zhang, J. Pinkas, T. A. Keating, R. Chari, H. K. Erickson and J. M. Lambert, *Bioconjug. Chem.*, 2017, **28**, 1371–1381.
- 92 D. Y. Jackson, *Org. Process Res. Dev.*, 2016, **20**, 852–866.
- 93 S. J. Moon, S. V. Govindan, T. M. Cardillo, C. A. D’Souza, H. J. Hansen and D. M. Goldenberg, *J. Med. Chem.*, 2008, **51**, 6916–6926.
- 94 L. Turell, R. Radi and B. Alvarez, *Free Radic. Biol. Med.*, 2013, **65**, 244–253.
- 95 T. H. Pillow, J. D. Sadowsky, D. Zhang, S. F. Yu, G. Del Rosario, K. Xu, J. He, S. Bhakta, R. Ohri, K. R. Kozak, E. Ha, J. R. Junutula and J. A. Flygare, *Chem. Sci.*, 2016, **8**, 366–370.
- 96 R. V. J. Chari, B. A. Martell, J. L. Gross, S. B. Cook, S. A. Shah, W. A. Blättler, S. J. McKenzie and V. S. Goldmacher, *Cancer Res.*, 1992, **52**, 127–31.
- 97 G. M. Dubowchik and R. A. Firestone, *Bioorg. Med. Chem. Lett.*, 1998, **8**, 3341–3346.
- 98 G. M. Dubowchik, R. A. Firestone, L. Padilla, D. Willner, S. J. Hofstead, K. Mosure, J. O. Knipe, S. J. Lasch and P. A. Trail, *Bioconjug. Chem.*, 2002, **13**, 855–869.
- 99 S. Kolodych, C. Michel, S. Delacroix, O. Koniev, A. Ehkirch, J. Eberova, S. Cianférani, B. Renoux, W. Krezel, P. Poinot, C. D. Muller, S. Papot and A. Wagner, *Eur. J. Med. Chem.*, 2017, **142**, 376–382.
- 100 J. C. Kern, M. Cancilla, D. Dooney, K. Kwasnjuk, R. Zhang, M. Beaumont, I. Figueroa, S. C. Hsieh, L. Liang, D. Tomazela, J. Zhang, P. E. Brandish, A. Palmieri, P. Stivers, M. Cheng, G. Feng, P. Geda, S. Shah, A. Beck, D. Bresson, J. Firdos, D. Gately, N. Knudsen, A. Manibusan, P. G. Schultz, Y. Sun and R. M. Garbaccio, *J. Am. Chem. Soc.*, 2016, **138**, 1430–1445.
- 101 J. D. Bargh, S. J. Walsh, A. Isidro-Llobet, S. Omarjee, J. S. Carroll and D. R. Spring, *Chem. Sci.*, 2020, **11**, 2375–2380.
- 102 J. C. Kern, D. Dooney, R. Zhang, L. Liang, P. E. Brandish, M. Cheng, G. Feng, A. Beck, D. Bresson, J. Firdos, D. Gately, N. Knudsen, A. Manibusan, Y. Sun and R. M. Garbaccio, *Bioconjug. Chem.*, 2016, **27**, 2081–2088.
- 103 J. D. Bargh, S. J. Walsh, N. Ashman, A. Isidro-Llobet, J. S. Carroll and D. R. Spring, *Chem. Commun.*, 2021, **57**, 3457.
- 104 S. J. Gregson, L. A. Masterson, B. Wei, T. H. Pillow, S. D. Spencer, G. D. Kang, S. F. Yu, H. Raab, J. Lau, G. Li, G. D. Lewis Phillips, J. Gunzner-Toste, B. S. Safina, R. Ohri, M. Darwish, K. R. Kozak, J. Dela Cruz-Chuh, A. Polson, J. A. Flygare and P. W. Howard, *J. Med. Chem.*, 2017, **60**, 9490–9507.
- 105 E. Oflazoglu, I. J. Stone, K. Gordon, C. G. Wood, E. A. Repasky, I. S. Grewal, C. L. Law and H. P. Gerber, *Clin. Cancer Res.*, 2008, **14**, 6171–6180.
- 106 B. Shi, M. Wu, Z. Li, Z. Xie, X. Wei, J. Fan, Y. Xu, D. Ding, S. H. Akash, S. Chen and S. Cao, *Cancer*

- Med.*, 2019, **8**, 1793–1805.
- 107 O. Koniev and A. Wagner, *Chem. Soc. Rev.*, 2015, **44**, 5495–5551.
 - 108 S. J. Walsh, J. D. Bargh, F. M. Dannheim, A. R. Hanby, H. Seki, A. J. Counsell, X. Ou, E. Fowler, N. Ashman, Y. Takada, A. Isidro-Llobet, J. S. Parker, J. S. Carroll and D. R. Spring, *Chem. Soc. Rev.*, 2021, **50**, 1305–1353.
 - 109 P. Agarwal and C. R. Bertozzi, *Bioconjug. Chem.*, 2015, **26**, 176–192.
 - 110 J. F. DiJoseph, D. C. Armellino, E. R. Boghaert, K. Khandke, M. M. Dougher, L. Sridharan, A. Kunz, P. R. Hamann, B. Gorovits, C. Udata, J. K. Moran, A. G. Popplewell, S. Stephens, P. Frost and N. K. Damle, *Blood*, 2004, **103**, 1807–1814.
 - 111 L. Wang, G. Amphlett, W. A. Blättler, J. M. Lambert and W. Zhang, *Protein Sci.*, 2005, **14**, 2436–2446.
 - 112 A. Wakankar, Y. Chen, Y. Gokarn and F. S. Jacobson, *MAbs*, 2011, **3**, 161–172.
 - 113 R. Ohri, S. Bhakta, A. Fourie-O'Donohue, J. dela Cruz-Chuh, S. P. Tsai, R. Cook, B. Wei, C. Ng, A. W. Wong, A. B. Bos, F. Farahi, J. Bhakta, T. H. Pillow, H. Raab, R. Vandlen, P. Polakis, Y. Liu, H. Erickson, J. R. Junutula and K. R. Kozak, *Bioconjug. Chem.*, 2018, **29**, 473–485.
 - 114 B.-Q. Shen, K. Xu, L. Liu, H. Raab, S. Bhakta, M. Kenrick, K. L. Parsons-Reponte, J. Tien, S.-F. Yu, E. Mai, D. Li, J. Tibbitts, J. Baudys, O. M. Saad, S. J. Scales, P. J. McDonald, P. E. Hass, C. Eigenbrot, T. Nguyen, W. A. Solis, R. N. Fuji, K. M. Flagella, D. Patel, S. D. Spencer, L. A. Khawli, A. Ebens, W. L. Wong, R. Vandlen, S. Kaur, M. X. Sliwowski, R. H. Scheller, P. Polakis and J. R. Junutula, *Nat. Biotechnol.*, 2012, **30**, 184–189.
 - 115 P. Strop, S. H. Liu, M. Dorywalska, K. Delaria, R. G. Dushin, T. T. Tran, W. H. Ho, S. Farias, M. G. Casas, Y. Abdiche, D. Zhou, R. Chandrasekaran, C. Samain, C. Loo, A. Rossi, M. Rickert, S. Krimm, T. Wong, S. M. Chin, J. Yu, J. Dilley, J. Chaparro-Riggers, G. F. Filzen, C. J. O'Donnell, F. Wang, J. S. Myers, J. Pons, D. L. Shelton and A. Rajpal, *Chem. Biol.*, 2013, **20**, 161–167.
 - 116 A. A. Wakankar, M. B. Feeney, J. Rivera, Y. Chen, M. Kim, V. K. Sharma and Y. J. Wang, *Bioconjug. Chem.*, 2010, **21**, 1588–1595.
 - 117 G. Chaubet, F. Thoreau and A. Wagner, *Drug Discov. Today Technol.*, 2018, **30**, 21–26.
 - 118 M. Hayakawa, N. Toda, N. Carrillo, N. J. Thornburg, J. E. Crowe and C. F. Barbas, *ChemBioChem*, 2012, **13**, 2191–2195.
 - 119 A. R. Nanna, X. Li, E. Walseng, L. Pedzisa, R. S. Goydel, D. Hymel, T. R. Burke, W. R. Roush and C. Rader, *Nat. Commun.*, 2017, **8**, 1–9.
 - 120 D. S. Wilbur, M. K. Chyan, H. Nakamae, Y. Chen, D. K. Hamlin, E. B. Santos, B. T. Kornblit and B. M. Sandmaier, *Bioconjug. Chem.*, 2012, **23**, 409–420.
 - 121 M. J. Matos, B. L. Oliveira, N. Martínez-Sáez, A. Guerreiro, P. M. S. D. Cal, J. Bertoldo, M. Maneiro, E. Perkins, J. Howard, M. J. Deery, J. M. Chalker, F. Corzana, G. Jiménez-Osés and G. J. L. Bernardes, *J. Am. Chem. Soc.*, 2018, **140**, 4004–4017.
 - 122 I. Dovgan, S. Ursuegui, S. Erb, C. Michel, S. Kolodych, S. Cianférani and A. Wagner, *Bioconjug. Chem.*, 2017, **28**, 1452–1457.
 - 123 A. Andrikopoulou, E. Zografos, M. Lontos, K. Koutsoukos, M. A. Dimopoulos and F. Zagouri, *Clin. Breast Cancer*, 2020, **21**, e212–e219.
 - 124 H. Liu, C. Chumsae, G. Gaza-Bulseco, K. Hurkmans and C. H. Radziejewski, *Anal. Chem.*, 2010,

- 82**, 5219–5226.
- 125 F. Debaene, A. Bœuf, E. Wagner-Rousset, O. Colas, D. Ayoub, N. Corvaia, A. Van Dorsselaer, A. Beck and S. Cianféroni, *Anal. Chem.*, 2014, **86**, 10674–10683.
 - 126 M. M. C. Sun, K. S. Beam, C. G. Cervený, K. J. Hamblett, R. S. Blackmore, M. Y. Torgov, F. G. M. Handley, N. C. Ihle, P. D. Senter and S. C. Alley, *Bioconjug. Chem.*, 2005, **16**, 1282–1290.
 - 127 C. Bahou, E. A. Love, S. Leonard, R. J. Spears, A. Maruani, K. Armour, J. R. Baker and V. Chudasama, *Bioconjug. Chem.*, 2019, **30**, 1048–1054.
 - 128 S. C. Alley, D. R. Benjamin, S. C. Jeffrey, N. M. Okeley, D. L. Meyer, R. J. Sanderson and P. D. Senter, *Bioconjug. Chem.*, 2008, **19**, 759–765.
 - 129 A. D. Baldwin and K. L. Kiick, *Bioconjug. Chem.*, 2011, **22**, 1946–1953.
 - 130 R. P. Lyon, J. R. Setter, T. D. Bovee, S. O. Doronina, J. H. Hunter, M. E. Anderson, C. L. Balasubramanian, S. M. Duniho, C. I. Leiske, F. Li and P. D. Senter, *Nat. Biotechnol.*, 2014, **32**, 1059–1062.
 - 131 L. N. Tumey, M. Charati, T. He, E. Sousa, D. Ma, X. Han, T. Clark, J. Casavant, F. Loganzo, F. Barletta, J. Lucas and E. I. Graziani, *Bioconjug. Chem.*, 2014, **25**, 1871–1880.
 - 132 H. Seki, S. J. Walsh, J. D. Bargh, J. S. Parker, J. Carroll and D. R. Spring, *Chem. Sci.*, 2021, **12**, 9060–9068.
 - 133 M.-A. Kasper, A. Stengl, P. Ochtrup, M. Gerlach, T. Stoschek, D. Schumacher, J. Helma, M. Penkert, E. Krause, H. Leonhardt and C. P. R. Hackenberger, *Angew. Chemie Int. Ed.*, 2019, **58**, 11631–11636.
 - 134 S. Kolodych, O. Koniev, Z. Baatarkhuu, J. Y. Bonnefoy, F. Debaene, S. Cianféroni, A. Van Dorsselaer and A. Wagner, *Bioconjug. Chem.*, 2015, **26**, 197–200.
 - 135 E. V. Vinogradova, C. Zhang, A. M. Spokoyny, B. L. Pentelute and S. L. Buchwald, *Nature*, 2015, **526**, 687–691.
 - 136 M. J. Matos, C. D. Navo, T. Hakala, X. Ferhati, A. Guerreiro, D. Hartmann, B. Bernardim, K. L. Saar, I. Compañón, F. Corzana, T. P. J. Knowles, G. Jiménez-Osés and G. J. L. Bernardes, *Angew. Chemie*, 2019, **131**, 6712–6716.
 - 137 J. R. Junutula, H. Raab, S. Clark, S. Bhakta, D. D. Leipold, S. Weir, Y. Chen, M. Simpson, S. P. Tsai, M. S. Dennis, Y. Lu, Y. G. Meng, C. Ng, J. Yang, C. C. Lee, E. Duenas, J. Gorrell, V. Katta, A. Kim, K. McDorman, K. Flagella, R. Venook, S. Ross, S. D. Spencer, W. Lee Wong, H. B. Lowman, R. Vandlen, M. X. Sliwowski, R. H. Scheller, P. Polakis and W. Mallet, *Nat. Biotechnol.*, 2008, **26**, 925–932.
 - 138 J. R. Junutula, S. Bhakta, H. Raab, K. E. Ervin, C. Eigenbrot, R. Vandlen, R. H. Scheller and H. B. Lowman, *J. Immunol. Methods*, 2008, **332**, 41–52.
 - 139 N. Dimasi, R. Fleming, H. Zhong, B. Bezabeh, K. Kinneer, R. J. Christie, C. Fazenbaker, H. Wu and C. Gao, *Mol. Pharm.*, 2017, **14**, 1501–1516.
 - 140 A. Kumar, K. Kinneer, L. Masterson, E. Ezeadi, P. Howard, H. Wu, C. Gao and N. Dimasi, *Bioorganic Med. Chem. Lett.*, 2018, **28**, 3617–3621.
 - 141 C. S. Neumann, K. C. Olivas, M. E. Anderson, J. H. Cochran, S. Jin, F. Li, L. V. Loftus, D. W. Meyer, J. Neale, J. C. Nix, P. G. Pittman, J. K. Simmons, M. L. Ulrich, A. B. Waight, A. Wong, M. C. Zaval, W. Zeng, R. P. Lyon and P. D. Senter, *Mol. Cancer Ther.*, 2018, **17**, 2633–2642.

- 142 T. H. Pillow, P. Adhikari, R. A. Blake, J. Chen, G. Del Rosario, G. Deshmukh, I. Figueroa, K. E. Gascoigne, A. V. Kamath, S. Kaufman, T. Kleinheinz, K. R. Kozak, B. Latifi, D. D. Leipold, C. Sing Li, R. Li, M. M. Mulvihill, A. O'Donohue, R. K. Rowntree, J. D. Sadowsky, J. Wai, X. Wang, C. Wu, Z. Xu, H. Yao, S. Yu, D. Zhang, R. Zang, H. Zhang, H. Zhou, X. Zhu and P. S. Dragovich, *ChemMedChem*, 2020, **15**, 17–25.
- 143 S. Bhakta, H. Raab and J. R. Junutula, *Methods Mol. Biol.*, 2013, **1045**, 189–203.
- 144 C. J. Noren, S. J. Anthony-Cahill, M. C. Griffith and P. G. Schultz, *Science*, 1989, **244**, 182–188.
- 145 J. W. Chin, *Nature*, 2017, **550**, 53–60.
- 146 T. J. Hallam, E. Wold, A. Wahl and V. V. Smider, *Mol. Pharm.*, 2015, **12**, 1848–1862.
- 147 J. Y. Axup, K. M. Bajjuri, M. Ritland, B. M. Hutchins, C. H. Kim, S. A. Kazane, R. Halder, J. S. Forsyth, A. F. Santidrian, K. Stafin, Y. Lu, H. Tran, A. J. Seller, S. L. Biroc, A. Szydluk, J. K. Pinkstaff, F. Tian, S. C. Sinha, B. Felding-Habermann, V. V. Smider and P. G. Schultz, *Proc. Natl. Acad. Sci. U. S. A.*, 2012, **109**, 16101–6.
- 148 R. K. V. Lim, S. Yu, B. Cheng, S. Li, N. J. Kim, Y. Cao, V. Chi, J. Y. Kim, A. K. Chatterjee, P. G. Schultz, M. S. Tremblay and S. A. Kazane, *Bioconjug. Chem.*, 2015, **26**, 2216–2222.
- 149 A. H. St. Amant, F. Huang, J. Lin, D. Lemen, C. Chakiath, S. Mao, C. Fazenbaker, H. Zhong, J. Harper, W. Xu, N. Patel, L. Adams, B. Vijayakrishnan, P. W. Howard, M. Marelli, H. Wu, C. Gao, J. Read de Alaniz and R. J. Christie, *Bioconjug. Chem.*, 2019, **30**, 2340–2348.
- 150 A. H. St. Amant, F. Huang, J. Lin, K. Rickert, V. Oganessian, D. Lemen, S. Mao, J. Harper, M. Marelli, H. Wu, C. Gao, J. Read de Alaniz and R. J. Christie, *Angew. Chemie Int. Ed.*, 2019, **58**, 8489–8493.
- 151 E. S. Zimmerman, T. H. Heibeck, A. Gill, X. Li, C. J. Murray, M. R. Madlansacay, C. Tran, N. T. Uter, G. Yin, P. J. Rivers, A. Y. Yam, W. D. Wang, A. R. Steiner, S. U. Bajad, K. Penta, W. Yang, T. J. Hallam, C. D. Thanos and A. K. Sato, *Bioconjug. Chem.*, 2014, **25**, 351–361.
- 152 P. E. Brandish, A. Palmieri, S. Antonenko, M. Beaumont, L. Benso, M. Cancilla, M. Cheng, L. Fayadat-Dilman, G. Feng, I. Figueroa, J. Firdos, R. Garbaccio, L. Garvin-Queen, D. Gately, P. Geda, C. Haines, S. Hsieh, D. Hodges, J. Kern, N. Knudsen, K. Kwasnjuk, L. Liang, H. Ma, A. Manibusan, P. L. Miller, L. Y. Moy, Y. Qu, S. Shah, J. S. Shin, P. Stivers, Y. Sun, D. Tomazela, H. C. Woo, D. Zaller, S. Zhang, Y. Zhang and M. Zielstorff, *Bioconjug. Chem.*, 2018, **29**, 2357–2369.
- 153 M. P. Vanbrunt, K. Shanebeck, Z. Caldwell, J. Johnson, P. Thompson, T. Martin, H. Dong, G. Li, H. Xu, F. D'Hooge, L. Masterson, P. Bariola, A. Tiberghien, E. Ezeadi, D. G. Williams, J. A. Hartley, P. W. Howard, K. H. Grabstein, M. A. Bowen and M. Marelli, *Bioconjug. Chem.*, 2015, **26**, 2249–2260.
- 154 G. Yin, H. T. Stephenson, J. Yang, X. Li, S. M. Armstrong, T. H. Heibeck, C. Tran, M. R. Masikat, S. Zhou, R. L. Stafford, A. Y. Yam, J. Lee, A. R. Steiner, A. Gill, K. Penta, S. Pollitt, R. Baliga, C. J. Murray, C. D. Thanos, L. M. McEvoy, A. K. Sato and T. J. Hallam, *Sci. Rep.*, 2017, **7**, 1–13.
- 155 H. Schneider, L. Deweid, O. Avrutina and H. Kolmar, *Anal. Biochem.*, 2020, **595**, 113615.
- 156 F. Lhospice, D. Brégeon, C. Belmant, P. Dennler, A. Chiotellis, E. Fischer, L. Gauthier, A. Boëdec, H. Rispaud, S. Savard-Chambard, A. Represa, N. Schneider, C. Paturel, M. Sapet, C. Delcambre, S. Ingoure, N. Viaud, C. Bonnafeous, R. Schibli and F. Romagné, *Mol. Pharm.*, 2015, **12**, 1863–1871.
- 157 Y. Anami, W. Xiong, X. Gui, M. Deng, C. C. Zhang, N. Zhang, Z. An and K. Tsuchikama, *Org.*

- Biomol. Chem.*, 2017, **15**, 5635–5642.
- 158 K. Zheng, C. Bantog and R. Bayer, *MAbs*, 2011, **3**, 568–576.
 - 159 D. Reusch and M. L. Tejada, *Glycobiology*, 2015, **25**, 1325–1334.
 - 160 M. K. Leabman, Y. G. Meng, R. F. Kelley, L. E. DeForge, K. J. Cowan and S. Iyer, *MAbs*, 2013, **5**, 896–903.
 - 161 P. Strop, T.-T. Tran, M. Dorywalska, K. Delaria, R. Dushin, O. K. Wong, W.-H. Ho, D. Zhou, A. Wu, E. Kraynov, L. Aschenbrenner, B. Han, C. J. O'Donnell, J. Pons, A. Rajpal, D. L. Shelton and S.-H. Liu, *Mol. Cancer Ther.*, 2016, **15**, 2698–2708.
 - 162 P. Strop, K. Delaria, D. Foletti, J. M. Witt, A. Hasa-Moreno, K. Poulsen, M. G. Casas, M. Dorywalska, S. Farias, A. Pios, V. Lui, R. Dushin, D. Zhou, T. Navaratnam, T. T. Tran, J. Sutton, K. C. Lindquist, B. Han, S. H. Liu, D. L. Shelton, J. Pons and A. Rajpal, *Nat. Biotechnol.*, 2015, **33**, 694–696.
 - 163 M. Dorywalska, P. Strop, J. A. Melton-Witt, A. Hasa-Moreno, S. E. Farias, M. Galindo Casas, K. Delaria, V. Lui, K. Poulsen, C. Loo, S. Krimm, G. Bolton, L. Moine, R. Dushin, T. T. Tran, S. H. Liu, M. Rickert, D. Foletti, D. L. Shelton, J. Pons and A. Rajpal, *Bioconjug. Chem.*, 2015, **26**, 650–659.
 - 164 P. M. Drake, A. E. Albers, J. Baker, S. Banas, R. M. Barfield, A. S. Bhat, G. W. De Hart, A. W. Garofalo, P. Holder, L. C. Jones, R. Kudirka, J. McFarland, W. Zmolek and D. Rabuka, *Bioconjug. Chem.*, 2014, **25**, 1331–1341.
 - 165 P. M. Drake, A. Carlson, J. M. McFarland, S. Bañas, R. M. Barfield, W. Zmolek, Y. C. Kim, B. C. B. Huang, R. Kudirka and D. Rabuka, *Mol. Cancer Ther.*, 2018, **17**, 161–168.
 - 166 J. Lee, H.-J. Choi, M. Yun, Y. Kang, J.-E. Jung, Y. Ryu, T. Y. Kim, Y. Cha, H.-S. Cho, J.-J. Min, C.-W. Chung and H.-S. Kim, *Angew. Chemie*, 2015, **127**, 12188–12192.
 - 167 R. R. Beerli, T. Hell, A. S. Merkel and U. Grawunder, *PLoS One*, 2015, **10**, e0131177.
 - 168 V. Siegmund, B. Piater, B. Zakeri, T. Eichhorn, F. Fischer, C. Deutsch, S. Becker, L. Toleikis, B. Hock, U. A. K. Betz and H. Kolmar, *Sci. Rep.*, 2016, **6**, 1–9.
 - 169 N. Forte, V. Chudasama and J. R. Baker, *Drug Discov. Today Technol.*, 2018, **30**, 11–20.
 - 170 P. Bryant, M. Pabst, G. Badescu, M. Bird, W. McDowell, E. Jamieson, J. Swierkosz, K. Jurlewicz, R. Tommasi, K. Henseleit, X. Sheng, N. Camper, A. Manin, K. Kozakowska, K. Peciak, E. Laurine, R. Grygorash, A. Kyle, D. Morris, V. Parekh, A. Abhilash, J. W. Choi, J. Edwards, M. Frigerio, M. P. Baker and A. Godwin, *Mol. Pharm.*, 2015, **12**, 1872–1879.
 - 171 M. Pabst, W. McDowell, A. Manin, A. Kyle, N. Camper, E. De Juan, V. Parekh, F. Rudge, H. Makwana, T. Kantner, H. Parekh, A. Michelet, X. B. Sheng, G. Popa, C. Tucker, F. Khayrzad, D. Pollard, K. Kozakowska, R. Resende, A. Jenkins, F. Simoes, D. Morris, P. Williams, G. Badescu, M. P. Baker, M. Bird, M. Frigerio and A. Godwin, *J. Control. Release*, 2017, **253**, 160–164.
 - 172 G. Badescu, P. Bryant, M. Bird, K. Henseleit, J. Swierkosz, V. Parekh, R. Tommasi, E. Pawlisz, K. Jurlewicz, M. Farys, N. Camper, X. Sheng, M. Fisher, R. Grygorash, A. Kyle, A. Abhilash, M. Frigerio, J. Edwards and A. Godwin, *Bioconjug. Chem.*, 2014, **25**, 1124–1136.
 - 173 F. F. Schumacher, J. P. M. Nunes, A. Maruani, V. Chudasama, M. E. B. Smith, K. A. Chester, J. R. Baker and S. Caddick, *Org. Biomol. Chem.*, 2014, **12**, 7261–7269.
 - 174 J. P. M. Nunes, M. Morais, V. Vassileva, E. Robinson, V. S. Rajkumar, M. E. B. Smith, R. B.

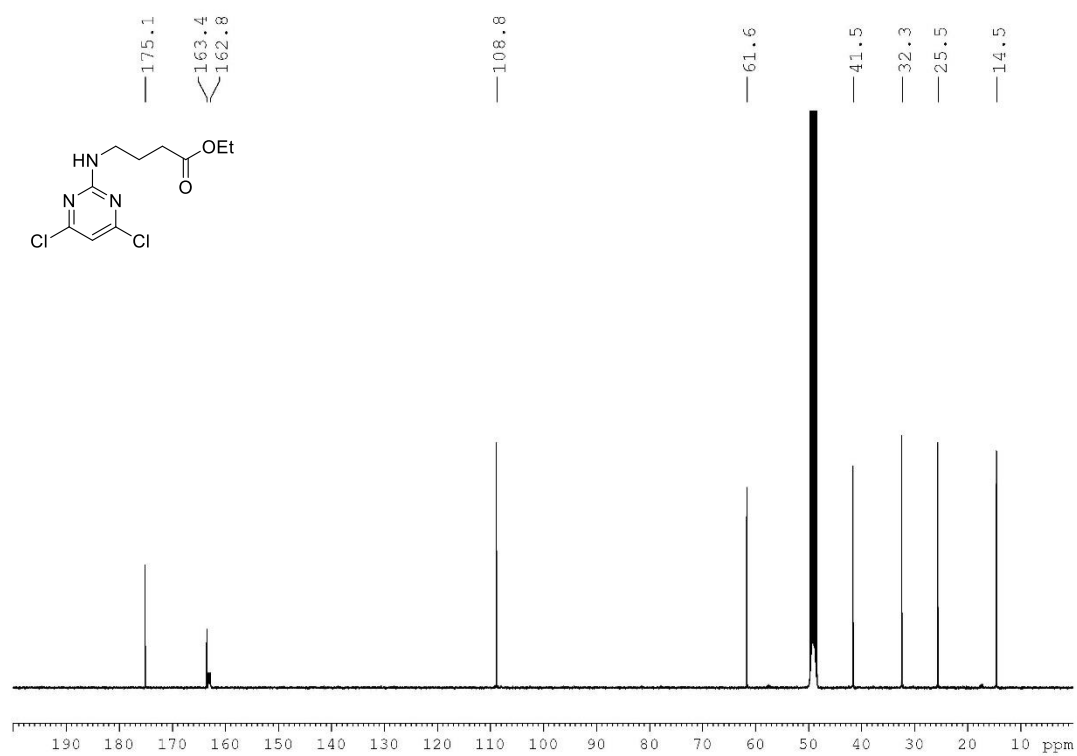
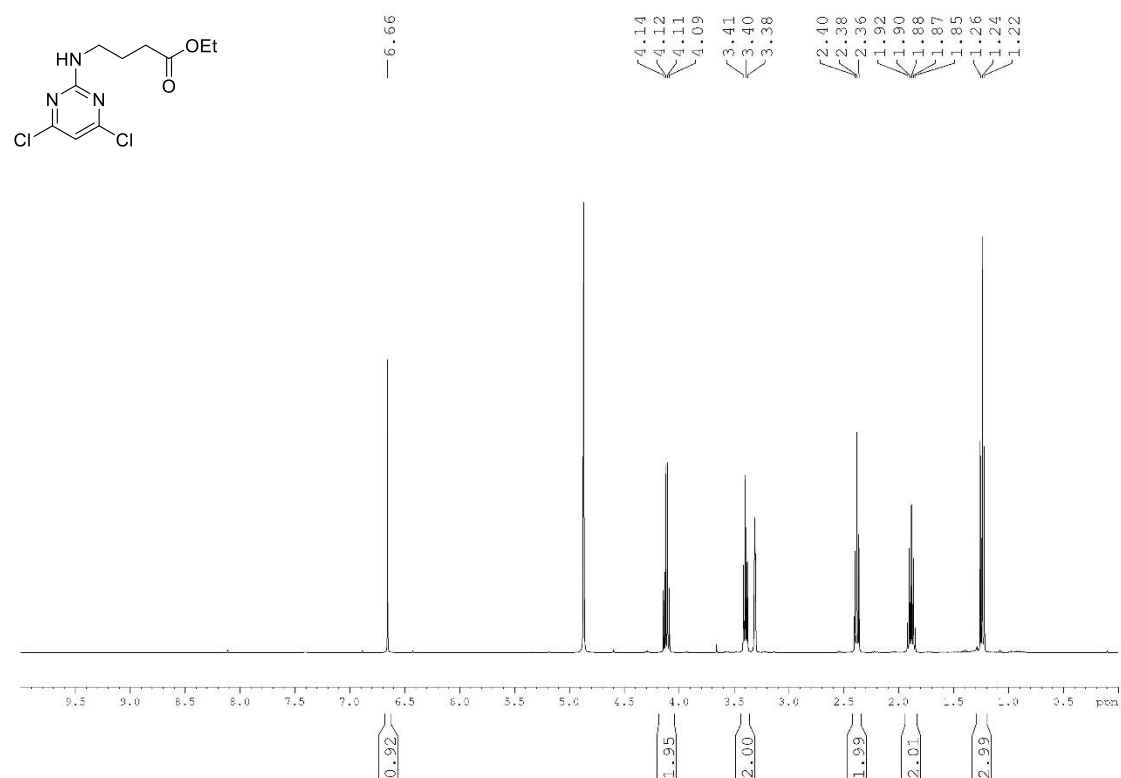
- Pedley, S. Caddick, J. R. Baker and V. Chudasama, *Chem. Commun.*, 2015, **51**, 10624–10627.
- 175 C. R. Behrens, E. H. Ha, L. L. Chinn, S. Bowers, G. Probst, M. Fitch-Bruhns, J. Monteon, A. Valdiosera, A. Bermudez, S. Liao-Chan, T. Wong, J. Melnick, J. W. Theunissen, M. R. Flory, D. Houser, K. Venstrom, Z. Levashova, P. Sauer, T. S. Migone, E. H. Van Der Horst, R. L. Halcomb and D. Y. Jackson, *Mol. Pharm.*, 2015, **12**, 3986–3998.
 - 176 M. Morais, J. P. M. Nunes, K. Karu, N. Forte, I. Benni, M. E. B. Smith, S. Caddick, V. Chudasama and J. R. Baker, *Org. Biomol. Chem.*, 2017, **15**, 2947–2952.
 - 177 A. Maruani, M. E. B. Smith, E. Miranda, K. A. Chester, V. Chudasama and S. Caddick, *Nat. Commun.*, 2015, **6**, 6645.
 - 178 E. Robinson, J. P. M. Nunes, V. Vassileva, A. Maruani, J. C. F. Nogueira, M. E. B. Smith, R. B. Pedley, S. Caddick, J. R. Baker and V. Chudasama, *RSC Adv.*, 2017, **7**, 9073–9077.
 - 179 S. Shao, M.-H. Tsai, J. Lu, T. Yu, J. Jin, D. Xiao, H. Jiang, M. Han, M. Wang and J. Wang, *Bioorg. Med. Chem. Lett.*, 2018, **28**, 1363–1370.
 - 180 F. Bryden, J. M. M. Rodrigues, H. Savoie, V. Chudasama, A. Beeby, M. H. Y. Cheng, R. W. Boyle and A. Maruani, *Bioconjug. Chem.*, 2017, **29**, 176–181.
 - 181 A. N. Marquard, J. C. T. Carlson and R. Weissleder, *Bioconjug. Chem.*, 2020, **31**, 1616–1623.
 - 182 O. Koniev, I. Dovgan, B. Renoux, A. Ekhkirch, J. Eberova, S. Cianférani, S. Kolodych, S. Papot and A. Wagner, *Med. Chem. Commun.*, 2018, **9**, 827–830.
 - 183 S. J. Walsh, S. Omarjee, W. R. J. D. Galloway, T. T. L. Kwan, H. F. Sore, J. S. Parker, M. Hyvönen, J. S. Carroll and D. R. Spring, *Chem. Sci.*, 2019, **10**, 694–700.
 - 184 S. J. Walsh, J. Iegre, H. Seki, J. D. Bargh, H. F. Sore, J. S. Parker, J. S. Carroll and D. R. Spring, *Org. Biomol. Chem.*, 2020, **18**, 4224–4230.
 - 185 A. J. Counsell, S. J. Walsh, N. S. Robertson, H. Sore and D. R. Spring, *Org. Biomol. Chem.*, 2020, **18**, 4739–4743.
 - 186 C. E. Stieger, L. Franz, F. Körlin and C. P. R. Hackenberger, *Angew. Chemie - Int. Ed.*, 2021, **60**, 15359–15364.
 - 187 Q.-Y. Hu and H. Imase, *Methods for making conjugates from disulfide-containing proteins*, *Inter Pat Appl WO2014/083505*, 2014.
 - 188 M. T. W. Lee, A. Maruani, D. A. Richards, J. R. Baker, S. Caddick and V. Chudasama, *Chem. Sci.*, 2017, **8**, 2056–2060.
 - 189 Q.-Y. Hu and M. Allan, *Method for making conjugates from disulfide-containing proteins*, *Pat Appl US2019/0381126*, 2019.
 - 190 J. B. White, R. Fleming, L. Masterson, B. T. Ruddell, H. Zhong, C. Fazenbaker, P. Strout, K. Rosenthal, M. Reed, V. Muniz-Medina, P. Howard, R. Dixit, H. Wu, M. J. Hinrichs, C. Gao and N. Dimasi, *MAbs*, 2019, **11**, 500–515.
 - 191 M. T. W. Lee, A. Maruani, J. R. Baker, S. Caddick and V. Chudasama, *Chem. Sci.*, 2016, **7**, 799–802.
 - 192 C. Bahou, D. A. Richards, A. Maruani, E. A. Love, F. Javaid, S. Caddick, J. R. Baker and V. Chudasama, *Org. Biomol. Chem.*, 2018, **16**, 1359–1366.
 - 193 E. O. Sapphire, P. W. H. I. Parren, R. Pantophlet, M. B. Zwick, G. M. Morris, P. M. Rudd, R. A.

- Dwek, R. L. Stanfield, D. R. Burton and I. A. Wilson, *Science*, 2001, **293**, 1155–1159.
- 194 B. J. Reizman and K. F. Jensen, *Org. Process Res. Dev.*, 2012, **16**, 1770–1782.
- 195 S. A. Weissman and N. G. Anderson, *Org. Process Res. Dev.*, 2015, **19**, 1605–1633.
- 196 P. M. Murray, F. Bellany, L. Benhamou, D. K. Bučar, A. B. Tabor and T. D. Sheppard, *Org. Biomol. Chem.*, 2016, **14**, 2373–2384.
- 197 C. J. Taylor, H. Seki, F. M. Dannheim, M. J. Willis, G. Clemens, B. A. Taylor, T. W. Chamberlain and R. A. Bourne, *React. Chem. Eng.*, 2021, **6**, 1404–1411.
- 198 M. Pittelkow, R. Lewinsky and J. B. Christensen, *Synthesis*, 2002, **15**, 2195–2202.
- 199 A. Markiv, R. Beatson, J. Burchell, R. V. Durvasula and A. S. Kang, *BMC Biotechnol.*, 2011, **11**, 117.
- 200 S. Y. Mao and J. M. Mullins, *Methods Mol. Biol.*, 2010, **588**, 43–48.
- 201 D. Wang, S. He, X. Wang, Y. Yan, J. Liu, S. Wu, S. Liu, Y. Lei, M. Chen, L. Li, J. Zhang, L. Zhang, X. Hu, X. Zheng, J. Bai, Y. Zhang, Y. Zhang, M. Song and Y. Tang, *Nat. Biomed. Eng.*, 2020, **4**, 1150–1158.
- 202 J. E. Sykes and B. B. Chomel, in *Canine and Feline Infectious Diseases*, Elsevier Inc., 2013, pp. 132–140.
- 203 L. N. Goswami, Q. Cai, L. Ma, S. S. Jalisatgi and M. F. Hawthorne, *Org. Biomol. Chem.*, 2015, **13**, 8912–8918.
- 204 M. E. B. Smith, M. B. Caspersen, E. Robinson, M. Morais, A. Maruani, J. P. M. Nunes, K. Nicholls, M. J. Saxton, S. Caddick, J. R. Baker and V. Chudasama, *Org. Biomol. Chem.*, 2015, **13**, 7946–7949.
- 205 N. Forte, M. Livanos, E. Miranda, M. Morais, X. Yang, V. S. Rajkumar, K. A. Chester, V. Chudasama and J. R. Baker, *Bioconjug. Chem.*, 2018, **29**, 486–492.
- 206 A. S. Rosenberg, *AAPS J.*, 2006, **8**, E501–E507.
- 207 A. Goyon, L. Sciascera, A. Clarke, D. Guillarme and R. Pell, *J. Chromatogr. A*, 2018, **1539**, 19–29.
- 208 D. L. Holliday and V. Speirs, *Breast Cancer Res.*, 2011, **13**, 215.
- 209 O. Hernandez-Alba, A. Ehkirch, A. Beck and S. Cianféroni, in *Methods in Molecular Biology*, Humana Press Inc., 2020, vol. 2078, pp. 197–211.
- 210 R. Fleming, in *Methods in Molecular Biology*, Humana Press Inc., 2020, vol. 2078, pp. 147–161.
- 211 A. Cusumano, D. Guillarme, A. Beck and S. Fekete, *J. Pharm. Biomed. Anal.*, 2016, **121**, 161–173.
- 212 J. Ouyang, *Methods Mol. Biol.*, 2013, **1045**, 275–283.
- 213 J. A. Queiroz, C. T. Tomaz and J. M. S. Cabral, *J. Biotechnol.*, 2001, **87**, 143–159.
- 214 R. P. Lyon, T. D. Bovee, S. O. Doronina, P. J. Burke, J. H. Hunter, H. D. Neff-Laford, M. Jonas, M. E. Anderson, J. R. Setter and P. D. Senter, *Nat. Biotechnol.*, 2015, **33**, 733–735.
- 215 J. Charoenpattarapreeda, S. J. Walsh, J. S. Carroll and D. R. Spring, *Angew. Chemie Int. Ed.*,

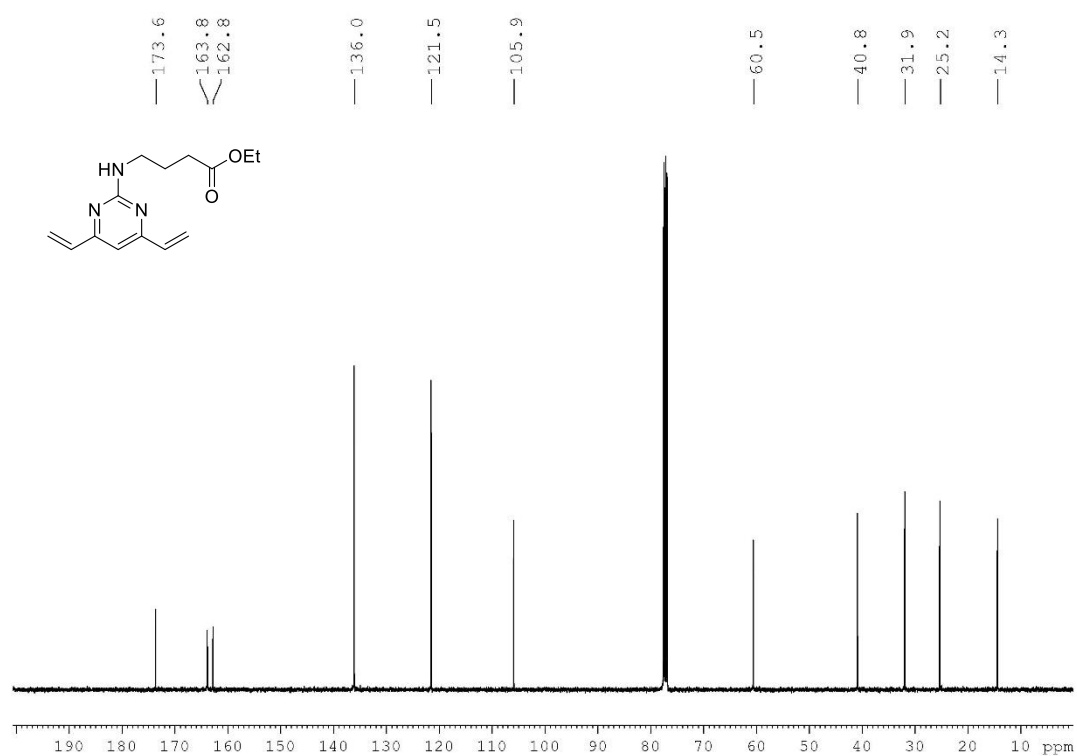
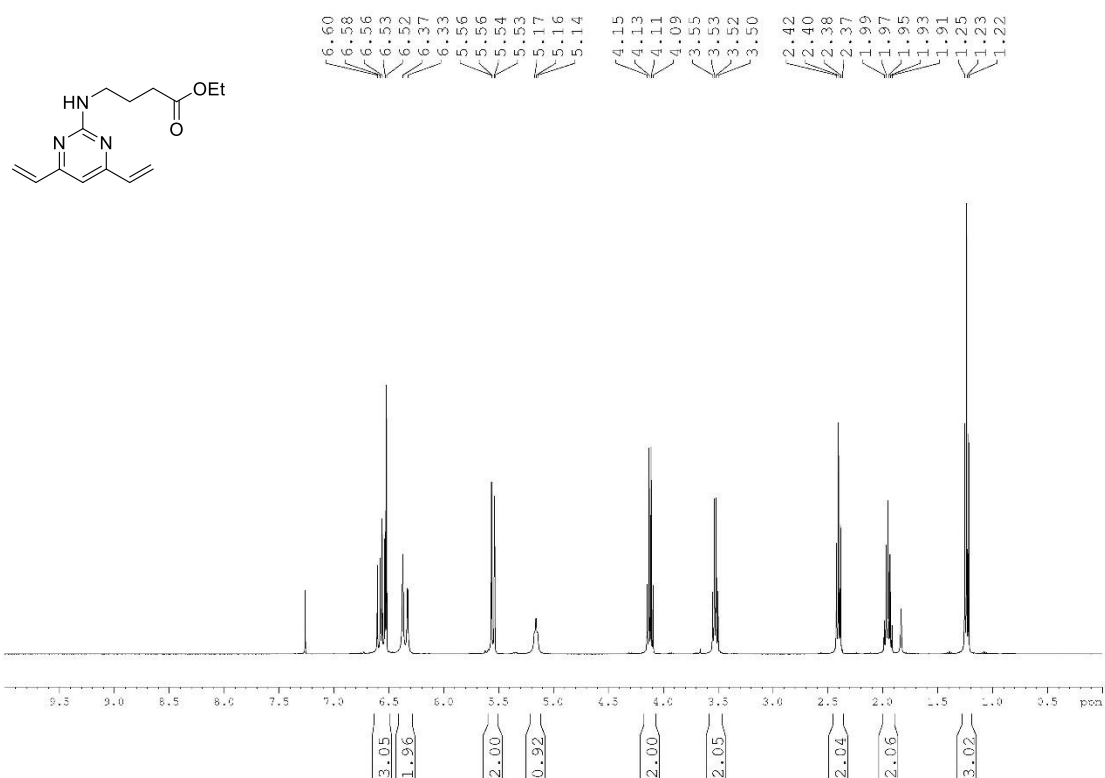
- 2020, **59**, 23045–23050.
- 216 P. W. Howard, Z. Chen, S. J. Gregson, L. A. Masterson, A. C. Tiberghien, N. Cooper, M. Fang, M. J. Coffils, S. Klee, J. A. Hartley and D. E. Thurston, *Bioorganic Med. Chem. Lett.*, 2009, **19**, 6463–6466.
 - 217 F. Bryden, C. Martin, S. Letast, E. Lles, I. Viéitez-Villemin, A. Rousseau, C. Colas, M. Brachet-Botineau, E. Allard-Vannier, C. Larbouret, M. C. Viaud-Massuard and N. Joubert, *Org. Biomol. Chem.*, 2018, **16**, 1882–1889.
 - 218 D. M. Goldenberg and R. M. Sharkey, *MAbs*, 2019, **11**, 987–995.
 - 219 Y. Yao, L. Yu, X. Su, Y. Wang, W. Li, Y. Wu, X. Cheng, H. Zhang, X. Wei, H. Chen, R. Zhang, L. Gou, X. Chen, Y. Xie, B. Zhang, Y. Zhang, J. Yang and Y. Wei, *J. Control. Release*, 2015, **220**, 5–17.
 - 220 T. M. Cardillo, S. V. Govindan, R. M. Sharkey, P. Trisal and D. M. Goldenberg, *Clin. Cancer Res.*, 2011, **17**, 3157–3169.
 - 221 R. H. J. Mathijssen, R. J. van Alphen, J. Verweij, W. J. Loos, K. Nooter, G. Stoter and A. Sparreboom, *Clin. Cancer Res.*, 2001, **7**, 2182–94.
 - 222 H. Zhao, C. Lee, P. Sai, Y. H. Choe, M. Boro, A. Pendri, S. Guan and R. B. Greenwald, *J. Org. Chem.*, 2000, **65**, 4601–4606.
 - 223 N. J. Agard, J. A. Prescher and C. R. Bertozzi, *J. Am. Chem. Soc.*, 2004, **126**, 15046–15047.
 - 224 B. L. Oliveira, Z. Guo and G. J. L. Bernardes, *Chem. Soc. Rev.*, 2017, **46**, 4895–4950.
 - 225 C. T. Orozco, M. J. Edgeworth, P. W. A Devine, A. R. Hines, O. Cornwell, X. Wang, J. J. Phillips, P. Ravn, S. E. Jackson and N. J. Bond, *bioRxiv*, 2020, 2020.09.28.317339. This article is a preprint and has not been certified by peer review.
 - 226 R. E. Kontermann, *Curr. Opin. Biotechnol.*, 2011, **22**, 868–876.
 - 227 M. Cavaco, M. A. R. B. Castanho and V. Neves, *Pept. Sci.*, 2018, **110**, e23095.
 - 228 J. Torchia, K. Weiskopf and R. Levy, *Proc. Natl. Acad. Sci. U. S. A.*, 2016, **113**, 5376–5381.
 - 229 S. Hirasawa, Y. Kitahara, Y. Okamatsu, T. Fujii, A. Nakayama, S. Ueno, C. Ijichi, F. Futaki, K. Nakata and M. Taki, *Bioconjug. Chem.*, 2019, **30**, 2323–2331.
 - 230 A. Jaakkonen, G. Volkmann and H. Iwai, *Int. J. Mol. Sci.*, 2020, **21**, 4011.
 - 231 R. J. Gubeli, S. Sonzini, A. Podmore, P. Ravn, O. A. Scherman and C. F. Van Der Walle, *Chem. Commun.*, 2016, **52**, 4235–4238.
 - 232 A. Makino, E. Hara, I. Hara, E. Ozeki and S. Kimura, *Langmuir*, 2014, **30**, 669–674.
 - 233 C. G. Collins, J. M. Baumes and B. D. Smith, *Chem. Commun.*, 2011, **47**, 12352–12354.
 - 234 B. G. Pasupuleti, K. Khongsti, B. Das and G. Bez, *Eur. J. Med. Chem.*, 2020, **186**, 111908.
 - 235 V. Bala, S. Rao, P. Li, S. Wang and C. A. Prestidge, *Mol. Pharm.*, 2016, **13**, 287–294.

Appendix A – NMR spectra

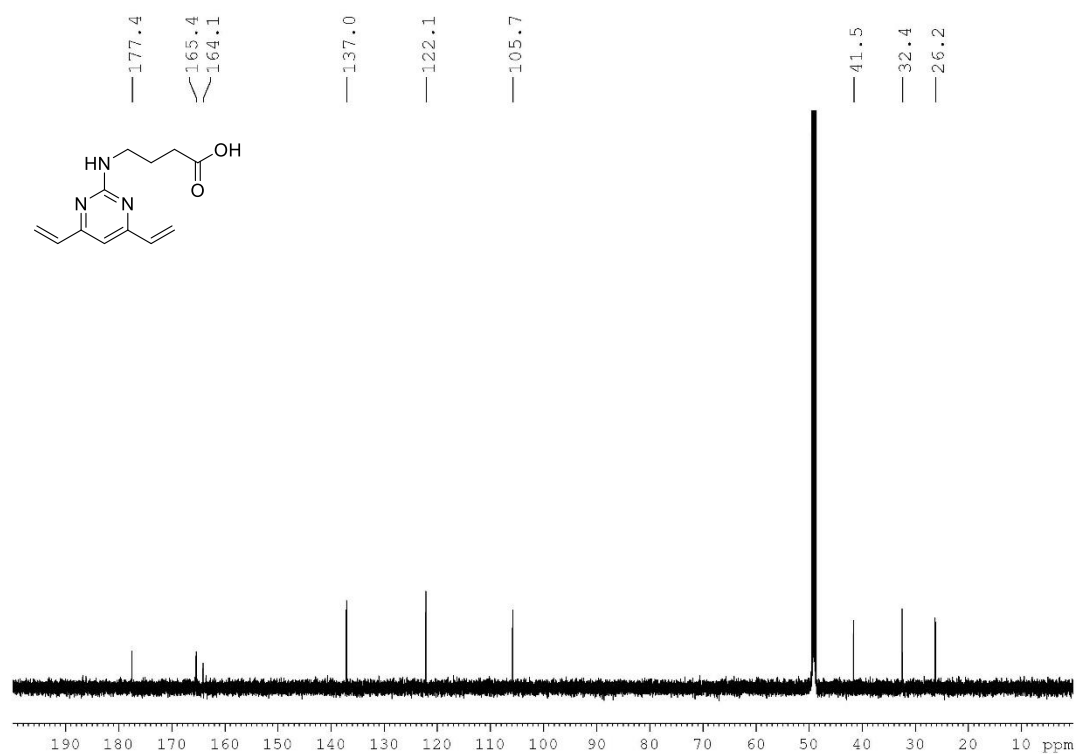
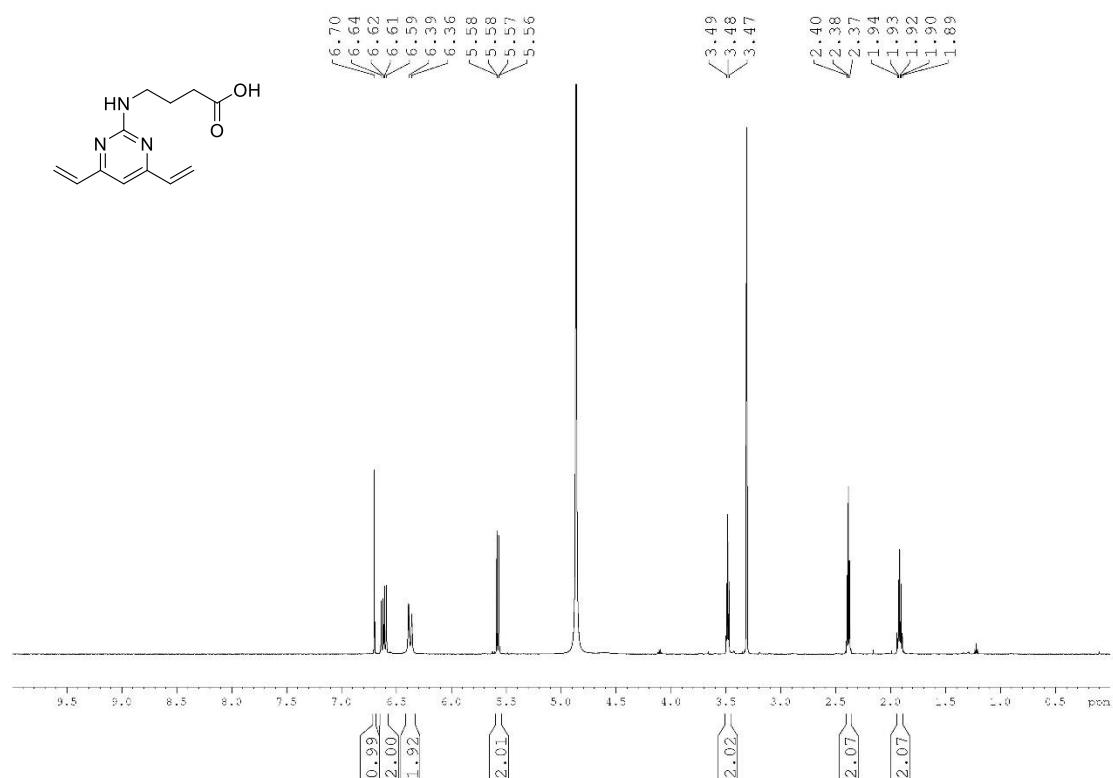
Ethyl 4-((4,6-dichloropyrimidin-2-yl)amino)butanoate (1)



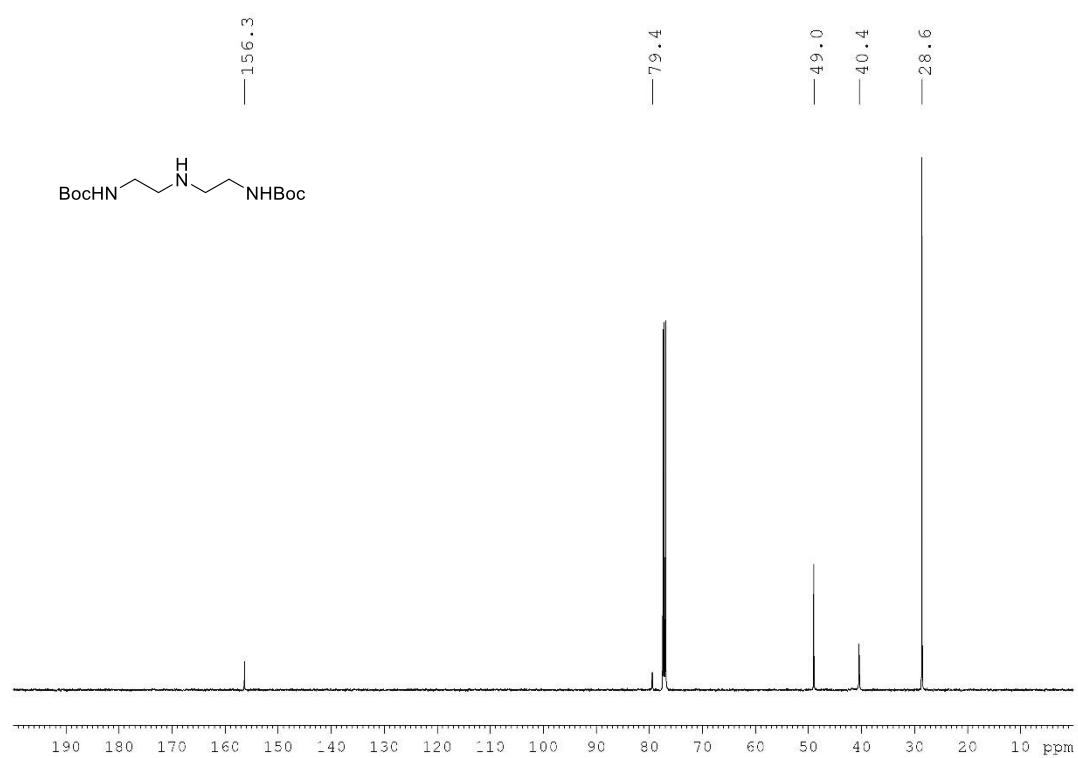
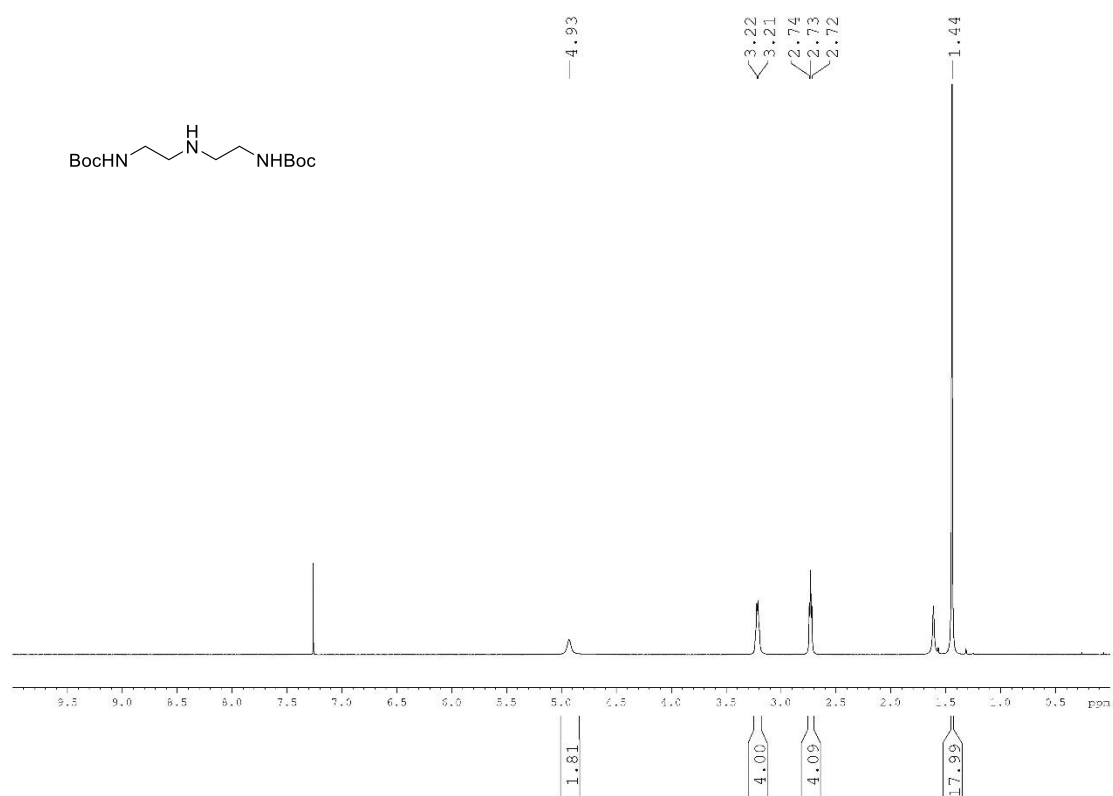
Ethyl 4-((4,6-divinylpyrimidin-2-yl)amino)butanoate (3)



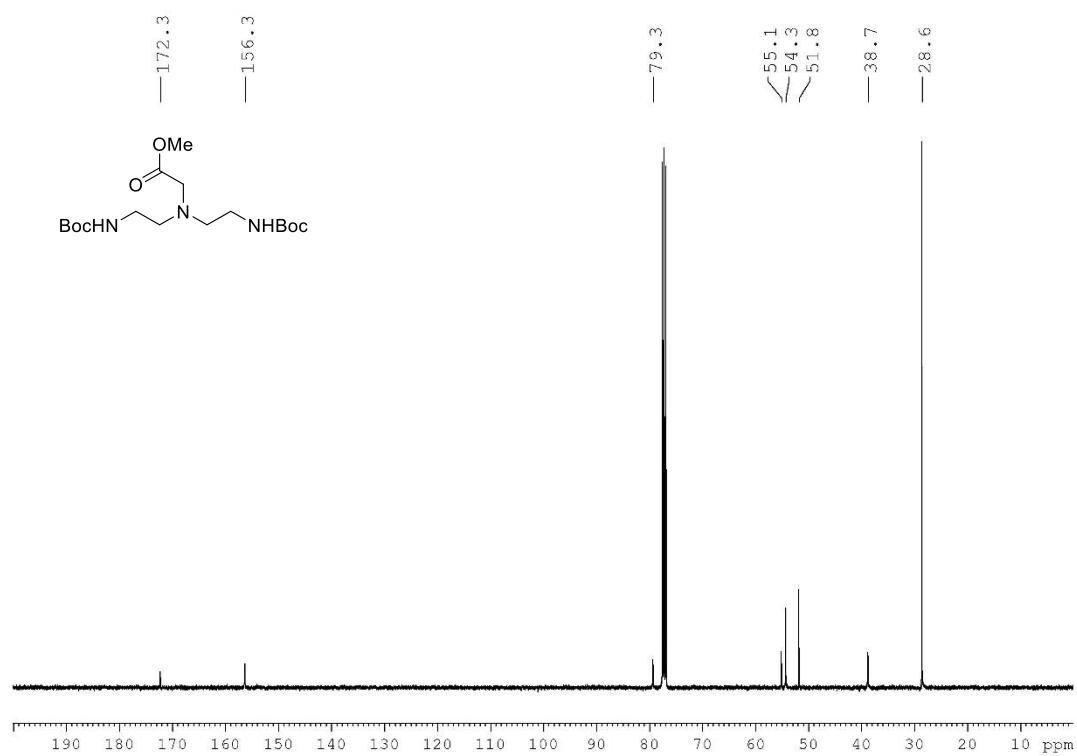
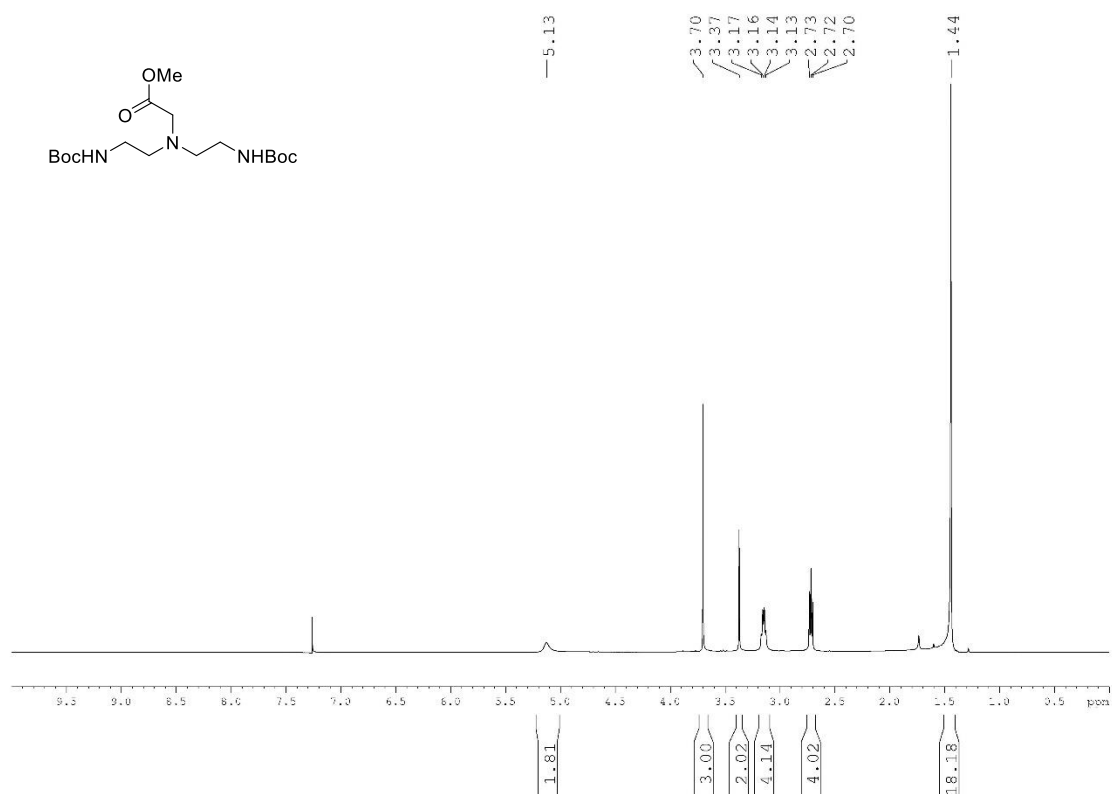
4-((4,6-divinylpyrimidin-2-yl)amino)butanoic acid (4)



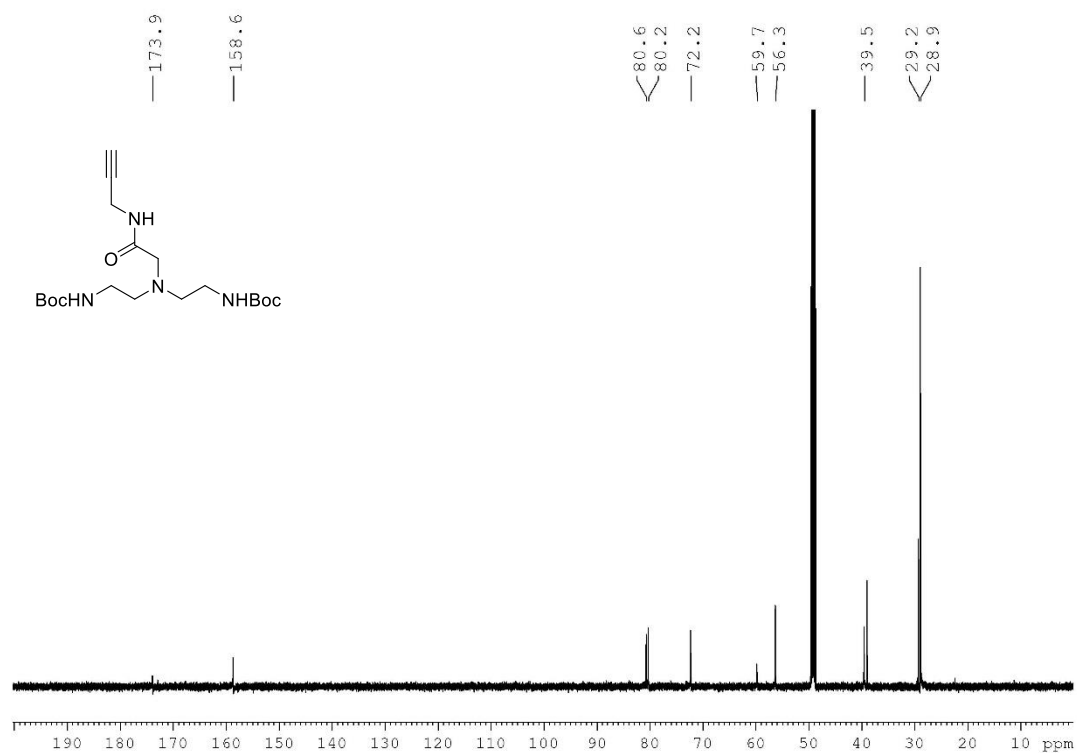
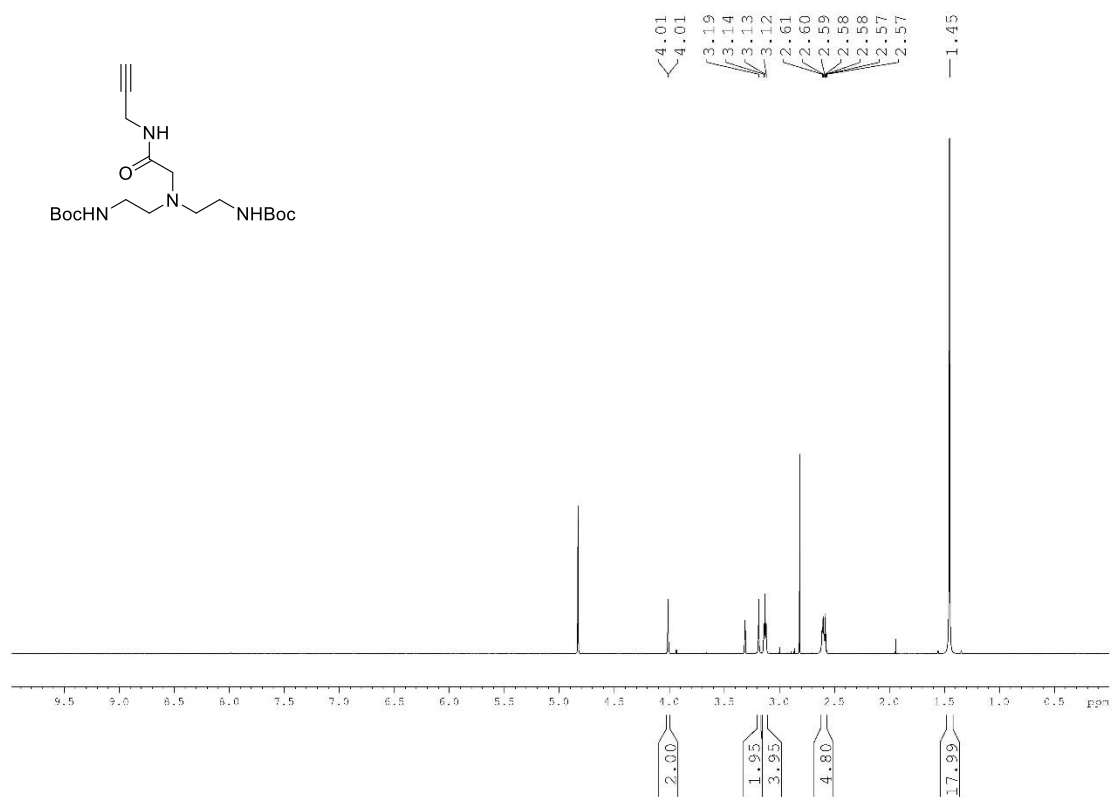
Di-*tert*-butyl (azanediylbis(ethane-2,1-diyl))dicarbamate (5)



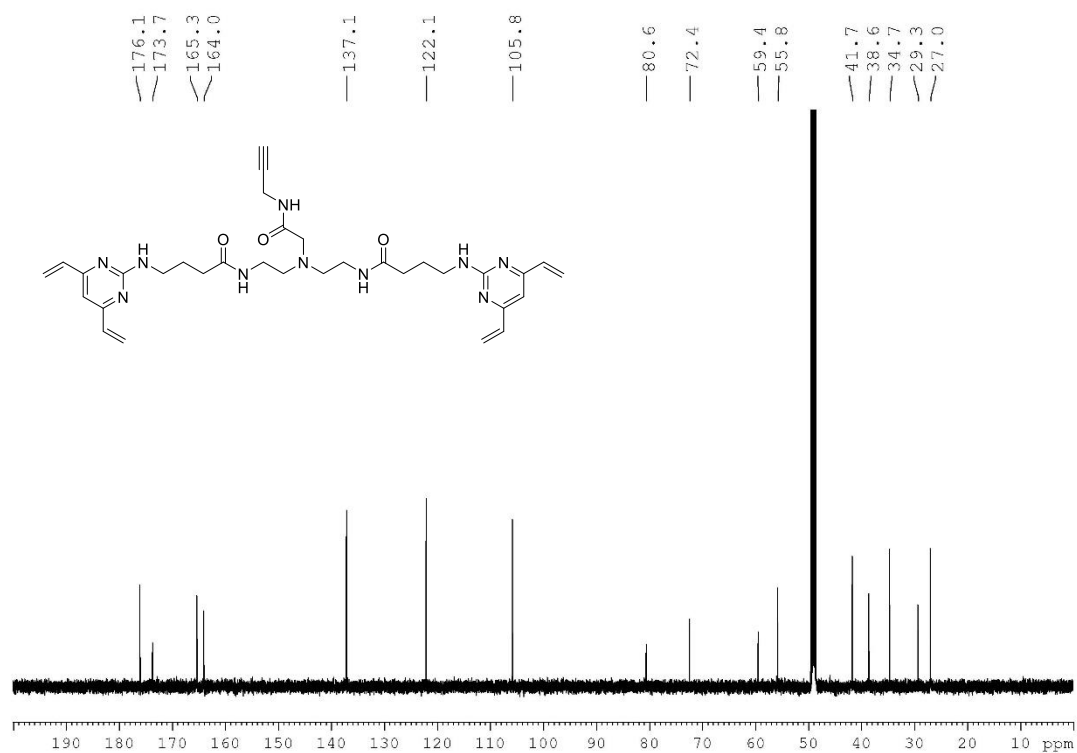
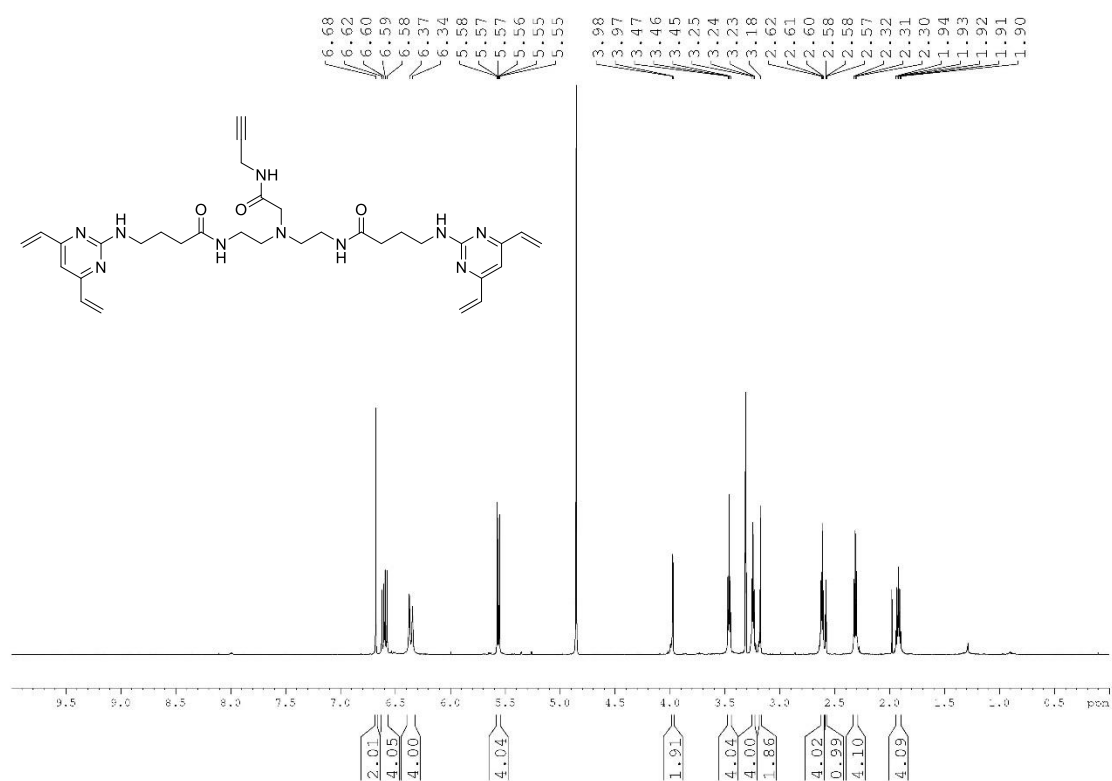
Methyl bis(2-((*tert*-butoxycarbonyl)amino)ethyl)glycinate (6)



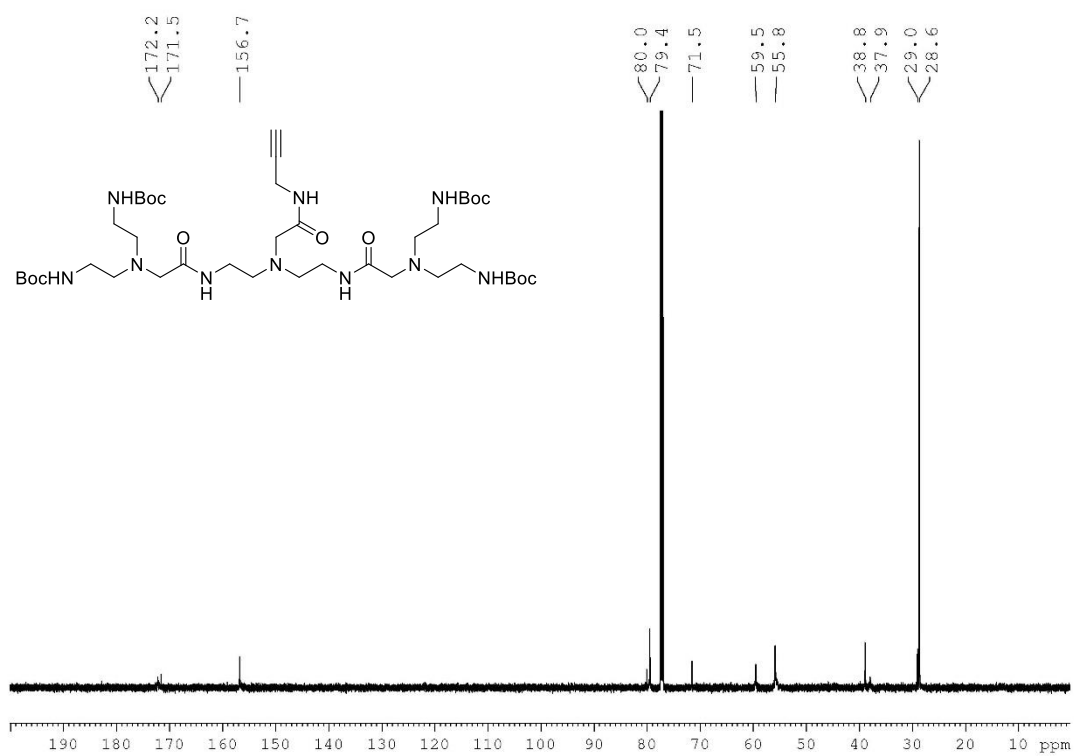
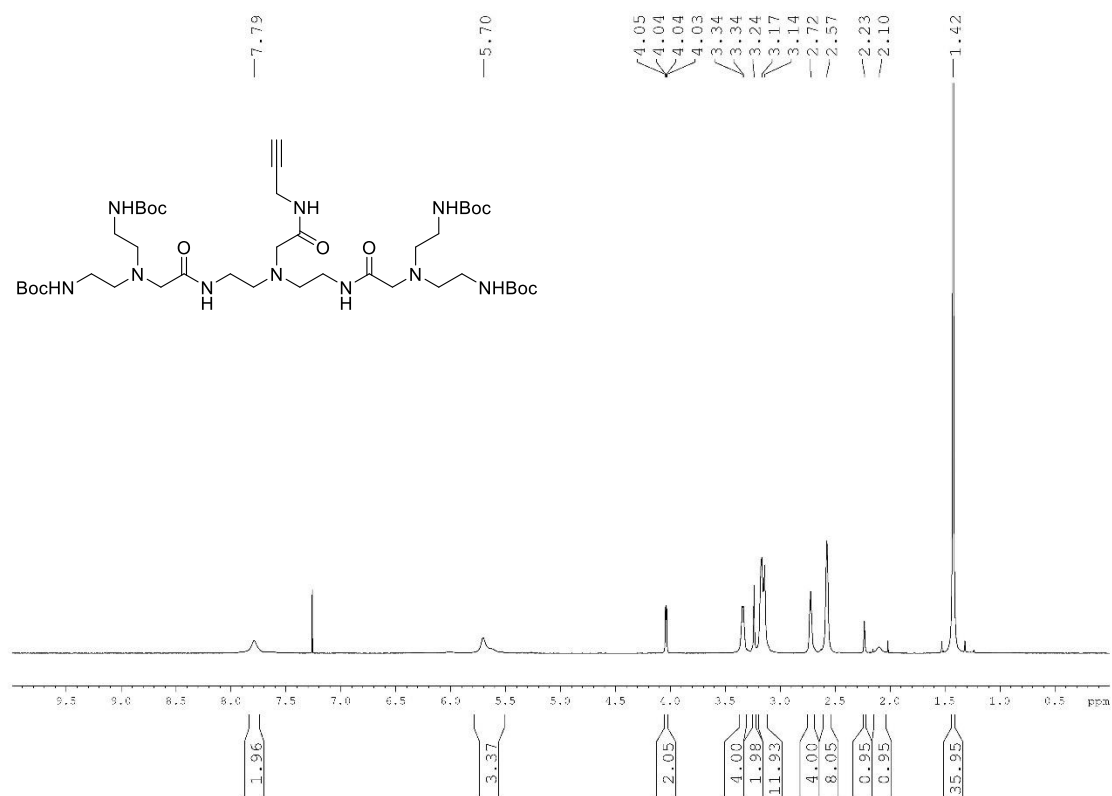
Di-*tert*-butyl (((2-oxo-2-(prop-2-yn-1-ylamino)ethyl)azanediyl)bis(ethane-2,1-diyl))dicarbamate (8)



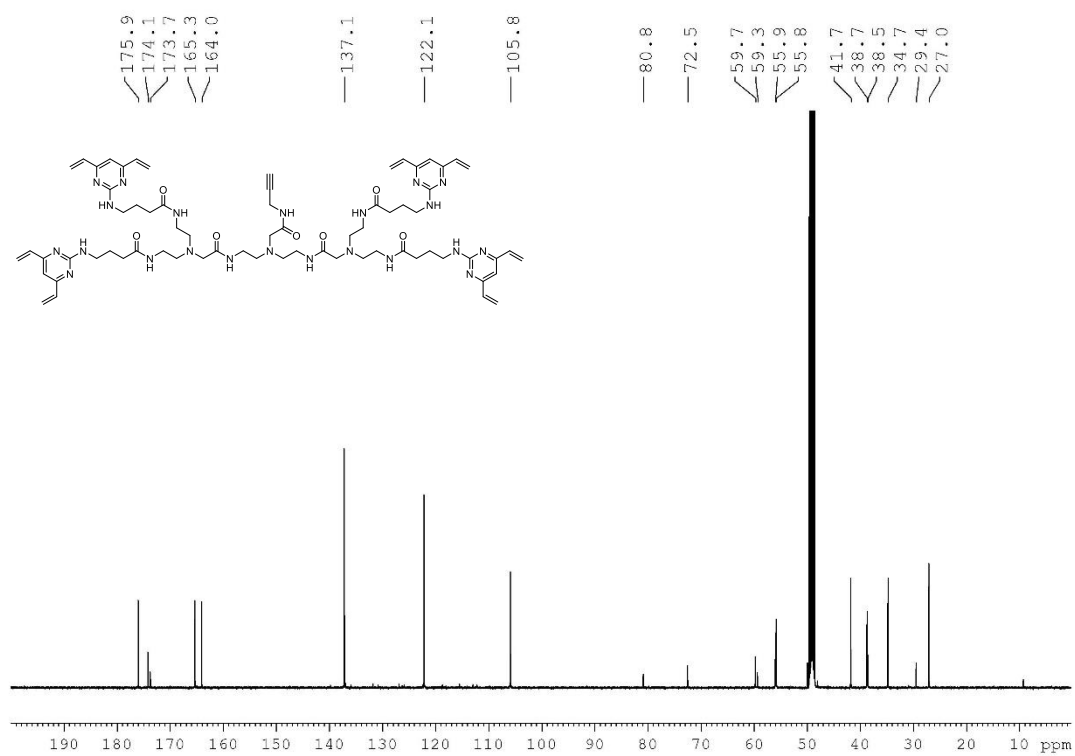
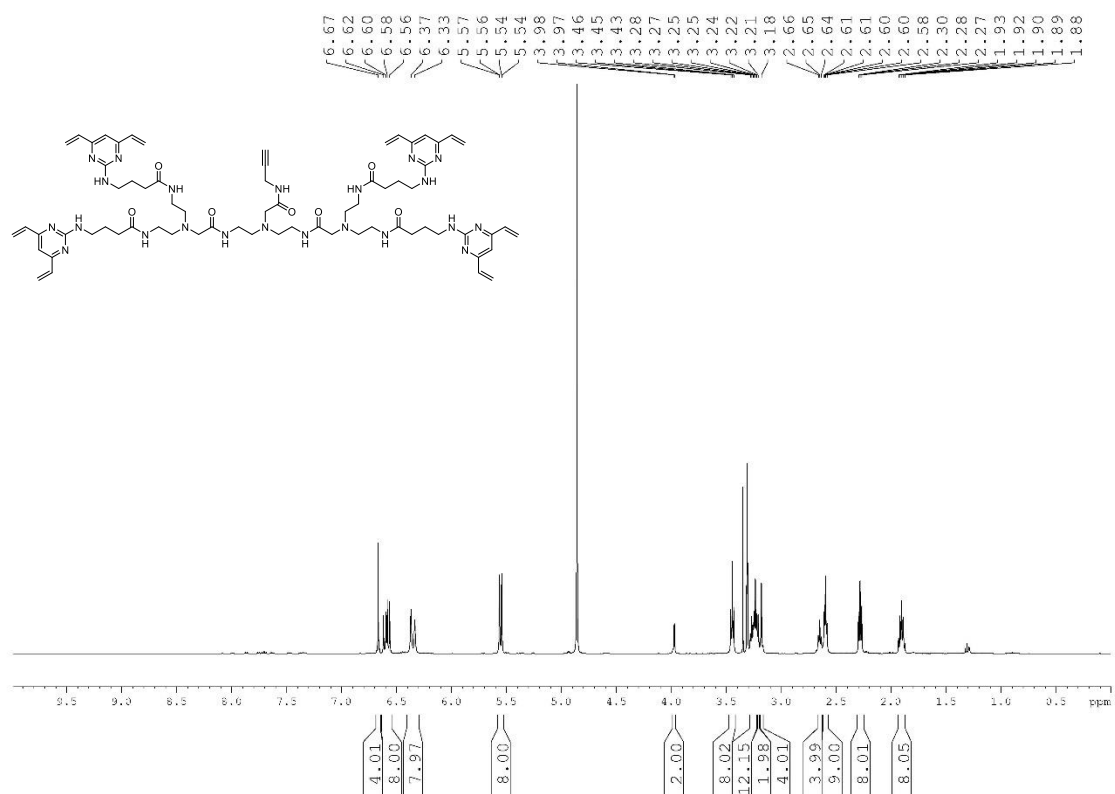
***N,N'*-(((2-oxo-2-(prop-2-yn-1-ylamino)ethyl)azanediyl)bis(ethane-2,1-diyl))bis(4-((4,6-divinylpyrimidin-2-yl)amino)butanamide) (10)**



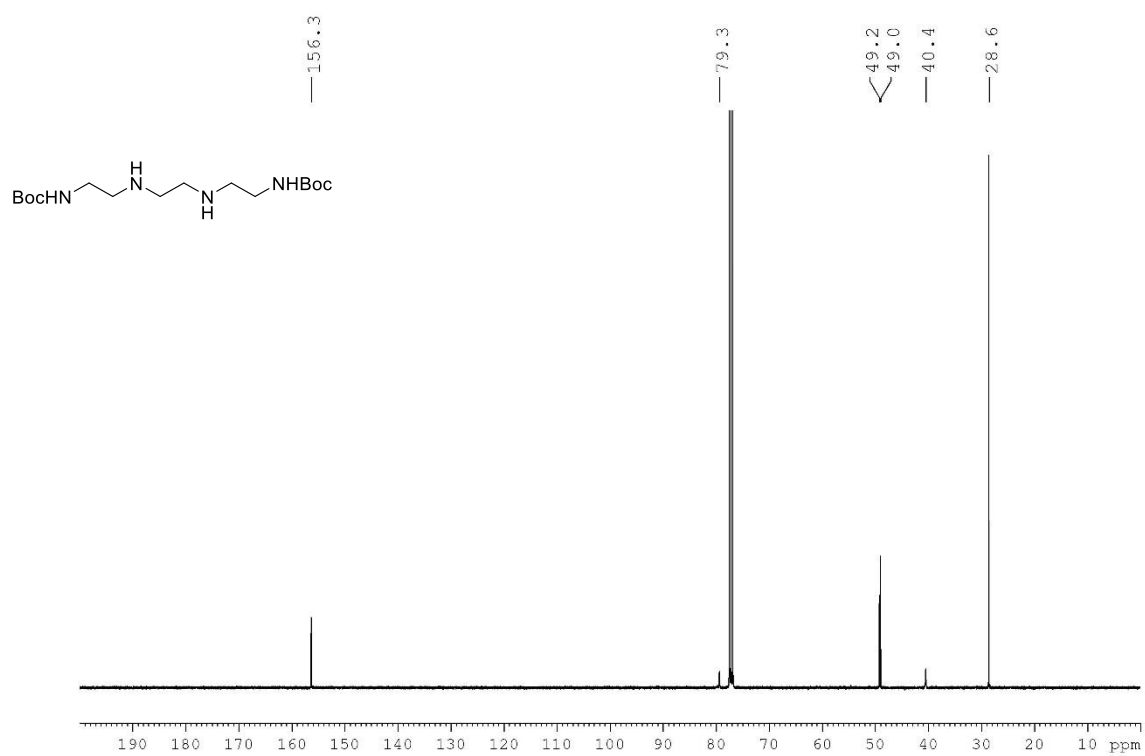
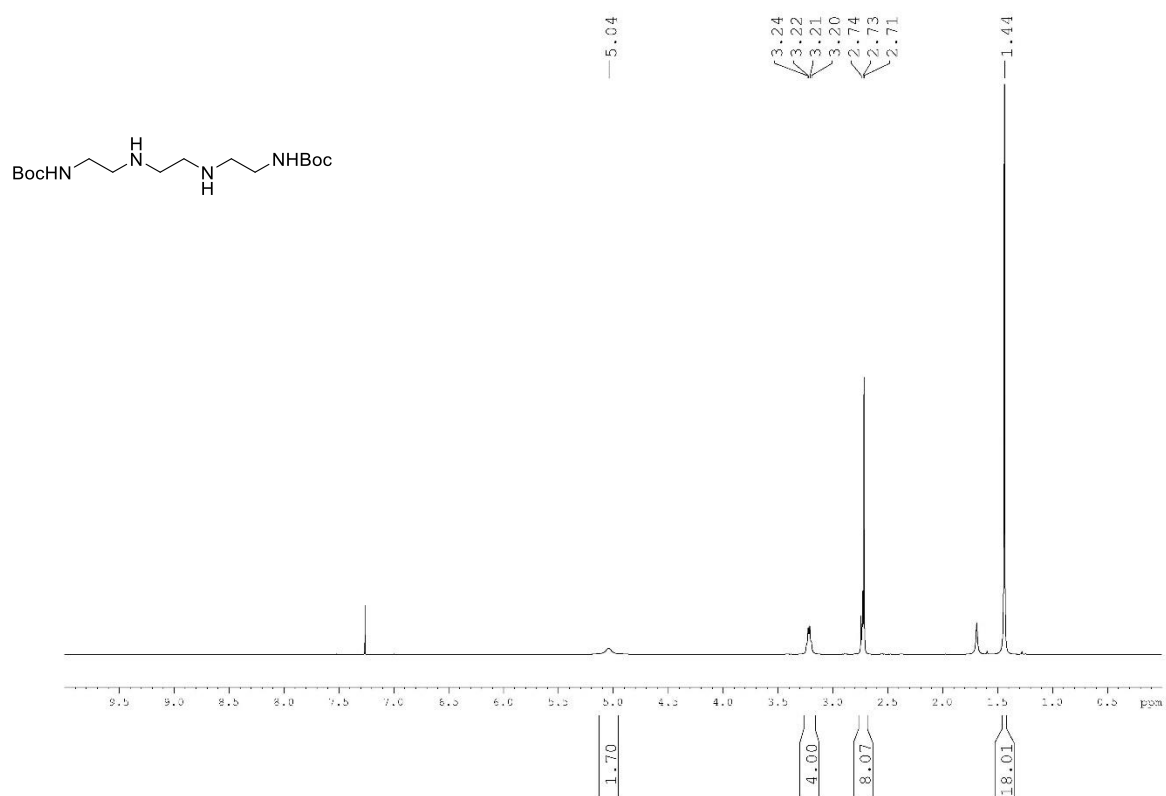
Tetra-*N*-Boc-amine backbone, (alkyne)₁ (14)



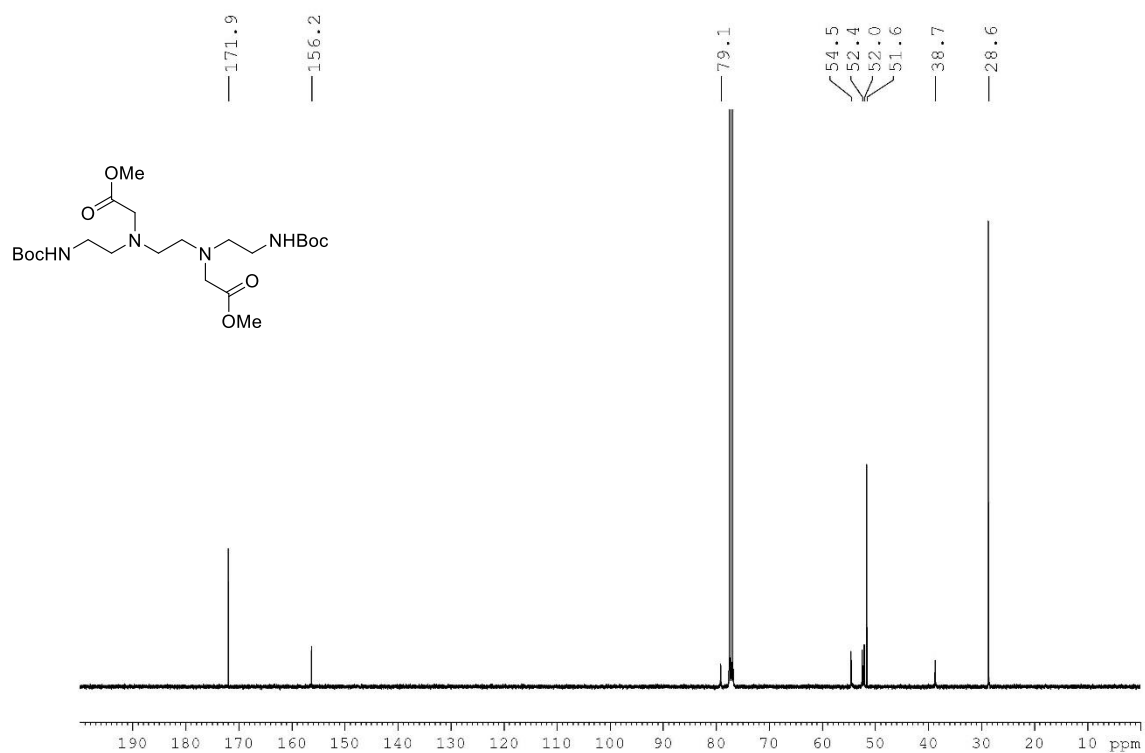
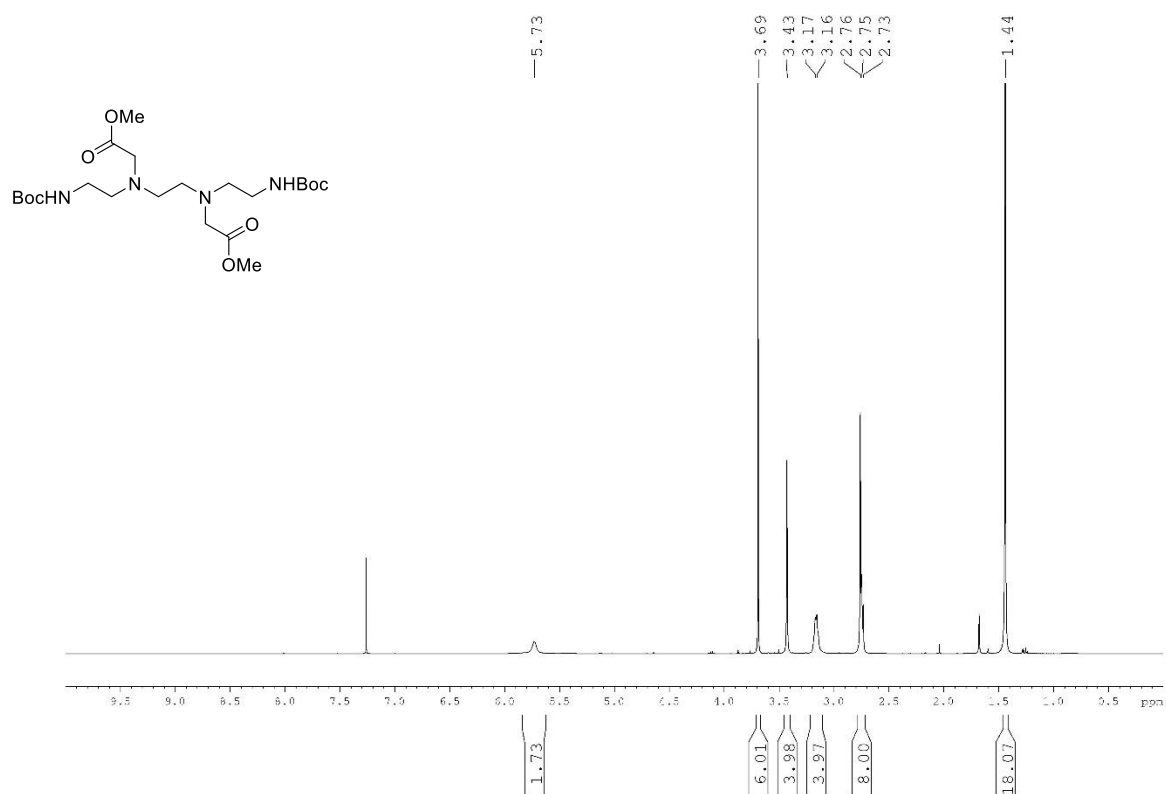
TetraDVP-alkyne₁ (15)



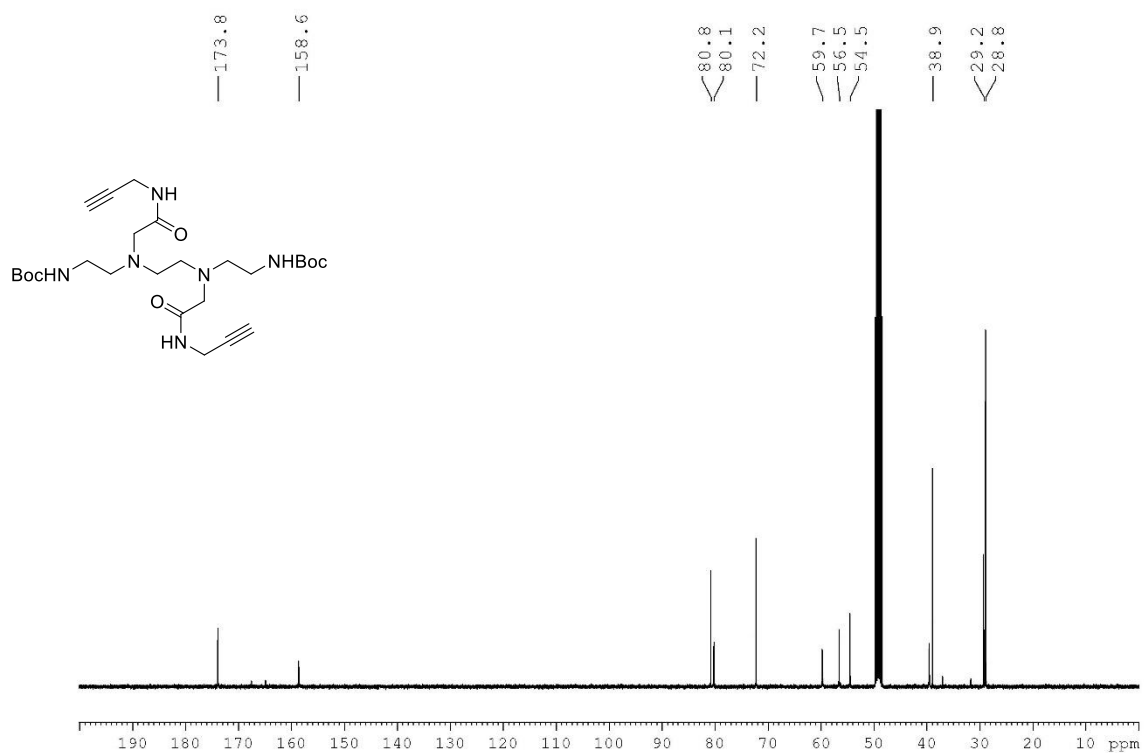
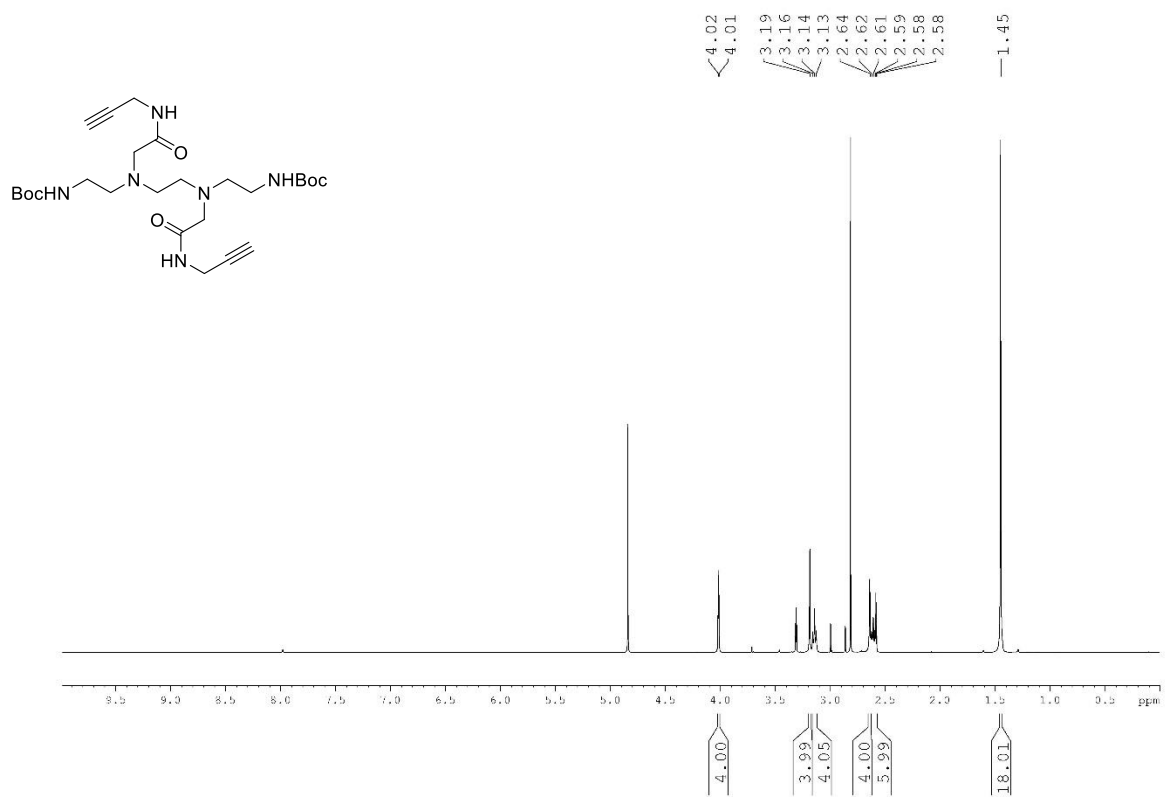
Di-*tert*-butyl ((ethane-1,2-diylbis(azanediy))bis(ethane-2,1-diyl))dicarbamate (16)



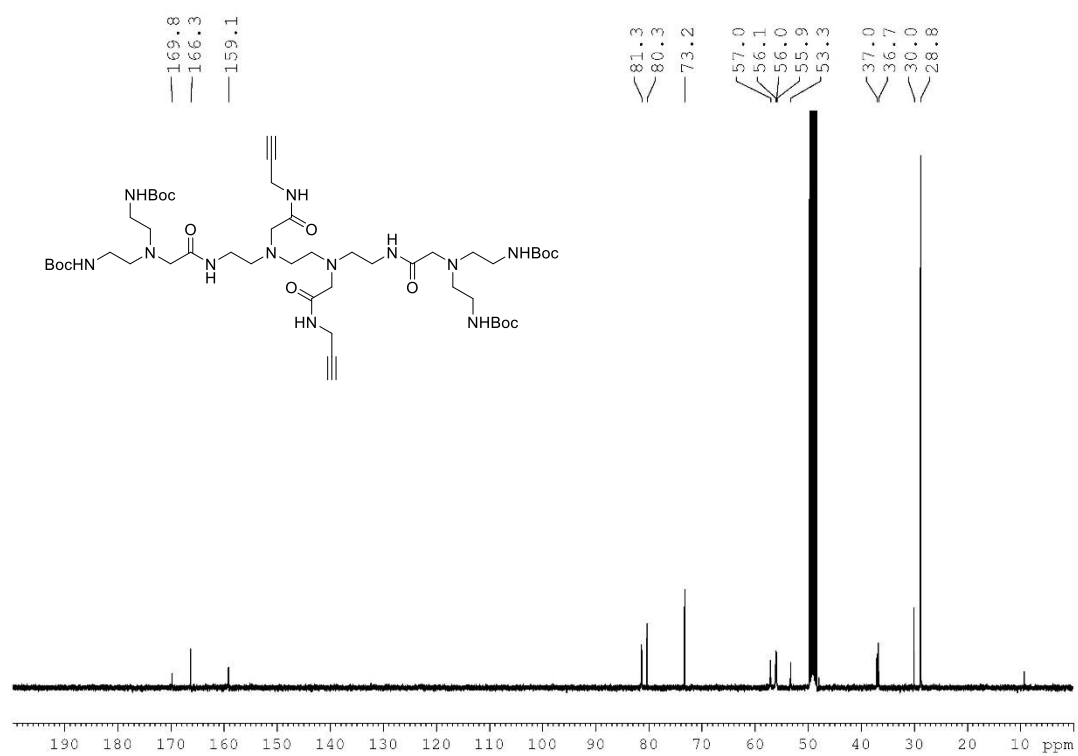
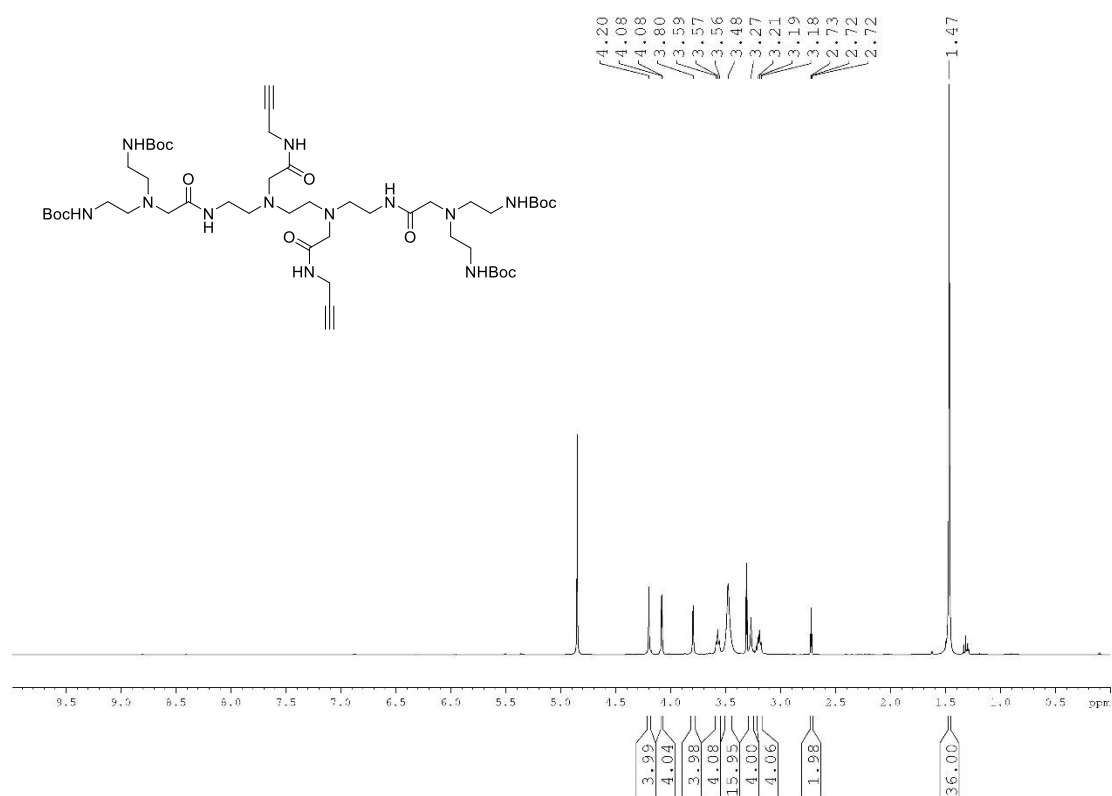
Methyl 11-(2-((*tert*-butoxycarbonyl)amino)ethyl)-8-(2-methoxy-2-oxoethyl)-2,2-dimethyl-4-oxo-3-oxa-5,8,11-triazatridecan-13-oate (17)



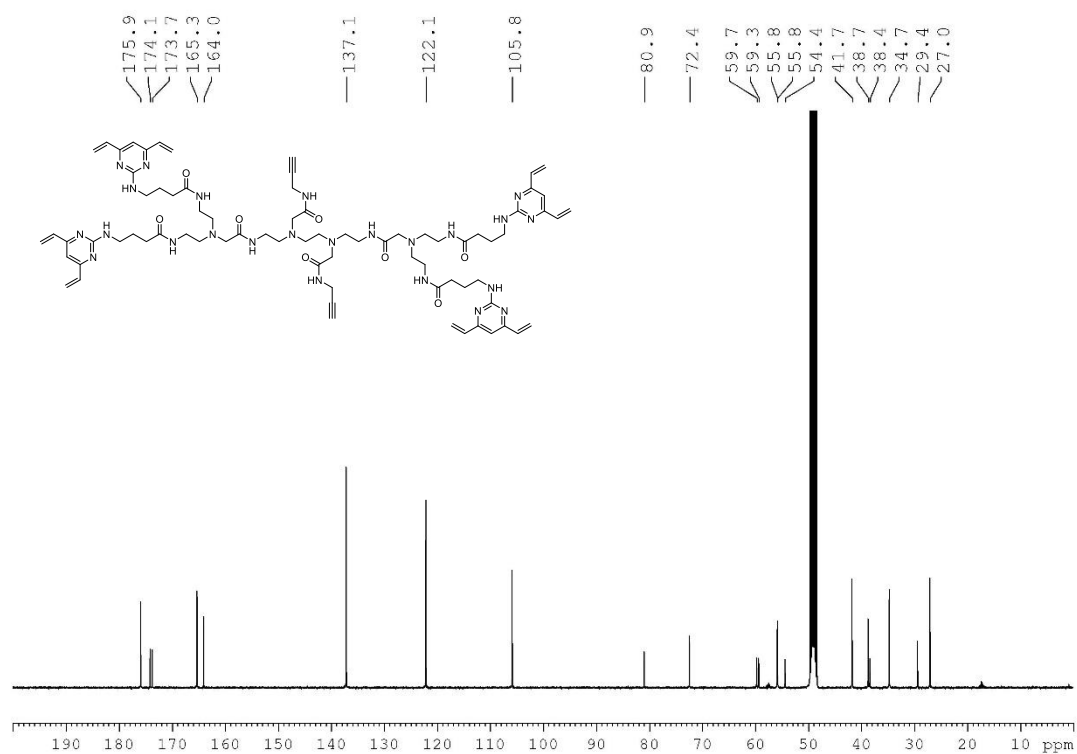
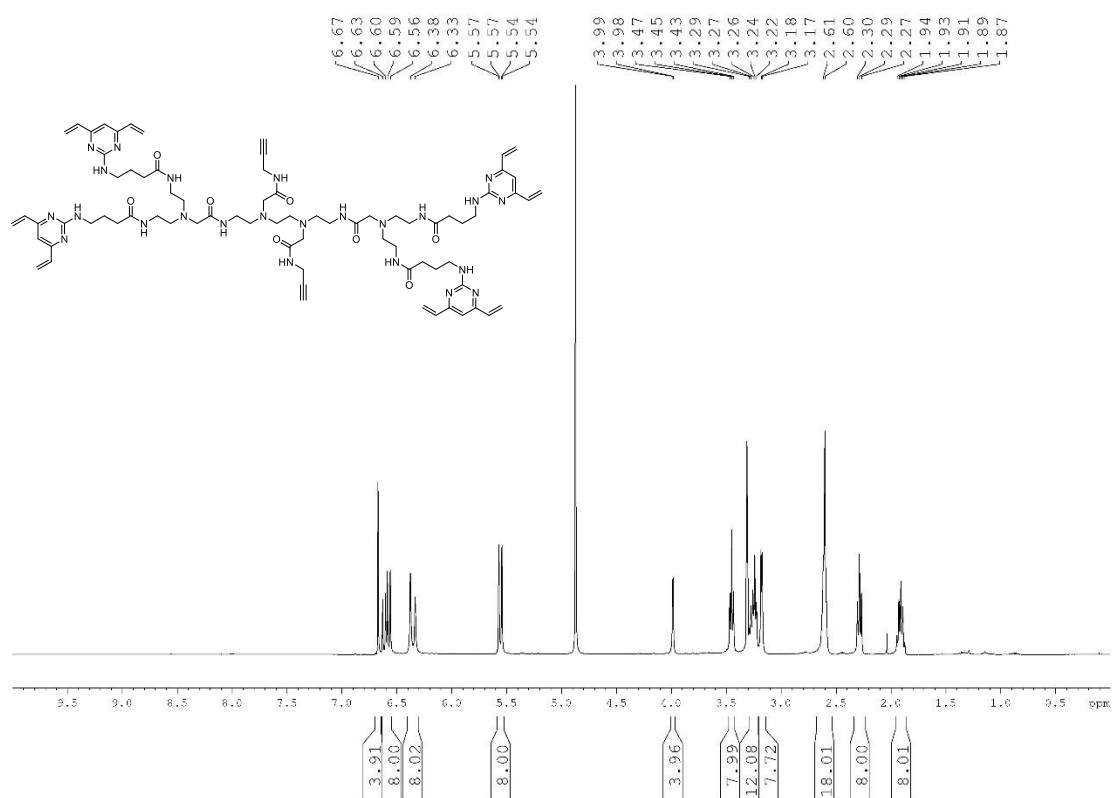
Di-*tert*-butyl ((5,12-dioxo-4,7,10,13-tetraazahexadeca-1,15-diyne-7,10-diyl)bis(ethane-2,1-diyl))dicarbamate (19)



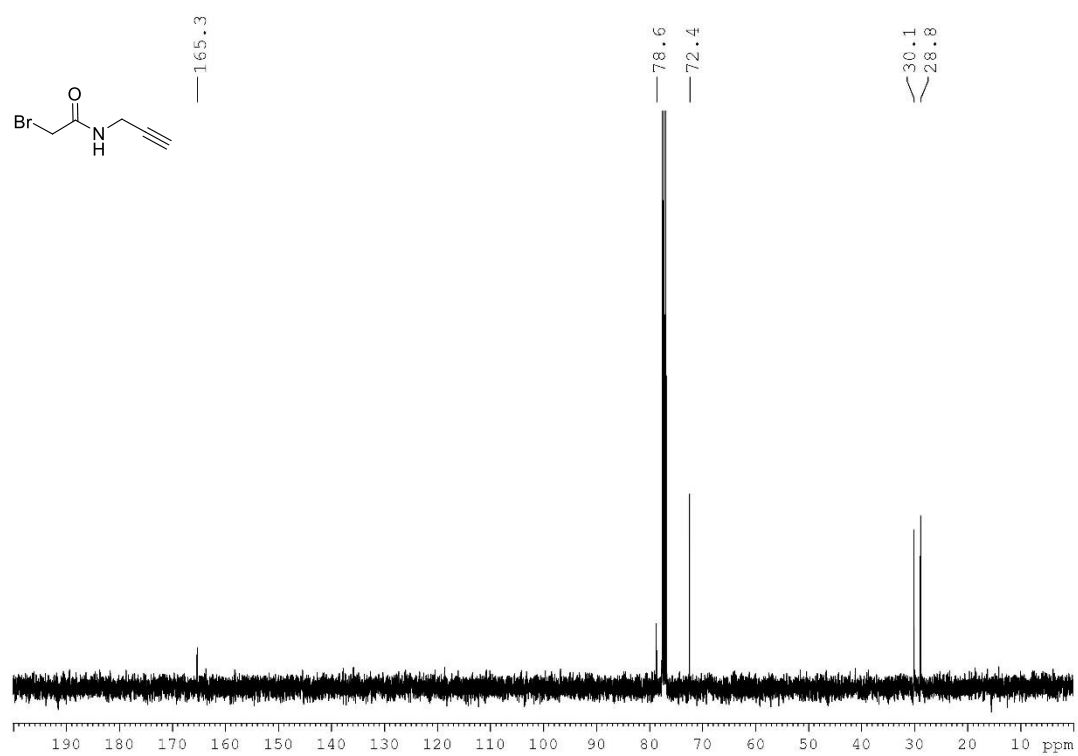
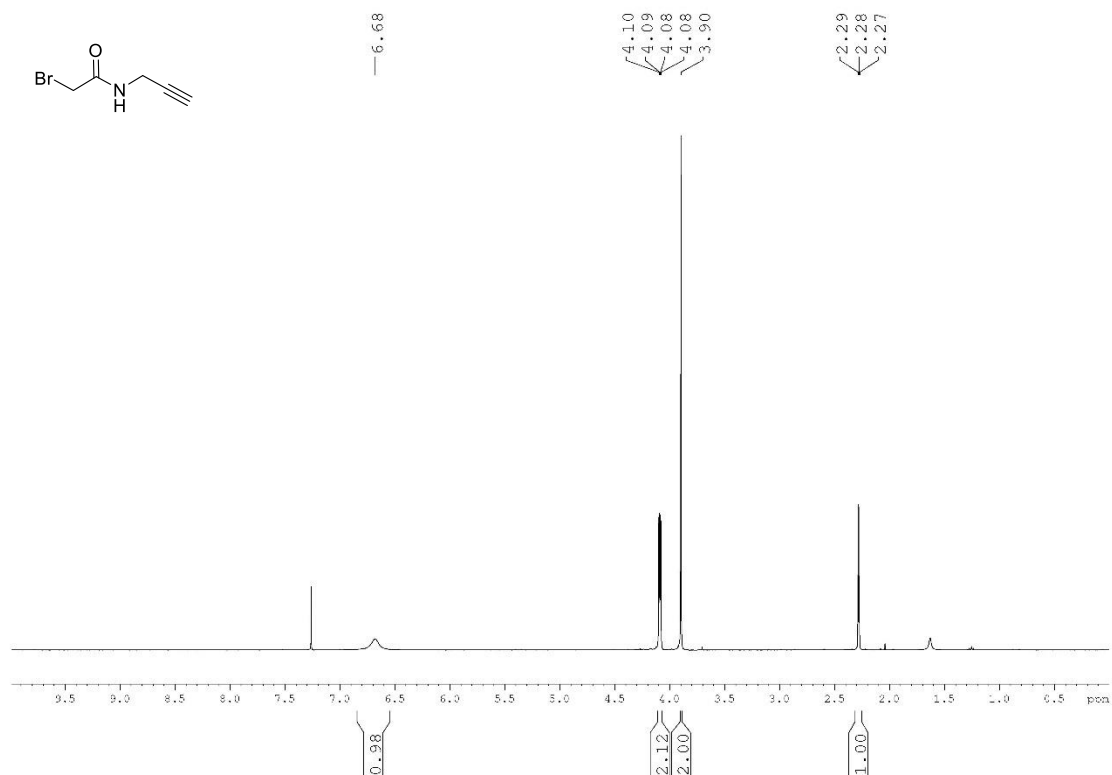
Tetra-*N*-Boc-amine backbone, (alkyne)₂ (20)



TetraDVP-alkyne₂ (21)



2-bromo-N-(prop-2-yn-1-yl)acetamide (23)



Chemical structure of the compound is shown above the spectrum. The structure is a linear peptide derivative with BocHN- and -NHBoc protecting groups. The spectrum displays peaks corresponding to the structure, with chemical shifts (ppm) and integrations (area) labeled above and below the peaks, respectively.

Chemical shifts (ppm) labeled above the spectrum:

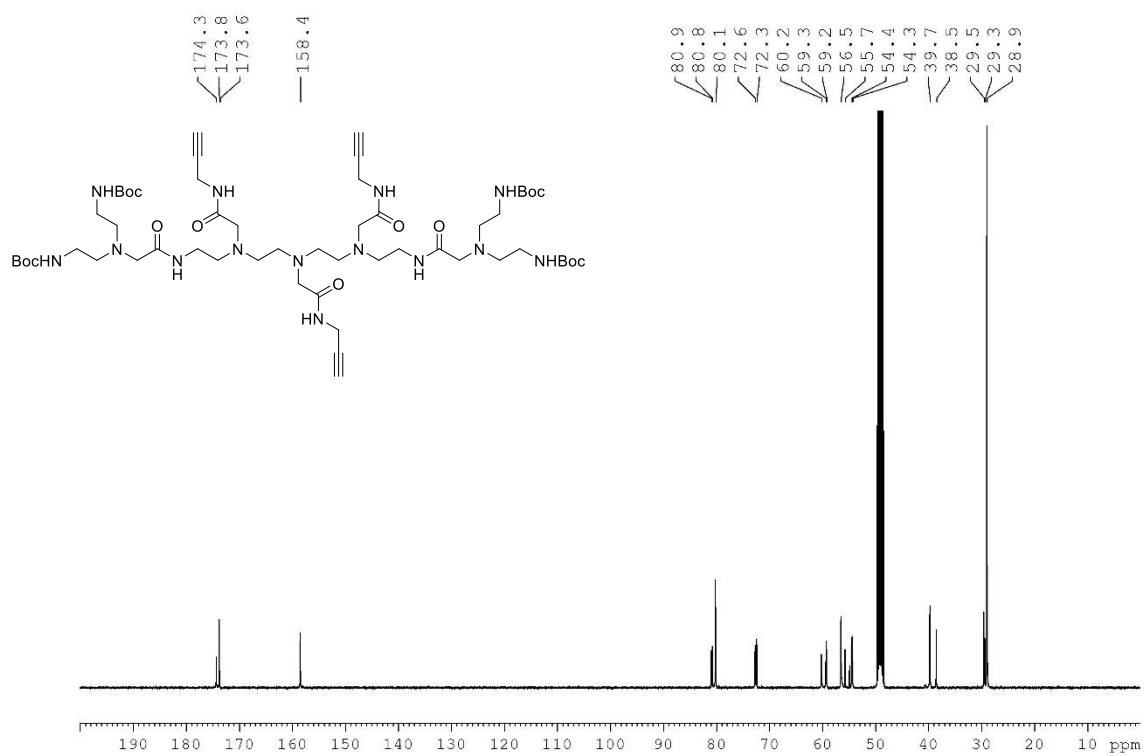
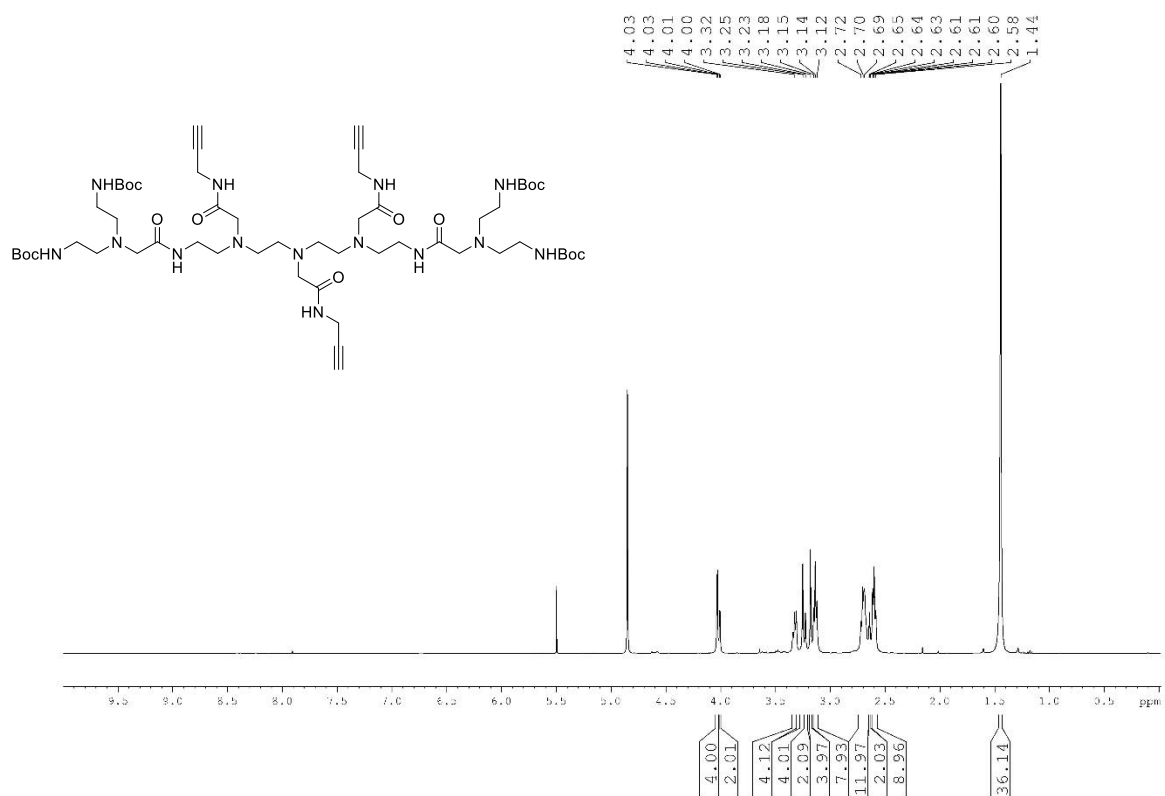
- 7.63
- 6.21
- 3.35
- 3.11
- 3.06
- 2.77
- 2.70
- 2.56
- 1.40

Integrations (area) labeled below the spectrum:

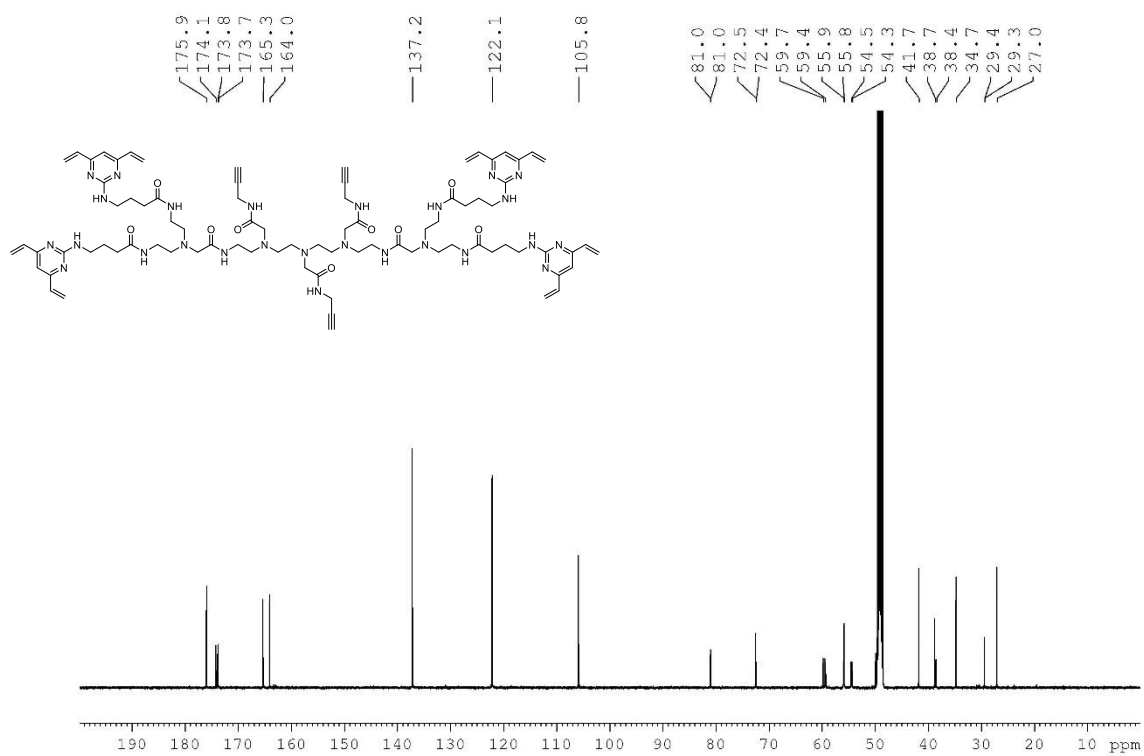
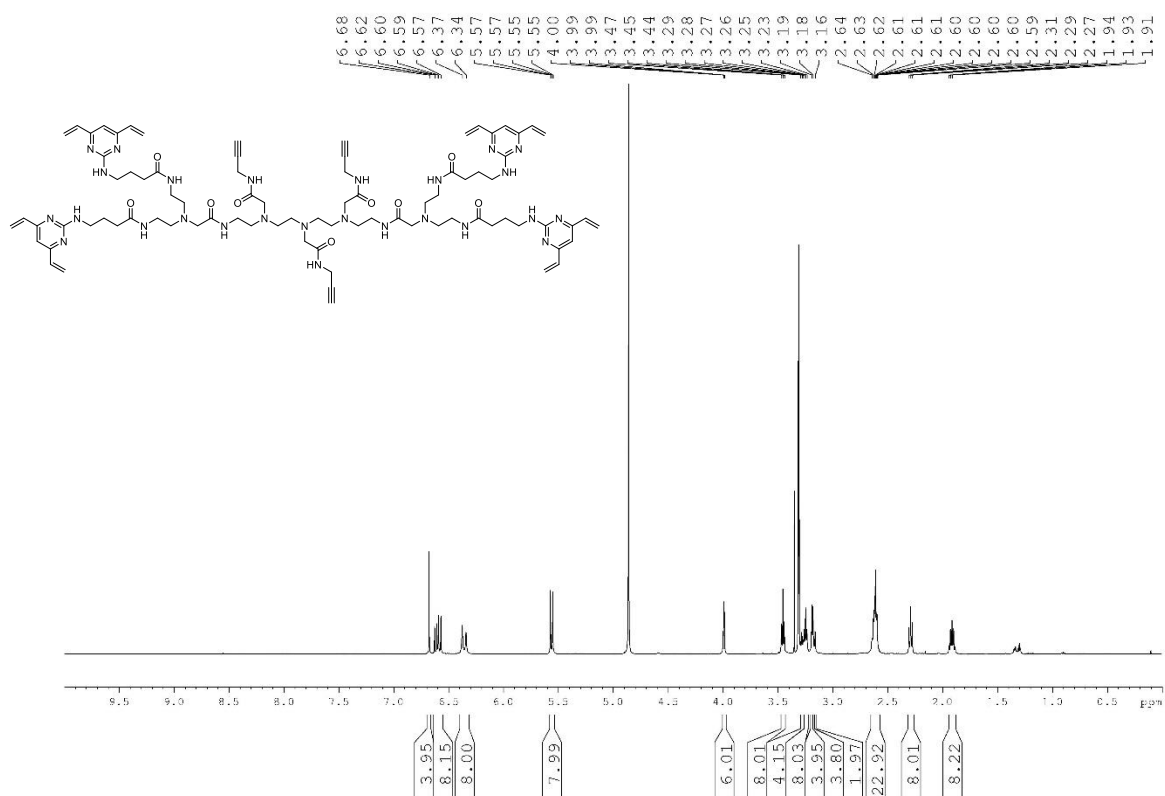
- 0.74
- 1.74
- 4.03
- 12.00
- 11.68
- 8.02
- 36.40



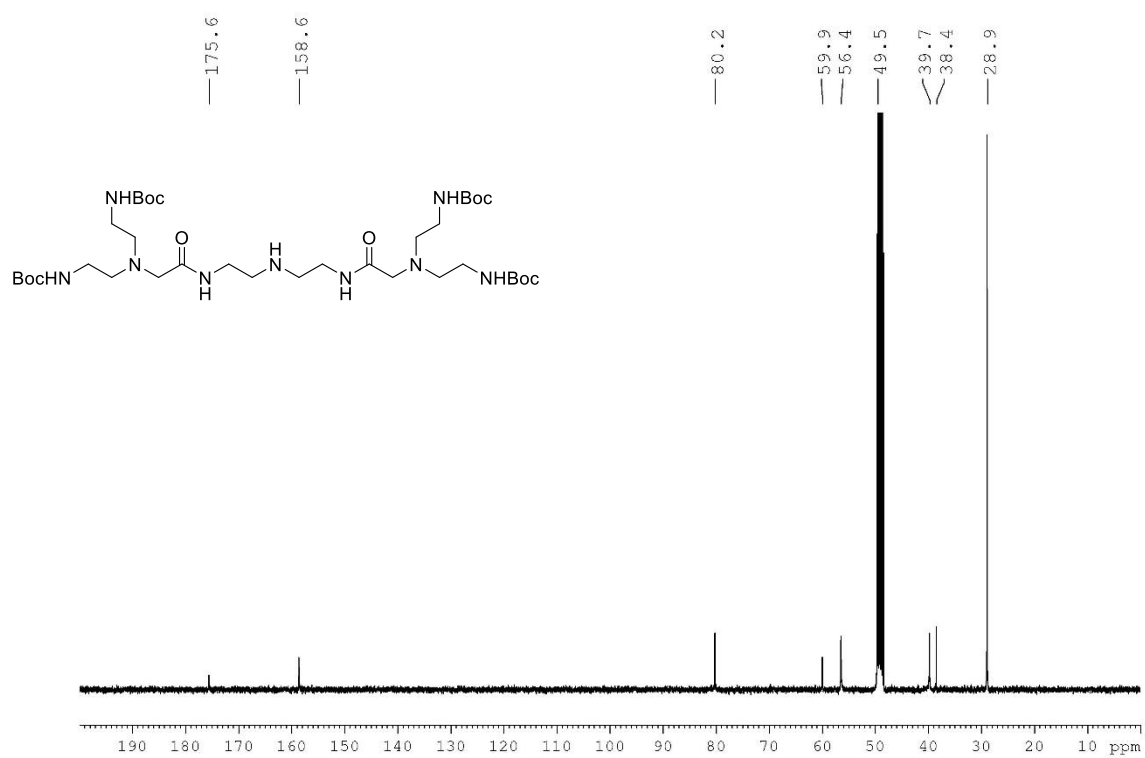
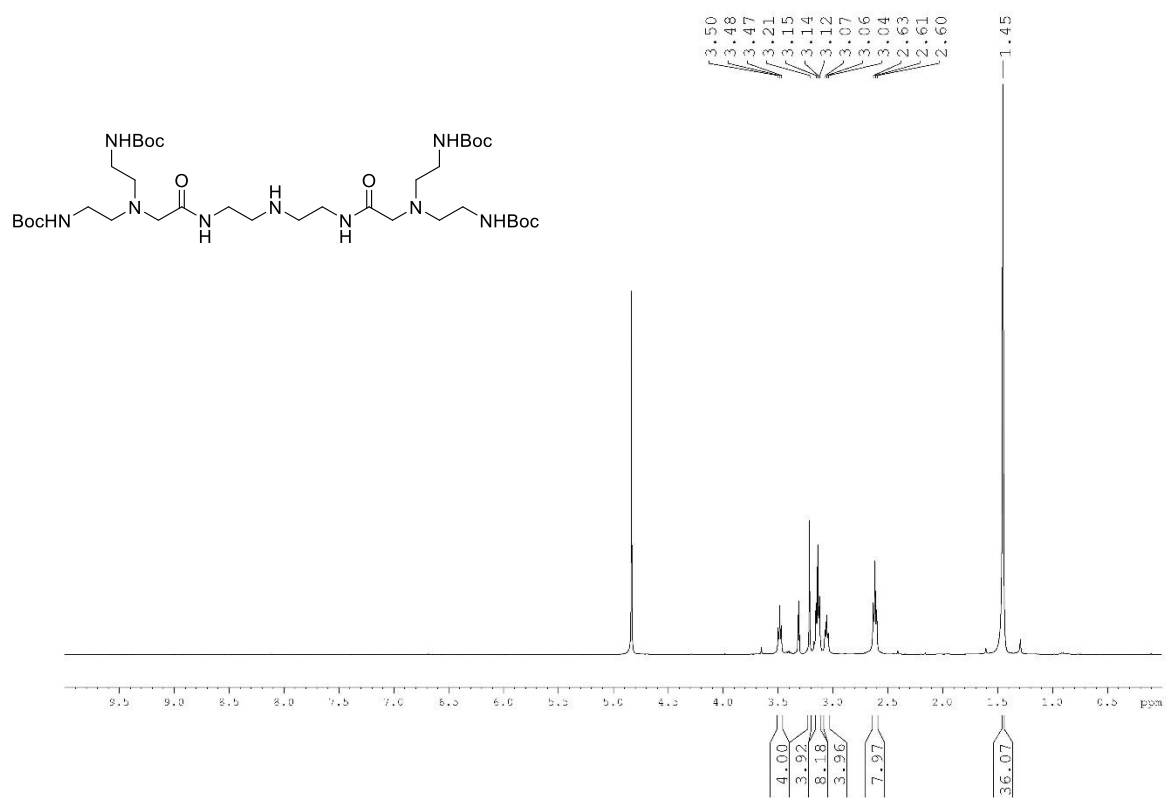
Tetra-*N*-Boc-amine backbone, (alkyne)₃ (25)



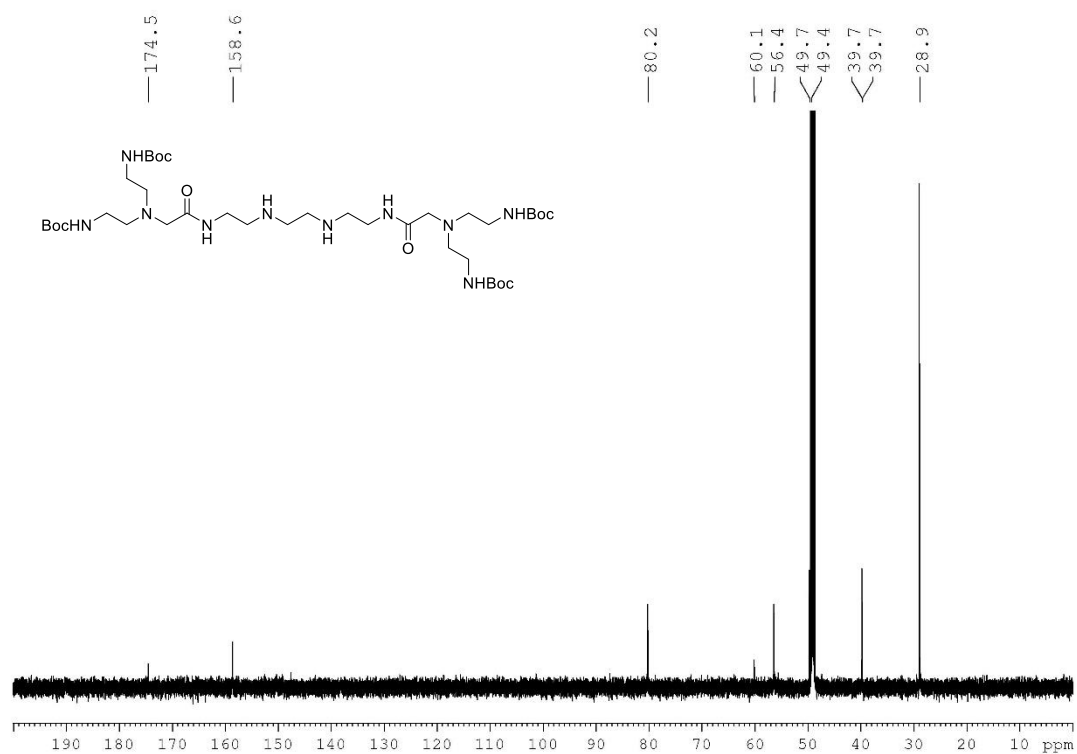
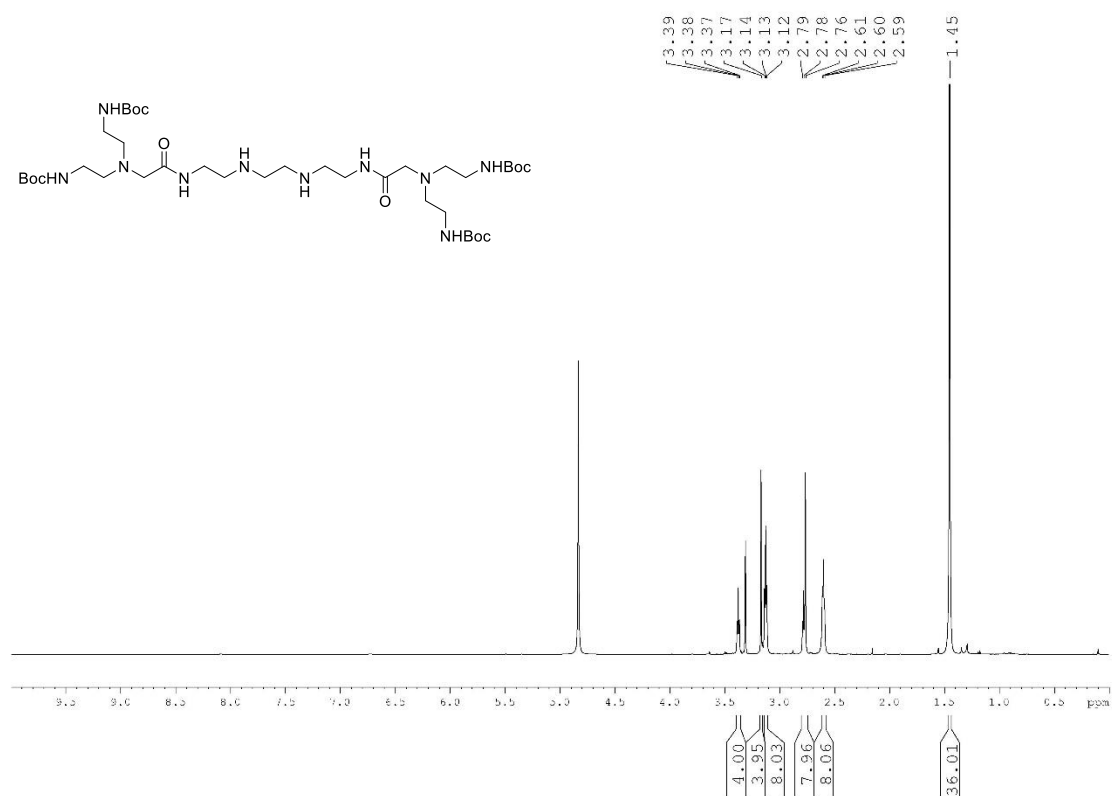
TetraDVP-alkyne₃ (26)



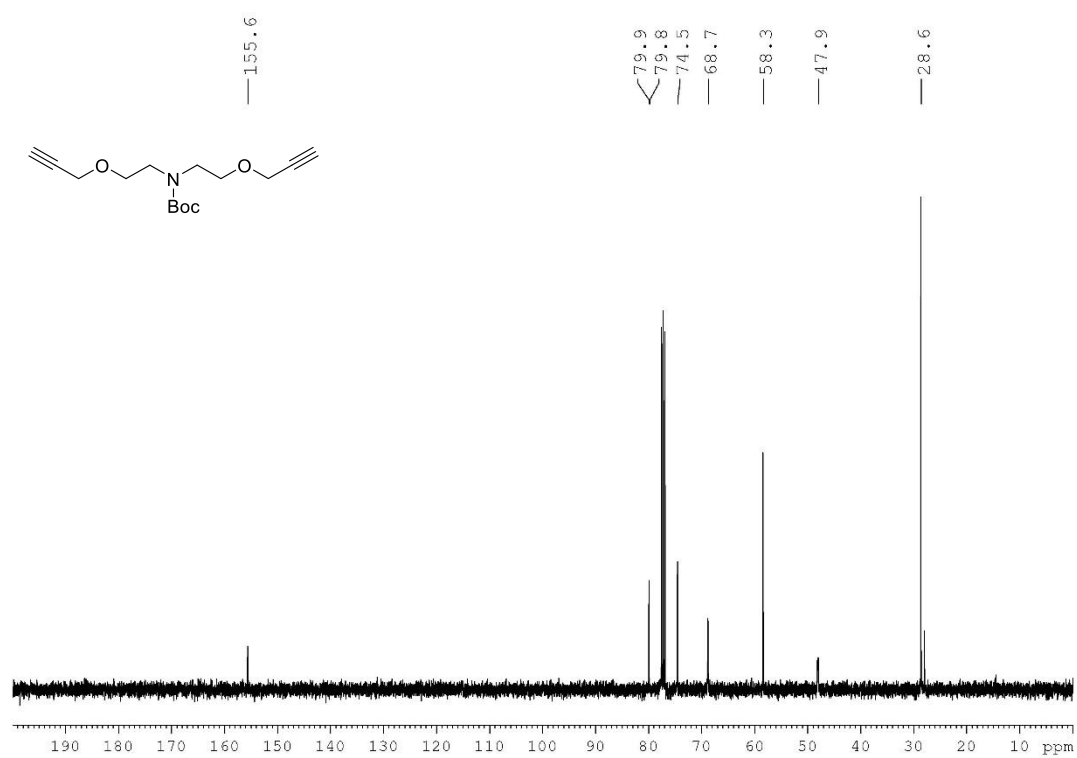
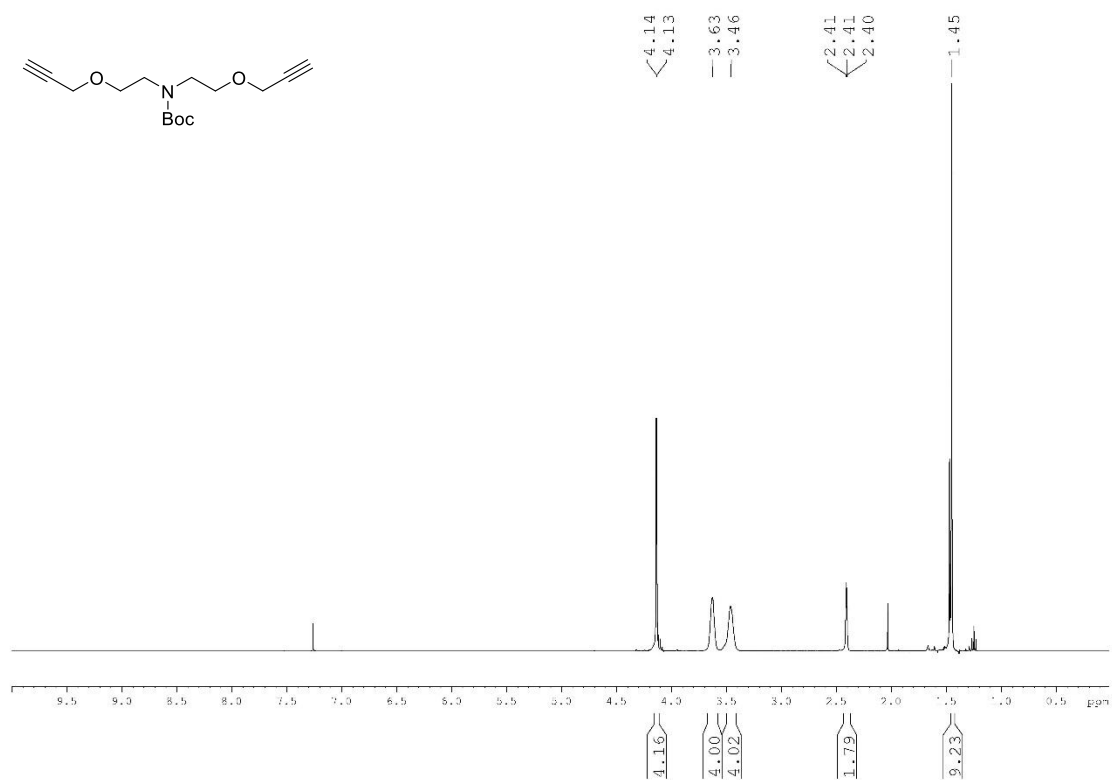
Tetra-*N*-Boc-amine backbone, (NH)₁ (27)



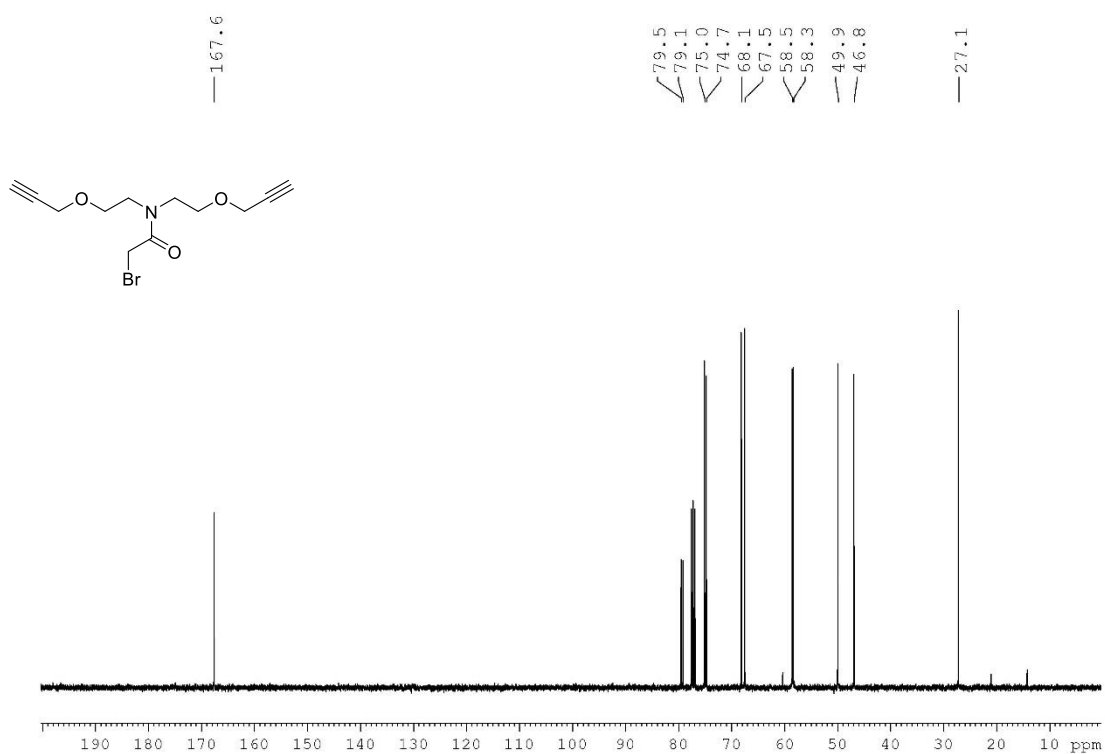
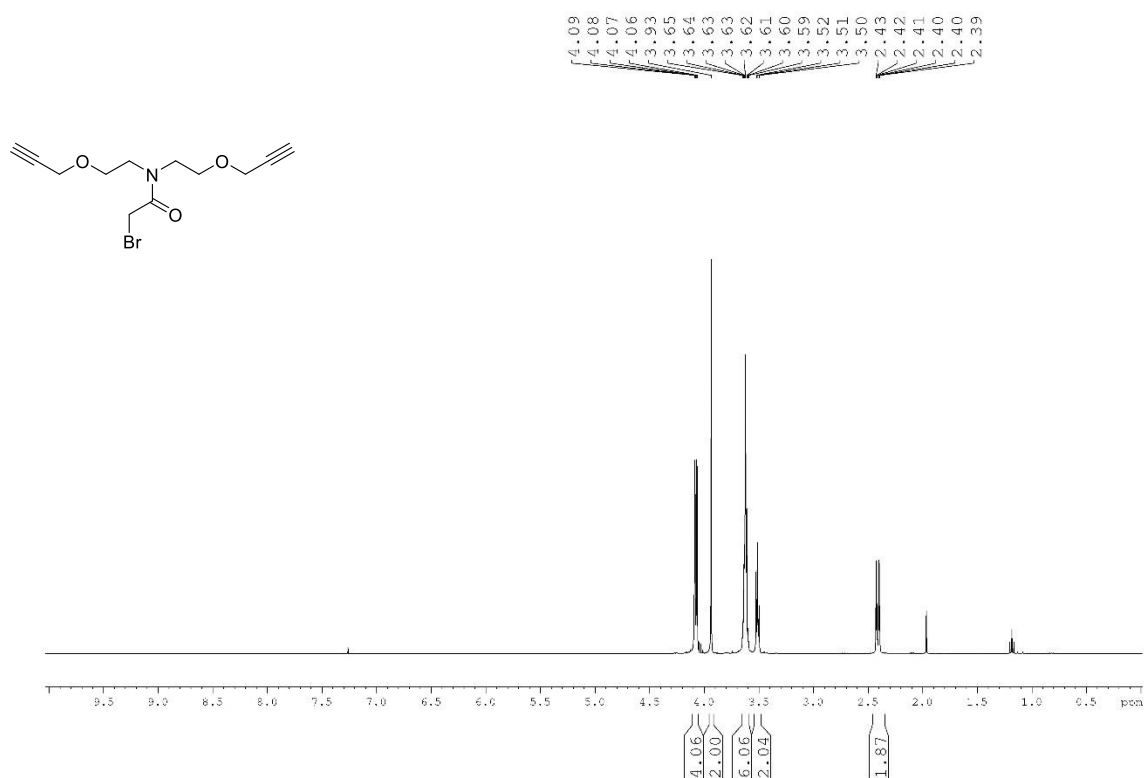
Tetra-*N*-Boc-amine backbone, (NH)₂ (28)



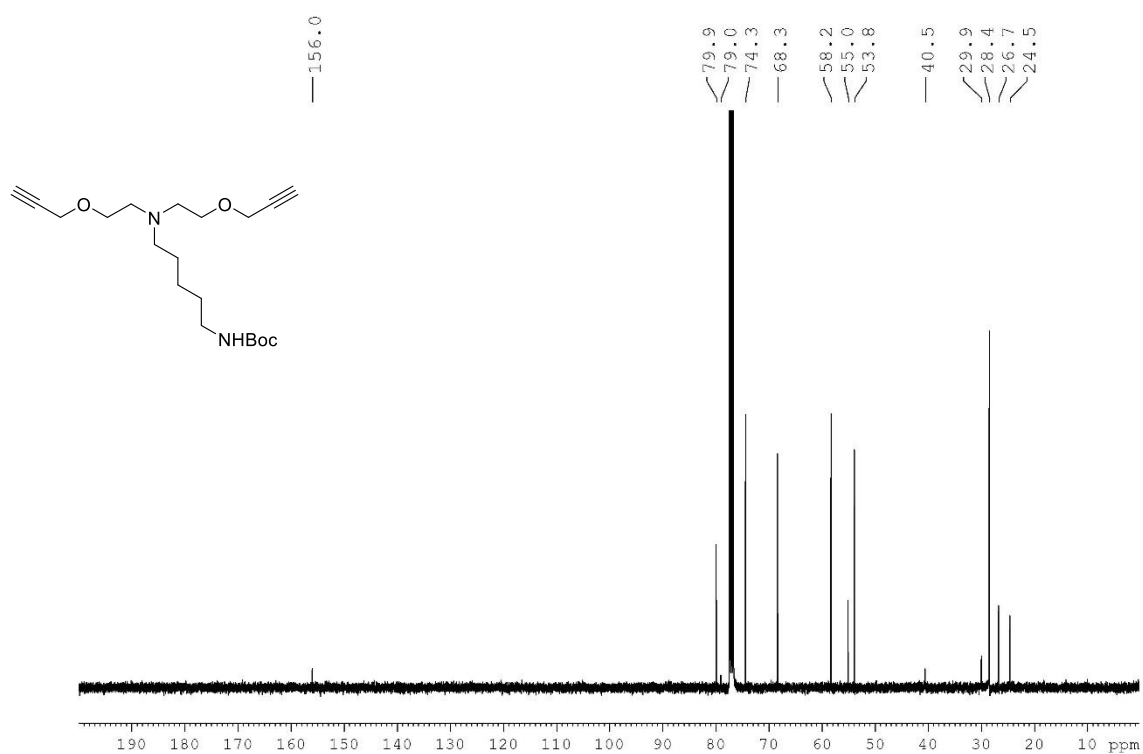
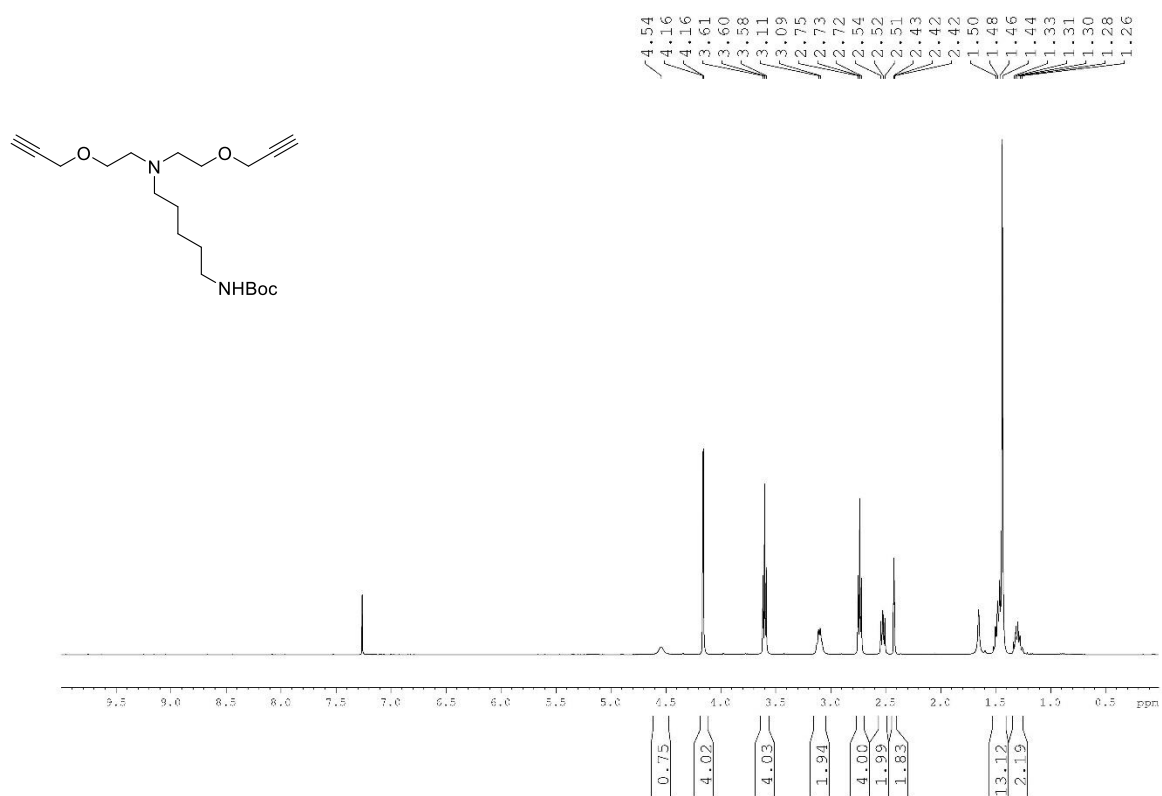
***tert*-butyl bis(2-(prop-2-yn-1-yloxy)ethyl)carbamate (29)**



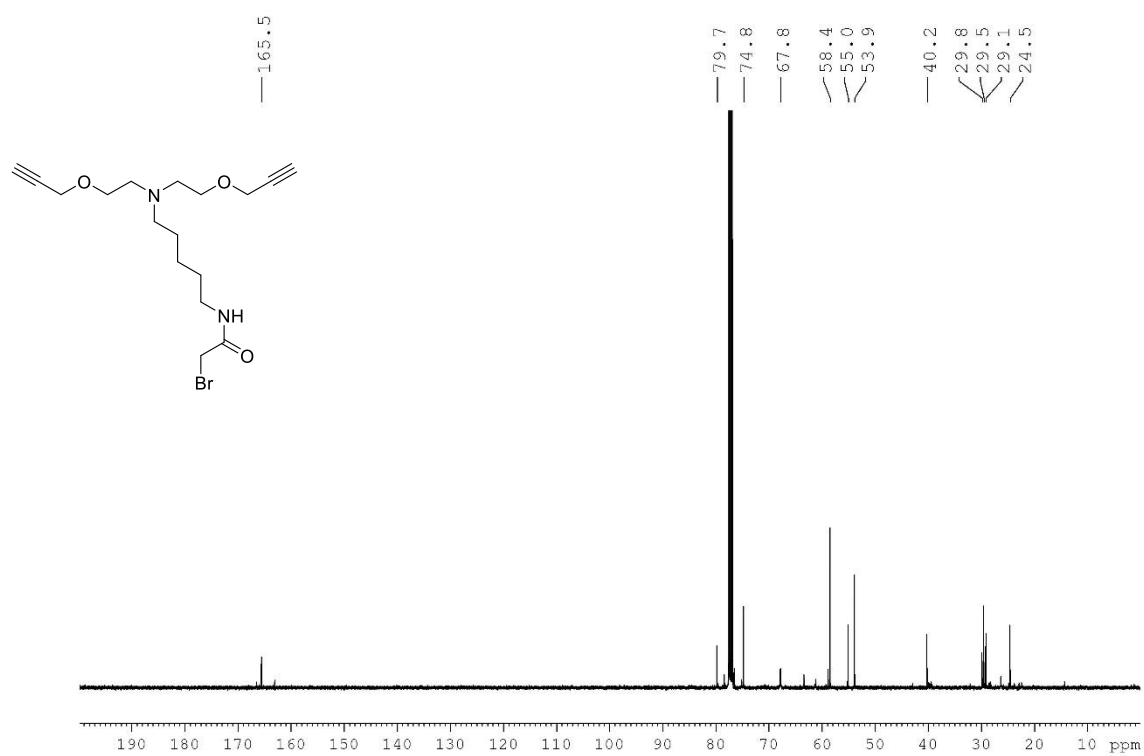
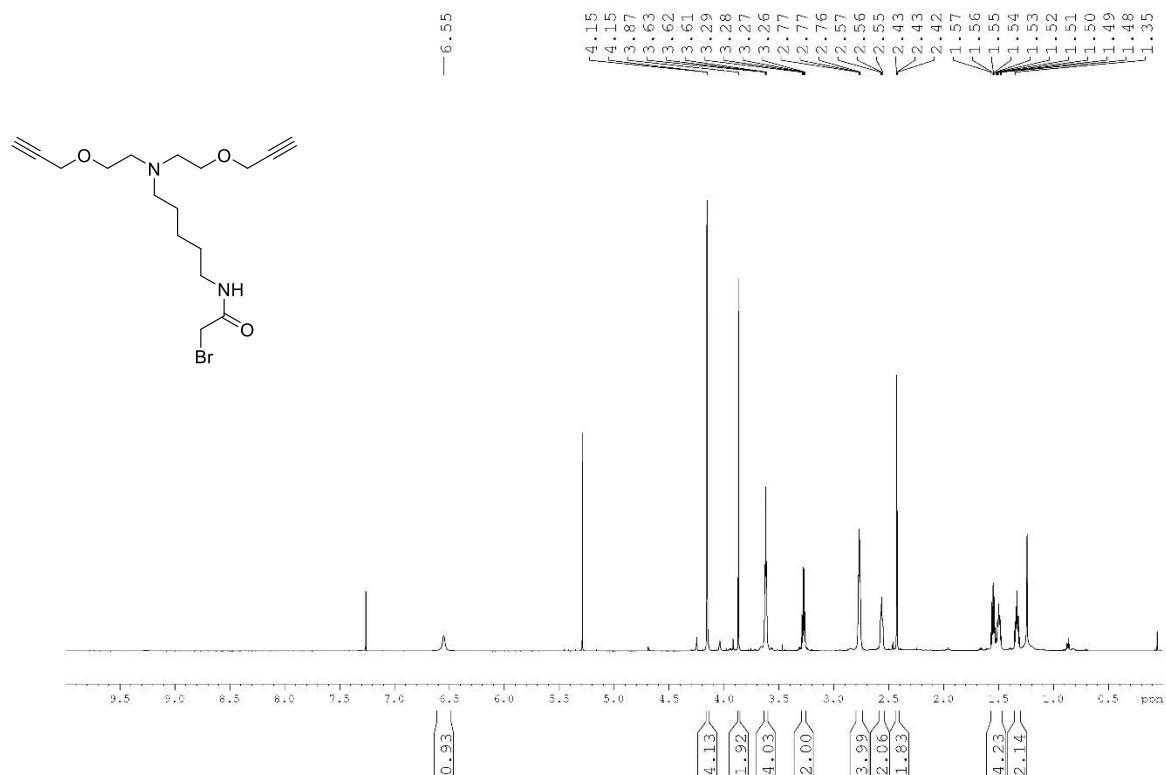
2-bromo-*N,N*-bis(2-(prop-2-yn-1-yloxy)ethyl)acetamide (30)



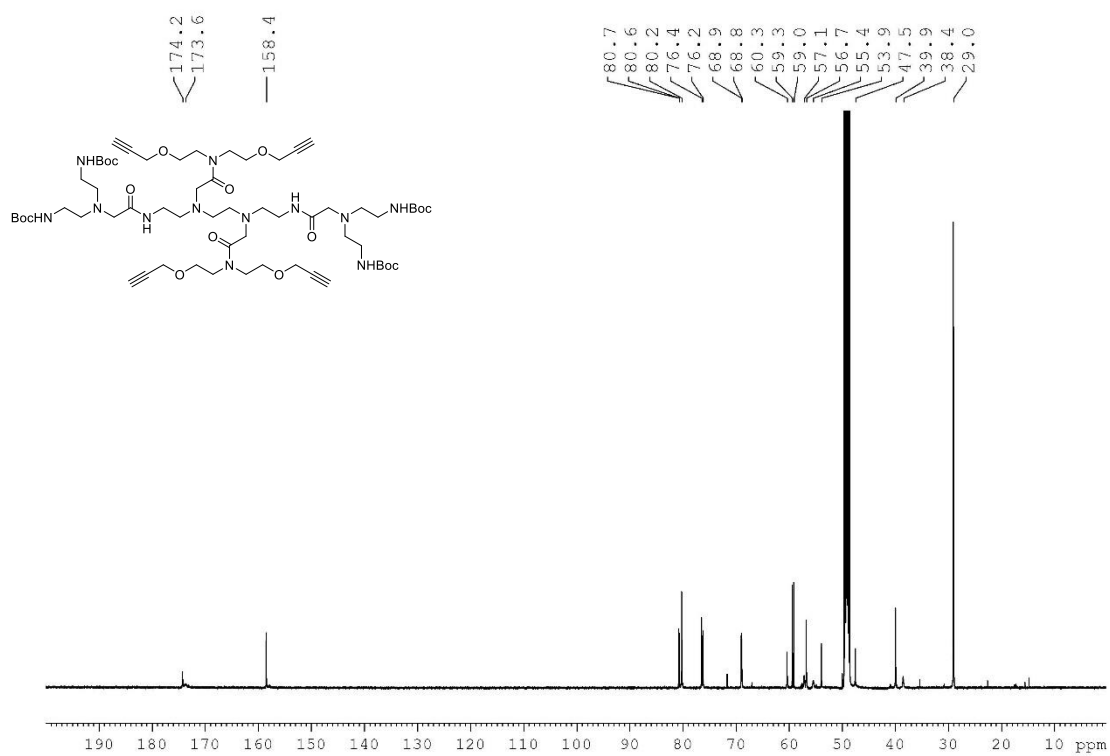
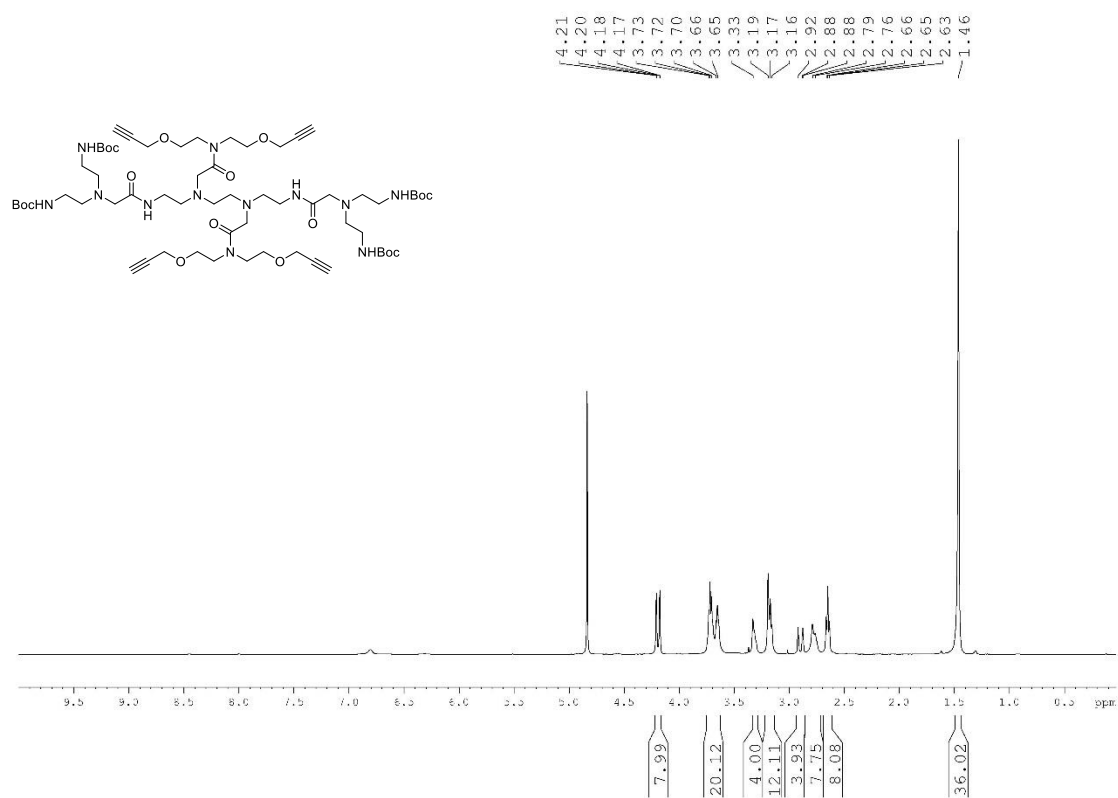
***tert*-butyl (5-(bis(2-(prop-2-yn-1-yloxy)ethyl)amino)pentyl)carbamate (31)**



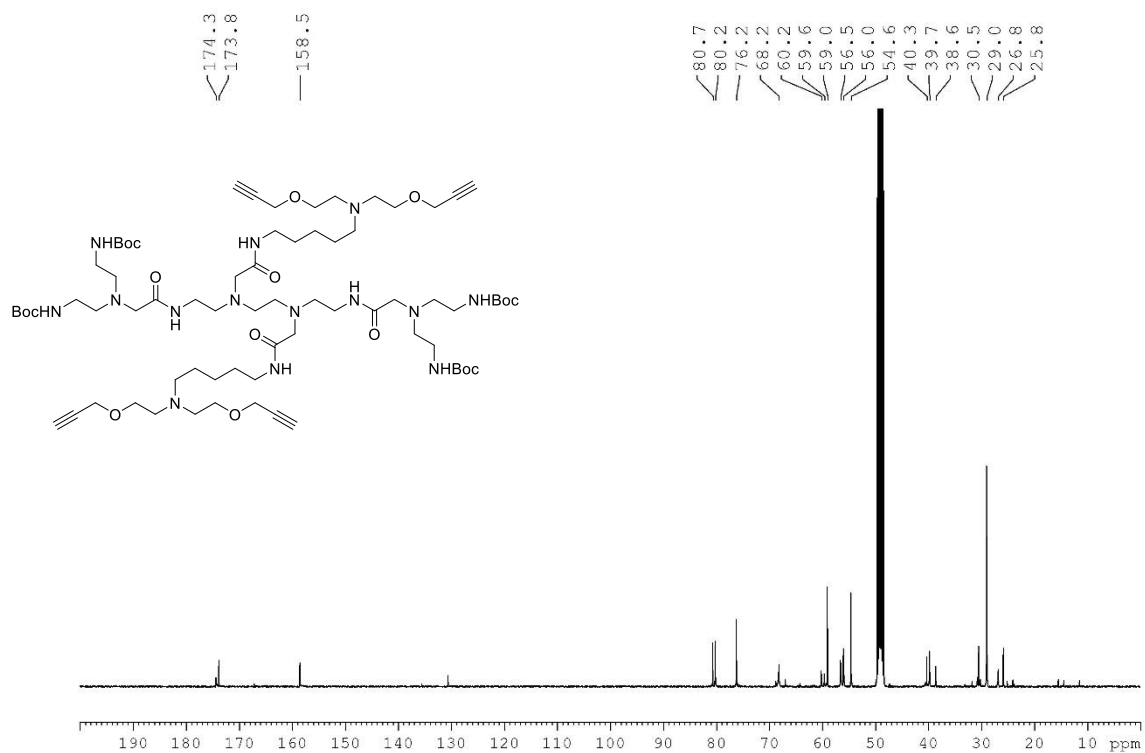
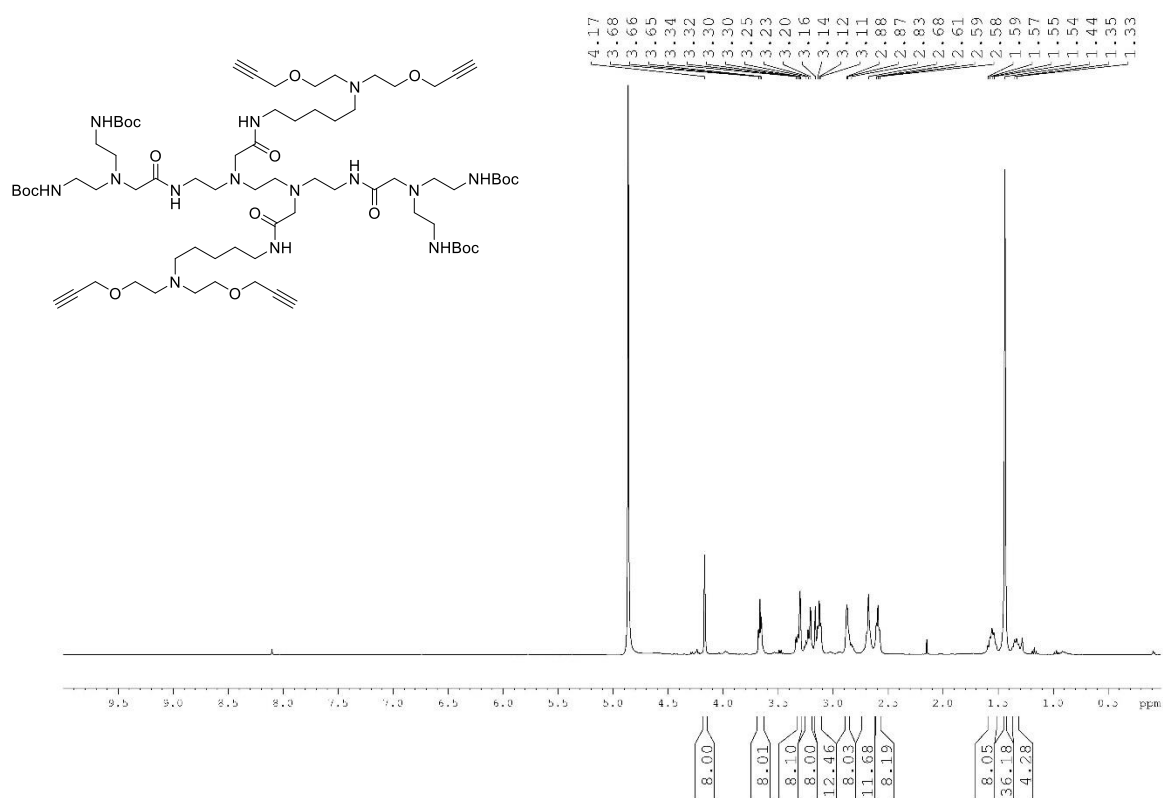
***N*-(5-(bis(2-(prop-2-yn-1-yloxy)ethyl)amino)pentyl)-2-bromoacetamide (32)**



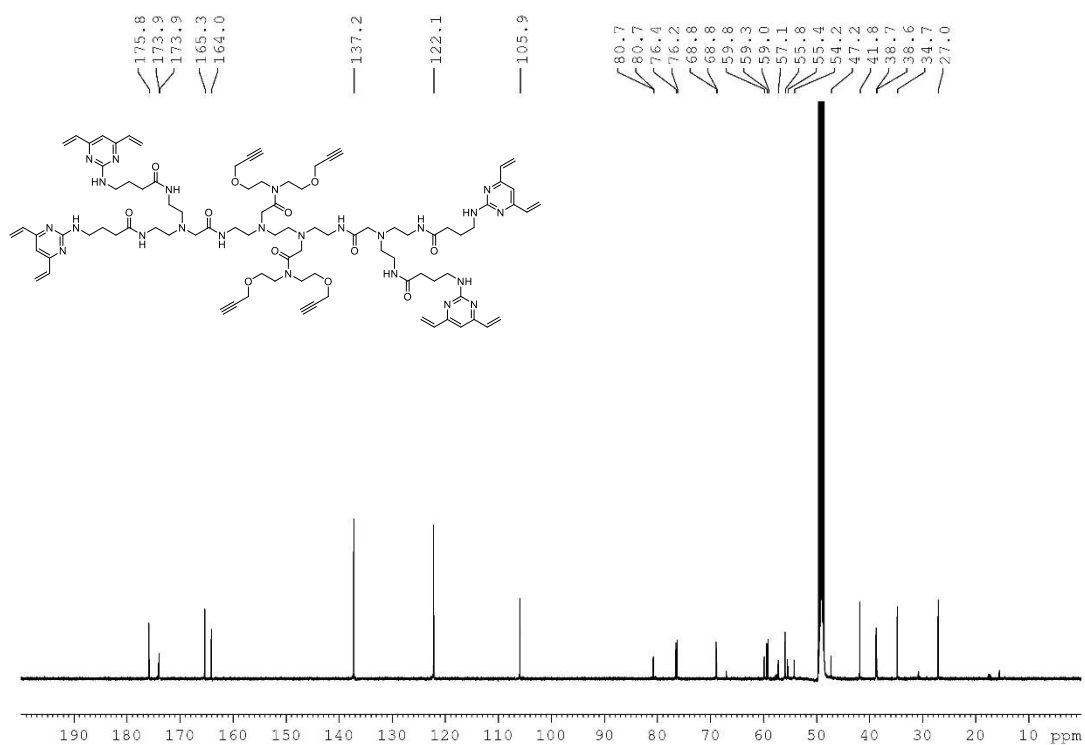
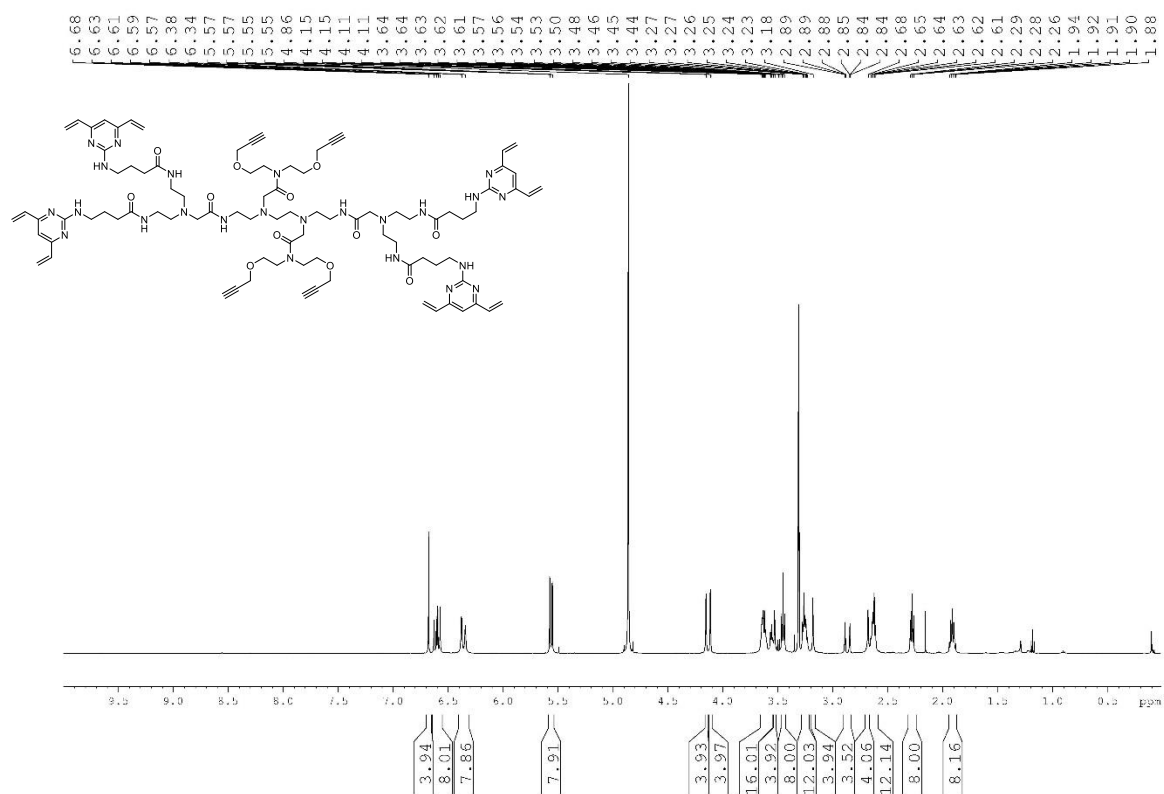
Tetra-*N*-Boc-amine backbone, ((alkyne)₂)₂ (33)



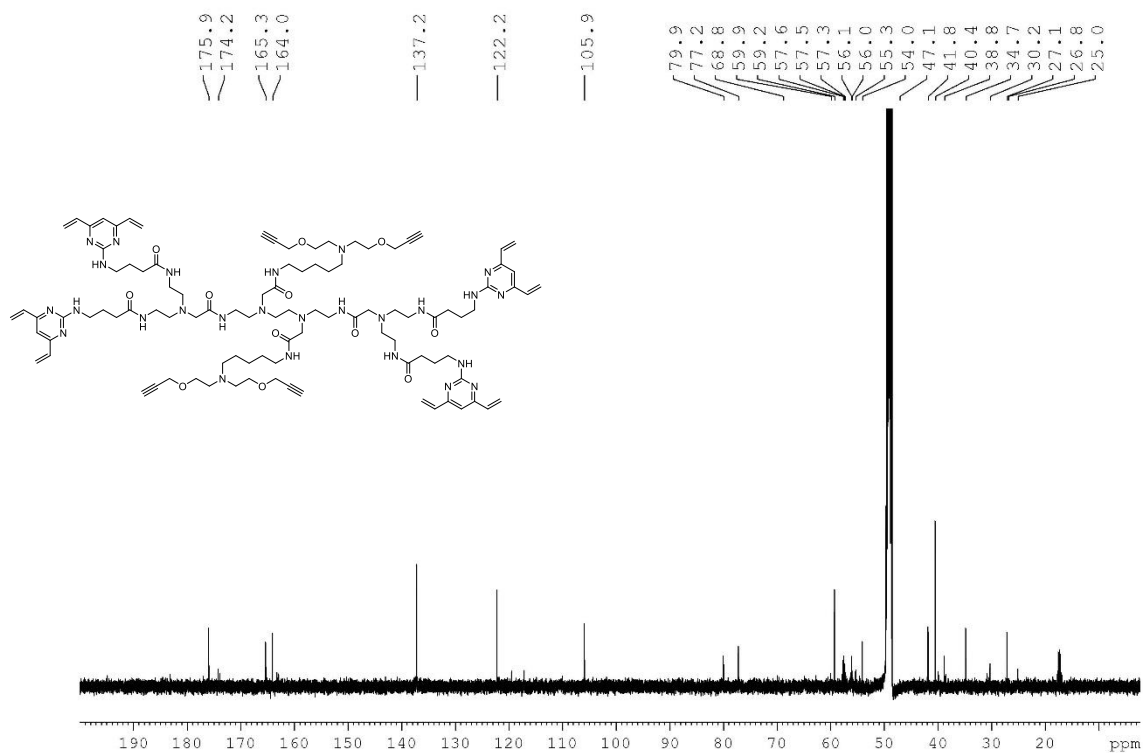
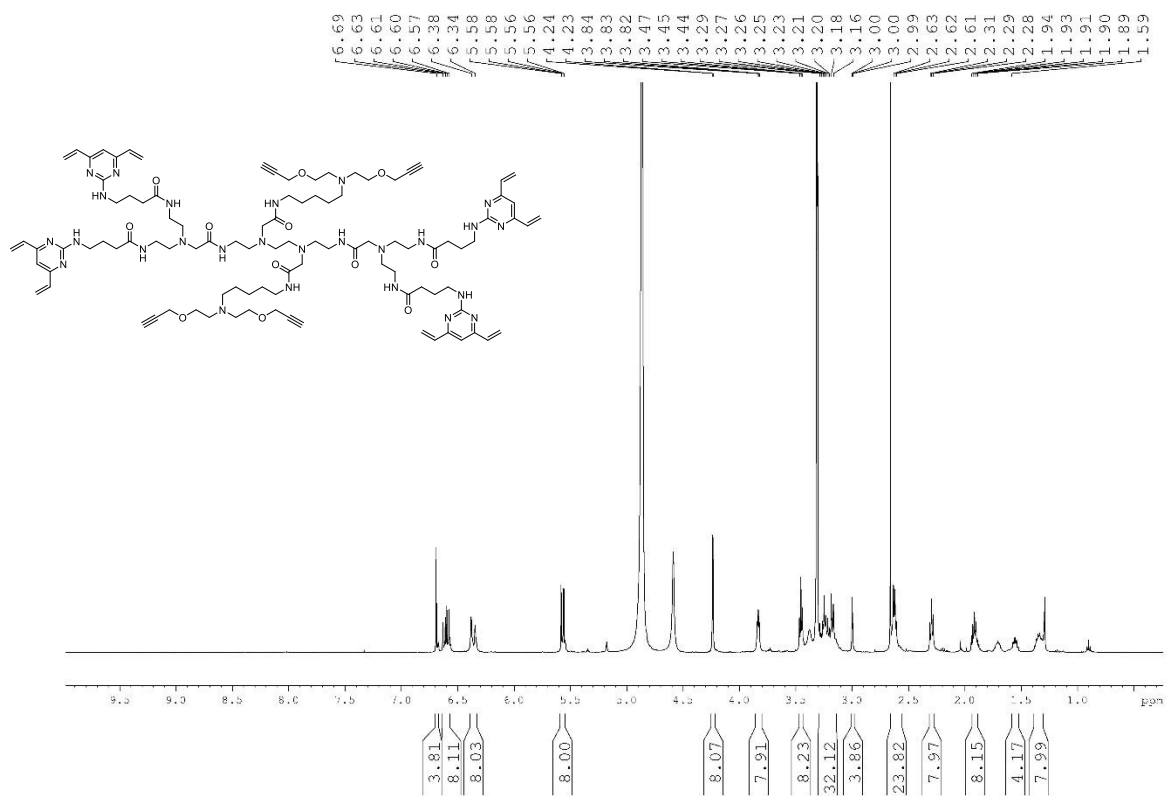
Tetra-*N*-Boc-amine backbone, (pentane-(alkyne)₂)₂ (34)



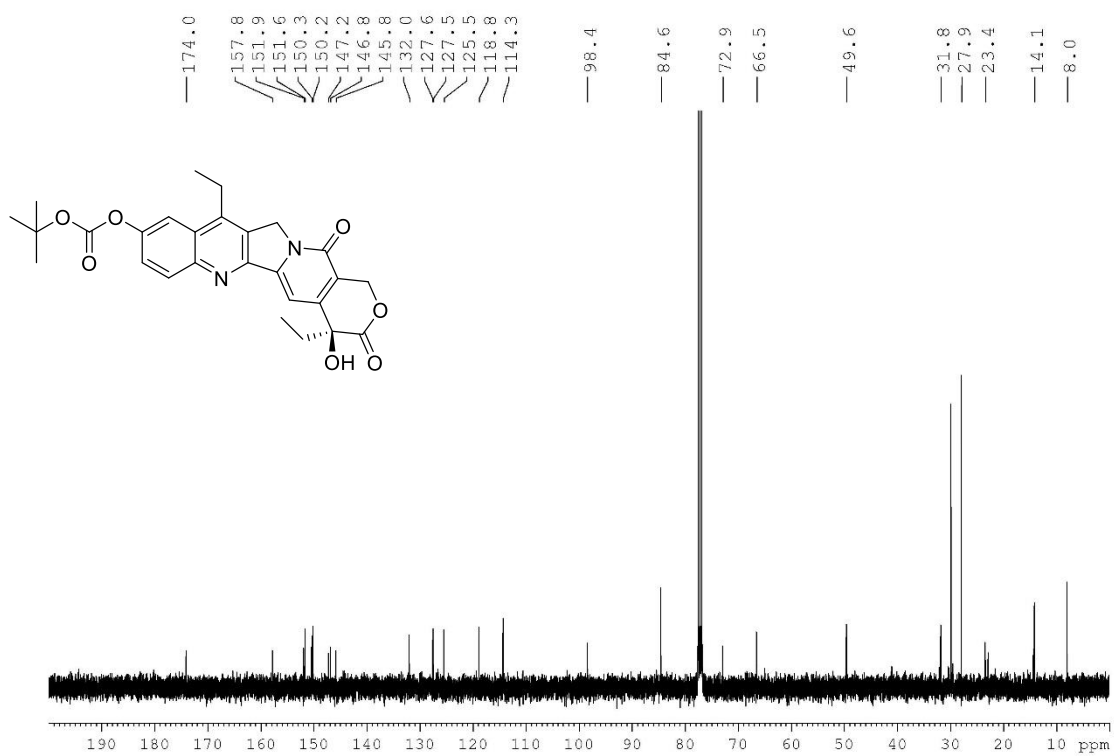
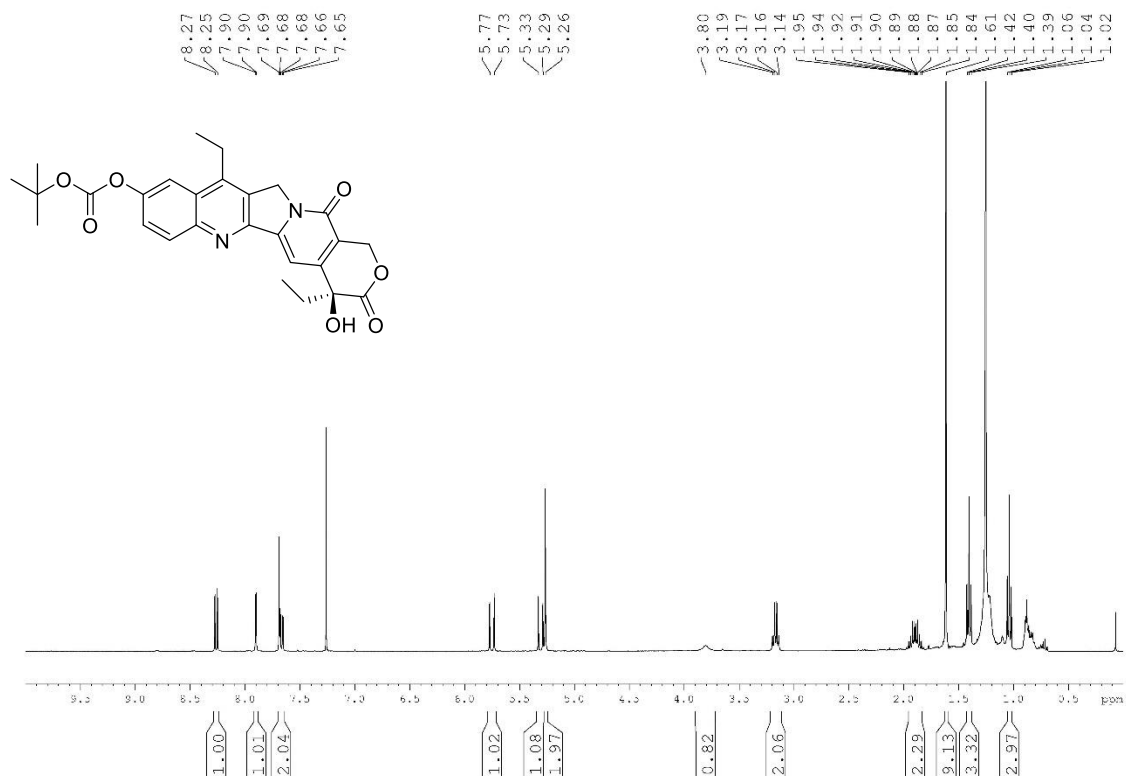
TetraDVP-((alkyne)₂)₂ (35)



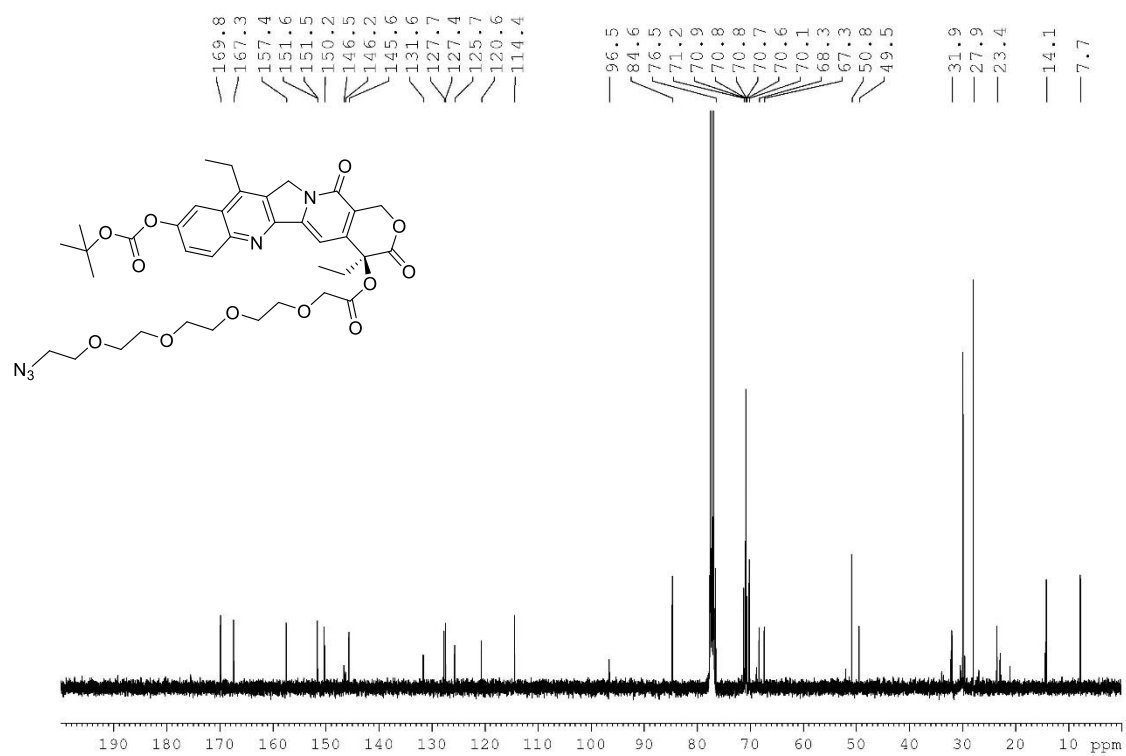
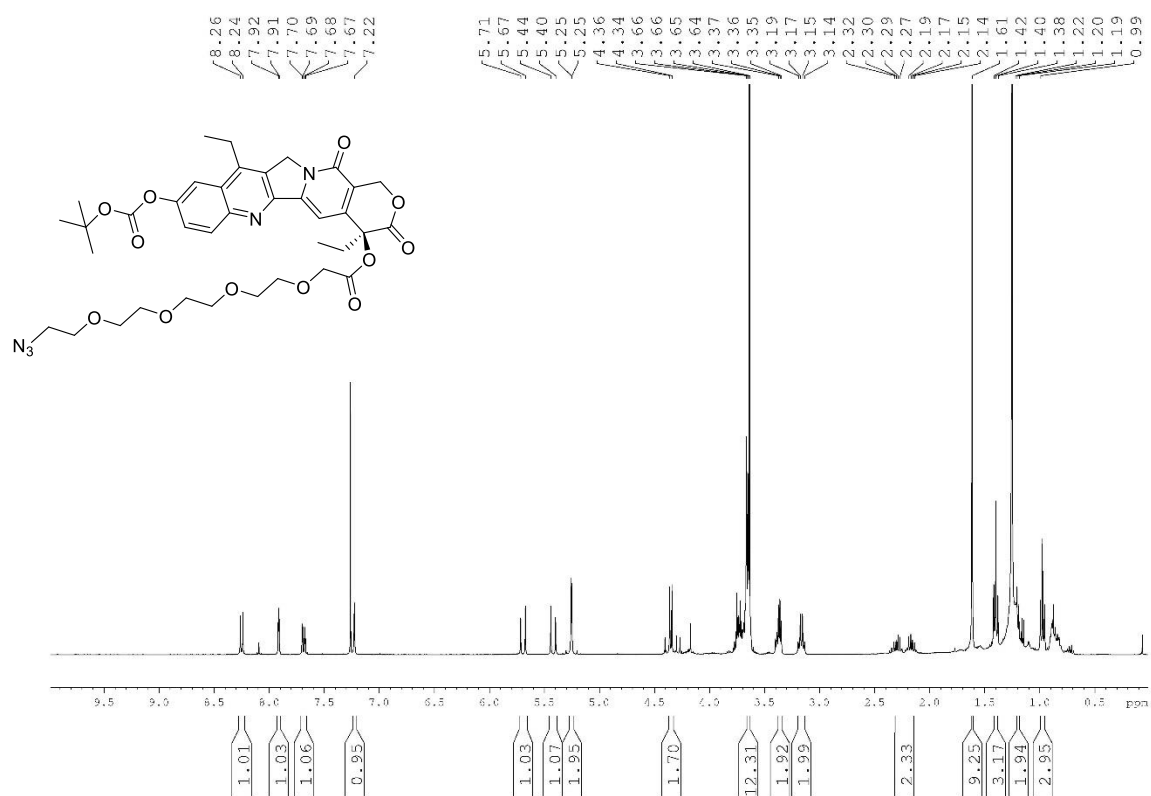
TetraDVP-(pentane-(alkyne)₂)₂ (36)



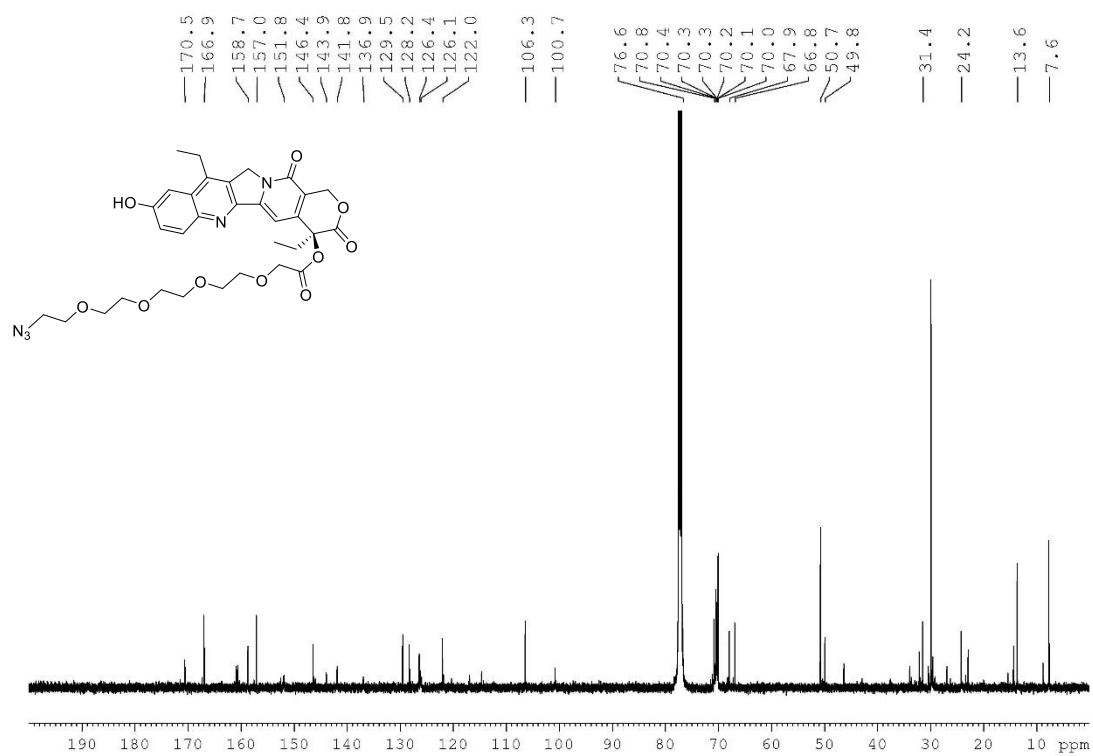
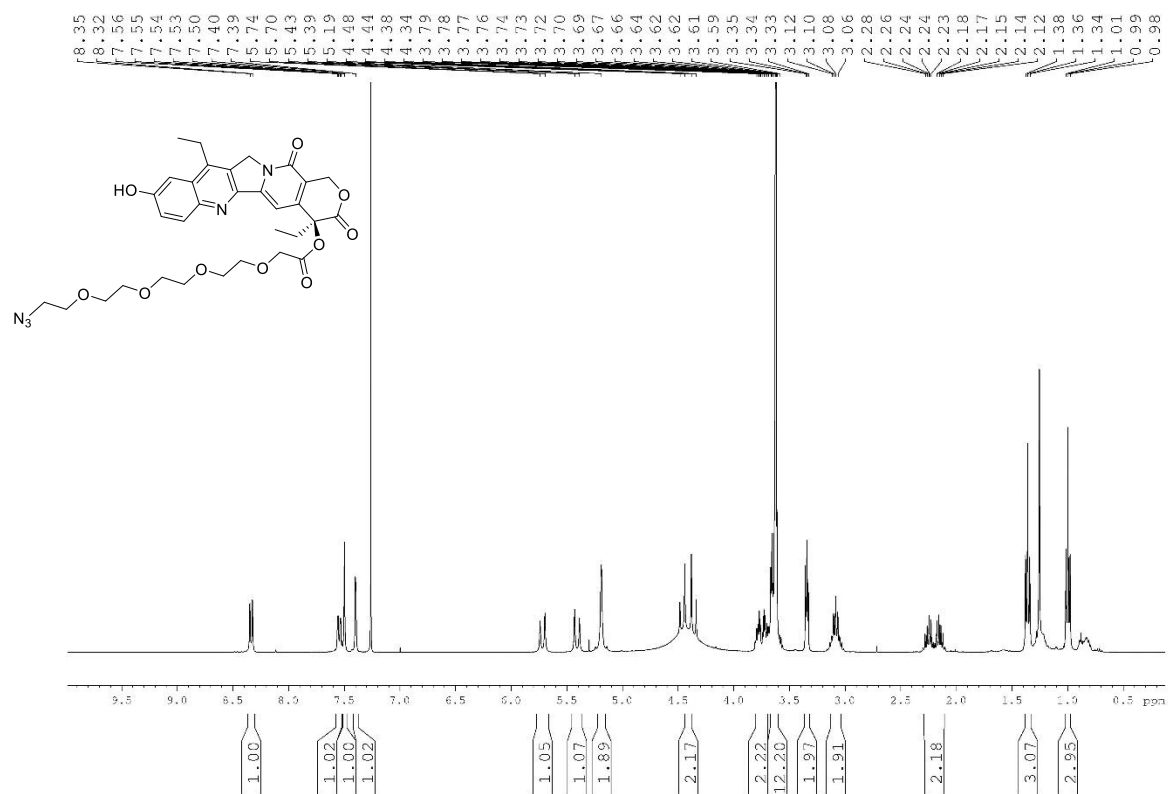
SN-38-Boc (65)



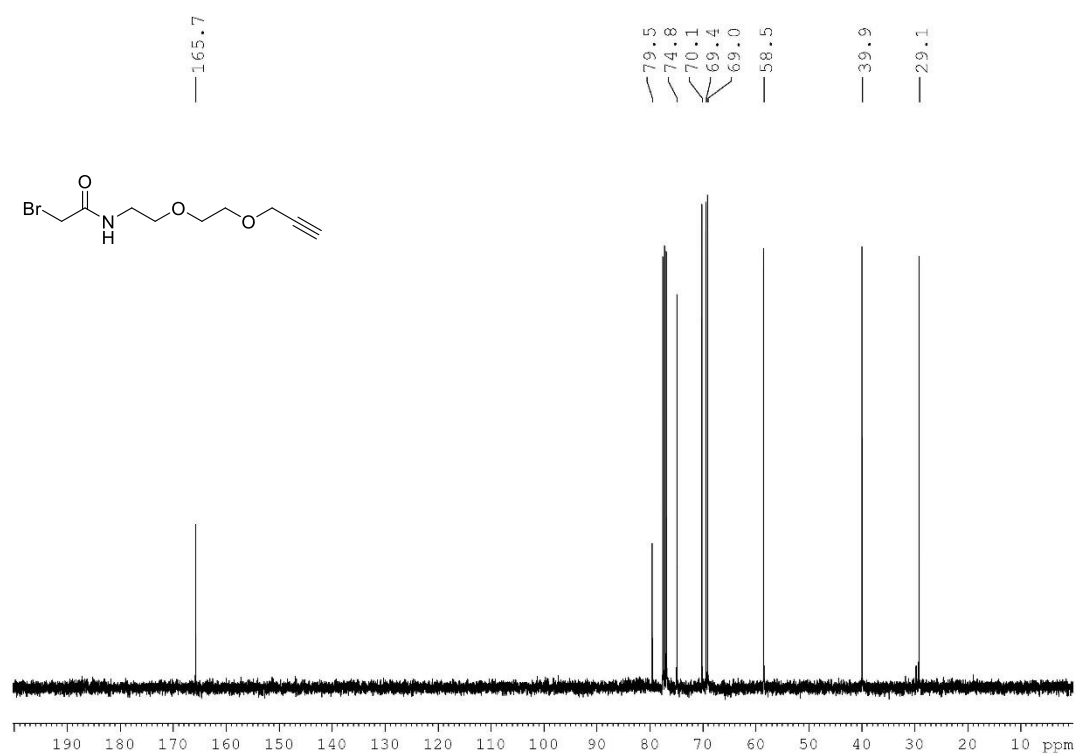
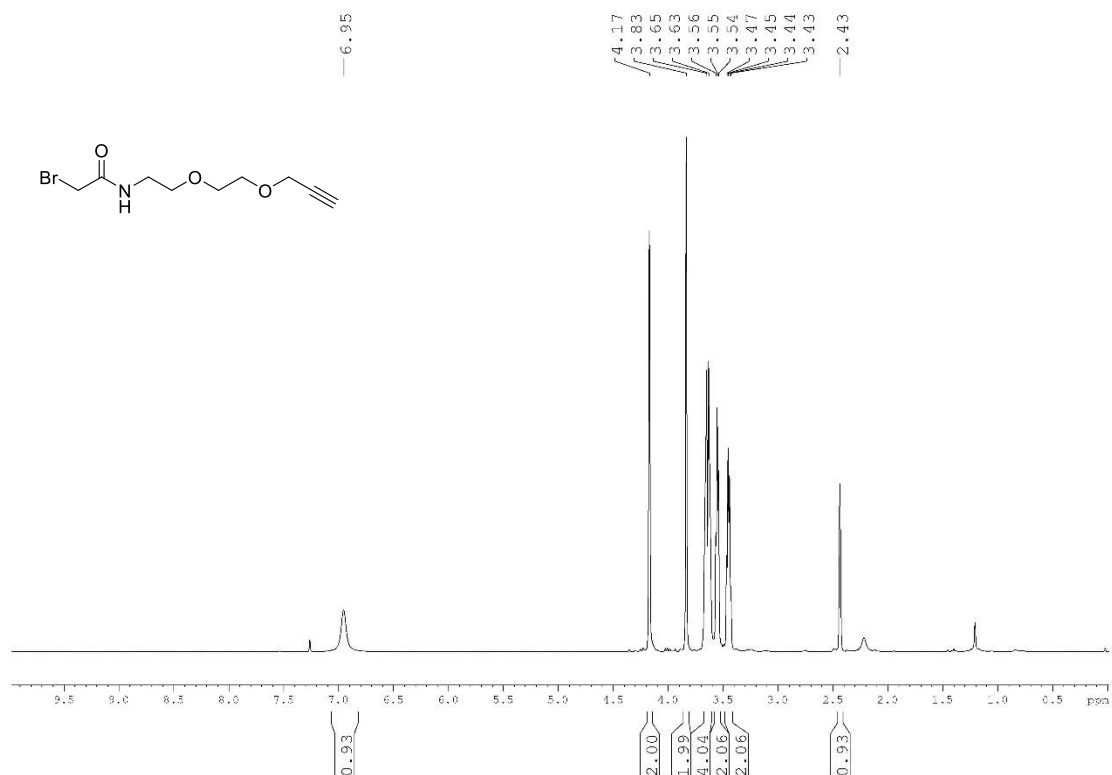
SN-38-Boc-azide (66)



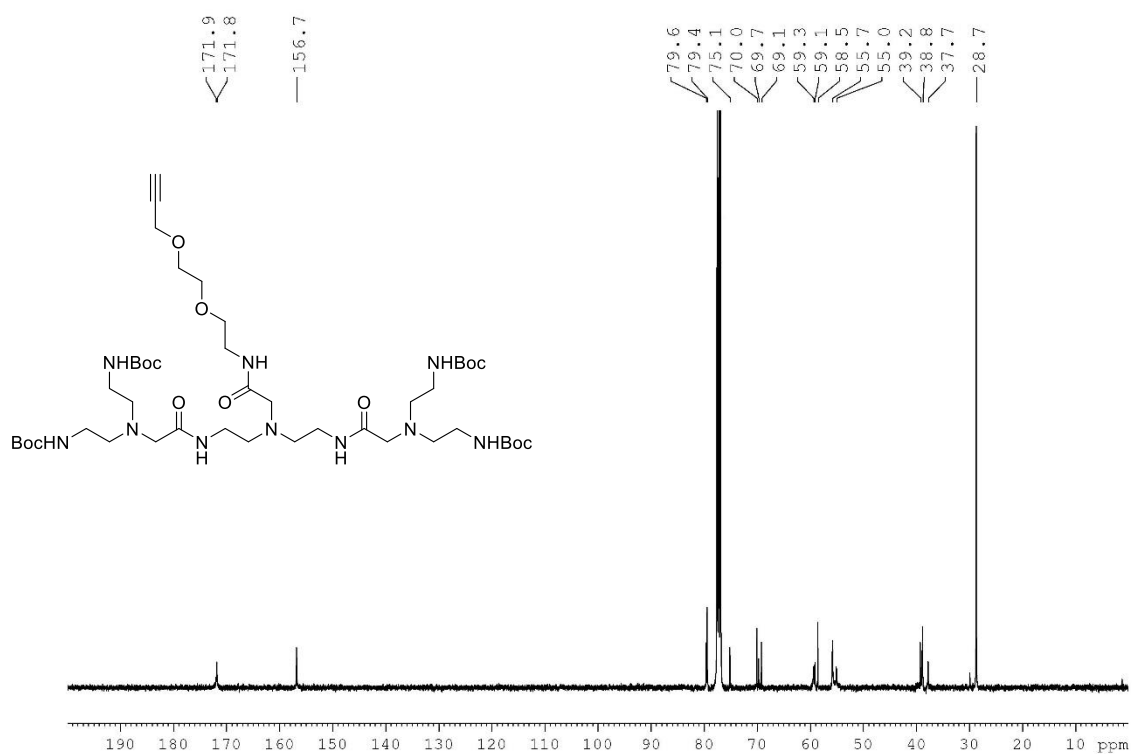
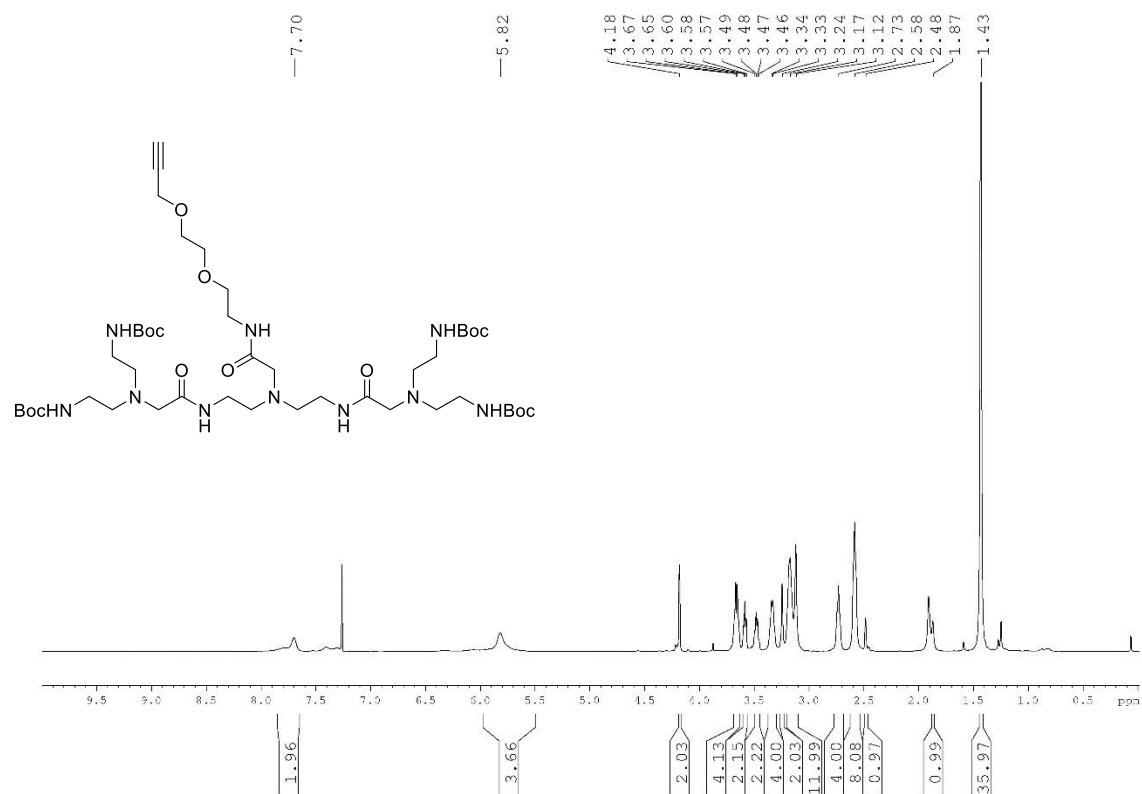
SN-38-azide (67)



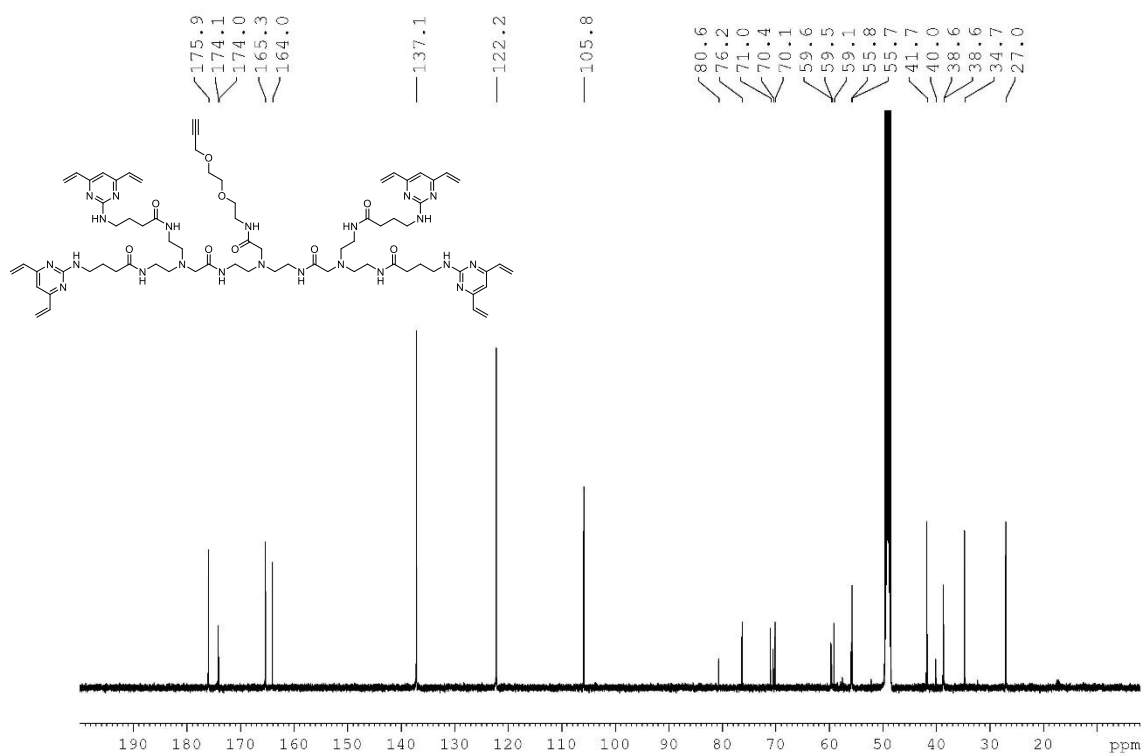
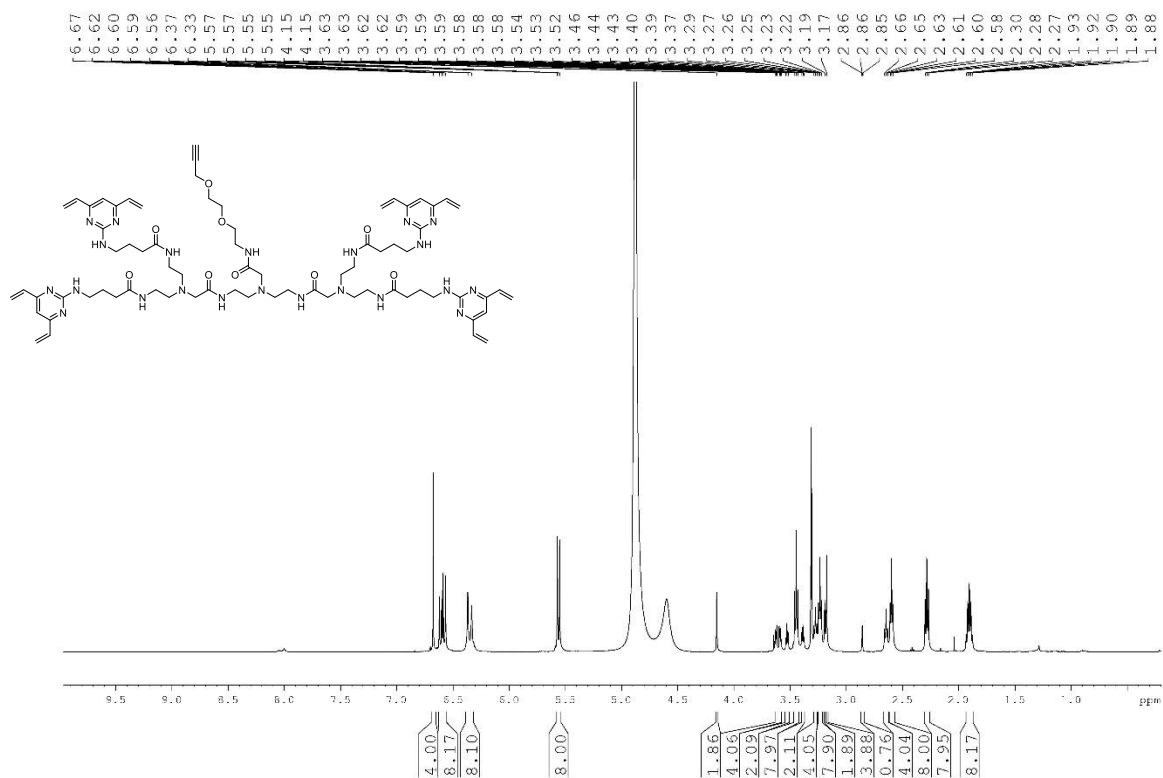
2-bromo-N-(2-(2-(prop-2-yn-1-yloxy)ethoxy)ethyl)acetamide (74)



Tetra-*N*-Boc backbone, PEG2-alkyne (75)



TetraDVP-PEG2-alkyne (76)



DoE optimisation of the S_NAr between 2,4,6-trichloropyrimidine and ethyl 4-aminobutyrate hydrochloride

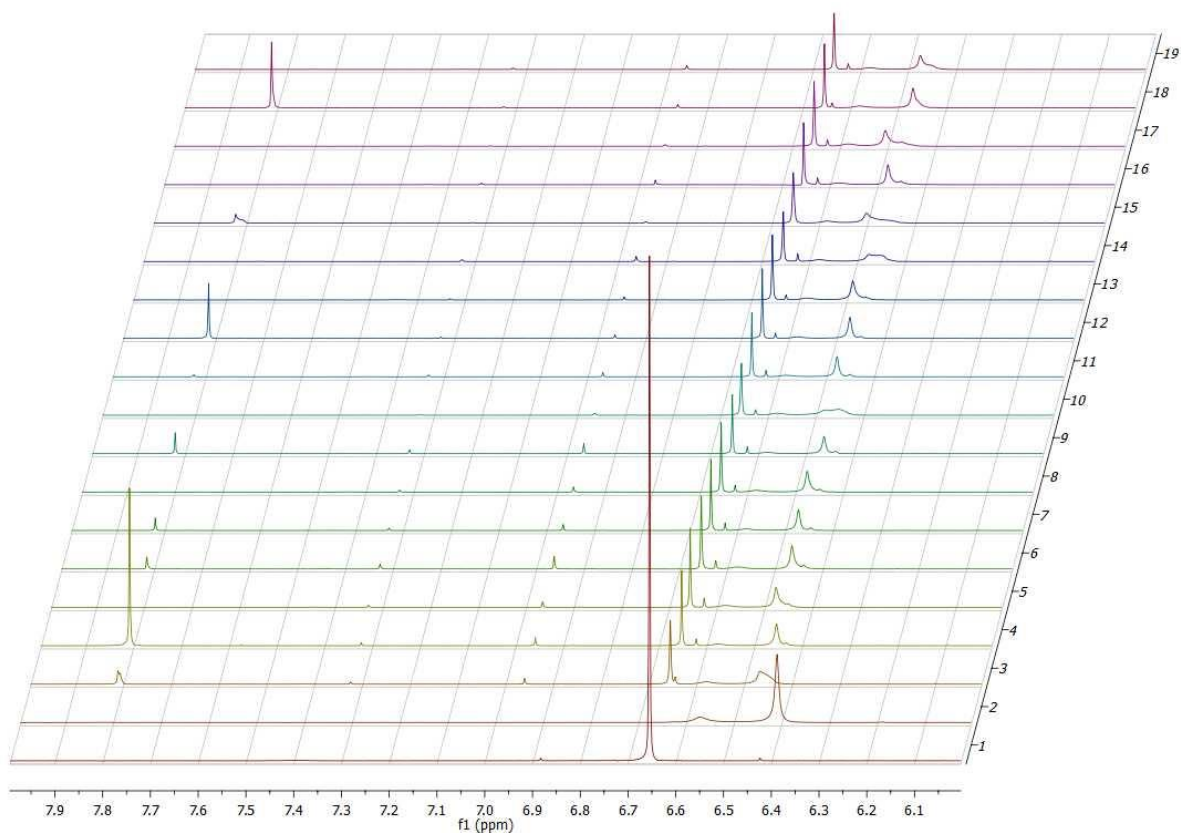


Figure A1: Analysis of the reaction between 2,4,6-trichloropyrimidine and ethyl 4-aminobutyrate hydrochloride by 1H NMR. Rows: 1 = Ethyl 4-((4,6-dichloropyrimidin-2-yl)amino)butanoate (**1**); 2 = Ethyl 4-((2,6-dichloropyrimidin-4-yl)amino)butanoate (**2**); 3-19 = Optimisation experiments. Reaction conditions and integration values can be found in Table 2 in Chapter 3.2.

Appendix B – HPLC traces

SN-38-azide (67)

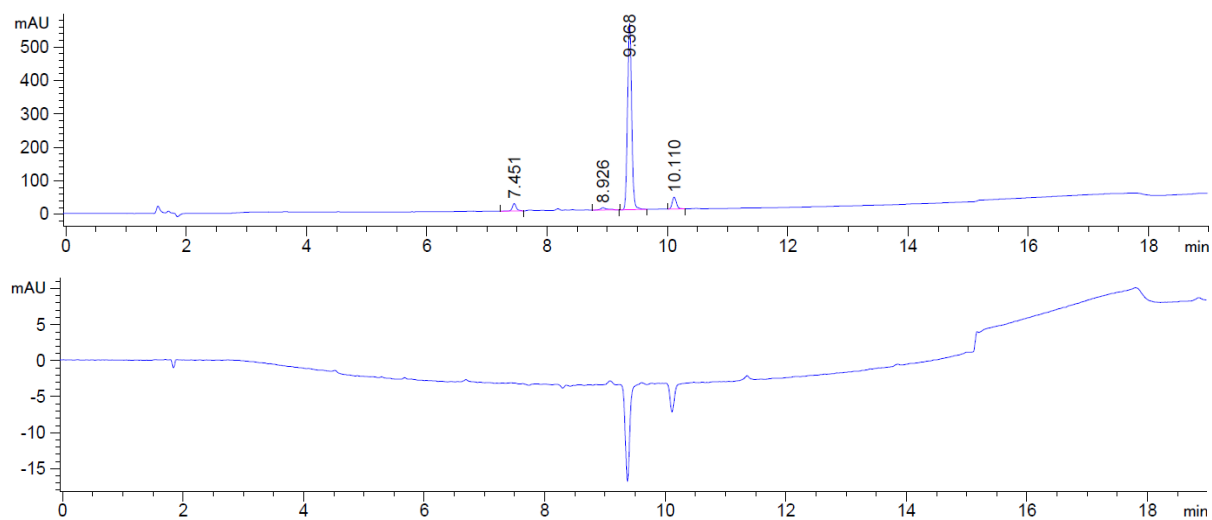
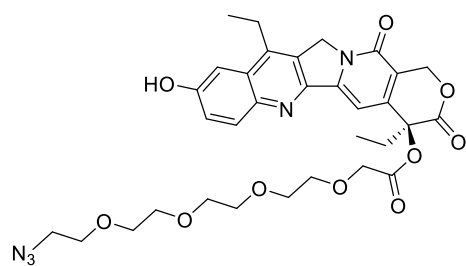


Figure B1: HPLC analysis of compound **67**. Top = 220 nm. Bottom = 254 nm.

TetraDVP-Val-Cit-PABC-MMAE (72)

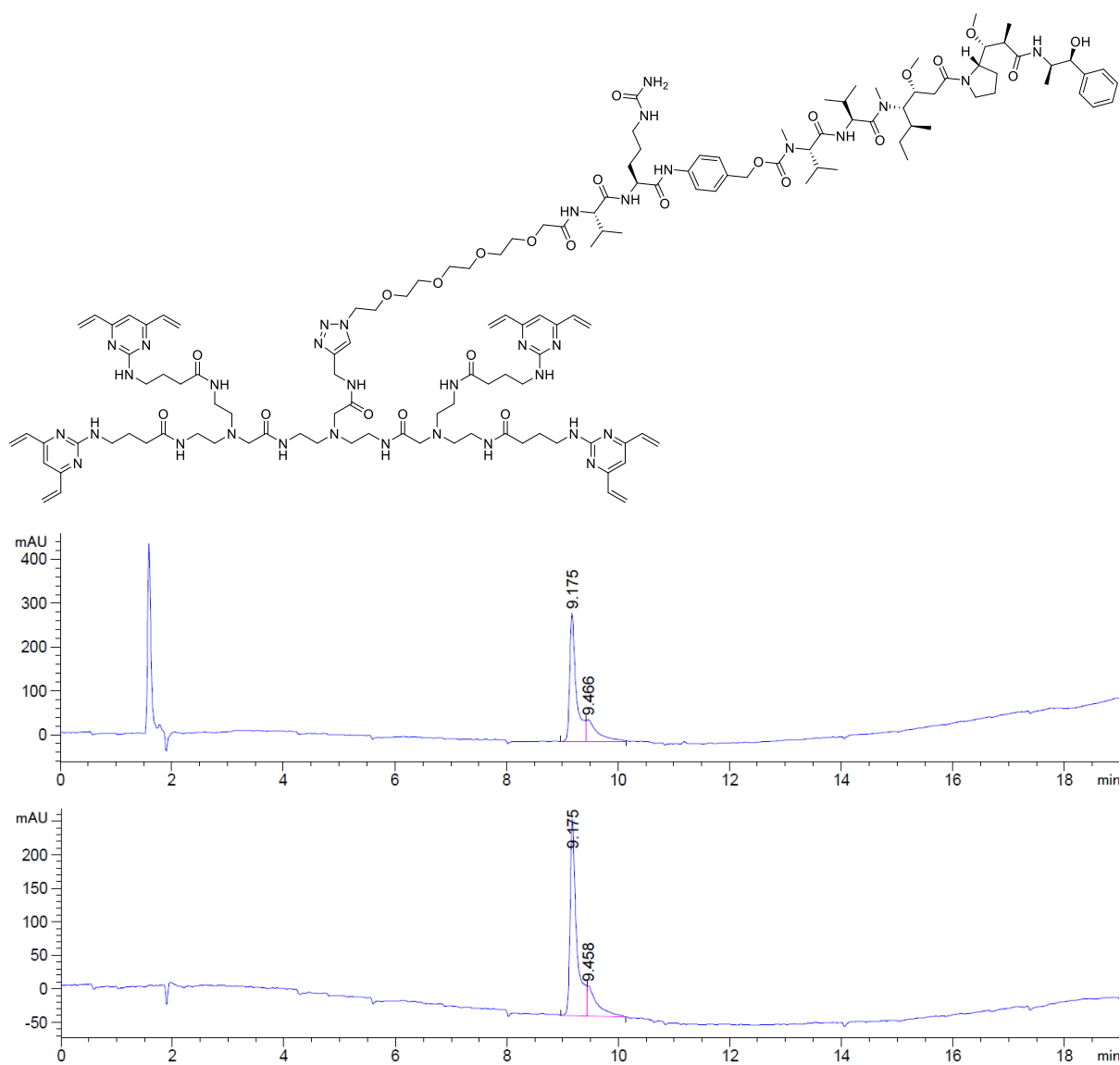


Figure B2: HPLC analysis of compound **72**. Top = 220 nm. Bottom = 254 nm.

Appendix C – Protein LC-MS

Procedure for LC-MS analysis:

Protein LC-MS was performed on a Xevo G2-S TOF mass spectrometer coupled to an Acquity UPLC system using an Acquity UPLC BEH300 C4 column (1.7 μm , 2.1 \times 50 mm). H₂O with 0.1% formic acid (solvent A) and 95% MeCN and 5% H₂O with 0.1% formic acid (solvent B) were used as the mobile phase at a flow rate of 0.2 mL/min. The gradient was programmed as follows: 95% A for 0.93 min, then a gradient to 100% B over 4.28 min, then 100% B for 1.04 minutes, then a gradient to 95% A over 1.04 min. The electrospray source was operated with a capillary voltage of 2.0 kV and a cone voltage of 190 V. Nitrogen was used as the desolvation gas at a total flow rate of 850 L/h. Total mass spectra were reconstructed from the ion series using the MaxEnt 1 algorithm preinstalled on MassLynx 4.2 software according to the manufacturer's instructions. Trastuzumab samples were deglycosylated with PNGase F (New England Biolabs) prior to LC-MS analysis.

Only the region of the total ion chromatogram (TIC) between 3.25-3.75 min was analysed. Peaks outside of this range did not contain proteinogenic signals and were excluded. Analysis was conducted in the same way for all protein LC-MS traces.

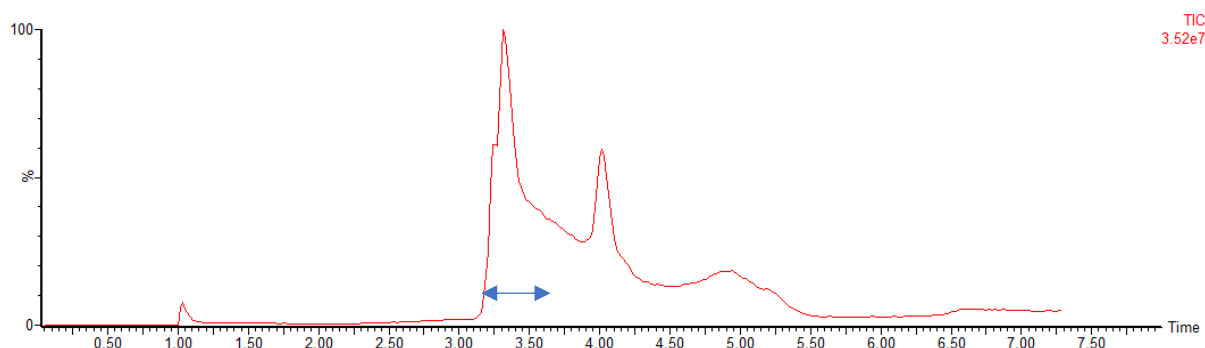


Figure C1: Typical TIC trace of trastuzumab samples. The blue arrow indicates the region was the TIC that was analysed.

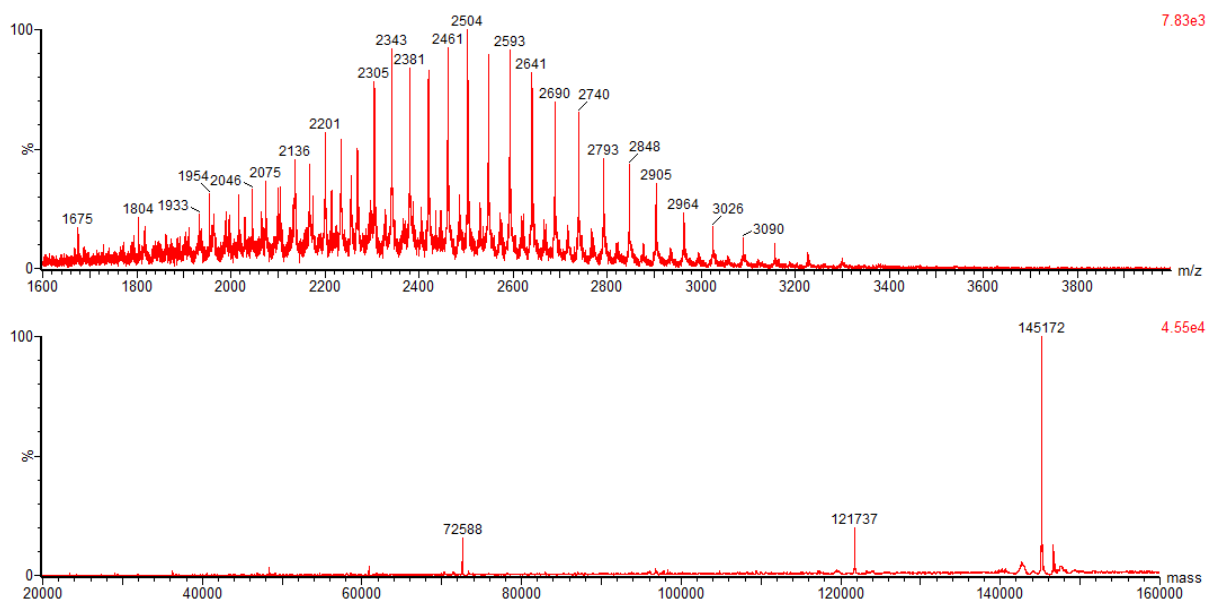


Figure C2: LC-MS of unmodified trastuzumab. Top = non-deconvoluted MS. Bottom = deconvoluted MS; expected 145,160 Da, observed 145,172 Da.

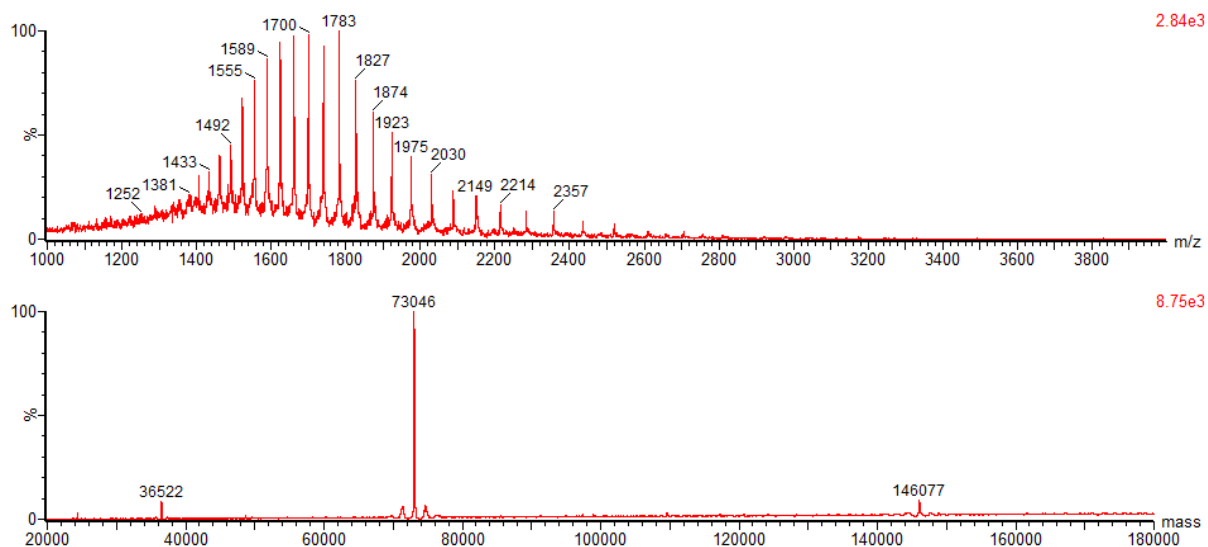


Figure C3: Analysis of the reaction between trastuzumab and DVP **4** by LC-MS. Top = non-deconvoluted MS. Bottom = deconvoluted MS; expected 73,061 Da (half antibody) and 146,123 Da (full antibody), observed 73,046 and 146,077 Da.

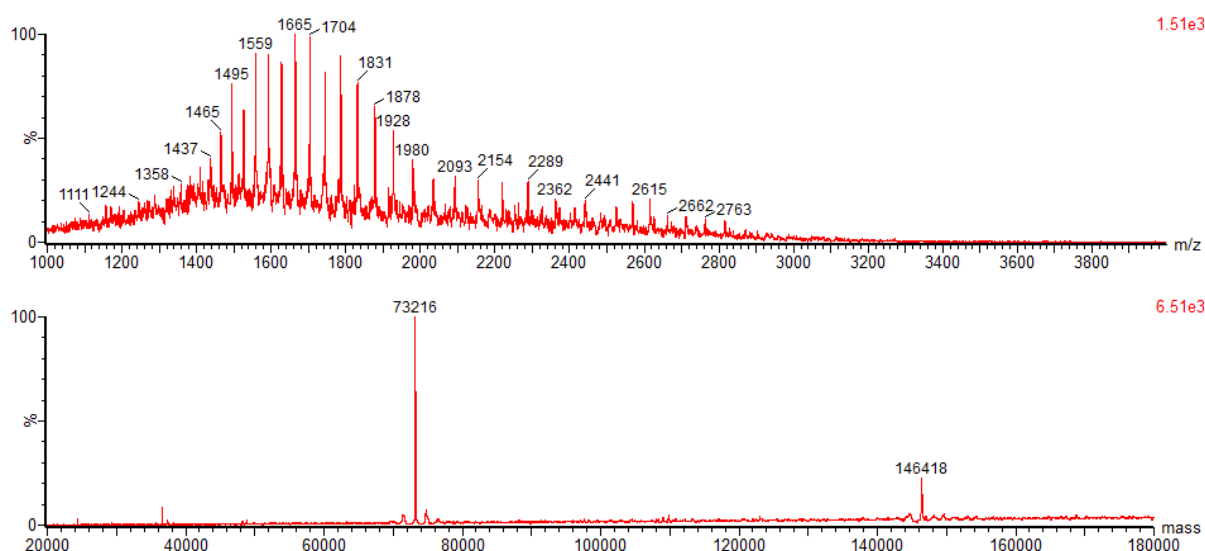


Figure C4: Analysis of the reaction between trastuzumab and BisDVP **10** by LC-MS. Top = non-deconvoluted MS. Bottom = deconvoluted MS; expected 73,224 Da (half antibody) and 146,448 Da (full antibody), observed 73,216 and 146,418 Da.

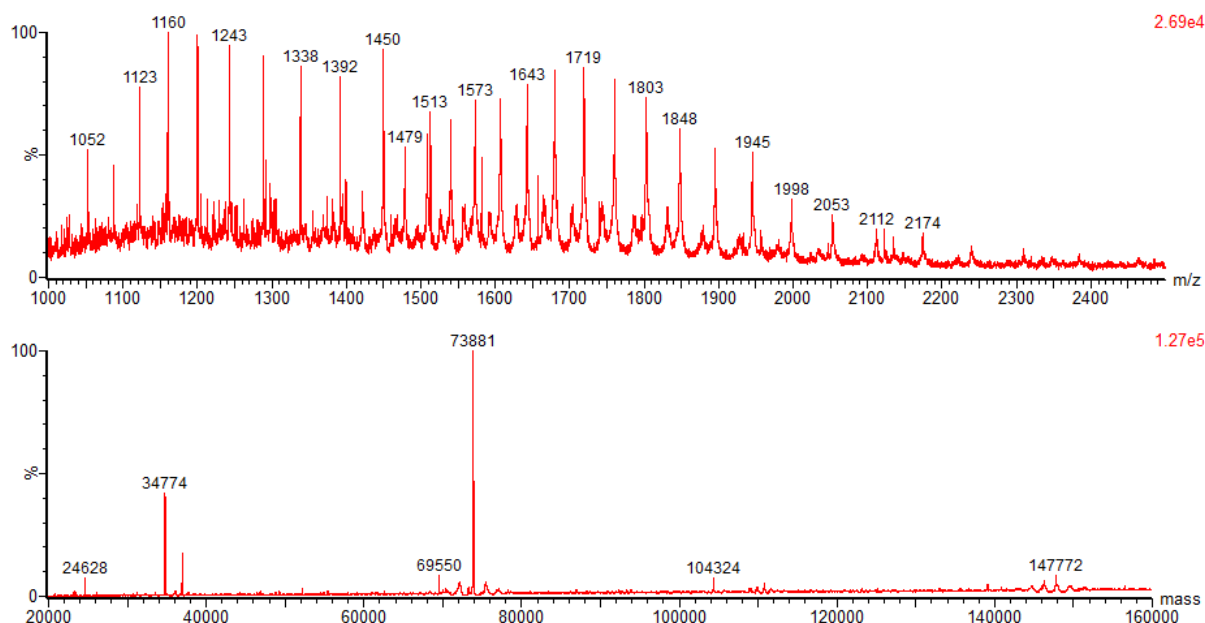


Figure C5: Analysis of the reaction between BisDVP ALC **12** and AlexaFluor™ 488 azide by LC-MS. Top = non-deconvoluted MS. Bottom = deconvoluted MS; expected 73,881 Da (half antibody) and 147,762 Da (full antibody), observed 73,881 Da and 146,772 Da. The peak at 34,774 Da corresponds to PNGase F.

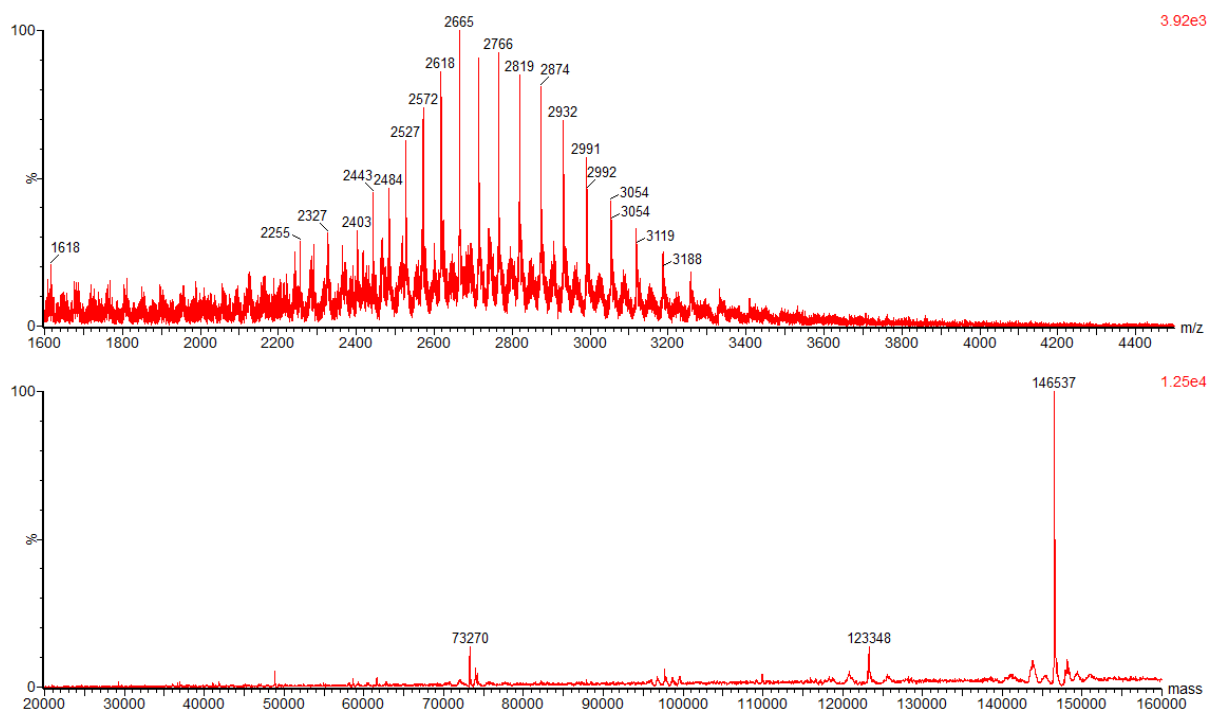


Figure C6: Analysis of the reaction between trastuzumab and TetraDVP **15** by LC-MS. Top = non-deconvoluted MS. Bottom = deconvoluted MS; expected 146,536 Da, observed 146,537 Da.

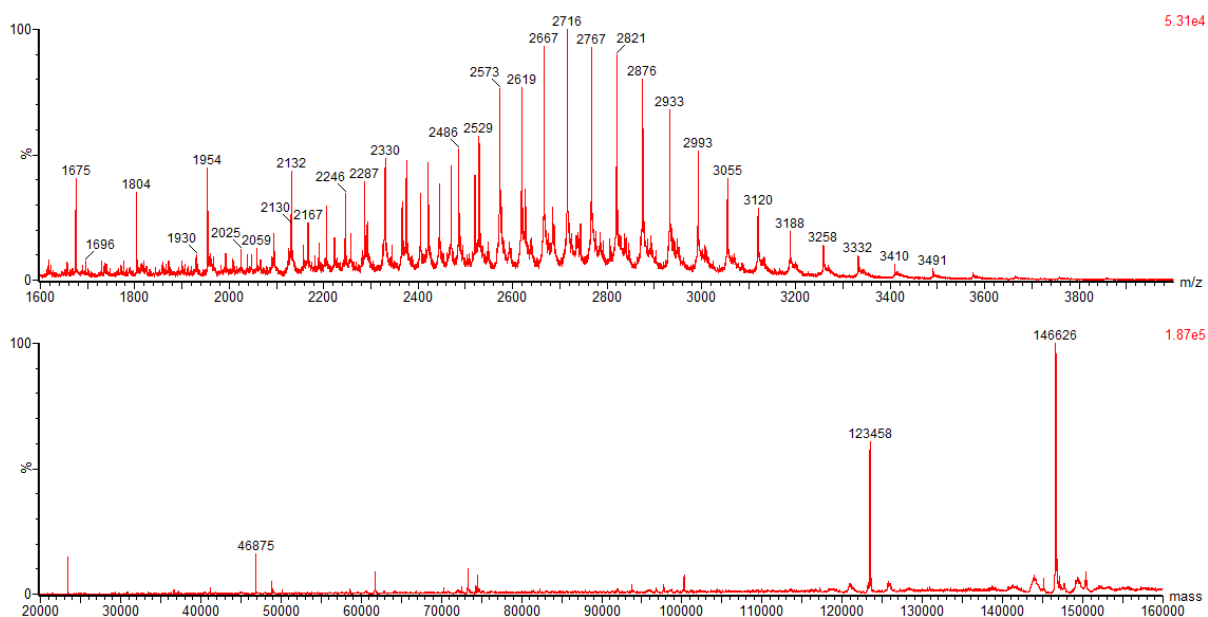


Figure C7: Analysis of the reaction between trastuzumab and TetraDVP **21** by LC-MS. Top = non-deconvoluted MS. Bottom = deconvoluted MS; expected 146,674 Da, observed 146,626 Da.

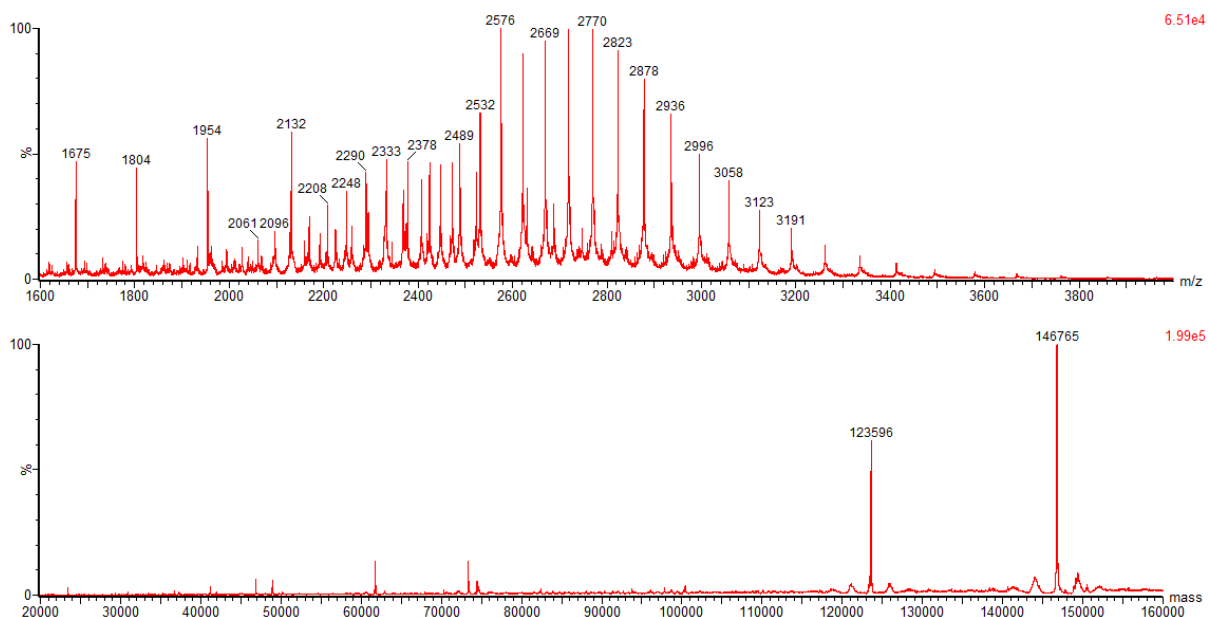


Figure C8: Analysis of the reaction between trastuzumab and TetraDVP **26** by LC-MS. Top = non-deconvoluted MS. Bottom = deconvoluted MS; expected 146,812 Da, observed 146,765 Da.

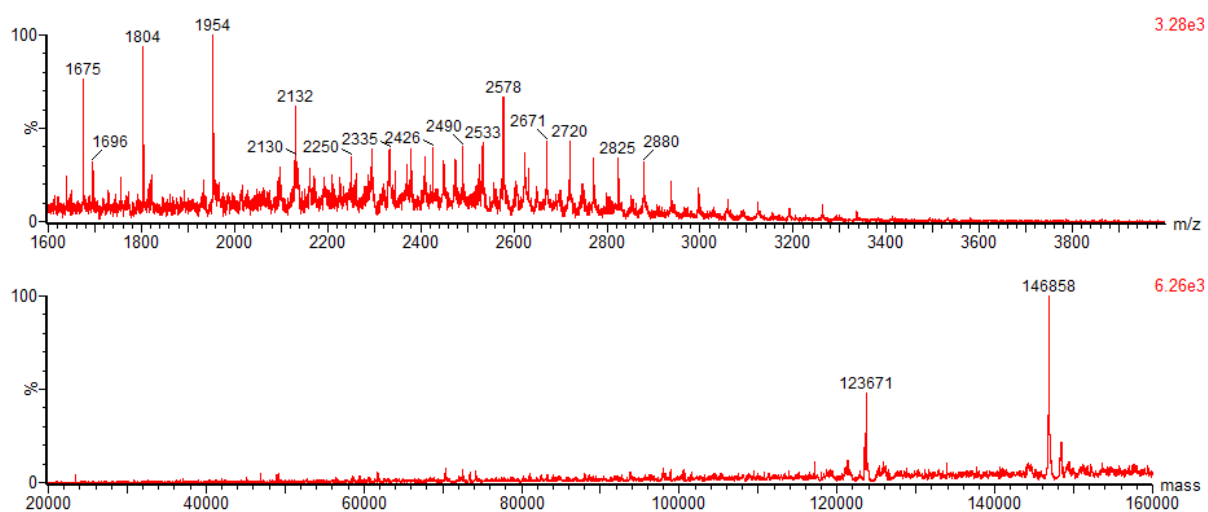


Figure C9: Analysis of the reaction between trastuzumab and TetraDVP **35** by LC-MS. Top = non-deconvoluted MS. Bottom = deconvoluted MS; expected 146,926 Da, observed 146,858 Da.

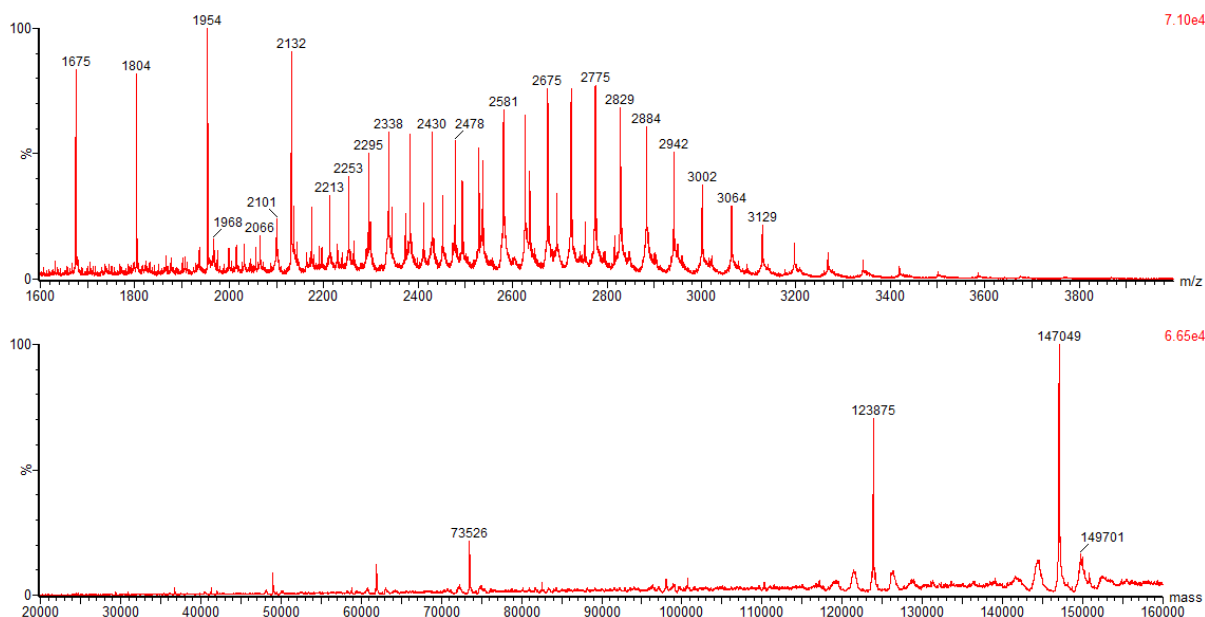


Figure C10: Analysis of the reaction between trastuzumab and TetraDVP **36** by LC-MS. Top = non-deconvoluted MS. Bottom = deconvoluted MS; expected 147,096 Da, observed 147,049 Da.

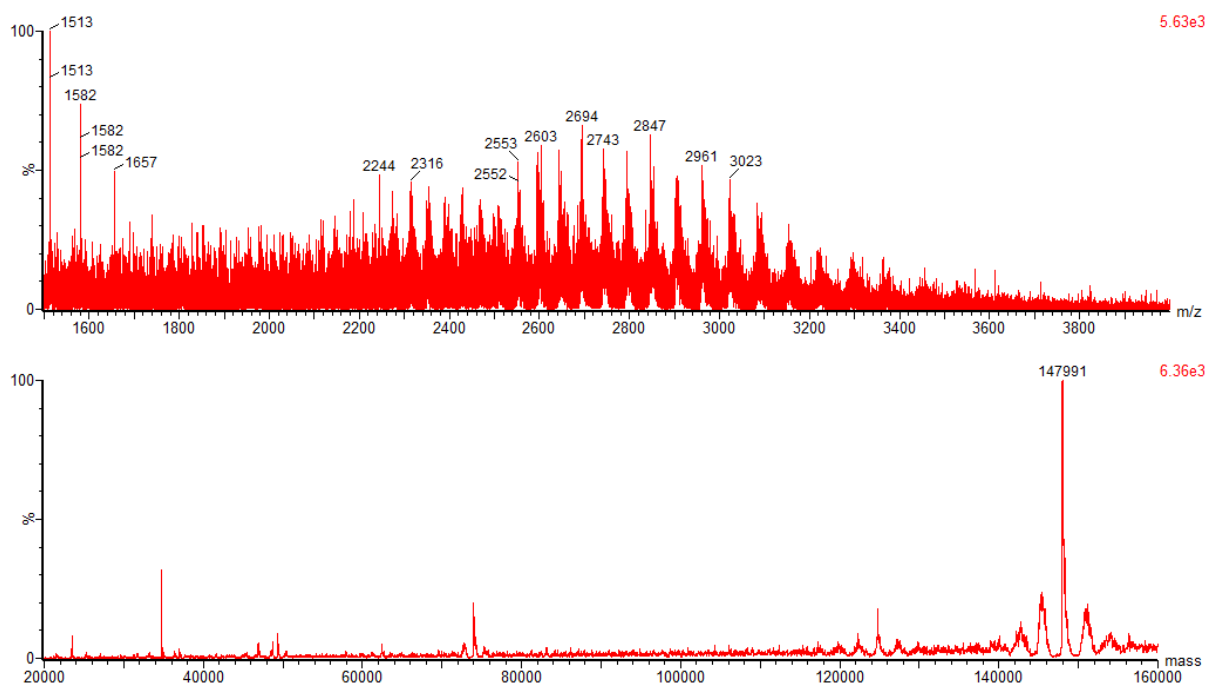


Figure C11: Analysis of the reaction between bis-alkyne ALC **38** and AlexaFluor™ 488 azide by LC-MS. Top = non-deconvoluted MS. Bottom = deconvoluted MS; expected 147,988 Da, observed 147,991 Da.

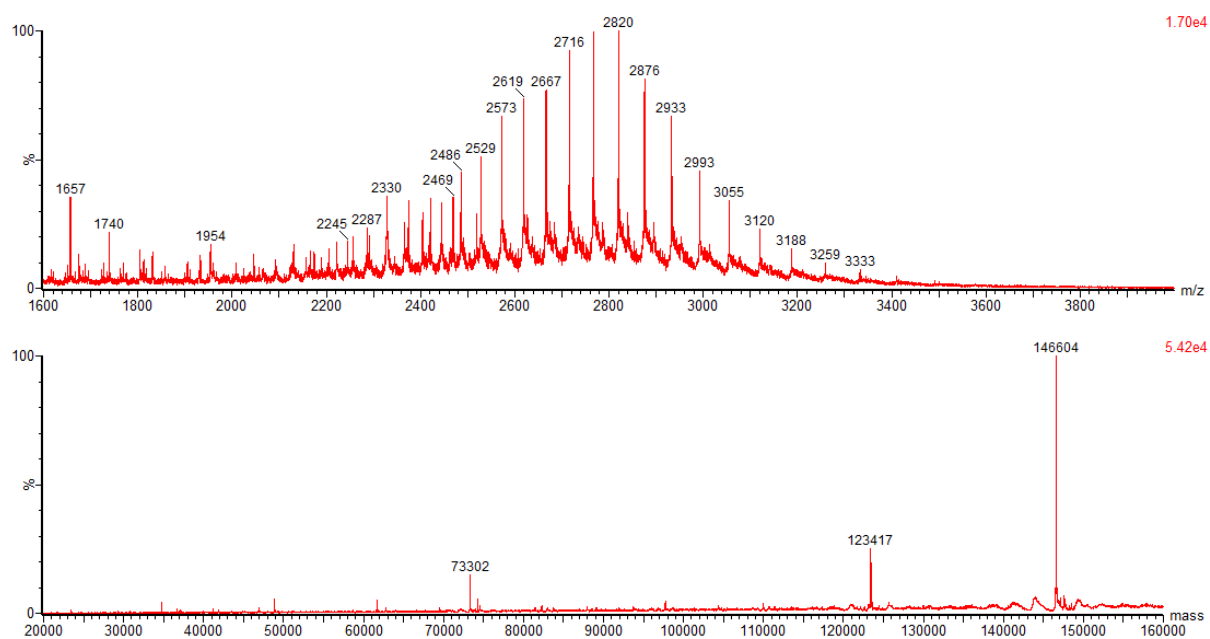


Figure C12: Analysis of the reaction between trastuzumab and TetraDVP **76** by LC-MS. Top = non-deconvoluted MS. Bottom = deconvoluted MS; expected 146,624 Da, observed 146,604 Da.

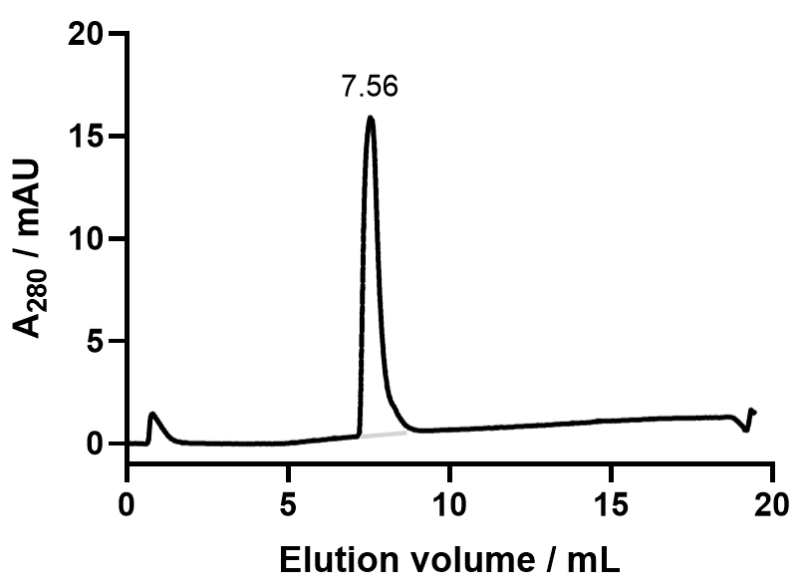
Appendix D – HIC traces

Procedure for HIC analysis:

Hydrophobic interaction chromatography (HIC) was carried out using a Tosoh Bioscience TSKgel Butyl-NPR column (4.6 mm ID x 3.5 cm L) at a flow rate of 0.6 mL/min. Proteins were eluted using a linear gradient of Solvent B in Solvent A (Solvent A: 1.5 M ammonium sulfate, 25 mM NaPi, pH 7; Solvent B: 25% isopropyl alcohol in 25 mM NaPi, pH 7).

TetraDVP ALC 37

HIC gradient: 0-100% B over 20 column volumes (CVs)

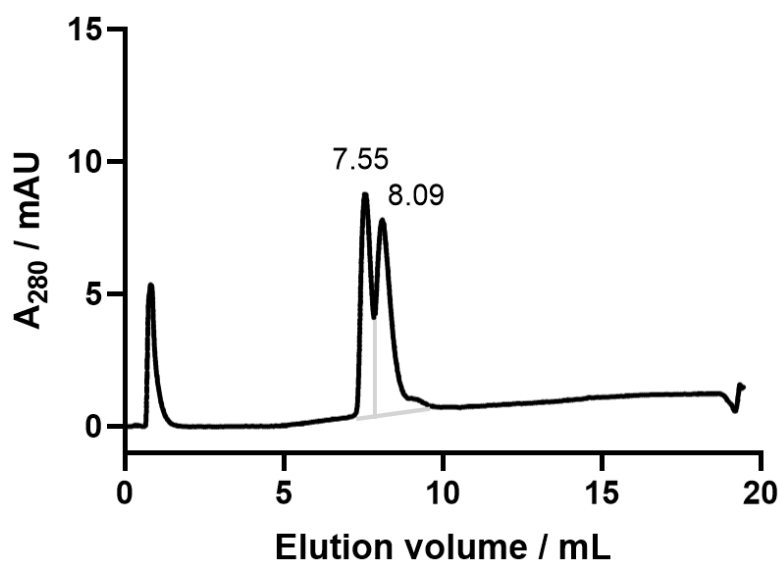


Peak Retention / mL	Area %
7.56	>99

TetraDVP PEG₄-Val-Cit-PABC-MMAE ADC 48

(from the reaction of ALC 37 with 24 equiv. N₃-PEG₄-Val-Cit-PABC-MMAE 47)

HIC gradient: 0-100% B over 20 CVs

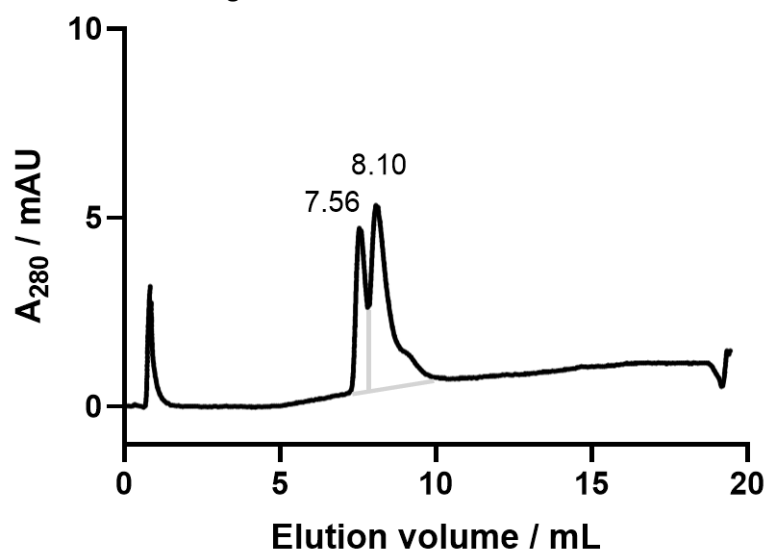


Peak Retention / mL	Area %
7.55	44.6
8.09	55.4

TetraDVP PEG₄-Val-Cit-PABC-MMAE ADC 48

(from the reaction of ALC 37 with 48 equiv. N₃-PEG₄-Val-Cit-PABC-MMAE 47)

HIC gradient: 0-100% B over 20 CVs

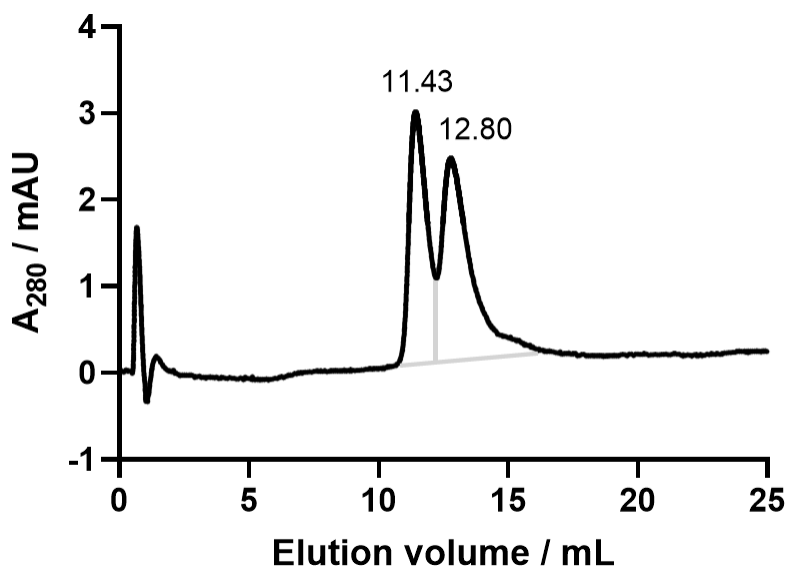


Peak Retention / mL	Area %
7.56	36.4
8.10	64.6

TetraDVP PEG₄-Val-Cit-PABC-MMAE ADC 48

(from the reaction of ALC 37 with 100 equiv. N₃-PEG₄-Val-Cit-PABC-MMAE 47)

HIC gradient: 0-70% B over 35 CVs

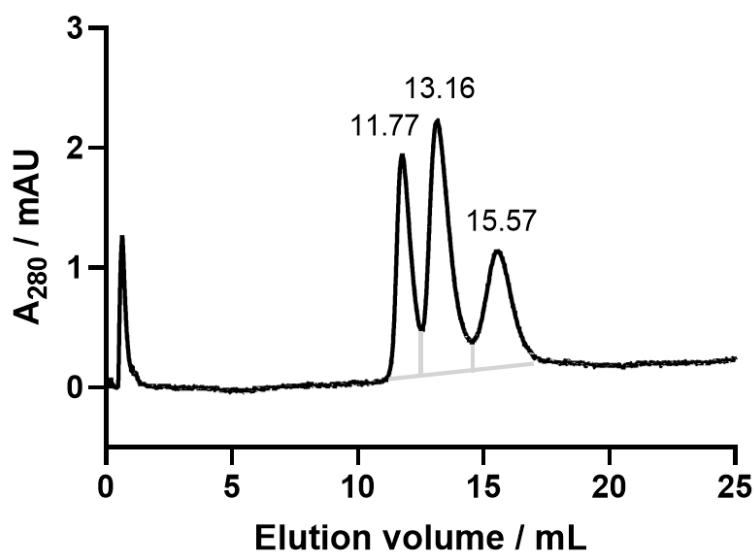


Peak Retention / mL	Area %
11.43	45.0
12.80	55.0

TetraDVP PEG₄-Val-Cit-PABC-MMAE ADC 49

(from the reaction of ALC 38 with 100 equiv. N₃-PEG₄-Val-Cit-PABC-MMAE 47)

HIC gradient: 0-70% B over 35 CVs

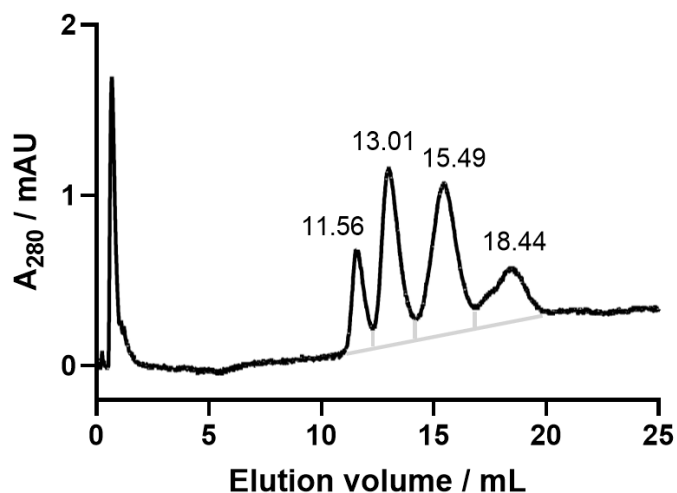


Peak Retention / mL	Area %
11.77	27.7
13.16	44.9
15.57	27.4

TetraDVP PEG₄-Val-Cit-PABC-MMAE ADC 50

(from the reaction of ALC 39 with 100 equiv. N₃-PEG₄-Val-Cit-PABC-MMAE 47)

HIC gradient: 0-70% B over 35 CVs

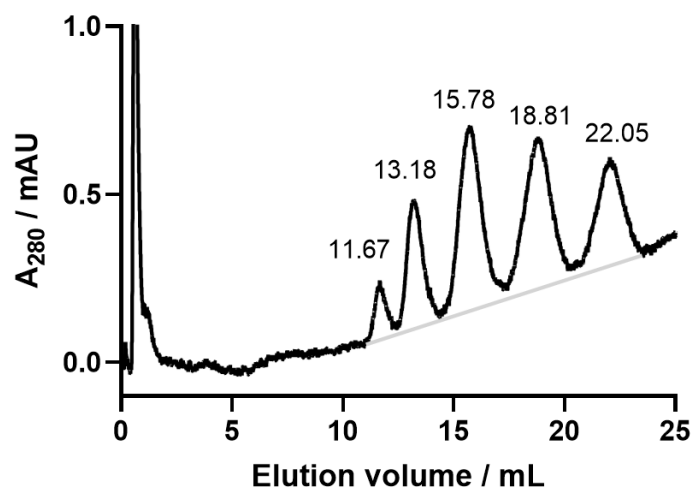


Peak Retention / mL	Area %
11.56	11.3
13.01	32.6
15.49	40.2
18.44	15.2

TetraDVP PEG₄-Val-Cit-PABC-MMAE ADC 51

(from the reaction of ALC 41 with 100 equiv. N₃-PEG₄-Val-Cit-PABC-MMAE 47)

HIC gradient: 0-70% B over 35 CVs

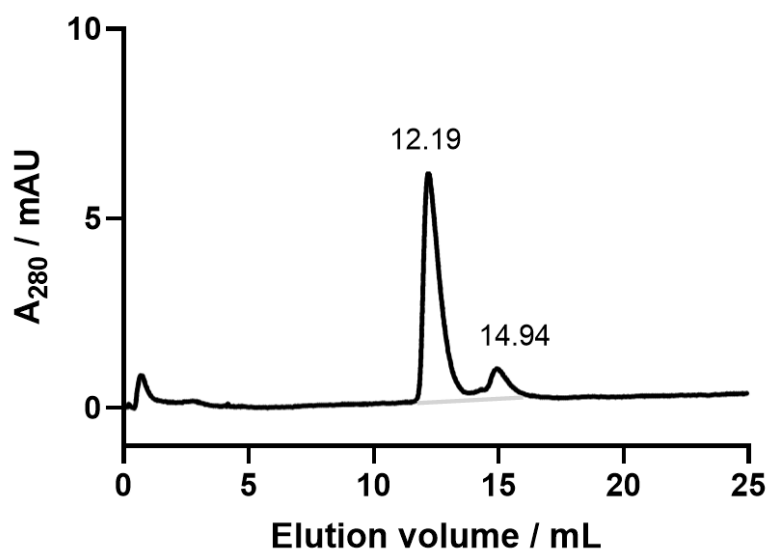


Peak Retention / mL	Area %
11.67	4.5
13.18	16.0
15.78	29.3
18.81	29.3
22.05	20.9

TetraDVP PEG₂₄-Val-Cit-PABC-MMAE ADC 53

(from the reaction of ALC 37 with 100 equiv. N₃-PEG₂₄-Val-Cit-PABC-MMAE 52)

HIC gradient: 0-70% B over 35 CVs

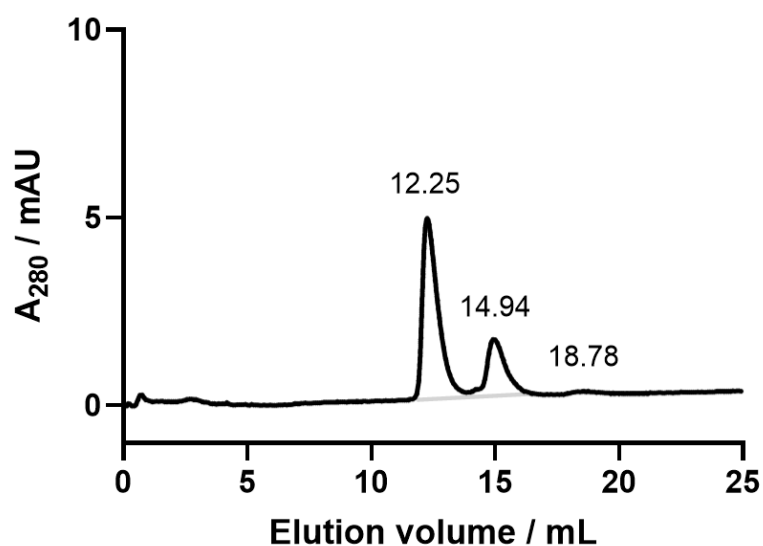


Peak Retention / mL	Area %
12.19	86.6
14.94	13.4

TetraDVP PEG₂₄-Val-Cit-PABC-MMAE ADC 54

(from the reaction of ALC 38 with 100 equiv. N₃-PEG₂₄-Val-Cit-PABC-MMAE 52)

HIC gradient: 0-70% B over 35 CVs

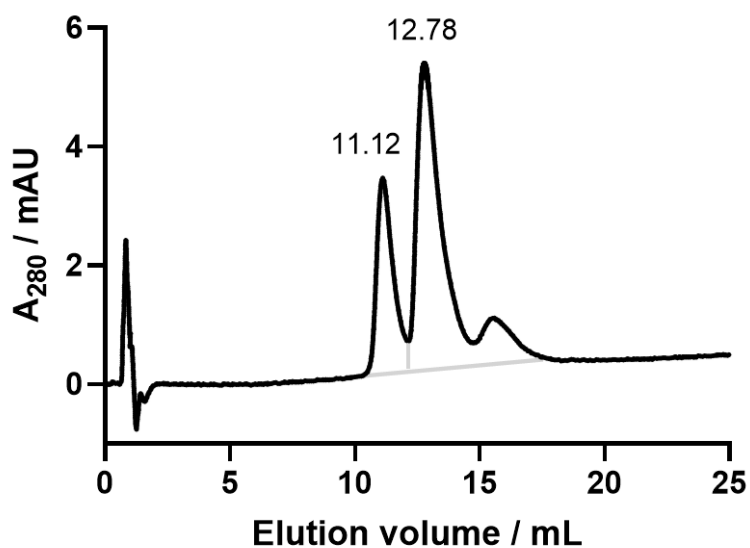


Peak Retention / mL	Area %
12.25	71.4
14.94	26.9
18.78	1.7

TetraDVP PEG₄-Glu₂-PEG₂-Val-Cit-PABC-MMAE ADC 56

(from the reaction of ALC 37 with 100 equiv. N₃-PEG₄-Glu₂-PEG₂-Val-Cit-PABC-MMAE 55)

HIC gradient: 0-70% B over 35 CVs

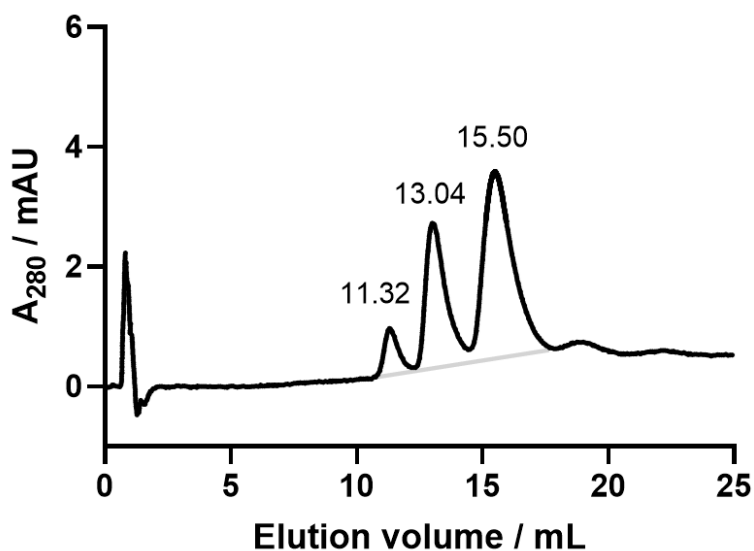


Peak Retention / mL	Area %
11.12	30.9
12.78	69.1

TetraDVP PEG₄-Glu₂-PEG₂-Val-Cit-PABC-MMAE ADC 57

(from the reaction of ALC 38 with 100 equiv. N₃-PEG₄-Glu₂-PEG₂-Val-Cit-PABC-MMAE 55)

HIC gradient: 0-70% B over 35 CVs

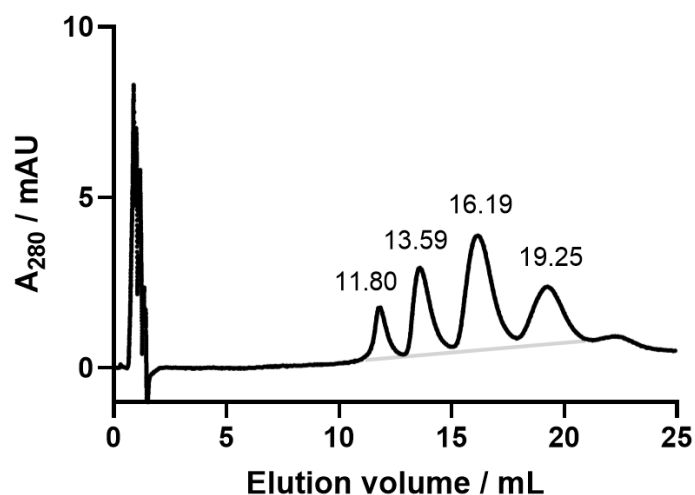


Peak Retention / mL	Area %
11.32	6.3
13.04	31.4
15.50	62.3

TetraDVP PEG₄-Glu₂-PEG₂-Val-Cit-PABC-MMAE ADC 58

(from the reaction of ALC 39 with 100 equiv. N₃-PEG₄-Glu₂-PEG₂-Val-Cit-PABC-MMAE 55)

HIC gradient: 0-60% B over 35 CVs

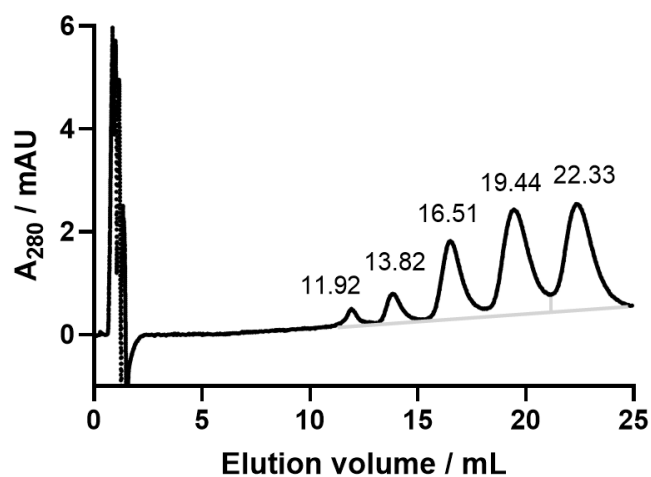


Peak Retention / mL	Area %
11.80	8.4
13.59	20.9
16.19	42.5
19.25	28.3

TetraDVP PEG₄-Glu₂-PEG₂-Val-Cit-PABC-MMAE ADC 59

(from the reaction of ALC 41 with 100 equiv. N₃-PEG₄-Glu₂-PEG₂-Val-Cit-PABC-MMAE 55)

HIC gradient: 0-60% B over 35 CVs

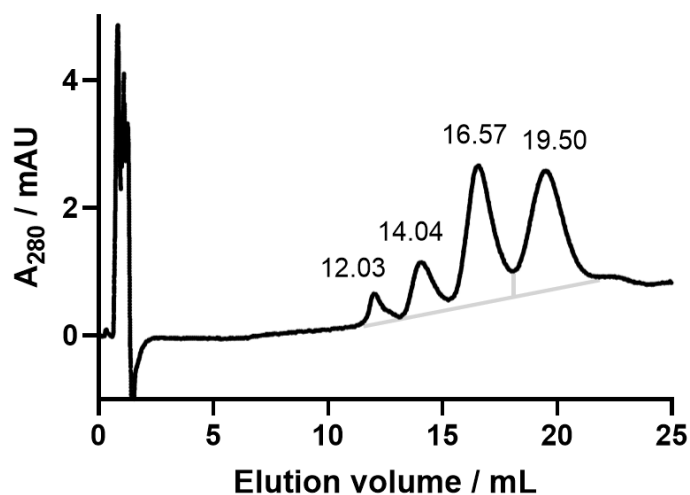


Peak Retention / mL	Area %
11.92	2.4
13.82	5.7
16.51	19.4
19.44	35.0
22.33	37.5

TetraDVP PEG₄-Glu₂-PEG₂-Val-Cit-PABC-MMAE ADC 58

(from the reaction of ALC 39 with 200 equiv. N₃-PEG₄-Glu₂-PEG₂-Val-Cit-PABC-MMAE 55)

HIC gradient: 0-70% B over 35 CVs

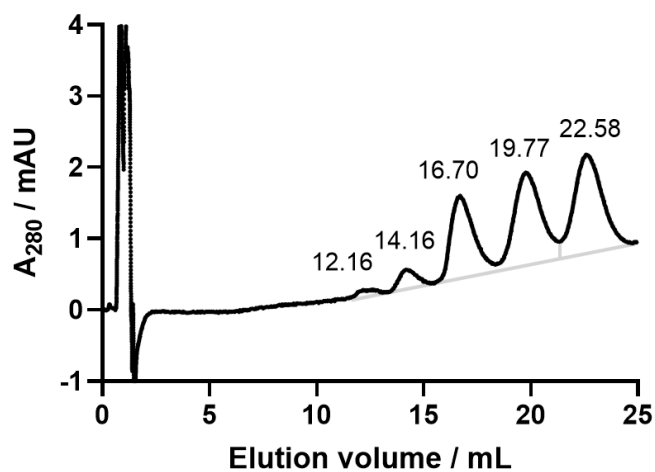


Peak Retention / mL	Area %
12.03	4.3
14.04	9.7
16.57	40.6
19.50	45.4

TetraDVP PEG₄-Glu₂-PEG₂-Val-Cit-PABC-MMAE ADC 59

(from the reaction of ALC 41 with 200 equiv. N₃-PEG₄-Glu₂-PEG₂-Val-Cit-PABC-MMAE 55)

HIC gradient: 0-70% B over 35 CVs

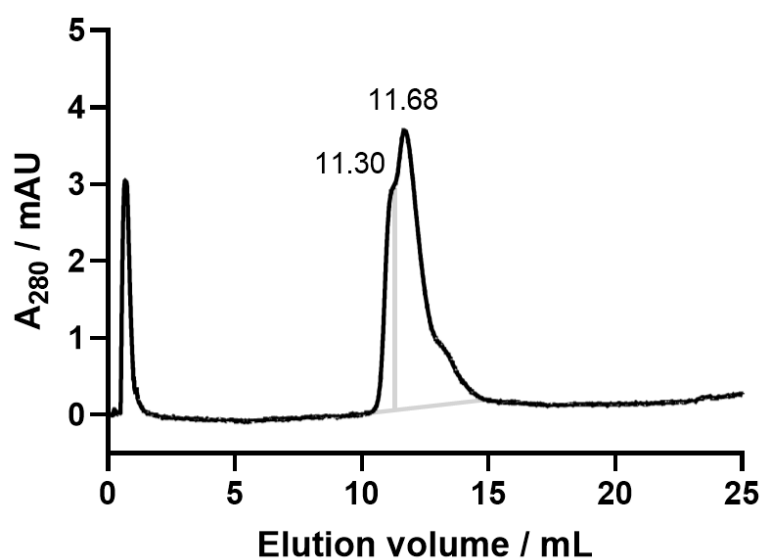


Peak Retention / mL	Area %
12.16	1.2
14.16	4.2
16.70	25.8
19.77	31.2
22.58	37.7

TetraDVP PEG₄-MMAE ADC 61

(from the reaction of ALC 37 with 100 equiv. N₃-PEG₄-MMAE 60)

HIC gradient: 0-70% B over 35 CVs

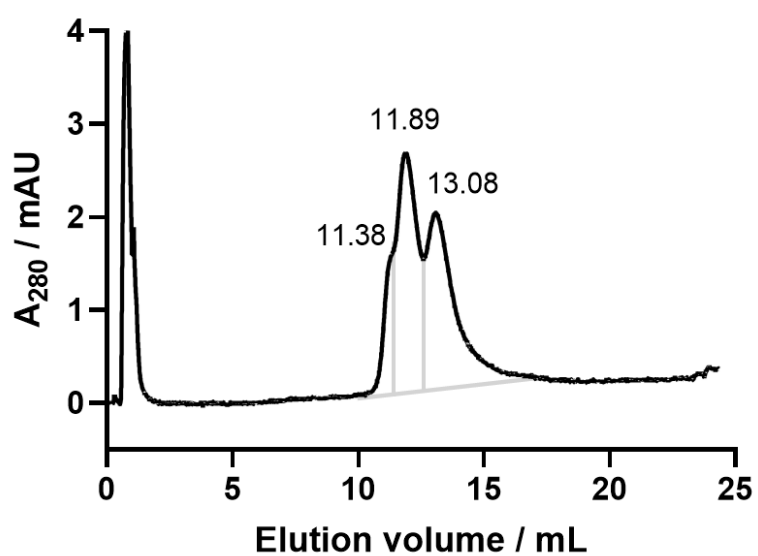


Peak Retention / mL	Area %
11.30	20.4
11.68	79.6

TetraDVP PEG₄-MMAE ADC 62

(from the reaction of ALC 38 with 100 equiv. N₃-PEG₄-MMAE 60)

HIC gradient: 0-70% B over 35 CVs

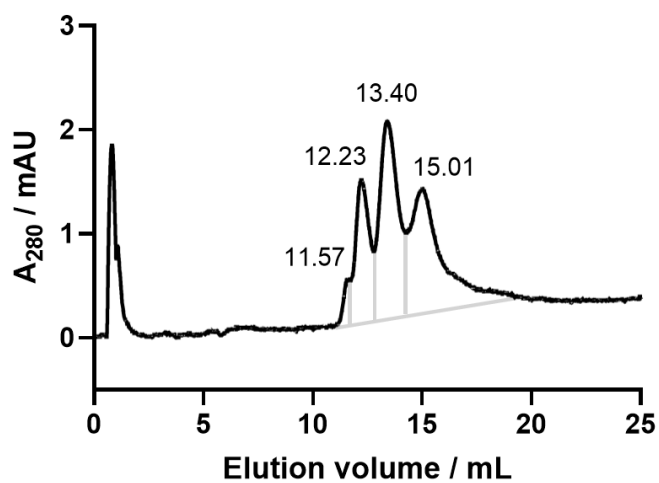


Peak Retention / mL	Area %
11.38	11.1
11.89	46.6
13.08	42.3

TetraDVP PEG₄-MMAE ADC 63

(from the reaction of ALC 39 with 100 equiv. N₃-PEG₄-MMAE 60)

HIC gradient: 0-70% B over 35 CVs

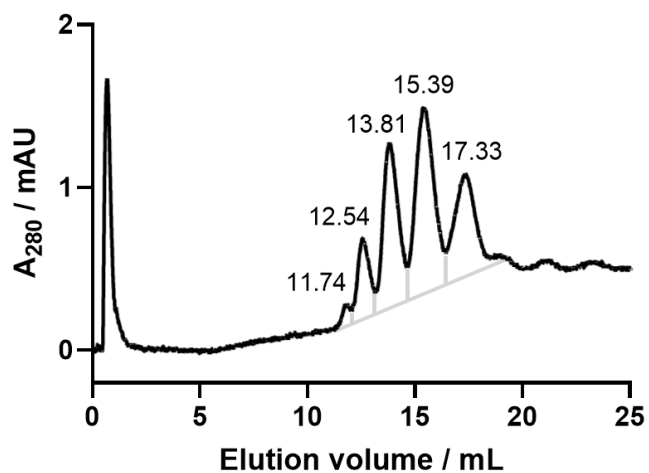


Peak Retention / mL	Area %
11.57	3.2
12.23	21.9
13.40	40.4
15.01	34.5

TetraDVP PEG₄-MMAE ADC 64

(from the reaction of ALC 41 with 100 equiv. N₃-PEG₄-MMAE 60)

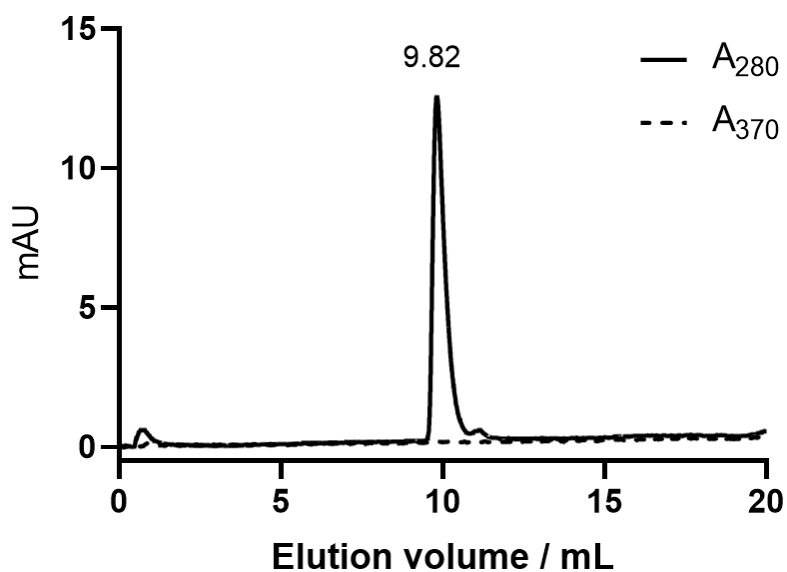
HIC gradient: 0-70% B over 35 CVs



Peak Retention / mL	Area %
11.74	0.6
12.54	7.3
13.81	26.6
15.39	39.7
17.33	25.8

TetraDVP ALC 37

HIC gradient: 0-60% B over 20 CVs

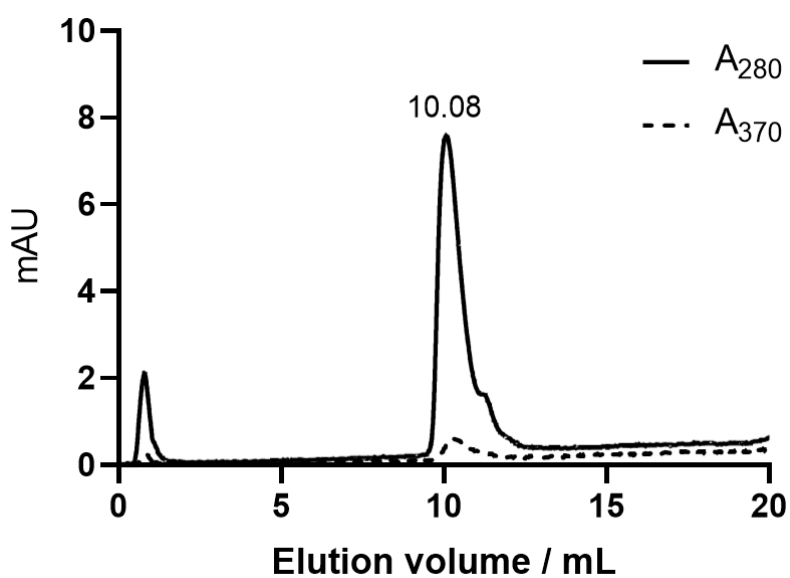


Peak Retention / mL	Area %
9.82	>99

TetraDVP PEG₄-SN-38 ADC 68

(from the reaction of ALC 37 with 100 equiv. N₃-PEG₄-SN-38 67)

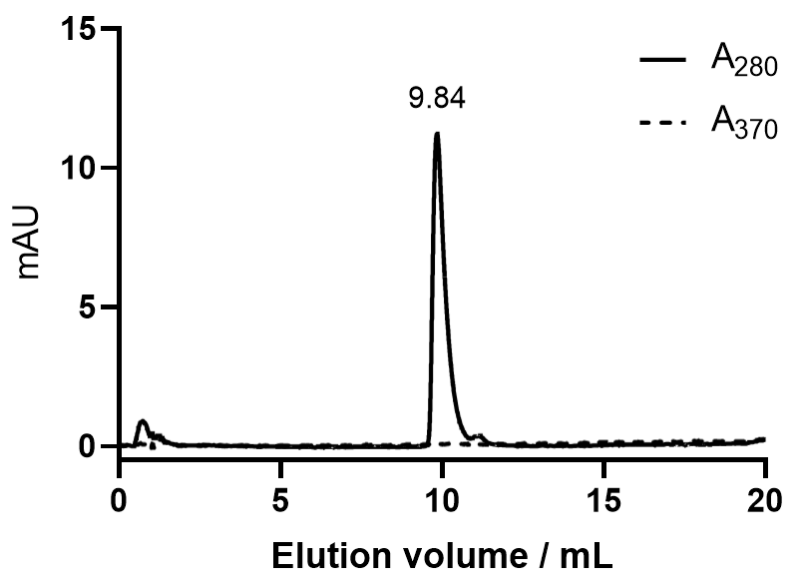
HIC gradient: 0-60% B over 20 CVs



Peak Retention / mL	Area %
10.08	>99

TetraDVP ALC 38

HIC gradient: 0-60% B over 20 CVs

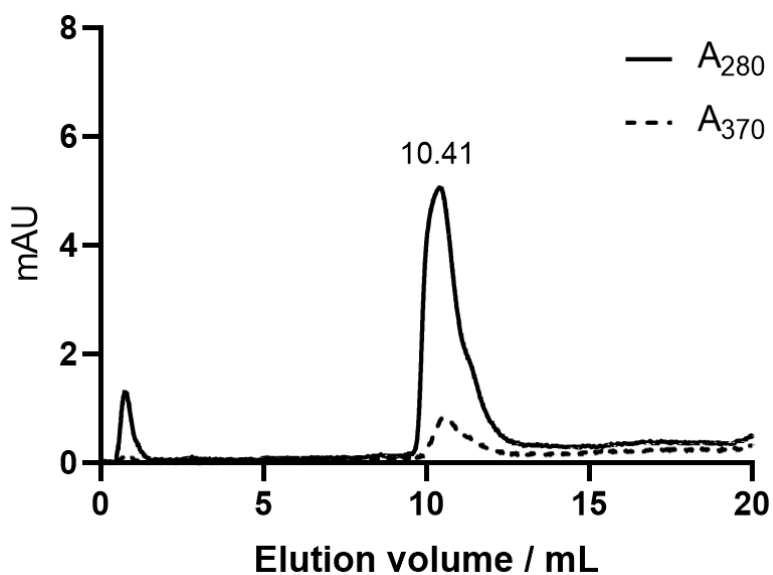


Peak Retention / mL	Area %
9.84	>99

TetraDVP PEG₄-SN-38 ADC 69

(from the reaction of ALC 38 with 100 equiv. N₃-PEG₄-SN-38 67)

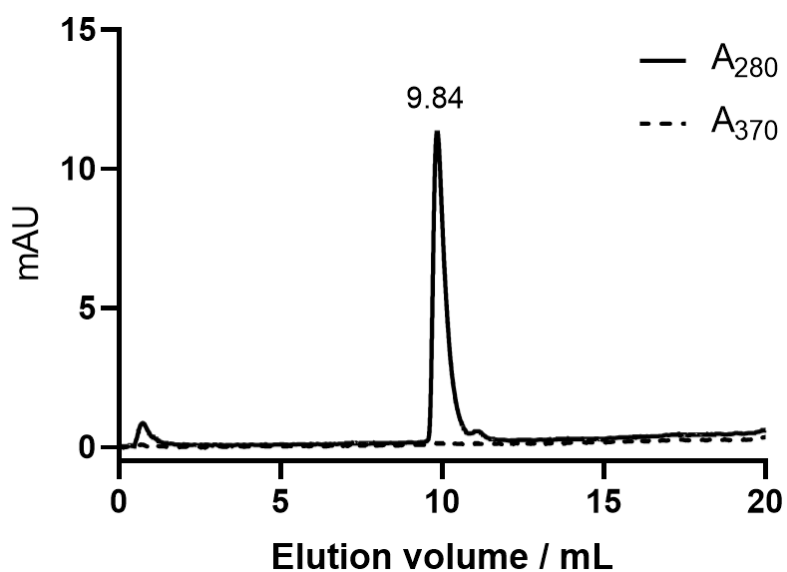
HIC gradient: 0-60% B over 20 CVs



Peak Retention / mL	Area %
10.41	>99

TetraDVP ALC 39

HIC gradient: 0-60% B over 20 CVs

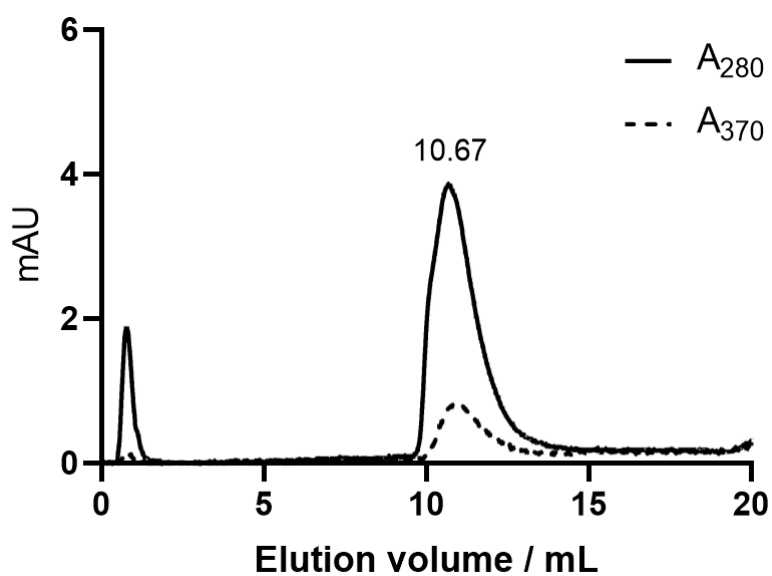


Peak Retention / mL	Area %
9.84	>99

TetraDVP PEG₄-SN-38 ADC 70

(from the reaction of ALC 39 with 100 equiv. N₃-PEG₄-SN-38 67)

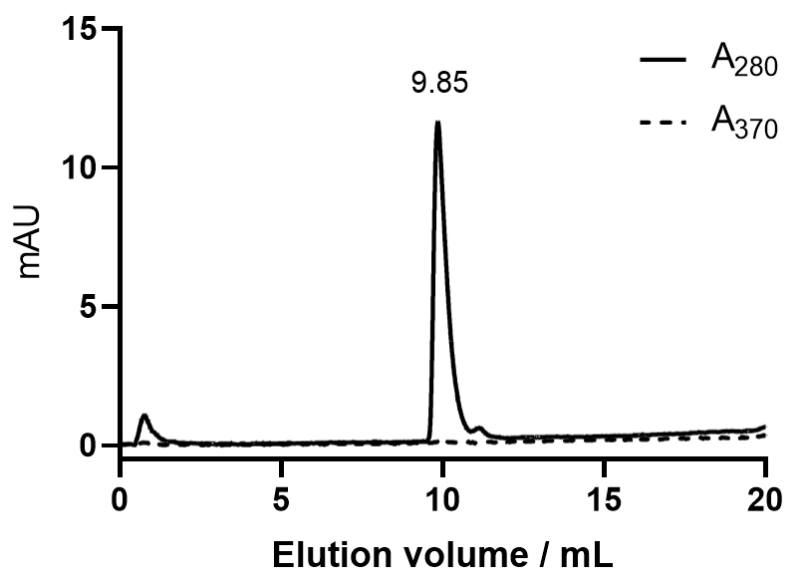
HIC gradient: 0-60% B over 20 CVs



Peak Retention / mL	Area %
10.67	>99

TetraDVP ALC 41

HIC gradient: 0-60% B over 20 CVs

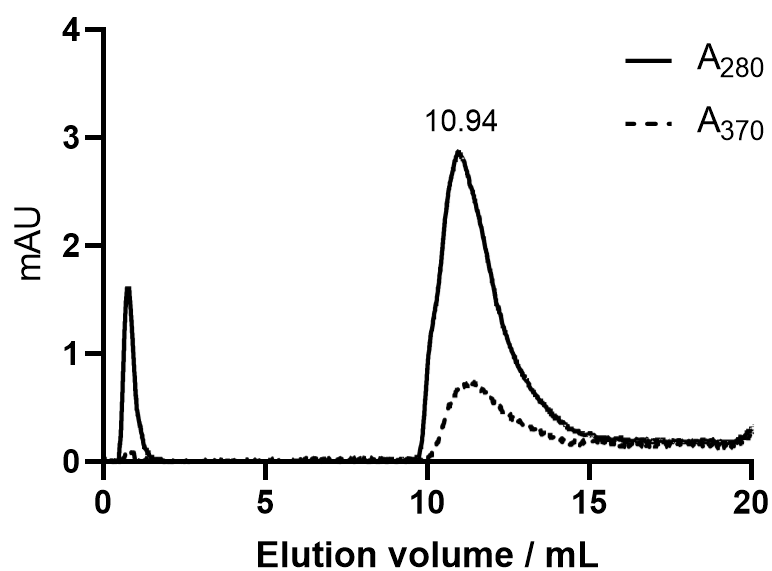


Peak Retention / mL	Area %
9.85	>99

TetraDVP PEG₄-SN-38 ADC 71

(from the reaction of ALC 41 with 100 equiv. N₃-PEG₄-SN-38 67)

HIC gradient: 0-60% B over 20 CVs

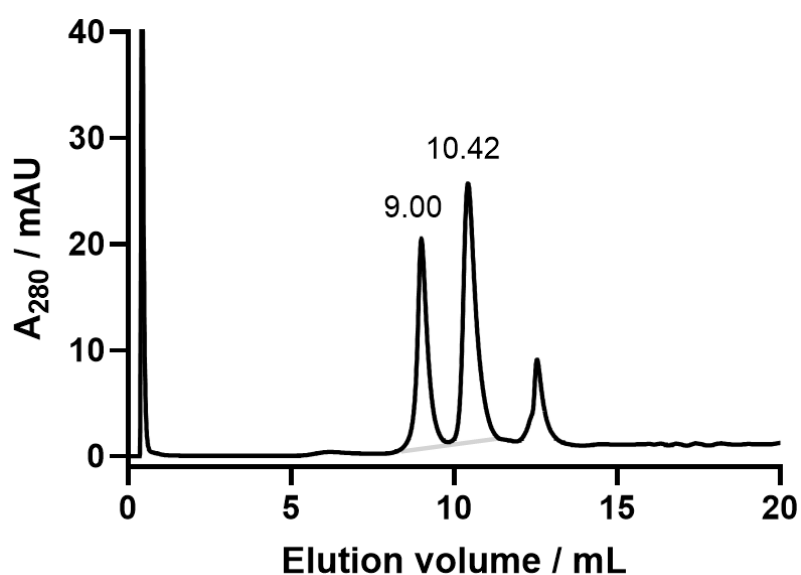


Peak Retention / mL	Area %
10.94	>99

TetraDVP PEG₂₄-Val-Cit-PABC-MMAE ADC 78

(from the reaction of ALC 77 with 100 equiv. N₃-PEG₂₄-Val-Cit-PABC-MMAE 52)

HIC gradient: 0-100% B over 25 CVs

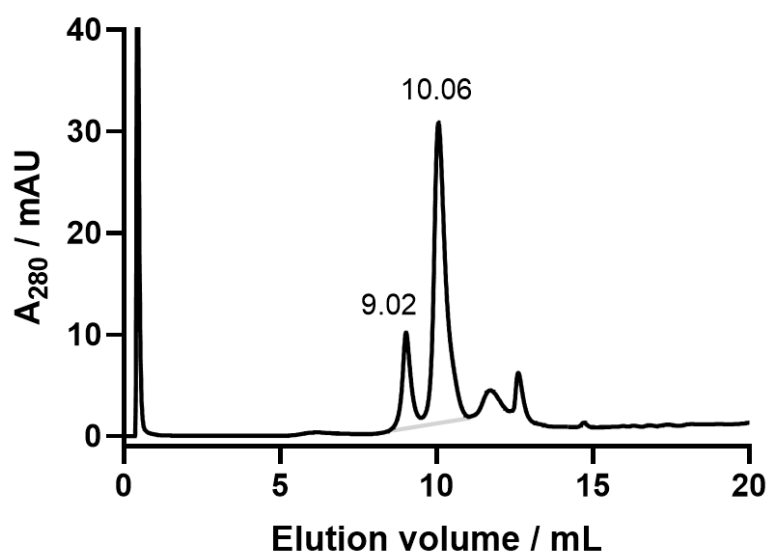


Peak Retention / mL	Area %
9.00	38.9
10.42	61.1

TetraDVP PEG₄-Glu₂-PEG₂-Val-Cit-PABC-MMAE ADC 79

(from the reaction of ALC 77 with 100 equiv. N₃-PEG₄-Glu₂-PEG₂-Val-Cit-PABC-MMAE 55)

HIC gradient: 0-100% B over 25 CVs

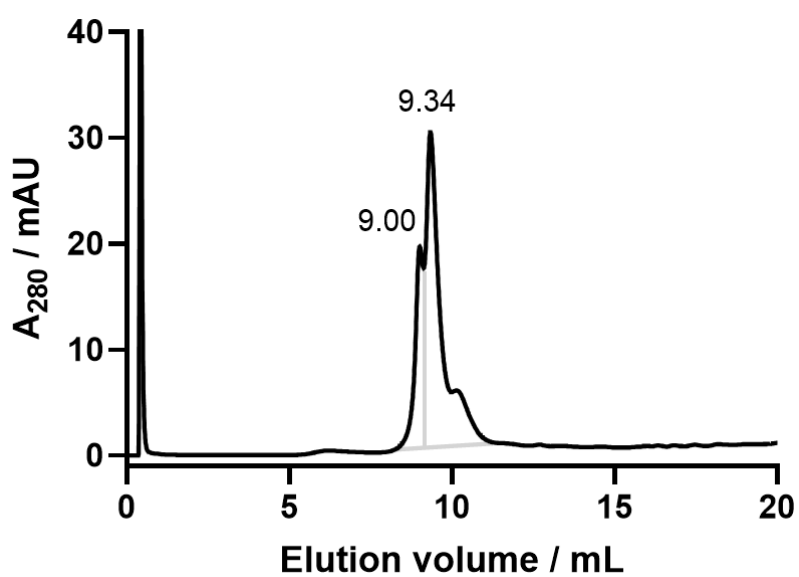


Peak Retention / mL	Area %
9.02	17.4
10.06	82.6

TetraDVP PEG₂₄-Val-Cit-PABC-MMAE ADC 80

(from the reaction of ALC **77** with 100 equiv. N₃-PEG₄-MMAE **60**)

HIC gradient: 0-100% B over 25 CVs



Peak Retention / mL	Area %
9.00	29.3
9.34	70.7

Appendix E – Publications

Friederike M. Dannheim, Stephen J. Walsh and David R. Spring, Conjugating reagents and conjugates thereof, Pat Appl GB2110726.3, 2021.

Connor J. Taylor, Hikaru Seki, **Friederike M. Dannheim**, Mark J. Willis, Graeme Clemens, Brian A. Taylor, Thomas W. Chamberlain and Richard A. Bourne, An Automated Computational Approach to Kinetic Model Discrimination and Parameter Estimation, *React. Chem. Eng.* 2021, **6**, 1404-1411.

Stephen J. Walsh*, Jonathan D. Bargh*, **Friederike M. Dannheim***, Abigail R. Hanby*, Hikaru Seki*, Andrew J. Counsell*, Xiaoxu Ou*, Elaine Fowler*, Nicola Ashman*, Yuri Takada*, Albert Isidro-Llobet, Jeremy S. Parker, Jason S. Carroll and David R. Spring, Site-selective modification strategies in antibody-drug conjugates, *Chem. Soc. Rev.* 2021, **50**, 1305-1353. *Authors contributed equally.